Pro-angiogenic and metastatic properties of galectin-1 during epithelial ovarian cancer metastasis to the omentum

Submitted by Annelie R.T. Maskell to the University of Exeter as a thesis for the degree of Doctor of Philosophy in Medical Sciences in October 2021.

This thesis is available for Library use on the understanding that it is copyright material and that no quotation from the thesis may be published without proper acknowledgement.

I certify that all material in this thesis which is not my own work has been identified and that no material has previously been submitted and approved for the award of a degree by this or any other University.

Signature:……Annelie Maskell……..

Acknowledgements

There are numerous people and groups who have made this project possible. I would firstly like to thank my supervisors Dr Jacqueline Whatmore and Dr Nicholas Gutowski, for their support and guidance. Whilst supervisory meetings had to often steer me back on track, I have appreciated their kindness and sense of humour whilst doing so.

Thank you to Mr Michael Hannemann and the surgical and research team at the RD&E, and to Susan Westoby for help with organising sample collections. Above all, my thanks to the patients who kindly donated omental tissue.

Thank you to FORCE cancer charity for funding this project and for all the work that they do.

All my friends and colleagues in the IBCS office, past or present, deserve my thanks. A special thank you to Alex, Annie, and the HOMeso to my HOMEC, Gillian.

Thank you to the Manchester gals, and my Sheffield pals.

Thank you to SWAT roller derby for providing a wonderful outlet during these busy years, and an immeasurable amount of emotional support. There are too many people to name, but special thanks to Orla, Fayelord, Moisty, Sandypants, Annasaurus, Trash bags, Helen Hicks, Rocksar, and everyone in my intake.

Finally, thank you to my family for their support over the years. Big thanks to my sister, Kim.

Dedicated to all the other widening participation people out there in higher education, as well as Kevin King, Mrs Archer, and Claudia Riley.

Abstract

Epithelial ovarian cancer (EOC) frequently metastasises to the omentum. Metastatic growth requires angiogenesis (new blood vessel formation), to provide nutrients and oxygen to the growing secondary tumour. This process requires the activation of local microvascular endothelial cells (ECs), by tumour cell secreted pro-angiogenic factors, such as vascular endothelial growth factor (VEGF). The prognosis for patients with advanced metastatic EOC remains poor and the search for effective treatments is on-going. However, therapeutic targeting of angiogenesis and, in particular, the VEGF pathway has been relatively unsuccessful, suggesting the involvement of other pro-angiogenic factors that may offer alternative therapeutic targets.

Cathepsin-L (CL), a lysosomal protease, has been shown to induce galectin-1 (gal-1) secretion, a small glycoprotein, from disease-relevant human omental microvascular ECs (HOMECs). Gal-1 is upregulated in advanced EOC, and has been implicated in metastatic processes, including angiogenesis. The mechanisms by which gal-1 may contribute to HOMEC pro-metastatic and angiogenic activity are unknown, and therefore the aims of this thesis were to a) improve a method to isolate HOMECs from omental samples, b) to examine pro-metastatic and angiogenic effects of gal-1 in EOC cells and HOMECs, and c) to identify pro-proliferative gal-1 activated receptors and downstream signalling pathways in HOMECs.

HOMEC cultures were obtained by enzymatic digestions and immunoselection, and characterised with immunocytochemistry (ICC). A2780 and SKOV3 EOC cell lines secreted gal-1, and HOMECs secreted significantly more gal-1 in response to CL. Gal-1 pre-treatment of either A2780/SKOV3 cells or HOMEC monolayers, significantly increased A2780/SKOV3 cell adhesiveness to HOMEC monolayers. CL significantly increased extracellular surface gal-1 on HOMECs, and HOMECs were shown to be able to bind exogenous gal-1 to their cell surface. Exogenous gal-1 significantly induced HOMEC proliferation in WST-1 and BrdU assays, as well as HOMEC migration in chamber but not scratch assays. Receptor tyrosine kinase and intracellular phosphokinase arrays identified gal-1 induced phosphorylation of VEGF receptor 2 (VEGFR2)

and phospholipase Cγ1 (PLCγ1) independently of VEGF, findings which were confirmed by ELISA and flow cytometry. It was hypothesised that gal-1 was inducing pro-proliferative effects by binding to complex N-glycans on the cell surface (possibly on VEGFR2). Inhibition of complex N-glycan synthesis with swainsonine (SW) significantly inhibited gal-1 induced HOMEC proliferation, phosphorylation of VEGFR2, and preliminarily suggested inhibition of PLCγ1 phosphorylation. Gal-1 also significantly increased retention of VEGF activated VEGFR2 complexes at the cell surface.

In conclusion, these data suggest that gal-1 is a potential pro-metastatic and pro-angiogenic molecule that may contribute to metastasis of EOC to, and within the omentum. In disease-relevant microvascular ECs (HOMECs) gal-1 activates pro-angiogenic responses via the VEGF receptor independently of VEGF, potentially by binding to complex N-glycans on VEGFR2 and initiating pro-proliferative intracellular pathways. Thus gal-1 may represent a new therapeutic target for the treatment of advanced EOC.

List of contents

List of figures

List of tables

Abbreviations

AA	Arachidonic acid
ACE	Angiotensin-converting enzyme
AJs	Adherens junctions
Akt	Protein kinase B
AMANII	Alpha2-mannosidase
ANG II	Angiotensin II
Ang-1	Angiopoietin-1
Ang-2	Angiopoietin-2
BBB	Blood brain barrier
BCA	Bicinchoninic acid
bFGF	Basic fibroblast growth factor
BRCA1	Breast cancer type 1 susceptibility protein
BRCA2	Breast cancer type 2 susceptibility protein
BSA	Bovine serum albumin
$CaCl_2$	Calcium chloride
cAMP	Cyclic adenosine monophosphate
Cdc42	Cell division control protein 42
CL	Cathepsin-L
COX-1	Cyclooxygenase-1
COX-2	Cyclooxygenase-2
CTCF	Corrected total cell fluorescence
CTCs	Circulating tumour cells
CXCL12	CXC chemokine ligand 12
DLL4	Delta-like ligand 4
DMEM	Dulbecco's Modified Eagle's Medium
DMSO	Dimethyl sulfoxide
ECM	Extracellular matrix
ECs	Endothelial cells
EDHF	Endothelium derived hyperpolarising factor
EDTA	(Ethylenedinitrilo)tetra-acetic

eGCX	Endothelial glycocalyx
EGF	Epidermal growth factor
EGFR	Epidermal growth factor receptor
ELISA	Enzyme linked immunosorbent assay
EMT	Epithelial-mesenchymal transition
EOC	Epithelial ovarian cancer
EPCs	Endothelial progenitor cells
ER	Endoplasmic reticulum
ERK	Extracellular signal-regulated pathway
ET-1	Endothelin-1
FACS	Fluorescence activated cell sorting
FAK	Focal adhesion kinase
FCS	Foetal calf serum
FI	Fluorescence intensity
Gal-1	Galectin-1
Gal-3	Galectin-3
GJs	Gap junctions
GJs	Gap junctions
Grb2	Growth factor receptor-bound protein 2
GTP	Guanosine triphosphate
HBSS	Hank’s balanced salt solution
hCMEC/D3 cells	Human cerebral microvascular endothelial cells
HGF	Hepatocyte growth factor
HIFs	Hypoxia-inducible factors
HOFs	Human omental fibroblasts
HOMECs	Human omental microvascular endothelial cells
HOMesos	Human omental mesothelial cells
HRECs	Human retinal endothelial cells
HRP	Horseradish peroxidase
HUVECs	Human umbilical vein endothelial cells
ICC	Immunocytochemistry
JAMs	Junctional adhesion molecules
KCl	Potassium chloride

KO	Knockout
LDH	Lactate dehydrogenase
MAPK	H-ras/mitogen-activated protein kinase
MET	Mesenchymal-epithelial transition
MFI	Median fluorescent intensity
MMPs	Matrix metalloproteinases
MMT	Mesothelial-mesenchymal transition
MSCs	Mesenchymal stem cells
mTOR	Mammalian target of rapamycin
Na+-/K+-ATPase	Sodium-potassium pump
NaCl	Sodium Chloride
NO	Nitric oxide
NOS/eNOS	Nitric oxide synthase/endothelial nitric oxide synthase
NRP-1	Neuropilin-1
OSE	Ovarian surface epithelium
PBS	Phosphate buffered saline
PDGF	Platelet-derived growth factor
PFA	Paraformaldehyde
PI	Propidium iodide
PI3	Phosphatidylinositol 3-kinase pathway
PKC	Protein kinase C
PLC	Phospholipase C
PLCγ1	Phospholipase C gamma 1
pPLCγ1	Phosphorylated phospholipase C gamma 1
pVEGFR2	Phosphorylated vascular endothelial growth factor receptor 2
Raf	Rapidly accelerating fibrosarcoma
RhoA	ras homolog family member A
ROS	Reactive oxygen species
RPMI	Roswell Park Memorial Institute
RT	Room temperature
RTK	Receptor tyrosine kinase
SD	Standard deviation

Shb	SH2 domain-containing adaptor protein B
SIK2	Salt-inducible kinase 2
snRNPs	Small nuclear ribonucleoproteins
Src	Proto-oncogene c-Src
SSc	Systemic sclerosis
SU	SU5416
SW	Swainsonine
TCM	Tumour conditioned media
TGF-β	Transforming growth factor-β
TIMPs	Tissue inhibitor of metalloproteinases
TJs	Tight junctions
TNF-α	Tumour necrosis factor
tpm	Tilts per minute
TSPs	Thrombospondins
TXA_2	Thromboxane A_2
VE-cadherin	Vascular endothelial cadherin
VEGF	Vascular endothelial growth factor
VEGFR2	Vascular endothelial growth factor receptor 2
VSMCs	Vascular smooth muscle cells
vWF	von Willebrand factor
WST-1	Water soluble tetrazolium salt-1
ZO-1	Zona occludens-1

Chapter 1. Introduction

The vasculature, microvasculature, and endothelial cells will first be defined and discussed. The wider cellular biology of endothelial cells (ECs; the building blocks of the endothelium), shall be explored initially, followed by the process of angiogenesis. This project specifically studied angiogenesis within the omentum in the context of epithelial ovarian cancer, and therefore further discussion covers these areas. The introduction progresses to discuss the molecule of interest, galectin-1, and its current implications in angiogenesis and cancer development.

1.1 The vasculature

The vasculature refers to the network of blood vessels within the body. There are three main types of blood vessel: arteries, veins and capillaries. Each type of vessel has distinct phenotypical and functional differences. Further differences within each type are observed dependent on location. Arterial (arteries and arterioles) and venous (veins and venules) blood vessels are comprised of three layers: an outer layer (tunica externa), middle layer (tunica media) and an innermost layer (tunica interna), see figure 1.

The tunica externa is a sheath of connective tissue primarily composed of collagen and is typically thicker on veins. The tunica externa holds vessels in relative position by connecting to surrounding tissue. The tunica media consists of layers of smooth muscle and elastic fibres, and is thicker in arteries to regulate pressure; the smooth muscle can relax and contract to alter lumen diameter, resulting in vasodilation and vasoconstriction respectively. The tunica interna is lined with ECs which collectively make up the endothelium, the interface between circulating blood and the vessel wall. The endothelium is bound to connective tissue of the tunica media by a semi-permeable basement membrane. Capillaries only consist of this basement membrane and the layer of ECs, but also pericytes. Pericytes wrap around ECs, stabilise capillaries, and interact with ECs in order to regulate blood flow.

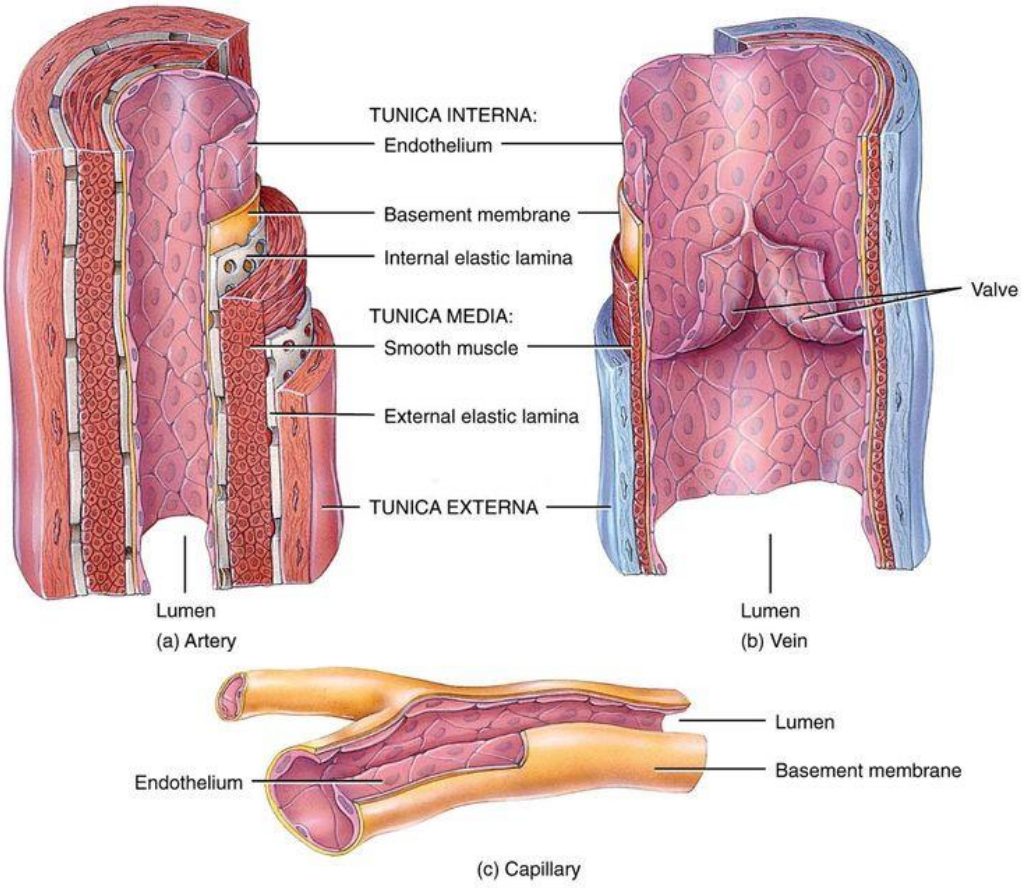

Figure 1. The three layer structure of arteries, veins and capillaries. The differences in the proportions of the three layers between arteries and veins is depicted; the thicker tunica media can be seen in the artery on the left. A valve is present in the vein on the right. The capillary, composed of the basement membrane and a single layer of endothelial cells (ECs) is shown beneath (Tortora and Derrickson, 2011).

1.1.1 The microvasculature

The vasculature supplies tissues with blood through the microvasculature: blood vessels with diameters of <100µm (Popel and Johnson, 2005). Microvessels within the microvasculature include arterioles, post-capillary venules, and capillaries. Capillaries are the smallest blood vessels (<10µm diameter), consisting of only the basement membrane and a single layer of ECs (see figure 1), and are the site of gas exchange to tissues (Guven *et al*, 2020). The microcirculation is also involved in the regulation of vascular permeability, and

therefore solute exchange. The location and functional requirement of capillaries varies between different capillary beds; different types of specialised capillary regulate permeability differently. There are two major types of specialised capillary: continuous (divided into fenestrated and non-fenestrated), and discontinuous capillaries see figure 2. Non-fenestrated capillaries have endothelium that is permeable to water and small solutes (<3nm), necessitating the transport of larger molecules through transendothelial channels or transcytosis processes. The high selectivity properties of non-fenestrated capillaries form part of the blood brain barrier, where permeability is tightly regulated (Aird, 2007a). Comparatively, fenestrated capillaries are more water and small solute permeable due to the presence of fenestrations (transcellular holes) and small intercellular gaps, but maintain a similar barrier to macromolecules to those of non-fenestrated capillaries (Satchell and Braet, 2009). These capillaries are located where there are large areas of molecular exchange, such as the kidneys and small intestine (Aird, 2007b). Discontinuous capillaries are so named due to interruptions or the absence of a basal lamina. These capillaries are the most permeable, and are found in areas where filtration of larger molecules and cells is required, such as the liver, spleen and bone marrow (Satchell and Braet, 2009).

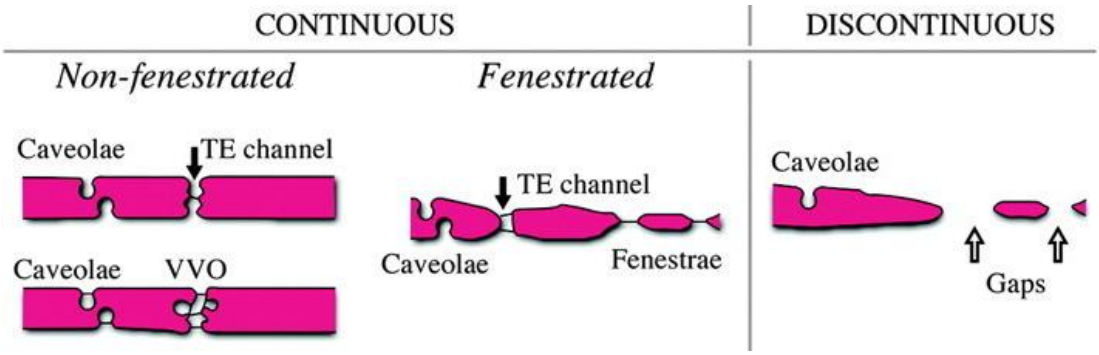

Figure 2. Characteristics of non-fenestrated, fenestrated and discontinuous capillaries. The differences in the basal lamina in each type of capillary is apparent; continuous and regular in non-fenestrated, continuous but more irregular in fenestrated, and interrupted or absent in discontinuous capillaries. Fenestrae in fenestrated capillaries allow for increased filtration without the barrier being permeable to macromolecules. Caveolae are involved in endocytosis and reactions to mechanical stress, and can be present in each type of capillary. Adapted from Aird (2007b).

1.1.2 The endothelium

A layer of ECs lines the entire vascular system (and lymphatic system, largely not discussed in this thesis) – this layer is called the endothelium. Whilst this layer was historically thought to be solely structural and inert, it is now known that the endothelium has many physiological roles, with pathophysiologies associated with endothelial dysfunction. Lymphatic ECs have similar structural and permeability regulation roles as vascular ECs, and are thought to have significant roles in inflammation and immunity (Fujimoto *et al*, 2020). Vascular ECs are known to be involved in inflammatory responses, including leukocyte adhesion and transmigration (Langer and Chavakis, 2009). The vascular endothelium also regulates haemostasis and maintains thromboresistance, and regulates vascular growth, tone, and permeability (Galley and Webster, 2004). Endothelium in different anatomical locations has a specific function owing to the needs of the organ/tissue, for example the differences in permeability described in 1.1.1. This heterogeneity of the endothelium and ECs (that extends to tissue-EC interactions) has led to research looking to characterise EC physiology in different capillary beds, as well as implying that EC research necessitates the use of capillary bed relevant ECs (Jambusaria *et al*, 2020).

1.1.2.1 Leukocyte adhesion to endothelium

Endothelial cells at rest have limited interaction with circulating leukocytes, sequestering leukocyte-interacting proteins such as P-selectin into storage granules, Weibel-Palade bodies and suppressing adhesion molecule transcription (Pober and Sessa, 2007). During inflammation, leukocytes are recruited to activated endothelium and exhibit a characteristic extravasation process that results in their activation and transmigration through the endothelial layer. This process can be broken down into a series of steps, with each step involving a different class of adhesion molecules either on the leukocytes or ECs. Initial leukocyte tethering is mediated through interactions between endothelial E and P-selectin and leukocyte L-selectin and α/β integrins. This tethering slows the speed of the circulating leukocytes and allows them to roll over the endothelium (Barreiro and Sánchez-Madrid, 2009). This

increased leukocyte contact with the endothelium presents leukocytes with endothelial chemokines, resulting in their activation and shift from a rounded to a polarised, pro-migratory morphology. The interaction between leukocytes and endothelial chemokines also leads to the next step: firm adhesion. ECs responding to inflammatory signalling have increased expression of the adhesion molecules intercellular adhesion molecule-1 and vascular cell adhesion molecule-1, which interact with leukocyte molecules lymphocyte function associated antigen-1 and very late antigen-4 (Muller, 2011); ECs expressing these markers are considered 'activated'. After firm adhesion, leukocytes are tightly bound to the endothelium but may migrate short distances to intercellular EC junctions, where most transmigration occurs, or may transmigrate through ECs in a paracellular manner (Langer and Chavakis, 2009).

1.1.2.2 The endothelium in haemostasis

Under normal physiological conditions, platelets circulate through blood vessels without adhering to the endothelium. The endothelium maintains platelets in a resting state by releasing nitric oxide (NO), prostacyclin and by expressing CD39, but also plays a role in platelet aggregation and thrombus formation during haemostasis (Coenen *et al*, 2017).

Following blood vessel damage, ECs (and other cells) are activated, and release tissue factor, which initiates the extrinsic pathway of coagulation. Additionally, the exposure of collagen within damaged vessel walls leads to the activation of the intrinsic coagulation pathway. Weibel-Palade bodies within activated ECs fuse with the plasma membrane and release von Willebrand factor (vWF); this and EC expression of P-selectin mediates initial platelet tethering (Hamilos *et al*, 2018). The platelets then roll and are activated in a similar manner to leukocytes, as described in 1.1.2.1. Their activation is induced by EC expressed disintegrin and metalloproteinase domain-containing protein-15 binding to the platelet glycoprotein IIb/IIIa receptor. The two pathways converge in the final common pathway, where a stable fibrin clot is formed (Yau *et al*, 2015). Activated platelets adhered to the endothelium are also thought to aid leukocyte recruitment and direct them to sites of transmigration (Roissant *et al*, 2018).

1.1.2.3 Endothelial regulation of vascular tone

All blood vessels under basal conditions exhibit vascular tone. This is to say, that vessels are not normally maximally relaxed. The endothelium regulates vascular tone through the release of both vasodilatory or vasoconstrictive factors in response to physical stimuli, hormones and platelet-derived substances (Rajendran *et al*, 2013). Endothelium derived vasodilatory factors include NO, prostacyclin, and endothelium derived hyperpolarising factor (EDHF). Endothelial derived vasoconstriction factors include endothelin-1 (ET-1), angiotensin II (ANG II), and thromboxane A_2 (TXA_2) (Sandoo *et al*, 2010).

Vasodilation

NO is important for the maintenance of basal vasodilator tone and is produced by the enzyme nitric oxide synthase (NOS, or eNOS specifically for endothelial NOS). Inactive eNOS is bound to caveolin, located in the caveolae of the cell membrane. This membrane bound eNOS detaches from caveolin in response to increased levels of intracellular calcium, and is activated. These changes in intracellular calcium levels provide short term regulation of NO production and consequently, vasodilation of the blood vessel. NO production is regulated further by phosphorylation of eNOS by protein kinases, which can be stimulated by shear stress. NO is freely diffusible, and diffuses into vascular smooth muscle cells (VSMCs) and binds to the soluble enzyme guanylyl cyclase, which catalyses the conversion of guanosine triphosphate (GTP) to cyclic guanosine monophosphate, leading to the relaxation of the vascular smooth muscle and therefore the blood vessel. NO also has a role in preventing the adhesion and activation of platelets and leukocytes as described in 1.1.2.1 and 1.1.2.2. When endothelium is damaged, tumour necrosis factor (TNF-α) and interleukin-1 stimulate the production of NO by activating iNOS, a calcium insensitive NOS (Rafikov *et al*, 2011).

Another vasodilator, prostacyclin, is produced by ECs by cyclooxygenase-1 (COX-1) and cyclooxygenase-2 (COX-2). COX-1 is expressed constitutively by ECs, whereas COX-2 is only expressed when there is damage to the endothelium and exposure to inflammatory cytokines. Both are enzymes that convert arachidonic acid (AA) to prostaglandin H_2, which is then converted to prostacyclin by prostacyclin synthase. Prostacyclin binds to receptors on VSMCs, leading to cyclic adenosine monophosphate production and

consequent protein kinase A activation and smooth muscle cell relaxation. Platelets also express prostacyclin receptors which when activated by prostacyclin, inhibit platelet aggregation. Prostacyclin induced vasodilation is inhibited in the presence of NO, but when NO is deficient or blocked, increased vasodilation occurs due to increased synthesis of prostacyclin (Sandoo *et al*, 2010).

If the vasodilatory action of both NO and prostacyclin is inhibited completely, endogenous endothelial vasodilation can still persist. This is due to hyperpolarisation of the endothelium by EDHFs. Exactly which factors cause the hyperpolarisation is site specific and it is thought that this non-NO/prostacyclin regulated vasodilation contributes more to regulation of vascular tone in resistance vessels. Implicated factors include AA derivatives, the epoxyeicosatrienoic acids, hydrogen peroxide, K+ efflux activation of the sodium-potassium pump (Na+/K+-ATPase), C-type natriuretic peptide, and transmission of EC hyperpolarisation to VSMCs via gap junctions (GJs). All factors act by increasing K+ conductance, causing depolarisation of the VSMCs (Ozkor and Quyyumi, 2011).

Vasoconstriction

Endothelial derived ET-1 is considered the most potent endogenous vasoconstrictor. Inflammatory cytokines such as interleukins and TNF-α stimulate ET-1 production and release from ECs. There are two endothelin receptor types, ET_A and ET_B; ET_A is primarily expressed by VSMCs, which also express ET_B. The activation of ET_A by ET-1 results in an increase in the release of sarcoplasmic Ca+ (which induces vascular muscle contraction), as does the activation of the ET_B subtype, ET_{B1} (Kowalczyk *et al*, 2015). Vasoconstrictive effects of ANG II are primarily mediated through G protein-dependent signalling following activation of the ANG II receptor type I expressed on VSMCs. Activated phospholipase C (PLC) produces inositol triphosphate (IP_3) which binds to the sarcoplasmic reticulum, allowing Ca+ efflux driven contraction (Mehta and Griendling, 2007). TXA_2 is a vasoconstrictor that works synergistically with prostacyclin. Whilst prostacyclin is produced from both COX-1 and COX-2, TXA_2 is solely produced by the COX-1 conversion of AA to prostaglandin H_2, from which thromboxane synthase produces TXA_2. The TXA_2 receptor is expressed on both VSMCs and platelets, its activation inducing

muscle contraction by increasing the release of sarcoplasmic Ca+. Activation of the TXA_2 receptor on platelets results in platelet aggregation (Chen, 2018).

1.1.2.4 Endothelial dysfunction

The functions of the endothelium described in 1.1.2.1-3, as well as 1.1.1, demonstrate the homeostatic role of the endothelium; inflammatory processes, platelets, vascular tone and permeability are all under endothelial regulation. A shift in endothelial homeostasis can lead to endothelial dysfunction and pathology. Typically, endothelial dysfunction is associated with reduced vasodilation due to decreased NO, increased inflammation and a pro-thrombotic state. During cardiovascular disease the macrovascular endothelium becomes pro-atherosclerotic due to a loss in leukocyte and platelet regulation (Versari *et al*, 2009). In the microvasculature, a loss of EC barrier function can increase permeability; as described in 1.1.1, permeability across different capillary beds varies and can be highly selective. This damage to the microvasculature is heavily implicated in diabetes, primarily as retinopathy, nephropathy and neuropathy (Shi and Vanhoutte, 2017).

1.2 Endothelial cells

The ‘building blocks’ of the endothelium, ECs, develop during a process called vasculogenesis; endothelial progenitor cells (EPCs) emerge from mesodermal precursors and develop into different subtypes. Transcriptional regulation determines the fate of these cells: erythroblast transformation specific variant 2 transcription factor (expressed transiently), gives rise to cells expressing endothelial growth factor receptor 2 (VEGFR2). These cells become arterial or venous ECs. Prolonged expression of this transcription factor instead drives cells towards a haemogenic fate (Marcelo *et al*, 2013). As mentioned in 1.1.2, ECs display heterogeneity, and it is thought that tissue-specific interactions between ECs and the microenvironment play a role in this during development and postnatal life. Broadly, macrovascular ECs lining larger vessels show distinct phenotypic differences compared with microvascular ECs (the ECs in the microvasculature). ECs also display differences between each capillary bed.

Despite this heterogeneity, there are EC specific characteristics and markers, although morphology can vary (Jambusaria *et al*, 2020).

1.2.1 Endothelial cell morphology

The shape and size of ECs varies depending on their location, although they are typically flat with a central nucleus, and a cell diameter between 10 - 20µm. Some ECs, are tall or cuboidal in shape; notably high endothelial venules – venules specifically adapted for high leukocyte trafficking. Those in pulmonary arteries and veins however, are rectangular and round respectively. The thickness of ECs can also vary, with some capillary ECs being less than 0.1µm, to 1µm thick ECs in the aorta (Aird, 2007a; Aird, 2007b). The shape of ECs can be influenced by shear stress, as haemodynamic forces influence cell polarity and can induce cytoskeletal remodelling. This remodelling is known to be mediated through ras GTPases such as ras homolog family member A (RhoA), ras-related C3 botulinum toxin substrate 1 and cell division control protein 42 homolog (Cdc42) (Tzima, 2006). Shear stress induced EC remodelling can be reproduced *in vitro*, for example cells grown under unidirectional flow (akin to ECs in straight arteries) polarise and elongate parallel to the flow direction. The nuclei of these cells also align to the direction of flow, and the reversibility of this process can be observed in the cells if flow is stopped. Monolayers of ECs display characteristic ‘cobblestone’ morphology, something that is often assessed by eye to quickly identify ECs and approximate their purity *in vitro* (Christiakov *et al*, 2016).

1.2.2 Endothelial cell markers

The presence of Weibel-Palade bodies is considered an ultrastructural marker of ECs. ECs share other markers common to cells originating from the same lineage: haematopoietic cells. However, these markers in context and used in tandem, can be used to identify ECs in labelling and staining techniques. Surface markers are typically used to identify cells for flow cytometry, particularly for fluorescence activated cell sorting (FACS) where viable cells may be desired for culture. The exact expression profile of an EC will depend on the vascular bed and influence of the local microenvironment, contributing to

EC heterogeneity. Despite the range in EC markers, there are constitutively expressed EC markers, which are summarised in table 1.

Marker	Ligands
CD31	CD31
Endoglin (CD105)	Transforming growth factor beta 1 and 3 (TGFβ1 and TGFβ3), in association with the TGFβ receptor type II
vWF	Factor VIII and some platelet glycoproteins
CD34	L-selectin
Angiotensin-converting enzyme (ACE/CD143)	Angiotensin

Table 1. Constitutively expressed endothelial cell markers. These factors are expressed by other cell types; CD31 by leukocytes, CD34 by haematopoietic stem and progenitor cells, and CD105 by chondrocytes, adapted from Ribatti et al (2020).

CD31 is a transmembrane homophilic adhesion protein expressed in intercellular EC junctions, binding to CD31 on adjacent ECs. It is a well-known junctional protein, and is involved in leukocyte transmigration as described in 1.1.2.1. Additionally CD31 is involved in EC migration, a function mediated through its intracellular signalling (Liu and Shi, 2012). Endoglin is also a transmembrane protein. Whilst constitutively expressed, endoglin expression is highly increased on proliferating ECs. The intracellular molecule vWF is normally stored in Weibel-Palade bodies, and its release mediates platelet tethering (see 1.1.2.2). These three markers all play a role in angiogenesis, the formation of new blood vessels from existing vasculature. CD34 is a shared marker with haematopoietic stem and progenitor cells, and ACE is a cell surface protease that converts angiotensin I to the vasoconstrictor angiotensin II (Goncharov *et al*, 2017).

Induced markers of ECs include cell adhesion molecules and selectins, which are expressed during inflammation and haemostasis (1.1.2.1-2). The expression of several receptor tyrosine kinases (RTKs) can be upregulated under certain conditions, notably VEGFR1 and 2, and tyrosine kinase with immunoglobulin-like and EGF-like domains (Tie) 1 and 2 receptors. All these

receptors are associated with angiogenesis and the regulation of EC permeability. Vascular endothelial cadherin (VE-cadherin) expression can also be increased, and is also involved in permeability regulation and angiogenesis. As with the constitutively expressed markers, these markers are not exclusive to ECs but confer EC properties that are used for both EC identification and research (Goncharov *et al*, 2017).

1.2.3 Endothelial cell junctions and transport

ECs are described as ‘gatekeepers’, owing to their function in controlling the passage of proteins and cells through the vascular wall, providing selective separation between interstitial fluid and blood. This regulation of permeability involves two different transport pathways: transcellular and paracellular. The transcellular route involves the movement of molecules through ECs; this is mediated via caveolae vesicles. Paracellular transport is movement between adjacent ECs, involving intercellular junctions. ECs from different capillary beds display heterogeneity in these transport pathways, as well as the molecules transported. It is worth noting that these processes, in particular the paracellular route, are associated with continuous endothelium, where cells are more closely organised than in discontinuous (see section 1.1.1) (Komarova and Malik, 2010).

1.2.3.1 Transcellular transport

The transcellular transport system primarily involves trafficking of albumin by endocytosis; albumin fuses to the plasma membrane in areas enriched with caveolin-1 on the luminal side of ECs. On the abluminal side, vesicles fuse with the plasma membrane and release contents via exocytosis. In addition to albumin, other macromolecules such as albumin-bound ligands and hormones are also transported this way (Komarova and Malik, 2010). ECs in different capillary beds show heterogeneity in the molecules they transport, in identity as well as amount. For example, ECs in the blood brain barrier (BBB) have fewer caveolae and therefore comparatively reduced transcellular transport, compared to continuous ECs in kidney glomeruli. Importantly, heterogeneity in transcellular transport exists in ECs from different vascular beds and contributes

to EC function. This could be essential in most capillaries but potentially pathogenic in larger vessels where the transport of molecules, such as lipids, into vessel walls may be harmful (Fung *et al*, 2017).

1.2.3.2 Paracellular transport: junctions

Paracellular transport occurs between ECs, via inter-endothelial junctions. These can be adherens (AJs), tight (TJs), or gap junctions (GJs). Briefly, AJs and TJs are involved in the adhesion and transmigration of cells, and GJs are the sites where fluid, ions and molecules pass between cells (Komarova and Malik, 2010).

1.2.3.3 Adherens junctions

Adherens junctions have a key role in endothelial permeability, by mediating EC-EC adhesion and transducing intracellular signals from a variety of stimuli. The adhesion is mediated by VE-cadherin, a molecule that binds homophilically, and neural cadherin, as well as others (see figure 3). VE-cadherin binds to β-catenin, and in turn, to cortical actin filaments (Lampugnani, 2010). The destabilisation of AJs can be induced by vascular endothelial growth factor (VEGF) and TNF-α by disrupting the binding of VE-cadherin to β-catenin. The breakdown of AJs increases permeability, disrupts signalling depending on AJ scaffolding, and can result in pathology (Rahimi, 2017). In addition to permeability, VE-cadherin is known to form complexes with VEGFR2 and promote EC stability. Activated VEGFR2 not complexed to VE-cadherin induces proliferation; in this sense, VE-cadherin has a role in the maturation of ECs during angiogenesis (Lampugnani, 2010).

1.2.3.4 Tight junctions

TJs are thought to be the junctions most in control of permeability, and are of particular importance in ECs that maintain highly selective barriers, like the BBB. TJs are composed primarily of claudins, which form homophilic and heterophilic dimerisations that determine the ultimate barrier properties between the ECs (Lampugnani, 2010). Most claudins contain a PDZ-binding domain, allowing them to bind to PDZ-containing proteins such as zona occludens-1 (ZO-1), a scaffolding protein, as shown in figure 3. Junctional adhesion molecules (JAMs) also contain a PDZ domain and these molecules can therefore also bind to ZO-1, and consequently to actin filaments. A particular JAM, JAM-A, is thought to be involved in the regulation of migration as well as barrier function, whilst JAM-C is implicated in tumour associated angiogenesis. Another important component in TJs is occludin, a protein that regulates electrical resistance between epithelial and endothelial cells, as well as regulating actin organisation (Rahimi, 2017).

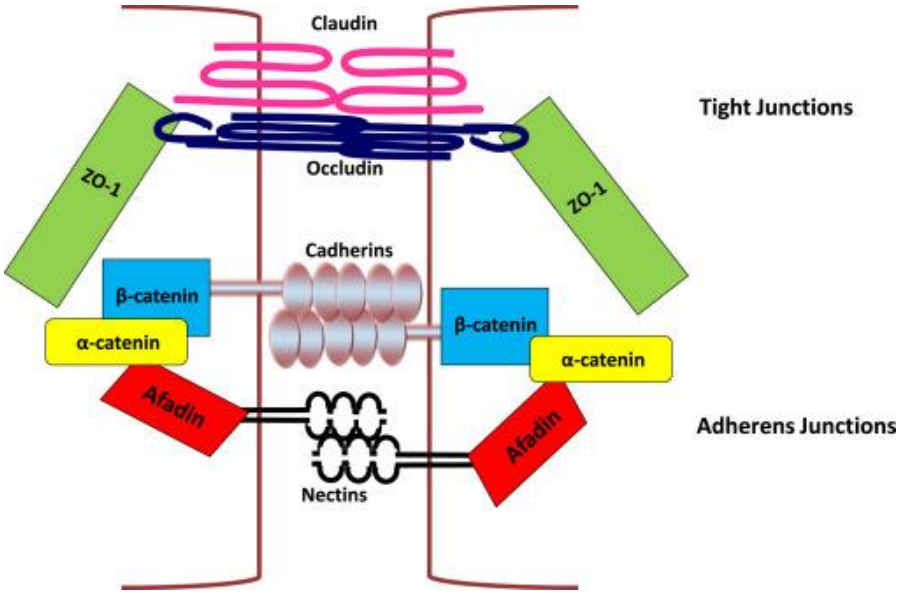

Figure 3. Schematic representation of an adherens and a tight junction. The tight junction is the most apically located of the intercellular junctions, with adherens junctions located immediately beneath. Interplay between the two junction types has been demonstrated, where mutations in tight junctions results in improperly formed adherens junctions. Adapted from Campbell *et al* (2017).

1.2.3.5 Gap junctions

GJs facilitate communication between ECs and cells adjacent to ECs, through structures located at the plasma membrane. Channels in one plasma membrane interact with a matched set of channels in an adjacent cell's plasma membrane, effectively connecting the cytoplasm of the two cells and facilitating communication. These channel structures consist of six connexin proteins that combine to form a hemichannel, as shown in figure 4. These hemichannels allow the transfer of ions, simple sugars, amino acids, nucleotides, and short polypeptides (Márquez-Rosado *et al*, 2012). The localisation of connexins to the plasma membrane, as well as their stability as a GJ component, is regulated by phosphorylation. The connexins forming hemichannels demonstrate heterogeneity depending on the location of ECs, and will therefore allow different movement of substances between cells (Figueroa and Duling, 2009). For example communication via connexin channels is thought to be involved in EDHF induced vasodilation; in the coronary arteries, GJs between ECs and VSMCs are involved in EDHF signalling in response to shear stress (Zhang *et al*, 2016). Studies have shown that GJ function is reduced during inflammation, and that pro-angiogenic signals such as VEGF negatively regulate connexin expression and therefore reduce GJ formation (Okamoto *et al*, 2019).

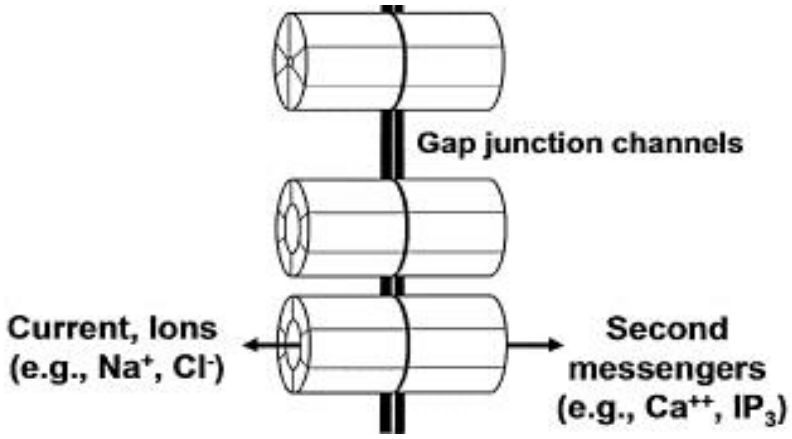

Figure 4. Gap junctions in the plasma membranes of two adjacent cells.
Hemichannels are shown comprising of six connexin subunits, the plasma membranes are depicted by the two black lines. The substances transported by the channels is largely dictated by the connexins, of which 20 different isoforms have been discovered adapted from (Figueroa and Duling, 2009).

1.2.4 Endothelial cell glycocalyx

On the surface of all cells there is a layer of glycans attached to various proteins and lipids: the glycocalyx. Proteins and lipids containing glycans are described as glycosylated. The endothelial glycocalyx (eGCX) lines the luminal surface of all blood vessels, and is primarily composed of proteoglycans, glycoproteins and glycolipids. Proteoglycans contain a core protein and glycosaminoglycan side chains. Collectively, these components form a meshwork structure that is in a dynamic balance between synthesis and degradation (Butler *et al*, 2020). The eGCX is an important regulator of endothelial permeability, tone, and both haemostasis and leukocyte adhesion; important functions of the endothelium as described in sections 1.2.1.1-3. Both the thickness and composition of the eGCX determines its properties, both of which display heterogeneity depending on the vessel location where the local microenvironment influences the eGCX (Uchimido *et al*, 2019). During disease processes, eGCX shedding can occur which can lead to an increase in endothelial inflammation, platelet aggregation, permeability, and a reduction in NO induced vasodilation (Kim *et al*, 2017). The eGCX also facilitates the binding of ligands and enzymes, and therefore has a role in regulating cell signalling; altered eGCX composition is associated with disease, and it has been shown that certain cancer cells can induce changes to the glycocalyx (Li *et al*, 2019).

1.2.5 Endothelial cell activation

As discussed earlier, ECs are considered activated after they express adhesion molecules in leukocyte tethering (see 1.1.2.1), and when they initiate haemostasis pathways (see 1.1.2.2). Although it is clear that ECs are involved in many regulatory processes, the change in their physiology during these contexts denotes their activated state. This activation to a response from the local microenvironment again, demonstrates heterogeneity. Moreover, ECs are typically quiescent in terms of proliferation. This can change during both physiological and pathological processes, and also requires the activation of ECs, which can lead to the initiation of angiogenesis (Liao, 2013). Angiogenesis is the formation of new blood vessels from existing vasculature. The process is normally inhibited through a molecular balance of anti and pro-angiogenic molecules, but the balance is tipped to a pro-angiogenic state when ECs are

activated, and both tethered leukocytes and platelets can release pro-angiogenic factors. This is termed ‘the angiogenic switch’, and is considered a hallmark in cancer development. Distant metastases can remain dormant as micrometastases (clusters of cancer cells between 0.2 - 2mm^3) for many years. In order to develop into bigger tumours beyond 2mm^3 (macrometastases), tumours must induce angiogenesis in order to obtain a blood supply (Ribatti *et al*, 2007). Angiogenesis is not always pathological however, as it is a part of wound healing and growth. The quiescent nature of adult ECs has posed a problem in *in vitro* research, as common ECs used in culture such as human umbilical vein endothelial cells (HUVECs) are foetal in origin, and are proliferative. This therefore complicates the study of the angiogenic switch as HUVECs are in this sense, already activated (Staton *et al*, 2009). There are also different types of angiogenesis, which warrants further consideration.

1.3 Angiogenesis

Angiogenesis is the formation of new blood vessels from pre-existing blood vessels. This differs from vasculogenesis, which is the formation of blood vessels during embryogenesis. The latter involves the differentiation of endothelial progenitor cells into ECs, although it is now believed that this is not exclusive to development; circulating endothelial progenitor cells have been identified and thought to be incorporated into new vessels during angiogenesis (Martin-Padura and Bertolini, 2009). ECs in adults are typically quiescent, except in certain physiological conditions such as endometrial regeneration during the menstruation cycle, during pregnancy in the placenta, and during wound healing. Angiogenesis also occurs during growth. The activation of angiogenesis requires the balance of anti and pro-angiogenic factors to be disrupted in favour of the pro-angiogenics. As discussed in 1.2.5, this is called the angiogenic switch. Anti and pro-angiogenic factors are produced by various cells within the local microenvironment in addition to ECs themselves. The aberrant activation of angiogenesis can be pathogenic, as observed in diabetic retinopathy and the development of tumours. There are two types of angiogenesis: sprouting and intussusceptive (Vailhé *et al*, 2001).

1.3.1 The angiogenic switch: anti and pro-angiogenic factors

As described in 1.2.5, ECs are typically quiescent due to a balance of anti and pro-angiogenic factors. Changes in the local microenvironment can lead to an increase in pro-angiogenic factors, leading to the angiogenic switch, and EC proliferation, migration and differentiation. After EC activation, EC intercellular junctions, as well as EC contact with supporting pericytes and VSMCs, start to breakdown. This disassembly and basement membrane degradation increases vascular permeability and allows fibrin deposition in the extra-vascular space. This provides a pathway for activated ECs to migrate along, and move towards pro-angiogenic signals (Bouïs *et al*, 2006). Anti and pro-angiogenic factors promoting EC proliferation and migration are summarised in table 2. These factors confer their activity by interacting with receptors on ECs, including receptor tyrosine kinases (RTKs). Both pro-angiogenic factors and their associated RTKs have been the target of anti-angiogenic therapies in diseases of aberrant angiogenesis (see section 1.6.3). ECs eventually form a lumen by aligning with other cells to form a neo-vessel. Once this stage is reached, the migration and proliferation of ECs must be inhibited, and a new basement membrane is formed. Supporting cells (pericytes, VSMCs) are recruited, and intercellular junctions (as described in 1.2.3) are formed between adjacent ECs.

Pro-angiogenic factors	Anti-angiogenic factors
*VEGF	*VEGF
*Basic fibroblast growth factor (bFGF)	Thrombospondins (TSPs)
*Epidermal growth factor (EGF)	Interferon(s)-α/β/γ
*Platelet-derived growth factor (PDGF)	Interleukin(s)-4/12/18
*Angiopoietin-1 (Ang-1)	Troponin-1
*Angiopoietin-2 (Ang-2)	*Angiopoietin-2 (Ang-2)
*Ephrins	Angiostatin
Angiogenin	Platelet factor-4
*Hepatocyte growth factor (HGF)	Endostatin
Thymidine phosphorylase	Tissue inhibitor of metalloproteinases (TIMPs)
Neuropeptide Y	
TNF-α	

Table 2. Examples of anti and pro-angiogenic factors in endothelial cell proliferation and migration. The balance, or imbalance of these factors, regulates the angiogenic state of ECs. Factors are secreted from cells in the microenvironment or other endothelial cells, * denotes factors that activate receptor tyrosine kinases. Note the pro and anti-angiogenic activity of VEGF and Ang-2; the angiogenic effect of some molecules is context dependent. Information taken from Bouïs et al (2006) and Burrell and Zadeh (2012).

Of the pro-angiogenic RTK ligands shown in table 2, the VEGF receptors and Tie receptors (the receptors for angiopoietins) are almost exclusively expressed on ECs (including lymphatic ECs). VEGF, namely VEGF-A, is described as the most potent pro-angiogenic factor due to its influence on extracellular matrix (ECM) degradation, tube formation, and increasing vessel permeability. The pro or anti-angiogenic effect of VEGF-A is determined by alternative splicing; the VEGF-A_{165} isoforms are pro-angiogenic, whereas the VEGF-A_{165}b isoform is anti-angiogenic (Harper and Bates, 2008). Going forward, this thesis uses the term 'VEGF' to refer to the pro-angiogenic isoform, VEGF-A_{165}, unless stated otherwise. Increasing vessel permeability initially drives angiogenic signalling but must be inhibited in mature vessels (Bates *et al*, 2002). In addition to promoting EC proliferation and migration signalling, pro-angiogenic signalling

increases the stability of neo-vessels, for example, PDGF signalling stabilises interactions between ECs and supporting cells. Ang-1 is also involved in neo-vessel stabilisation, as well as supporting cell recruitment and EC survival (Jeltsch *et al*, 2013). Angiogenin induces angiogenesis by activating signal pathways extracellularly, but also translocates to the nucleus and increases the expression of pro-survival proteins in ECs (Sheng and Xu, 2016). Other signalling regulates the identity of the ECs, for example ephrin-B2 expression drives an arterial fate, whereas ephrin-B4 expression results in a venous EC cell fate (Rudno-Rudzińska *et al*, 2017).

Physiological angiogenesis necessitates the degradation of the basement membrane and remodelling of the ECM in order to allow the migration of ECs and resultant neo-vessel establishment. This involves a variety of enzymatic processes from fibrinolytic and proteolytic systems, as well as certain factors involved in coagulation. Haemostasis and angiogenesis are interlinked processes that under physiological conditions, are under strict control. Angiogenesis must be prevented until after successful coagulation as neo-vessels are initially leaky and unstable and would therefore lead to excessive bleeding if grown prematurely (see table 2, where TSPs are anti-angiogenic). Pro-angiogenic factors involved in coagulation and ECM/basement membrane degradation in angiogenesis are shown in figure 5 (Hadjipanayi *et al*, 2015). Other processes that contribute to EC/basement membrane degradation are fibrinolysis, which involves serine proteases in the plasminogen activator-plasmin system, and proteolytic enzymes, including the matrix metalloproteinases (MMPs) (see figure 5). Collectively, these molecules are also required for capillary lumen formation (Pepper, 2001).

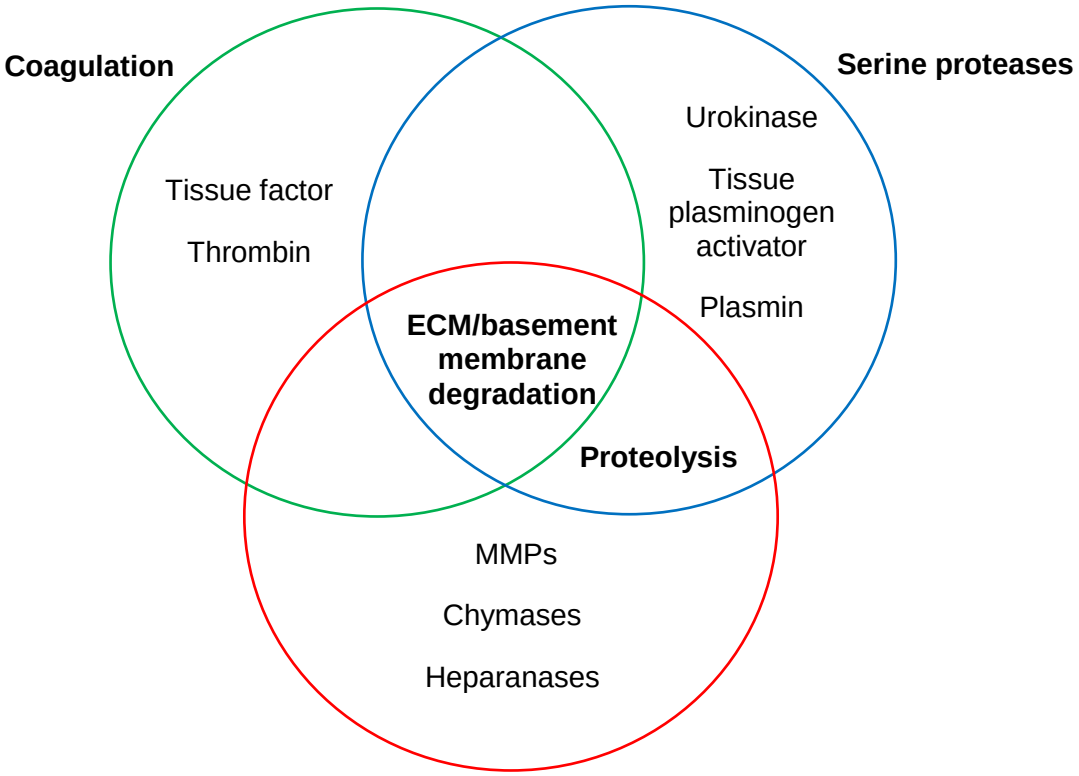

Figure 5. The source of molecules involved in the degradation of the extracellular matrix/basement membrane during angiogenesis. Molecules from the coagulation cascade are shown in the green circle, serine proteases from the fibrinolytic process in the blue, and proteolytic enzymes in the red. Information from Bouïs *et al* (2006).

The primary anti-angiogenic factors are the TSPs, angiostatin, and endostatin. It is not clear exactly how these factors act but it is thought to be a combination of inhibiting pro-angiogenic signals, inducing EC apoptosis, and inhibiting cell cycle progression (Huang and Bao, 2004; Kazerounian and Lawler, 2018). Anti-angiogenic molecules can antagonise the effects of pro-angiogenic molecules; Ang-2 directly antagonises Ang-1 by binding to Tie-2 but only weakly activating it. Moreover, without the presence of VEGF, Ang-2 induced activation of Tie-2 leads to EC death. However, when Ang-2 is present in higher levels, such as in the tumour microenvironment, the activation of Tie-2 is stronger and promotes angiogenesis. Cytokines such as interferons and interleukins can inhibit angiogenesis by preventing the release of growth factors from cells in the microenvironment (Jeltsch *et al*, 2013). ECM/basement membrane degradation molecules have been implicated in the generation of anti-angiogenic proteins such as angiostatin and endostatin, suggesting a regulatory mechanism. MMP activity is also regulated by TIMPs (see table 2), in a 1:1 ratio of molar stoichiometry. Therefore the correct balance of MMPs:TIMPs is essential for

appropriate ECM/basement membrane remodelling (Pepper, 2001). Another receptor for VEGF, VEGFR1 can suppress the pro-angiogenic signalling of VEGF-VEGFR2, by binding VEGF; VEGFR1 has a higher affinity for VEGF, but is only activated very weakly. This sequestration effectively nullifies potential VEGF pro-angiogenic signalling (Kowanetz and Ferrara, 2006).

1.3.2 Sprouting and intussusceptive angiogenesis

The most well-known form of angiogenesis is sprouting angiogenesis. Briefly, this consists initially of the enzymatic degradation of the surrounding ECM and the capillary basement membrane. This leads to increased vascular permeability and extravascular fibrin deposition, followed by the proliferation and migration of ECs towards pro-angiogenic signals. ECs also extend long filopodia (a sprout), that will join other EC sprouts, and hollow out to form the lumen of the new capillary. The filopodia secrete proteolytic enzymes which digest through the ECM and pave a way for the new capillary. Cells at the front of the sprout are called tip cells, and these are areas where there is a lot of VEGFR2 expression. Tip cells are initially selected for by imbalanced expression of delta-like ligand 4 (DLL4) and Notch signalling between adjacent ECs. These cells show increased DLL4 expression in response to VEGF, and this induces lateral inhibition in neighbouring cells. These adjacent cells then upregulate Notch which inhibits the expression of VEGFR2, as shown in figure 6. This allows the sprout to undergo guided growth towards higher concentrations of VEGF, led by the VEGFR2 expressing tip cells. The elongation of the sprout is achieved through EC proliferation; these are described as stalk cells (Santos-Oliveira *et al*, 2015). Sprouts develop vacuoles that coalesce to form the lumen, which becomes continuous with another sprout when the tips converge, typically at the source of the VEGF. This neo-vessel is remodelled and then stabilised by the recruitment of pericytes, becoming a mature capillary. Angiogenesis will cease when pro-angiogenic signals, namely VEGF, return to normal levels. EC proliferation and migration stops, the basement membrane is established, ECM is rebuilt, and EC junctions form (Pepper, 2001). Cells inducing pro-angiogenic factors from blood vessels will often be in areas of hypoxia, which drives the expression of hypoxia-inducible factors (HIFs) such as HIF-1α. This transcription factor upregulates the

expression of pro-angiogenic molecules such as VEGF (Zimna and Kurpisz, 2015).

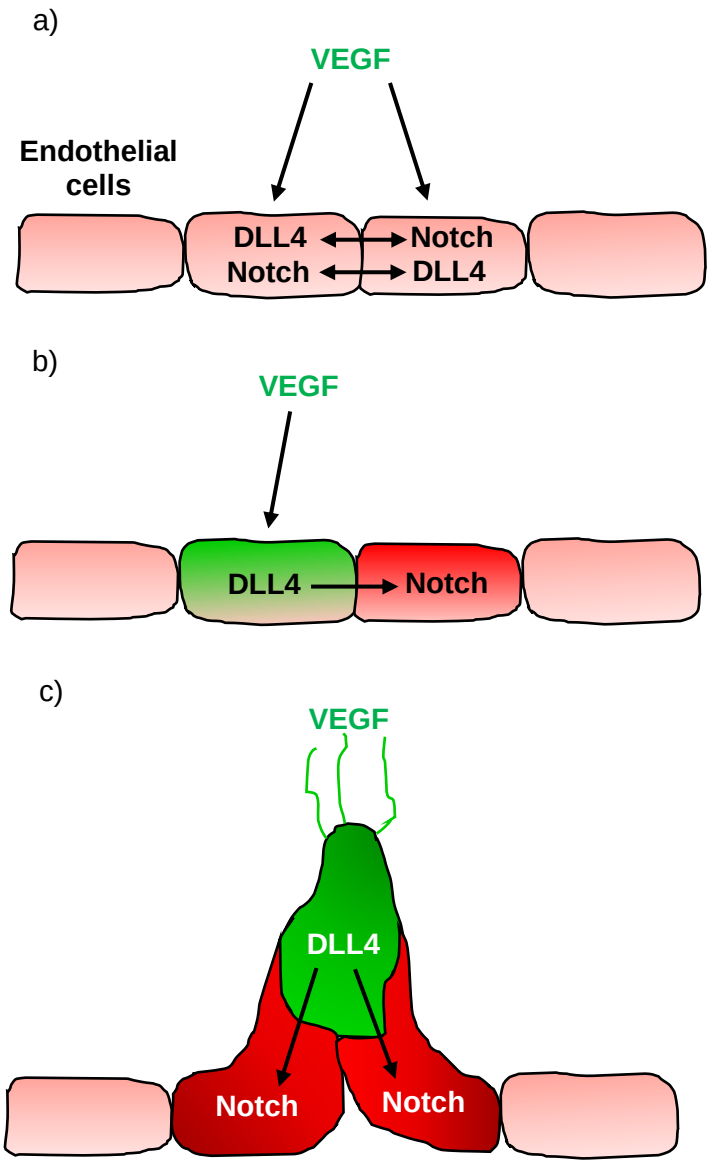

Figure 6. The selection of tip cells in sprouting angiogenesis by VEGF, DLL4 and Notch signalling. a) Shows the initial balanced signalling between DLL4 and Notch, before an increase in DLL4 in cells destined to be tip cells and lateral inhibition of adjacent cells by an increase in VEGFR2 expression which in turn downregulates Notch (b). In c), the tip cells can be seen migrating towards the source of VEGF (information from Santos-Oliveira *et al*, 2015).

Intussusceptive angiogenesis differs from sprouting in several ways, and is thought to be more involved in the remodelling of blood vessels. Rather than a sprout forming from a vessel wall, ECs on opposite sides of a lumen make contact with one another – in effect, sprouting in towards the luminal space, forming a transluminal bridge. This forms a structure called an intraluminal pillar that invading pericytes and fibroblasts cover. The intraluminal pillars increase in diameter and eventually separate into two separate vessels, as shown in figure 7 (Hillen and Griffioen, 2007).

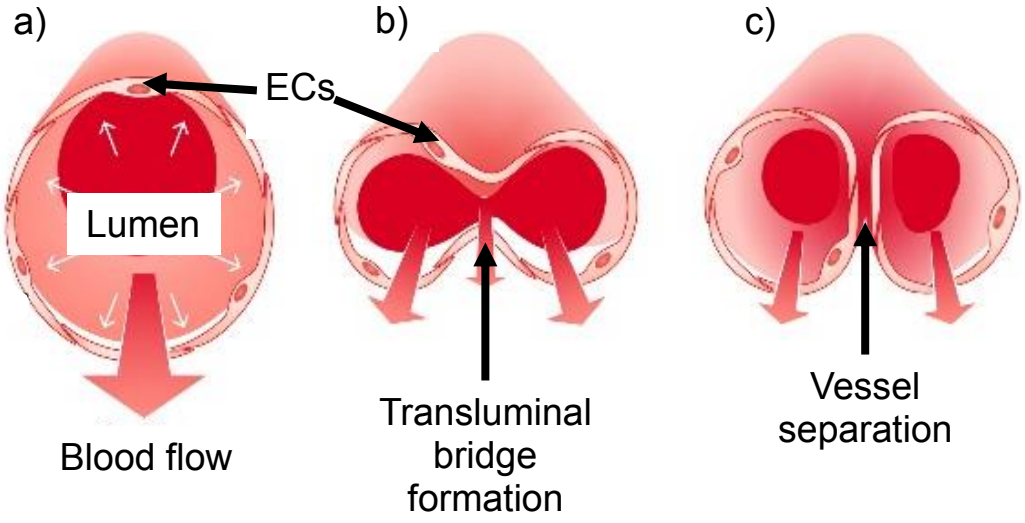

Figure 7. Representation of intussusceptive angiogenesis. a) Shows a capillary where the endothelial cells (ECs) are quiescent. In b) the ECs are moving in to the luminal space, where they form a transluminal bridge that will form the intraluminal pillar. In c) the vessel in shown to have split into two vessels (adapted from D'Amico *et al*, 2020).

1.3.3 Pathological angiogenesis

As discussed earlier in 1.3, ECs are normally quiescent and therefore, not undergoing angiogenesis. Pathological angiogenesis normally refers to the improper activation of angiogenesis, and is typically associated with the growth of improperly functional vessels. This is well documented in cancers, where tumours send pro-angiogenic signals out into the microenvironment in order to acquire a blood supply. This is also observed in diabetes complications such as diabetic retinopathy, nephropathy and neuropathy. There is also an association of pathological angiogenesis in several inflammatory autoimmune diseases such as rheumatoid arthritis and psoriasis (Elshabrawy *et al*, 2015). On the

other hand, impaired angiogenesis has been observed in other autoimmune diseases such as systemic sclerosis and is often seen as a result of aging (Cantatore *et al*, 2017).

1.3.3.1 Impaired angiogenesis

As we age, the ability of ECs to undergo angiogenesis is reduced. This is a problem as the elderly are at more risk of ischaemic injuries, where angiogenesis is required for proper healing. This has largely been attributed to a reduction in NO and resultant endothelial dysfunction; in aged ECs, increased levels of reactive oxygen species (ROS) decrease the availability of NO. The production of NO by eNOS is also reduced. NO has been implicated in the regulation of telomeres, with reductions in NO availability suggested to be a major contributor to EC senescence. Senescent ECs do not proliferate, but it is important to note the capability of ECs in the elderly to undergo angiogenesis, for example in tumour angiogenesis (Lähteenvuo and Rosenzweig, 2012; Ungvari *et al*, 2018). Systemic sclerosis (SSc) is an autoimmune disease where there is excessive collagen production, causing fibrosis and vascular injury; SSc is associated with impaired angiogenesis and therefore recovery from vascular injury is less efficient. Interestingly, high levels of VEGF have been reported in SSc patients, and it is now thought that this might be high levels of the anti-angiogenic VEGF-A_{165}b splice variant. Anti-angiogenic factors such as endostatin and angiostatin have also been shown to be upregulated, but there is evidence for a reduction in the expression of their receptors, reducing their contribution to the anti/pro-angiogenic balance (Manetti *et al*, 2011; Cantatore *et al*, 2017).

1.3.3.2 Pathological activation of angiogenesis

Rheumatoid arthritis

RA is an autoimmune disease where the lining of the joints, the synovium, is targeted by the immune system. Excessive leukocyte recruitment to inflamed joints induces angiogenesis in order to provide oxygen to joints as they become hypertrophic. Macrophages in the joints produce pro-inflammatory cytokines that stimulate the synovial tissue fibroblasts, which in turn go on to produce pro-

angiogenic factors such as VEGF, bFGF and interleukins (Elshabrawy *et al*, 2015).

Psoriasis

Psoriasis is an autoimmune disease characterised by raised areas of skin that can be red, scaly and have erythematous plaques. These skin lesions and plaques exhibit highly abnormal histopathology, with the dermis infiltrated by tortuous capillaries. Furthermore, these capillaries consist of activated ECs that express adhesion molecules promoting leukocyte recruitment. This results in further inflammation. Initially, surrounding keratinocytes are thought to secrete pro-angiogenic factors such as VEGF and Ang-1/2. After leukocytes reach the lesions they also contribute to pro-angiogenic signalling by releasing TNF-α (Chua and Arbiser, 2009).

Diabetes

Diabetes can result in severe pathological alterations to the microvasculature across multiple organs and tissues, and is also associated with macrovascular pathologies. In the retina, vascular changes lead to ischaemia which in turn triggers aberrant angiogenesis. These new blood vessels form improperly and are leaky and fragile due to the absence of TJs, causing the leakage of both inflammatory and pro-angiogenic factors from retinal vessels to the vitreous body (Abcouwer, 2013). Additionally, pathological angiogenesis has been observed in the kidney; the formation of abnormal vessels is associated with glomerular hypertrophy in diabetic nephropathy (Maeshima and Makino, 2010). These abnormally long and numerous capillaries possess thin basement membranes which result in increased permeability. It is thought that glomerular hypertension and NO deficiency, as well as increased VEGF expression drives this angiogenesis; studies blocking VEGF have shown attenuation of angiogenesis in the kidney (Nakagawa *et al*, 2009). There is also a role for pathological angiogenesis in diabetic neuropathy, despite the ability of hyperglycaemia alone to cause nerve dysfunction. The exact mechanisms of angiogenesis induced neuropathy are unclear, but the restoration of angiogenic activity in blood vessels supplying nerves has been observed (Fadini *et al*, 2019).

Cancer development

Tumour vascularisation is associated with poorer prognosis. Dormant or small (<2mm^3) tumours can remain unchanged for years and normally do not cause symptoms. This phase is called the avascular phase. Larger tumours generate symptoms and are more likely to become a serious health risk (Hanahan and Weinberg, 2011). Tumour cells can secrete a variety of different pro-angiogenic factors themselves, as well as influence other cells in the microenvironment to contribute to disrupting the anti/pro-angiogenic balance. There are multiple methods of angiogenesis through which a growing tumour can become vascularised in addition to sprouting and intussusceptive angiogenesis as described in section 1.3.2. These include co-option, EC progenitor recruitment, vasculogenic mimicry, the trans-differentiation of cancer stem cells, and mosaic vessels (Lugano *et al*, 2020).

Co-option essentially bypasses the need for tumour cells to induce angiogenesis; this is where tumours instead grow by using the pre-existing vessels from surrounding tissues. This occurs when tumour cells infiltrate and grow in the spaces between established vessels, and ultimately are in close enough proximity of a blood supply. Therefore this process is strictly speaking, non-angiogenic (Kuczynski *et al*, 2019). This process is notable in the early development of glioblastomas and interestingly, ECs in co-opted vessels show increased Tie-2 expression and Ang-2 synthesis, leading to a reduction in vessel number through methods described in 1.3.1. This results in hypoxia which then drives VEGF expression and induces angiogenesis (Auguste *et al*, 2005).

Vasculogenesis, the process of blood vessel formation in the embryo (described in 1.2) is also found in adults under certain circumstances, including in the development of cancer. This method of tumour vascularisation is again, not definable as angiogenesis as this concerns the development of new blood vessels from endothelial progenitor cells (EPCs) and not from pre-existing vessels. The EPCs mature into ECs and create sites of neovascularisation (see figure 8); this is mediated through the secretion of VEGF from tumour cells acting on VEGFR2 expressing EPCs (Kuczynski *et al*, 2019).

Vascular (or vasculogenic) mimicry is an interesting phenomenon where rapidly growing tumour cells can form vessel like structures in order to meet their oxygen and nutrient demands, see figure 8. Fast growing tumours are associated with hypoxia; as discussed previously, this can drive angiogenesis through HIF-1α and a resultant increase in VEGF expression, but tumour hypoxia is also thought to be an initiator of vascular mimicry. The hypoxia can induce VE-cadherin expression of tumour cells, thereby promoting the vascular mimicry phenotype of cell adhesion and allow tumour cells to form ‘vessels’. Moreover, tumour VE-cadherin phosphorylation and internalisation is associated with increased permeability, which can allow for further extravasation of tumour cells into the growing tumour (Fernández-Cortés *et al*, 2019).

The trans-differentiation of cancer stem cells into ECs is another mechanism of tumour angiogenesis. The resultant ECs (see figure 8), and sometimes VSMCs, express markers of the associated cell type, and may also harbour somatic mutations similar to the original tumour cells (Chen and Wu, 2016). The differentiation of cancer stem cells into ECs appears to be driven by Notch, but not VEGF. The extent of cancer stem cell involvement in tumour angiogenesis is likely dependent on the tumour type, but the VEGF independence of the process is one possible reason why anti-VEGF therapies are not very efficient (Huang *et al*, 2015).

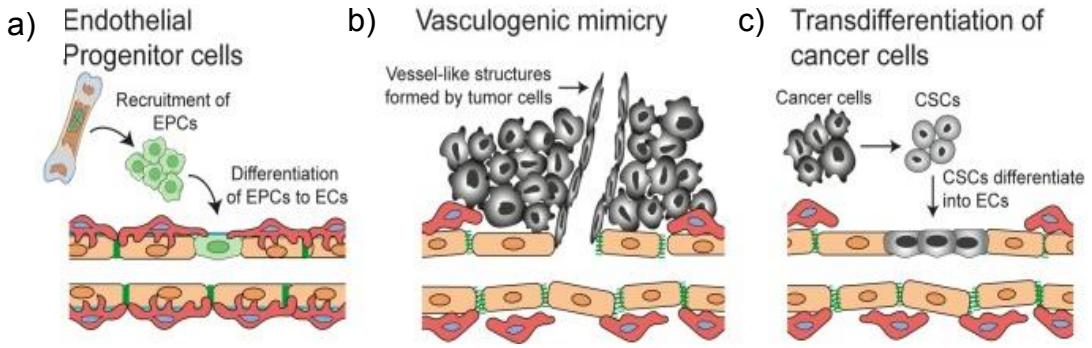

Figure 8. The endothelial progenitor cell, vascular mimicry, and trans-differentiation of cancer cells models of tumour angiogenesis. In a) endothelial progenitor cells (EPCs) from bone marrow are shown travelling to a vessel, before differentiating into endothelial cells (ECs) and becoming incorporated into the growing vessel. The development of a vessel like structure consisting of tumour cells in shown in b), where tumour cells show vascular mimicry to try and reach oxygen demands. The trans-differentiation of cancer stem cells into ECs in c) is mechanistically similar to a) except the ECs are derived from cancer stem cells and can share the same somatic mutations as the original cancer (adapted from Lugano *et al*, 2020).

Tumour cells have also been shown to sometimes infiltrate the wall of tumour associated vessels. Here, the tumour cells form the luminal surface in conjunction with ECs; essentially, tumour cells have become some of the building blocks of the vessel. This gives the tumour cells direct contact with the lumen in order to intravasate and spread into the circulation. The exact proportion of tumour cells can have implications on vessel function, and it is thought that these vessels are likely to be leaky and therefore problematic (Chang *et al*, 2000). Tumour angiogenesis is known to produce improperly formed vessels and can further affect the microenvironment and tumour development.

1.3.3.3 Features of tumour associated blood vessels

This discussion of tumour angiogenesis so far has not directly addressed the quality of the blood vessels formed. Tumour associated blood vessels are not well formed and have different morphological features to physiological vessels. As a result of this, despite increases in various pro-angiogenic factors in the

microenvironment, tumour hypoxia is commonly observed in fast growing cancers as neo-vessels cannot keep up with the oxygen and nutrient demand. This can lead to a necrotic tumour core, which is linked with a poor prognosis (Bredholt *et al*, 2015). Tumour vessels are tortuous and leaky, often have irregularities in their diameter and have thin vessel walls. There is also a deficiency in pericyte recruitment. Increased permeability leads to the release of more tumour secreted pro-angiogenic factors into the microenvironment, stimulating more aberrant angiogenesis. Since tumour cells also shed into the circulation, blood vessels near developing tumours can lead to haematogenous metastasis (Ruoslahti, 2002).

The ability of tumour cells to induce angiogenesis from their microenvironment varies depending on the type of tumour cells, and the microenvironment in which they are in, if they have metastasised. This concept of 'seed and soil', formed in the 19th century, still holds truth today (Langley and Fidler, 2011). This thesis focuses on epithelial ovarian cancer metastasis (the seeds) to the omentum (the soil), where tumour induced angiogenesis is very readily observed.

1.4 Epithelial ovarian cancer

Epithelial ovarian cancer (EOC) is the fifth most common cancer amongst women, the most lethal gynaecological cancer, and is responsible for approximately 4,500 deaths a year in the UK. The ovaries are located within the pelvic cavity, and are in close proximity with important anatomical structures (see figure 9), such as the colon, bladder, and peritoneum, which are common locations of local metastasis (Doufekas and Olaitan, 2014). The peritoneum is a thin membranous layer that lines the peritoneal and abdominal cavities. The peritoneal cavity is a potential space that exists between the pelvic/abdominal walls and the layers of peritoneum that cover the internal organs. In EOC, this space can become enlarged due to the presence of ascites, a pathological increase in the amount of peritoneal fluid typically present in this space. Disseminated cancer cells present in ascites can spread to more distant organs, such as the omentum (Swisher *et al*, 2016).

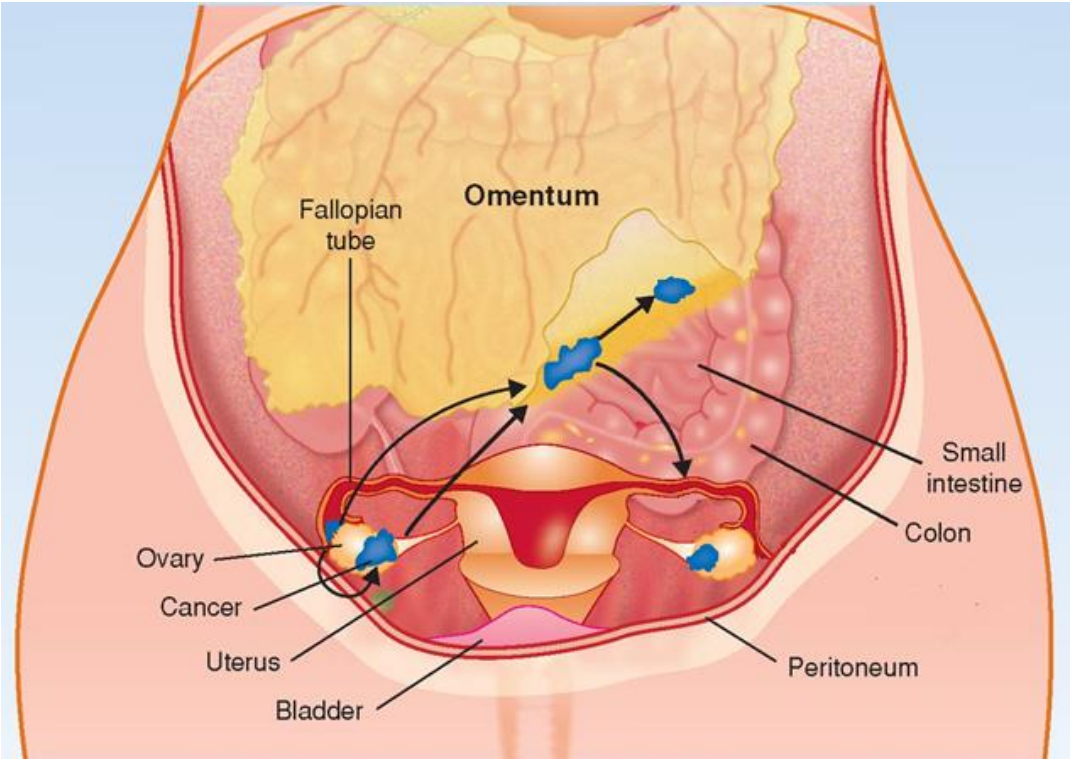

Figure 9. The location of ovaries within the body, and common sites of epithelial ovarian cancer (EOC) metastasis. EOC originates from the ovaries (or other closely related and situated tissues), and metastasises locally to the colon, bladder and peritoneum. The peritoneal cavity is shown as the area lined by the layer of peritoneum. Excess fluid here (ascites) is often present in advanced cases of EOC and can contain disseminated cancer cells. These cancer cells can metastasise to organs such as the omentum. Adapted from Swisher *et al* (2016).

EOC can be divided into serous, endometrioid, clear cell and mucinous subtypes. Endometrial cancer has a higher incidence rate but a lower mortality rate. Due to often vague symptoms that present late and a lack of effective screening tools, diagnosis often unfortunately occurs when the disease has already progressed and metastasised (Doufekas and Olaitan, 2014). Most women are diagnosed with advanced disease of high-grade serous type (the mean age at diagnosis is 62) (Neesham *et al*, 2020). This consequently limits the success of treatment. The most effective treatment is surgical cytoreduction followed by adjuvant chemotherapy, but even this has limited efficacy due to the often late diagnoses, and the overall five year survival rate remains at approximately 45% (Kuroki and Guntupalli, 2020). For high-grade serious type, the five year survival rate is 20 - 30% (Neesham *et al*, 2020). Effective treatments for EOC are therefore a research area of great interest.

1.4.1 Risk factors

The aetiology of EOC is uncertain and appears to be influenced by a multitude of factors. There appears to be some geographical influence, as there is an increased incidence in Northern and Western Europe, as well as North America. However the disease does occur in every geographical location. Interestingly, instances of other ovarian cancers such as germ cell ovarian cancers do not exhibit this geographical variance, suggesting that there are other risk factors involved in EOC (Bray *et al*, 2018), which will be discussed further.

1.4.1.1 Hereditary factors

Individuals with a first degree relative with EOC have a 2 - 5 fold increased risk of developing EOC compared to the risk in the general population. This risk appears to increase when there are additional first degree relatives with EOC (Soegaard *et al*, 2009). Overall, it is estimated that between 10 and 20% of EOC can be attributed to hereditary conditions (Daniilidis and Karagiannis, 2007; Lynch *et al*, 2009). The most common of these are mutations in the breast cancer type 1 and 2 susceptibility proteins (BRCA1 and BRCA2) which are thought to occur in about 65 - 90% of hereditary cases of EOC (Daniilidis and Karagiannis, 2007; Lynch *et al*, 2009). BRCA1 and BRCA2 are structurally

different proteins, but are both tumour suppressor genes involved in the repair of double stranded DNA breaks. Several different mutations can affect the expression and function of these proteins, reducing their capability to repair DNA and therefore increasing the risk of mutations that can lead to the development of cancer. Cancers as a result of BRCA mutations show high penetrance and are inherited in an autosomal dominant manner (Roy *et al*, 2011). However, not all people with BRCA gene mutations will develop EOC, and equally, BRCA mutations do not account for all cases of hereditary EOC. The mismatch repair gene mutations associated with hereditary nonpolyposis colorectal cancer families are also thought to confer an increased EOC risk of between 9 - 12% (Daniilidis and Karagiannis, 2007; Lynch *et al*, 2009). In Li-Fraumeni syndrome, p53 mutations result in an increased likelihood of developing several types of cancers. Whilst this is implicated in some cases of hereditary EOC, the exact mechanism of disease development is less understood due to the rarity of this syndrome. Therefore the contribution of Li-Fraumeni syndrome to hereditary EOC cases is likely very small (Toss *et al*, 2015).

An interesting but less researched genetic risk factor, is that of a greater genetic propensity to being taller. This link was based primarily on observational studies, until a study by Dixen-Suen *et al* (2018) used a Mendelian randomisation to study association between 609 single nucleotide polymorphisms associated with height and EOC. The study found a modest positive association between height and increased risk of developing EOC, reporting a 7 - 8% increase in risk per 5cm in height. It has been suggested that an increased exposure to growth hormones in taller women is responsible for the increased risk (Rodriguez *et al*, 2002).

1.4.1.2 Hormonal factors

There is evidence that various hormonal related factors influence the risk of developing EOC, namely the exposure to oestrogen and progesterone. There appears to be a link between the number of menstrual cycles experienced, where fewer reduces the risk. An earlier age at menarche, and late age of menopause have demonstrated this, as both are associated with an increased risk. The increased risk of longer menstrual life is however, modest (Schildkraut

et al, 2001). Interestingly the reduction in ovulation, both with oral contraceptives and through pregnancies, is associated with a lower EOC risk. The use of oral contraceptives reduces risk and the effect becomes apparent within a few months of use, with longer use further decreasing the risk. The risk reduction is also thought to last for over thirty years after oral contraceptive use has ceased (Fathalla, 2013). Additionally, there is a potential link between taking hormone replacement therapy and the risk of EOC, although the risk of short-term use during menopause as opposed to longer use has shown to bear less risk (Beral *et al*, 2007). This effect is termed 'the incessant ovulation' hypothesis, where it is proposed that inflammatory events during ovulation traumatises the ovarian surface epithelium (OSE) and subjects it to repeated oxidative stress, resulting in DNA damage and potentially the development of EOC (Fleming *et al*, 2006). Another hypothesis, 'the gonadotrophin' hypothesis proposes that excessive exposure to the gonadotrophin hormones, follicle stimulating hormone and luteinising hormone, increases the risk of developing EOC. The risk associated with gonadotrophins is thought to be cumulative with age, with a peak at menopause. The mechanism is thought to be direct, by stimulating the OSE to be transformative, or indirect, by stimulating oestrogen production (Fleming *et al*, 2006). Many EOCs express gonadotrophin receptors and can also be influenced to grow by gonadotrophins (Choi *et al*, 2007). Both the incessant ovulation and gonadotrophin theories are supported by evidence showing that breastfeeding decreases the risk of developing EOC; lactation suppresses the release of gonadotrophins, and the release of oestrogen (Reid *et al*, 2017).

1.4.1.3 Lifestyle factors

The effect of diet on EOC risk is still not completely clear, with proposed mechanisms associating certain foods with antioxidant activity, or having an effect on hormone levels. However, it is generally accepted that risk is reduced in diets high in fibre and phytochemicals, and less red meat. An increased frequency of EOC cases in diabetes type 2 patients still warrants further study, but it is thought that this may be related to diet (Han *et al*, 2014; Plagens-Rotman *et al*, 2018). The role of obesity and EOC risk has been studied extensively but findings remain inconsistent, with any link seemingly small and

concerning an increased risk of obesity leading to the development of certain lower grade types of EOC (Tworoger and Huang, 2016). A possible explanation for this increased risk could be due increased leptin in obese patients. Leptin is an adipokine implicated in the increased inflammation of the endometrium, and is thought to at least be partially responsible for the association between obesity and endometrial cancer. It has been suggested that this inflammation is also a possible risk factor for EOC (Ray *et al*, 2018).

An interesting factor that has been linked to EOC risk is the use of perineal talc. Talc is a mineral with similarities to asbestos, a known carcinogen, and is known to co-occur with asbestos. Most evidence suggesting a causal link between talc and EOC is retrospective, but has been sufficient to warrant its inclusion on the International Agency for Research on Cancer list of agents possibly carcinogenic to humans: group 2B agents (Tran *et al*, 2019).

1.4.1.4 Influence of other gynaecological diseases

As mentioned in 1.4.1.3, endometrial inflammation is a potential risk factor for EOC. However, the link between endometriosis and EOC is not entirely clear. Zafrakas *et al* (2014) conducted a review that showed an association between endometriosis and the development of clear-cell and endometrioid ovarian cancers, but not enough evidence to change clinical practice. A similar implication in pelvic inflammatory disease has yielded contradictory results overall in all types of ovarian cancer, but an increased risk of EOC with repeated cases of pelvic inflammatory disease (Rasmussen *et al*, 2017).

Increased risk conferred from polycystic ovary syndrome has been proposed, although studies have generally found little to no association. Increased cell turnover and increased gonadotrophins (see the gonadotrophin hypothesis in 1.4.1.2) were suspected contributors of risk (Ding *et al*, 2018).

1.4.2 Diagnosis and treatment

There is no national screening programme in the UK for any type of ovarian cancer, as there is no reliable test that can detect the cancer at an early stage. Diagnoses are typically made after symptoms present and risk factors are taken

into account, notably if the patient is over 50 years of age. Common symptoms include abdominal bloating, loss of appetite, pelvic/abdominal pain, weight loss, increased urinary frequency, and vaginal bleeding. Following clinical assessment, measurement of serum CA125 is usually performed; CA125 is a membrane protein on the surface of Müllerian cells undergoing abnormal division (Scholler and Urban, 2007). The conventional upper limit to warrant investigation for ovarian cancer is ≥35U/ml, which would be followed with scanning investigations (Funston *et al*, 2020). There is no national CA125 screening programme as CA125 is only elevated in approximately 50% of early stage ovarian cancers, but is elevated in other circumstances, including pregnancy and non-cancerous conditions such as uterine fibroids (Ledermann *et al*, 2013). There is prognostic value to CA125 however, as it is a useful indicator of whether advanced cancers are responding to treatment and for predicting disease reoccurrence (Piatek *et al*, 2020; Bachmann *et al*, 2021).

The treatment of ovarian cancer is determined by the stage at diagnosis, but most patients will have surgery. Disease is normally staged as a result of initial surgery. Many patients have additional surgeries. Typical surgeries involve hysterectomy, bi or unilateral salpingo-oophorectomy, and often debulking. Particularly advanced cases of ovarian cancer may require neoadjuvant chemotherapy prior to surgery, as well as adjuvant chemotherapy. Further maintenance therapies may be given following disease recurrence, including bevacizumab (a monoclonal antibody against VEGF) and poly ADP ribose polymerase inhibitors (Kuroki and Guntupalli, 2020).

1.4.3 Disease origin and subtype

Historically, it was believed that all EOCs originated from the surface epithelium of the ovary, a single layer of epithelial cells that cover the ovary surface. These cells were thought to invaginate to inside the ovary, form cysts, and become cancerous through an accumulation of genetic mutations. However it is now accepted that EOC can originate from multiple sites and that this is likely to explain the histopathological heterogeneity of the disease (Cardenas *et al*, 2016). This heterogeneity is apparent in the different subtypes of EOC: serous, mucinous, endometrioid and clear cell; it is thought that these subtypes arise from different anatomical locations as they contain cells from different areas, including outside of the ovary. Cells comprising these subtypes bear resemblance to epithelia from surrounding areas; serous EOCs are similar to epithelium in the fimbriae of the fallopian tube (but can also resemble the OSE), mucinous to endocervix epithelium, endometrioid to endometrial epithelium and clear cell to glycogen-rich epithelial cells found in the vagina (see figure 10) (Kim *et al*, 2018). In cases where local metastasis has occurred, it can be difficult to determine the origin of the cancer. This can have clinical implications as cancers originating from different sites often have different clinical outcomes (Moro *et al*, 2019).

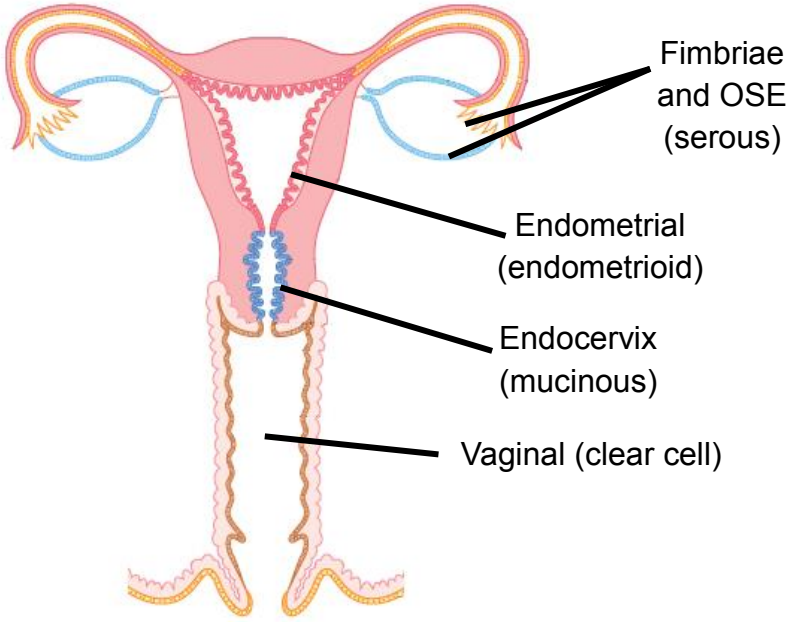

Figure 10. Origin of different epithelial ovarian cancer (EOC) subtypes. The anatomical origin of each subtype associated epithelium is labelled, and the subtype name is shown in brackets. OSE = ovarian surface epithelium (adapted from Obgyn Key, 2016).

1.4.4 Epithelial ovarian cancer staging

EOC is currently staged in the UK using the International Federation of Gynaecology and Obstetrics system (FIGO). This system uses three factors to classify EOC. This includes the extent of the tumour size (T); whether the tumour has spread outside of the ovary to the fallopian tube, or further pelvic organs. The spread to nearby lymph nodes (N) is also considered, as well as metastasis (M) to distant sites such as the liver and bones. Taken together, cancers are assigned a TNM stage. A simplified FIGO staging chart is shown in table 3, adapted from British Gynaecological Cancer Society (BGCS) epithelial ovarian cancer guidelines (2014).

Stage	TNM stage range	Description
IA-IC3	T1a-N0-M0 – T1c-N0-M0	Lowest stage IA tumours are limited to the ovary/fallopian tube on one side (capsule intact) and no cells in ascites, to highest stage IC3 tumours where tumours may be in both ovaries/fallopian tubes and there is presence of cells in ascites
IIA-IIB	T2a-N0-M0 – T2b-N0-M0	Lowest stage T2a tumours involves one or both ovaries/fallopian tubes with extension to or implants to the uterus and/or ovaries/fallopian tubes (depending on site of origin), to highest stage T2b tumours which have further extension to other pelvic intraperitoneal tissues
IIIA1-IIIC	T1/2-N1-M0 – T3c-N0/N1-M0	Lowest stage T1/T2-N1-M0 tumours have positive retroperitoneal lymph node spread, to highest stage T3c-N0/N1-M0 tumours, where there is macroscopic peritoneal metastasis beyond the pelvis of >2cm ± retroperitoneal lymph node spread (includes tumour extension to liver capsule and spleen without parenchymal involvement)
IVA-IVB	Any T, any N, M1	Lowest stage IVA cancers have pleural effusion with positive cytology, to highest stage IVB cancers, where there are parenchymal metastases to extra-abdominal organs

Table 3. A simplified explanation of the International Federation of Gynaecology and Obstetrics (FIGO) staging system, detailing the range between each stage.

As discussed in 1.4, the poor survival rate of EOC is generally attributed to late diagnoses. The most common type of EOC is high-grade serous EOC, being responsible for approximately 70% of all diagnoses, and this subtype is often diagnosed when the cancer has already progressed to stage III or IV (Kim *et al*, 2018). EOC is known to spread to distant organs such as the liver, lungs and even the bones and brain. Lymph node spread and the spread of EOC cells to

local peritoneal tissues precedes cancer cell dissemination into the peritoneal fluid, and consequently the omentum. However other routes of metastasis have more recently been investigated, and shall be discussed further (Deng *et al*, 2018).

1.4.5 Epithelial ovarian cancer metastasis

EOC is known to primarily metastasise transcoelomically. At the primary tumour site, local metastasis occurs through direct surface spread; transcoelomic spread refers to a cancer spreading by travelling through a body cavity before penetrating a distant surface. In the case of EOC, this is the peritoneal cavity. Disseminated cancer cells from the primary tumour shed into the peritoneal fluid within the peritoneal cavity, and subsequently adhere to and invade organs and tissues within the cavity. There is however, also evidence of EOC metastasis through the haematogenous (circulation) and lymphatic routes. This has challenged the previously held belief of the transcoelomic peritoneal metastasis route as the only metastatic route, and could have clinical implications in the management of the disease (Yeung *et al*, 2015).

1.4.5.1 Haematogenous metastasis in EOC

Haematogenous spread is when EOC cells from the primary tumour intravasate into the vasculature, travel to a secondary site, and extravasate out into the surrounding tissue. Evidence for a role of haematogenous metastasis originated from post-surgical observations. Tarin *et al* (1984) found that peritoneovenous shunts (a device to relieve ascites by directing fluid to the vena cava) in EOC patients were directing disseminated cancer cells into the blood, yet the disease was still mainly contained in the abdomen. However more recent studies have shown that increased circulating tumour cells (CTCs) are typically present in patients with advanced disease, and were associated with poorer responses to treatment and a poorer survival. This necessitated investigations into whether the increased CTCs caused the metastases, or resulted from the metastases after they were established (Cui *et al*, 2015). An *in vivo* study by Pradeep *et al* (2014) used a parabiosis mouse model involving one mouse with EOC and one without. The mice shared a blood supply, and it was found that CTCs from the

EOC mouse preferentially spread to the omentum of the other mouse before other peritoneal sites. The presence of metastases in the highly vascularised omentum was then able to facilitate further haematogenous spread (Yoo *et al*, 2007).

1.4.5.2 Transcoelomic metastasis in EOC

The transcoelomic route of metastasis in EOC can be divided into a series of steps: the detachment of cancer cells from the primary tumour, anoikis (programmed cell death following the loss of contact between anchorage-dependent cells and the ECM) resistance development, dissemination of cells into the peritoneal cavity, attachment of disseminated cancer cells to surfaces within the peritoneal cavity, attachment and invasion of the mesothelial layer of peritoneal tissues, and subsequent growth of new tumours at successful sites of invasion (Yousefi *et al*, 2020). These steps are shown in figure 11. Given that EOC arises from various epithelia, the detachment of cancer cells from the primary tumour primarily concerns the loss, or downregulation of epithelial (E)-cadherin. This is associated with epithelial-mesenchymal transition (EMT), where epithelial cells detach due to a decrease in E-cadherin and lose their cell polarity and cell-cell adhesion. The cells gain a migratory phenotype and have mesenchymal-like morphology. Cancer cells undergoing this change become mesenchymal-like cancer stem cells that can migrate to distant sites; these are the cells found in ascites in EOC that attach to and invade peritoneal surfaces, such as the omentum (Heerboth *et al*, 2015). In EOC, the activation of several signalling pathways can activate transcription factors (such as Snail and Slug), that affect E-cadherin expression. These pathways include those of ET-1, EGF, HGF and transforming growth factor-β (TGF-β) (Vergara *et al*, 2010).

After the cancer cells detach from the primary tumour, they need to develop resistance to anoikis. In EOC, anoikis resistance is thought to be acquired through an overexpression of Rab25 GTPase, a protein involved in vesicle trafficking, and B7-H4 protein, a negative regulator of T-cell responses (Salceda *et al*, 2005). Overexpression of Rab25 GTPase is associated with decreased disease-free survival in EOC (Cheng *et al*, 2004). In order for disseminated cells to reach peritoneal surfaces, there must be sufficient ascites in the peritoneal cavity. In EOC, excess peritoneal fluid accumulates due to increased tumour

secretion of VEGF, which increases the permeability of the peritoneal capillaries and in turn, the amount of fluid they leak into the cavity. This is coupled with reduced lymph drainage (Xu *et al*, 2000). Malignant ascites itself harbours factors that promote the cancer cell migration and invasion, including MMPs and CXC chemokine ligand 12 (CXCL12), the latter promoting upregulation of integrins for enhanced binding properties of disseminated cancer cells (Casey and Skubitz, 2000). Some cancer cells in ascites form spheroids, which have metastatic advantages as opposed to single disseminated cancer cells, as inner cells are protected from attacks by immune cells and anti-tumour drugs (Al Habyan *et al*, 2018).

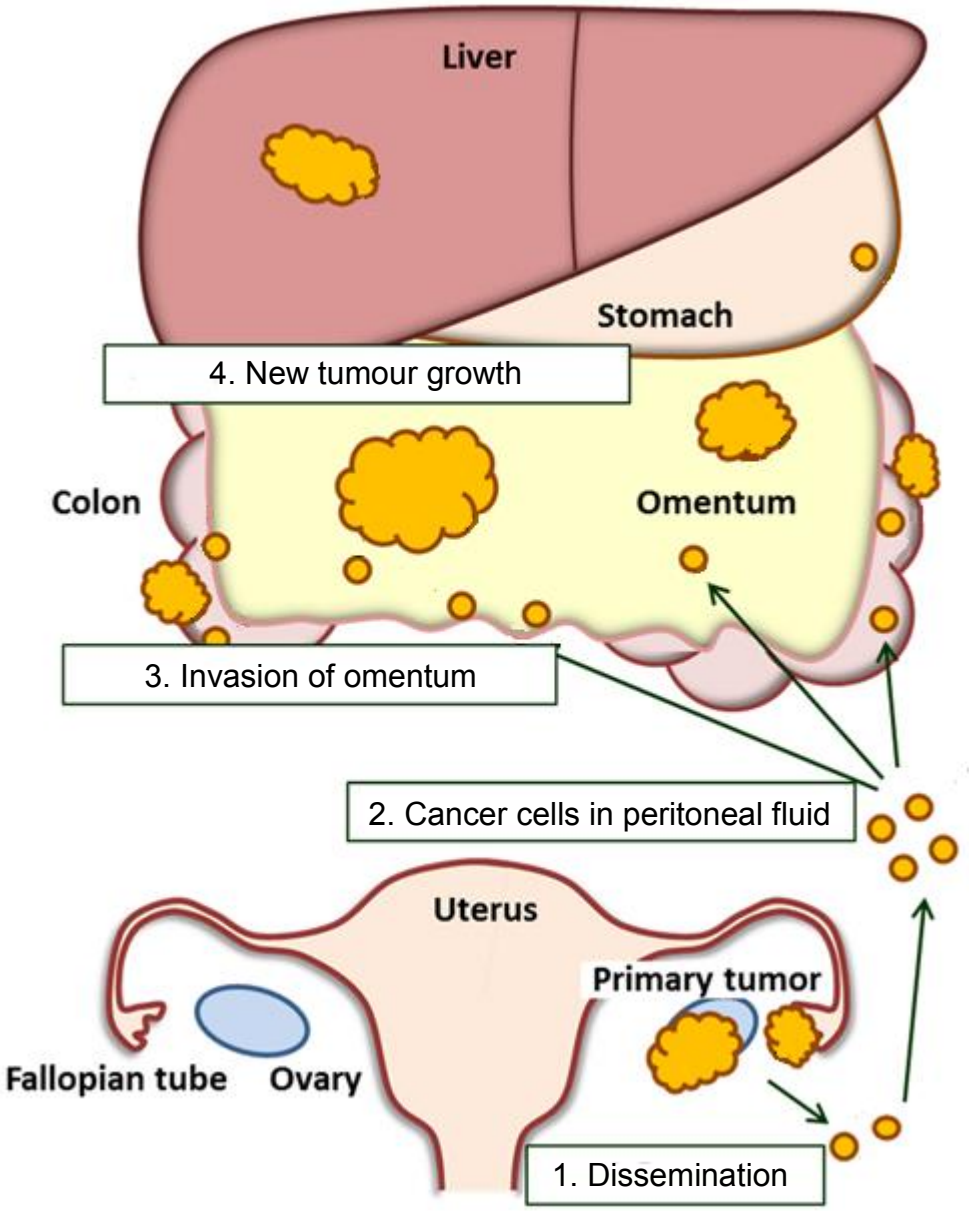

Figure 11. Transcoelomic metastasis of epithelial ovarian cancer (EOC). Cells from the primary tumour are shown disseminating into the peritoneal fluid (steps 1-2). Step 3 shows EOC cells in the peritoneal fluid attaching to and invading the omentum. The development of new tumours from these sites of metastases is shown in step 4 (including further sites such as the stomach and liver) (adapted from Nakamura *et al*, 2019).

Historically accepted as a passive process, there is now scope to believe that EOC transcoelomic metastasis via peritoneal dissemination may be at least partly, an adaptive process. This is to say that the capacity of the cancer cells at the primary site to disseminate and spread is not an inherent property, but is acquired or 'gifted'. One step undergoing research is the attachment of cancer cells to the omental mesothelium (the most superficial layer of the omentum,

which is composed of mesothelial cells), where there is suspected involvement of the mesothelial cells themselves (Kenny *et al*, 2014). After cancer cells arrive at a secondary site, they regain their epithelial phenotype by undergoing mesenchymal-epithelial transition (MET). E-cadherin expression and cell polarity are also regained. Disseminated EOC cells are known to express α5β1 integrin (the fibronectin receptor), which facilitates their binding to the mesothelium, which expresses fibronectin. Additionally, the ovarian cancer marker CA125 (that is overexpressed in EOC cells) promotes cell attachment to the mesothelium by binding to mesothelin expressed on the surface of the mesothelial cells (Rump *et al*, 2004). Cancer cell attachment is further facilitated through the action of secreted adipokines, such as adiponectin, from adipocytes within the omentum (Nieman *et al*, 2011). This preferential binding of EOC cells to the omentum is aligned with the seed and soil hypothesis of metastasis, with the omentum being the ideal 'soil' for the EOC 'seeds' (Sawada *et al*, 2008).

The omentum is one of the most preferred sites of EOC metastasis, and omental metastases are often present in patients with stage III-IV disease (Iwagoi *et al*, 2021). The metastasis in the omentum contributes further to disease development, and is the metastatic location focussed on in this thesis. Therefore the omentum, and the final steps in EOC transcoelomic metastasis, the invasion of the omental mesothelial layer by the cancer cells and subsequent growth of new omental tumours, are explored in greater detail below (section 1.5.3).

1.5 The omentum

The omentum has historically been thought of as solely a fat storage organ but is now known to have unique immune functions. Despite these functions however, complete omentectomy is a survivable procedure often performed in surgeries treating EOC. The fatty composition is known as a good 'soil' for metastasising EOC cells, and as mentioned in 1.4.5.2, this is not a passive process; the omentum is now thought to actively facilitate cancer cell binding and growth (Meza-Perez and Randall, 2017).

1.5.1 Omental macrostructure and general function

The omentum is a large apron-like infolding of visceral peritoneum largely composed of visceral fat. It is anatomically divided into the greater and lesser omentum; the greater omentum is derived from the dorsal mesentery, whilst the lesser omentum is derived from the ventral mesentery. The greater omentum extends from the greater curvature of the stomach, over the small intestines, and folds back on itself to fuse with the anterior surface of the transverse colon. The position within the abdominal and pelvic cavities, as well as the omental blood supply is shown in figure 12. The lesser omentum is typically much smaller, extending from the lesser curvature of the stomach and the liver (Collins *et al*, 2009). Commonly, both the greater and lesser omentum are discussed together, as 'the omentum'. The size of the omentum is hugely variable as it is varies naturally, but also increases and decreases with body fat percentage; it is known to range between 300 - 2000g with a surface area between 300 - 1500cm^2 (Di Nicola, 2019).

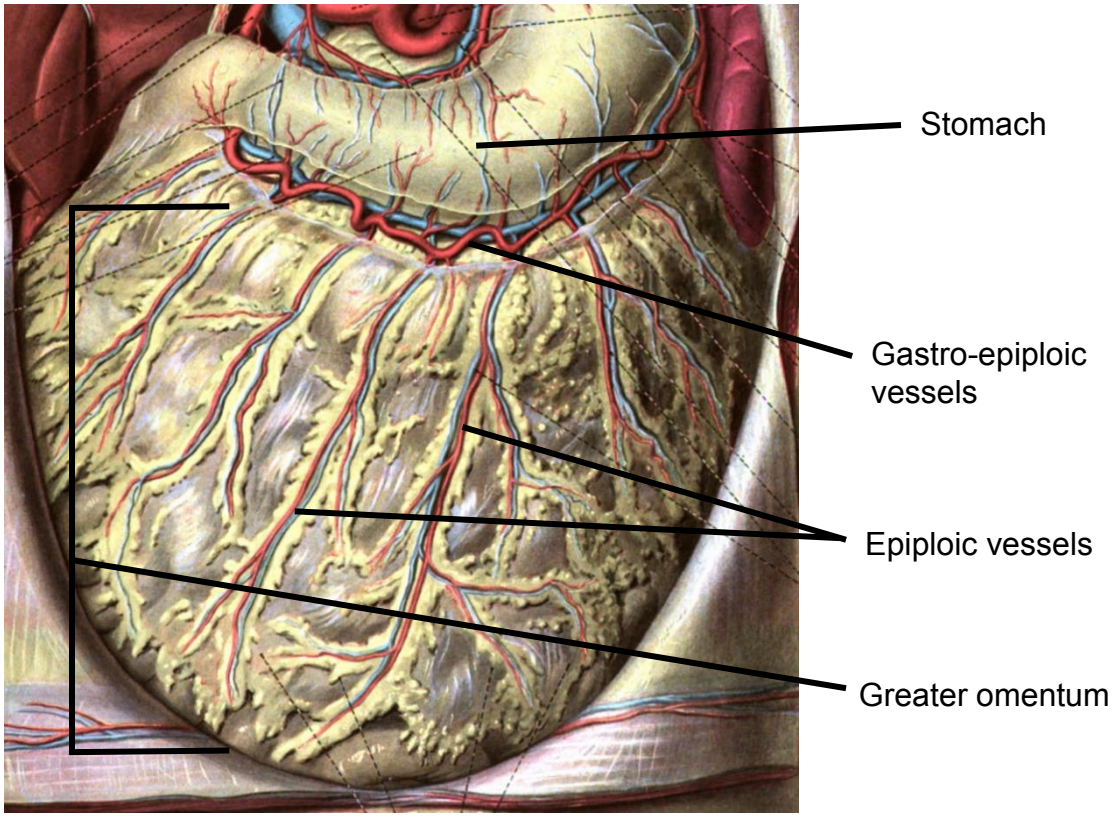

Figure 12. Diagram of the anterior view of the greater omentum. The greater omentum is shown superficially covering the abdominal organs, hanging down from the greater curvature of the stomach, into the abdominal and pelvic region. The greater omentum (and the lesser omentum) are supplied with blood from the right and left gastro-epiploic vessels; branches of the gastroduodenal and splenic arteries respectively, both of which derive from the coeliac trunk. Smaller epiploic vessels branch off from the right and left gastro-epiploic arteries (adapted from Di Nicola, 2019).

As a fatty organ, the omentum acts as a store for adipose tissue. This allows for general body heating and organ protection functions. Additionally, the omentum is a mobile immune organ; patrolling the abdominal cavity, it can shift to sites of local infection, controlling inflammation and promoting revascularisation and wound healing post-injury (Di Nicola, 2019). The omentum contains many lymph nodes that contribute to its properties as an immune organ (Collins *et al*, 2009).

1.5.2 Omental microstructure and immunological function

The omentum is primarily composed of adipocytes, but has a unique microstructure pertaining to its immunological functions. Histologically, the omentum is heterogeneous, containing areas composed primarily of connective tissue, and other areas richer in adipose tissue. However, all areas of the omentum have a layered structure. Most superficially is a layer of mesothelial cells that overlies a submesothelial layer that contains adipocytes, collagen and fibroblasts (Wang *et al*, 2020). The submesothelial layer is not uniform, with varying fenestrations and amounts and size of adipocytes. Within the adipose rich areas are the basic functional immunologic units measuring 0.3 - 3.5mm^3, called milky spots. Bordered by adipocytes, these units contain the immune cells: macrophages, B-lymphocytes, T-lymphocytes and mast cells. Interestingly, omental B and T lymphocytes are thought to mature in the omentum, making the omentum a sort of 'intestinal thymus'. These lymphocytes express different markers to lymphocytes found in the blood, spleen and lymph tissue. The cells are arranged around omental glomeruli (see figure 13), and the overlying mesothelium and omental endothelium are adapted to facilitate leukocyte transmigration (see section 1.1.2.1) through omental capillaries into the surrounding fat tissue (Di Nicola, 2019).

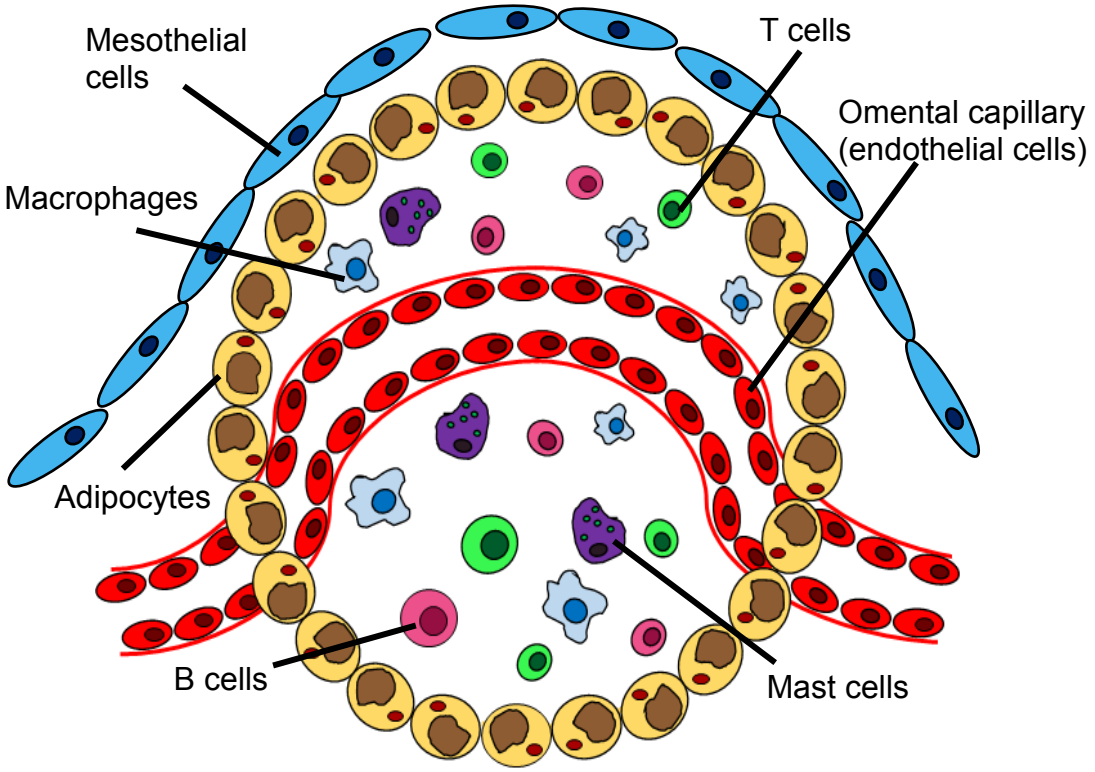

Figure 13. Cell types within, and structure of an omental milky spot. A layer of mesothelial cells (blue) lies superficially over adipocytes (yellow, shown with fat reservoirs) which surround an omental capillary. Together, these cells form the structure of a milky spot. An average number of 600 immune cells are present within a milky spot, including macrophages (70%), B and T lymphocytes (10% each), and mast cells (which together with stromal cells, constitute the remaining 10%). The milky spot structure facilitates leukocyte transmigration as well as solute transport within the omentum (information from Platell *et al*, 2000).

The omentum is able to launch both innate and adaptive immune responses, as implied by the presence of both cells of the innate and adaptive immune systems in the milky spots. Macrophages are deployed to areas of acute inflammation, their deployment aided by the motility of the omentum as a whole, but also due to their maturation within milky spots. Inflammation within the peritoneal cavity can be driven by the presence of pathogens and foreign material. Importantly, additional immune cells (leukocytes) are recruited through the omental glomeruli; activated B and T lymphocytes constitute the adaptive immune response (Meza-Perez and Randall, 2017). Once the omentum is forming an immune response, it is described as activated. However, activated omentum also refers to the omentum during regenerative and pro-angiogenic

activities. Omental capillaries are known to have high angiogenic capability when stimulated, a phenomenon involving signalling from multiple cell types within the omental microenvironment (discussed in section 1.6.1), including invading EOC cells (Di Nicola, 2019). These properties of the omentum enhance the metastasis of disseminated EOC cells (see 1.4.5.2), including the invasion of the mesothelial layer and the subsequent growth of new tumours.

1.5.3 Omental enhancement of EOC metastasis

1.5.3.1 Invasion of the omentum

Following attachment to the mesothelial layer (see section 1.4.5.2), EOC cells invade further into the mesothelium. This is promoted by both intrinsic and extrinsic factors. Lysophosphatidic acid and MMPs present in ascites extrinsically facilitate further invasion (see figure 5) by degrading ECM, providing a path for invading cancer cells. MMPs 2, 9 and 14 have specifically been implicated in EOC, and have been shown to deregulate claudin proteins in TJs (see section 1.2.3.4). Claudins are overexpressed, leading to abnormal structure and function of TJs (Wang *et al*, 2013). The action of MMPs can also activate the H-ras/mitogen-activated protein kinase (MAPK) pathway, which causes redistribution of focal adhesion kinase (FAK), promoting mesothelial cell migration. In addition to EOC cells, MMPs are known to be produced by different cell types within the omental microenvironment, including mesothelial cells, macrophages and fibroblasts (Yang and Huang, 2015).

Section 1.4.5.2 discusses how mesothelial cells can enhance the attachment of cancer cells to the omentum, primarily through mesothelial expression of fibronectin. Mesothelial cells are also however implicated in further invasion of the omental tissue. Fibronectin overexpression is also associated with enhanced migration and invasion of cancer cells, as fibronectin knockout (KO) studies in EOC metastases models have demonstrated a significant reduction in both processes. EOC cells that have attached to the mesothelial layer also secrete TGFβ1, which promotes mesothelial-mesenchymal transition (MMT) of mesothelial cells. This process can lead to mesothelial cells transforming into cancer associated fibroblasts (Pakula *et al,* 2019). This process of MMT results in a loss of E-cadherin, and therefore a reduction in the integrity of the

mesothelial barrier. This in turn offers a path of decreased resistance for cancer cell invasion (Kenny *et al,* 2014).

1.5.3.2 Omental metastasis development

Successfully invasive EOC cells in the omentum establish micrometastases. Development into macrometastases and larger tumours involves cells in the microenvironment as well as EOC cells themselves, including adipocytes, macrophages, mesenchymal stem cells (MSCs), fibroblasts, and endothelial cells. These cells in the tumour microenvironment interact with the cancer cells in a complex network of signalling pathways that play roles in cancer cell survival, proliferation and further metastasis (Motohara *et al*, 2019).

Given the preferential homing and subsequent metastatic success of EOC cells to the omentum, seemingly through both transcoelomic and haematogenous spread, the role of adipocytes has been an interesting point of study. Interestingly, EOC cells found at the interface between metastases and adipocytes contain more triglycerides. Nieman *et al* (2011) demonstrated that the EOC cells influence omental adipocytes to release triglycerides. In turn this allows the cancer cells to adapt to lipid metabolism by increasing β-oxidation of fatty acids. Furthermore, these 'cancer associated adipocytes' are stimulated to release adipokines such as interleukins, adiponectin and leptin; these have been shown to enhance the metastatic niche formed within the omentum (Nieman *et al*, 2011). Adipocytes have also been shown to directly promote EOC cell proliferation through mechanisms that are exclusive to omental metastasis; expression of salt-inducible kinase 2 (SIK2) occurs in omental metastases but not in primary tumours. SIK2 is activated by adipocytes, and increases EOC proliferation through the phosphatidylinositol 3-kinase (PI3 kinase) pathway (Miranda *et al*, 2016).

MSCs have regenerative properties, and are involved in the normal wound healing process. There is evidence to suggest that omental metastases inappropriately recruit MSCs – effectively, that MSCs treat these sites as wounds that do not heal. Co-culture studies of MSCs with EOC cell lines have shown an increase in the cancer cell proliferation, migration and invasion (Lis *et al*, 2012; Zhang *et al*, 2017). A potential role of MSCs in increasing NO

synthesis within EOC cells has been observed, where the MSCs secrete arginine which is utilised by EOC cells for NO production. This in turn reduces oxidative stress and increases growth rate (Salimian Rizi *et al,* 2015). MSC presence within solid tumours has been observed in many different tumour types, including EOC tumours, and it is thought that this presents the possibility that MSCs can contribute to cancer stemness – the ability of the cancer to self-renew and adapt to the local microenvironment (McLean *et al,* 2011).

Interestingly, MSCs can also be induced to become cancer associated fibroblasts by lysophosphatidic acid in ascites and EOC exosomes (Jeon *et al,* 2008; Cho *et al*, 2011). Additionally, omental fibroblasts can be transformed into cancer associated fibroblasts through EOC associated miRNAs that mediate TGFβ signalling (Mitra *et al*, 2012). Cancer associated fibroblasts within the omentum release cytokines, growth factors and matrix degrading proteins that promote the invasiveness and growth of metastases; notably hepatocyte growth factor (HGF) and MMP2. Cancer associated fibroblasts also increase EOC cell motility through the activation of the nuclear factor kappa-light-chain-enhancer of activated B cells (NF-κB) pathway. Cancer associated fibroblasts have been shown to secrete TNF-α which enhances the colony forming ability of EOC cells through the activation of epidermal growth factor receptor (EGFR), as well as CXCL12 which increases EOC cell proliferation (Lau *et al*, 2017). The reciprocal signalling between cancer associated fibroblasts and EOC cells drives the development of new tumours.

As well as the involvement of stromal cells in enhancing omental metastasis, there is thought to be significant involvement from immune cells, namely omental macrophages. Sections 1.5.1-2 discuss how the omentum functions as an immune organ. It is therefore interesting that EOC cells are able to metastasise and colonise the omentum so effectively (and preferentially). Interestingly, sites of omental EOC metastases have been found to primarily occur in close proximity to milky spots (see section 1.5.2) (Krishnan *et al*, 2015). Macrophages are stimulated by factors secreted by invading EOC cells, including colony-stimulating factor-1, and β-chemokines. In the case of omental macrophages, most become type M2 tumour associated macrophages (Duluc *et al*, 2007). These macrophages suppress the immune response to the EOC cells and also modify the ECM; both processes greatly enhance the growth of

new tumours. Furthermore, omental tumour associated macrophages have been shown to enhance cancer cell motility *in vitro* through the secretion of the β-chemokines CCL6 and CCL23. Both interact with the CCR1 receptor expressed on EOC cells (Krishnan *et al*, 2020).

The EOC cells themselves are resistant to cell death and undergo sustained and uncontrollable proliferation. Coupled with the interactions between the cells of the omental microenvironment, a metastatic niche within the omentum is established, and metastasis proceeds very successfully. The processes discussed in sections 1.4.5.1-2 and 1.5.3.1-2 are summed up in figure 14. The processes discussed so far cover all the hallmarks of cancer development except one: angiogenesis (Hanahan and Weinberg, 2011). However, EOC cells, as well as cells within the microenvironment secrete VEGF, which activates angiogenesis (Motohara *et al*, 2019). Tumour associated angiogenesis within EOC metastasis to the omentum is the focus of this thesis and will therefore be discussed in further detail.

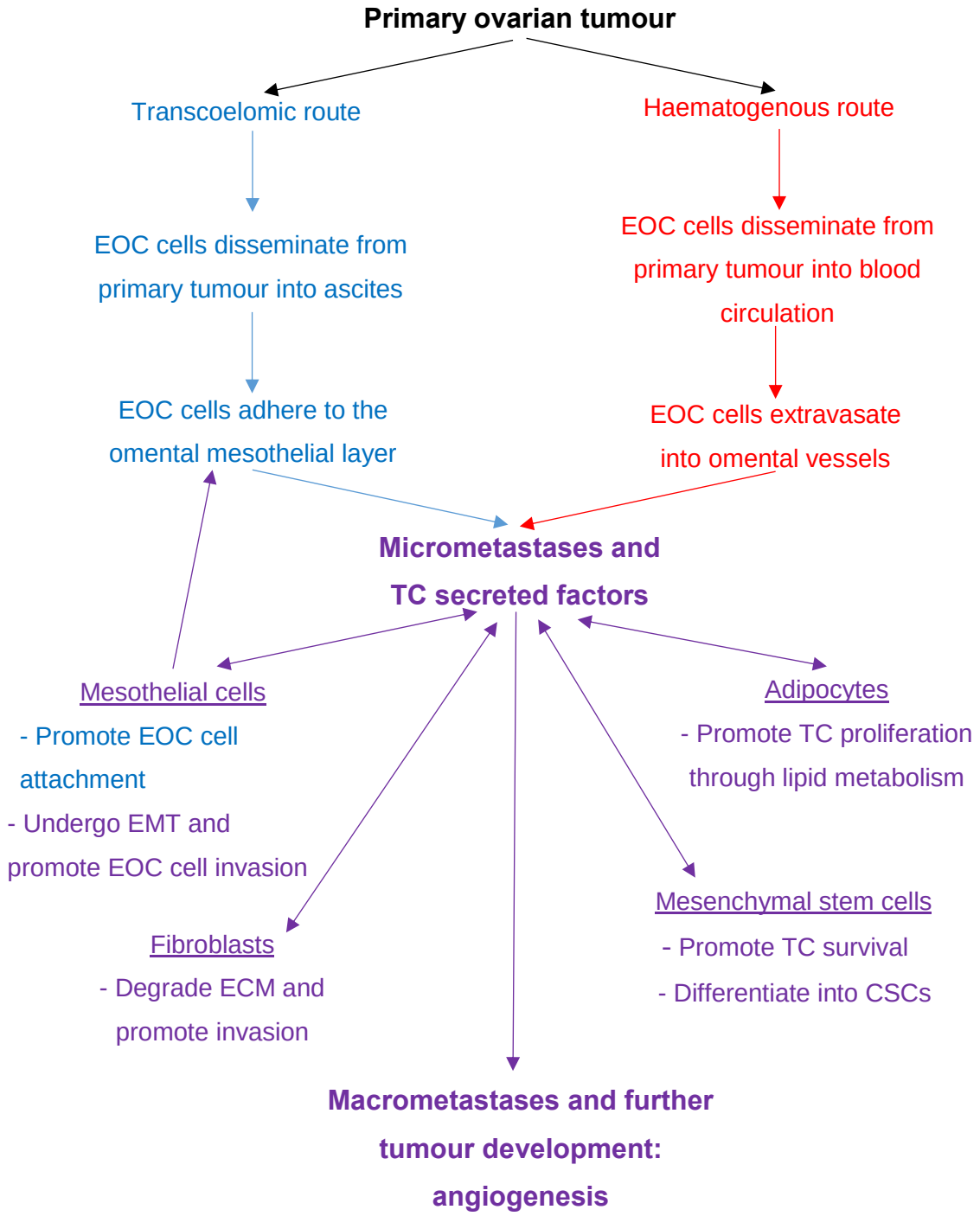

Figure 14. Summary of the transcoelomic and haematogenous routes of epithelial ovarian cancer (EOC) development and microenvironment involvement. The transcoelomic route is detailed in blue, haematogenous in red. Processes and cell involvement after EOC cells arrive at the omentum are detailed in purple. Note the involvement of mesothelial cells in the attachment of EOC cells to the omentum. ECM = extracellular matrix; CSCs = cancer stem cells. EMT = epithelial-mesenchymal transition.

1.6 Angiogenesis pathways in EOC omental metastasis

As mentioned previously, in order for metastases to develop into tumours beyond $2mm^3$, angiogenesis must be activated in order to form tumour associated blood vessels that provide a blood supply. Without this supply, EOC cell proliferation is limited due to a lack of nutrients and waste removal. Additionally, further haematogenous spread requires access to blood vessels. In order to activate the angiogenic switch (see section 1.3.1), EOC cells, as well as other cells in the microenvironment, secrete pro-angiogenic molecules. (Gavalas *et al*, 2013). The mechanisms of angiogenesis are discussed in section 1.3 (and 1.3 subsections). Pathological activation of angiogenesis within cancer is discussed in section 1.3.3.2; these processes will now be looked at specifically within the context of EOC omental metastasis.

1.6.1 Pro-angiogenic factors

As discussed throughout sections 1.4 to 1.5, EOC cells secrete a variety of factors into ascites and within the omentum, and also induce cells in the tumour microenvironment to secrete factors that contribute to tumour development. EOC cells and omental stromal cells influenced by EOC cells are known to secrete VEGF and a variety of other pro-angiogenic molecules, the most well-known of which are summarised in table 4.

Cell type	Pro-angiogenic molecule(s)	Reference(s)
EOC cells	VEGF MMP9, 7, 2 FGF1 FGF18 Ang-1 HGF PDGF	Yeung *et al* (2015)
Mesothelial cells	VEGF	Sako *et al* (2003)
Adipocytes	VEGF IL-6 HGF	Dai *et al* (2020)
Fibroblasts	VEGF CXCL12 FGFs Ang-1, Ang-2	Yeung *et al* (2015)
Macrophages	VEGF MMP9 IL-6, IL-8 EGF Tie-2	Yeung *et al* (2015) Heredia-Soto *et al* (2020)

Table 4. Primary pro-angiogenic molecules secreted into the epithelial ovarian cancer (EOC) tumour microenvironment.

Notably, most cell types secrete VEGF. As discussed in section 1.3.1, this is considered the most potent pro-angiogenic molecule. The factors in table 4 promote EC proliferation, migration and tubule formation, as well as vessel stabilisation, demonstrating the angiogenic facilitation from the omental microenvironment. Section 1.3.3.3 details how tumour vessels are improperly formed, and how their leakiness contributes to the continual production and secretion of pro-angiogenic factors. This is true in EOC, and VEGF is increased at sites of metastasis and found in ascites. Most anti-angiogenic therapies in EOC have looked to target VEGF and/or VEGFR2, with limited success (Gavalas *et al*, 2013).

1.6.2 VEGF pro-angiogenic signalling

As discussed in section 1.3.1, not all VEGF signalling promotes a pro-angiogenic phenotype. The biological activity of VEGF is mediated through the binding to and activation of VEGFRs; VEGFR2 is the receptor strongly associated with angiogenesis, and is the primary receptor activated by the VEGF-A_{165} isoform. This pro-angiogenic signalling is discussed further in this section.

1.6.2.1 VEGF-VEGFR2 pro-angiogenic signalling pathways

The signal transduction pathways triggered downstream of VEGF binding to and activating VEGFR2 are complex, and branch/converge at multiple points. However whilst not fully elucidated, there are certain pathways that have been well studied and documented. Initially, VEGF binding acts like a cross-linker, linking the two halves of VEGFR2, and inducing their dimerisation. VEGF binding to VEGFR2 is mediated through the Ig-like domain 3 portion of the extracellular part of the receptor. This receptor dimerisation triggers autophosphorylation on certain tyrosine residues, of which 5 of the 19 are considered to be the major phosphorylation sites: Y1175, Y1214, Y951, Y1054, and Y1059. Signalling pathways activated from these phosphorylation sites are associated with EC survival, proliferation and migration (Matsumoto and Mugishima, 2006). The simplified proliferation and migration signalling pathways are shown in figure 15. The signalling following VEGF induced activation of VEGFR2 can be inhibited *in vitro* by a number of small molecule inhibitors that target either VEGF or VEGFR2 (or all VEGFRs), for example targeting of VEGFRs with the inhibitor SU5416 (Mendel *et al*, 2000). The impact of such molecules for treating advanced EOC (in phase II and III trials) are discussed later in section 1.6.3.

Y1175 phosphorylation site

The Y1175 phosphorylation site is located in the C-terminal tail of the receptor. After phosphorylation, this site induces the phosphorylation of phosphoinositide phospholipase Cγ1 (PLCγ1). This leads to the release of Ca^{2+} from endoplasmic reticulum and the activation of protein kinase C (PKC), which in turn promotes EC proliferation through the extracellular signal-regulated (ERK)

pathway (see figure 15a). Y1175 phosphorylation is also known to promote EC migration by binding to SH2 domain-containing adaptor protein B (Shb), which then mediates cell migration through the FAK pathway. Moreover, the site is implicated in promoting cell survival through Shb mediated activation of the PI3 kinase pathway (Holmqvist *et al*, 2004), which can induce cell migration, regulate vascular permeability, and promote cell survival (Karar and Maity, 2011).

Y1214 phosphorylation site

Like Y1175, Y1214 is also located in the C-terminal tail, and is also associated with EC migration, through mediation of the growth factor receptor-bound protein 2 (Grb2)/Cdc42 pathway (see figure 15b). Interestingly, although Grb2 is an upstream stimulator of the ERK pathway, it is not thought to be an important branch of Y1214 pathway signalling (ERK signalling is instead thought to occur via Y1175 phosphorylation) (Takahashi *et al*, 2001).

Y951 phosphorylation site

The Y951 phosphorylation site is located in the kinase-insert domain 2 site. Upon phosphorylation, the adaptor molecule T-cell specific adaptor protein mediates EC migration through the proto-oncogene c-Src (Src) pathway (Gorgon *et al*, 2016). Migration is facilitated through the activation of the Rho family GTPase members, Rac and Rho, which stimulates actin reorganisation (see figure 15b) (Soga *et al*, 2001).

Y1054 and Y1059 phosphorylation sites

These phosphorylation sites are located within the kinase domain, and whilst not linked to any of the previously mentioned pathways, have been shown to be essential for VEGFR2 activation and degradation. This is evidenced by a significant decrease in VEGFR2 activation and internalisation of the VEGF-VEGFR2 complex in cells bearing Y1054 and Y1059 mutations (Dougher and Terman, 1999; Ewan *et al*, 2006).

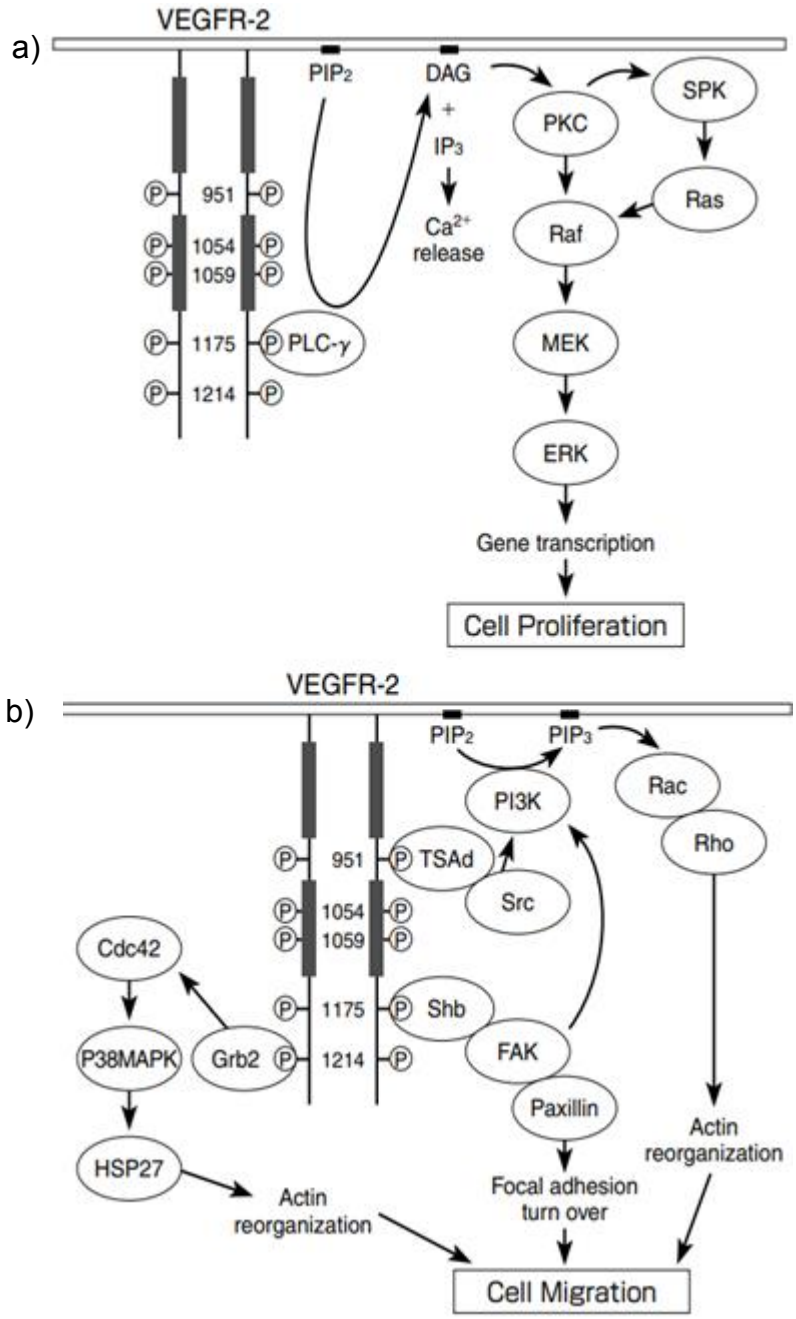

Figure 15. VEGF-VEGFR2 proliferation and migration pathways in endothelial cells. Following binding of the VEGF ligand, a) shows the signalling pathway stemming from the Y1175 phosphorylation site, which is associated with promoting EC proliferation. b) Depicts the signalling pathways that promote endothelial cell migration, from phosphorylation sites Y1214 and Y951. Note that Y1054 and Y1059 are not part of these pathways; these sites are however essential for normal receptor function (adapted from Matsumoto and Mugishima, 2006).

In reality, VEGF-VEGFR2 signalling within ECs is much more complicated, with the branching and converging of pathways meaning that signalling from these phosphorylation sites, and indeed the minor sites, demonstrates a great deal of crossover. For example, downstream signalling from Y1175 and Y951 is known to increase vascular permeability by increasing eNOS expression (Kowanetz and Ferrara, 2006). In addition to this pleiotropic effect of the VEGF ligand and of VEGFR2, VEGF-VEGFR2 signalling is also affected and regulated through internalisation (or lack thereof) of the ligand-receptor complex.

1.6.2.2 VEGF-VEGFR2 complex regulation

As an RTK, VEGFR2 is embedded within the plasma membrane. Whilst ECs can upregulate proteins involved in angiogenesis in response to pro-angiogenic signals, the 'strength' of the initial response of VEGFR2 to VEGF will depend on several factors. These include how much VEGFR2 is expressed and localised to the surface; VEGFR2 molecules exist both within the plasma membrane and within endosomes that can either be trafficked to the plasma membrane for function, or towards degradation routes (Jopling *et al*, 2014). VEGFR2 localisation within ECs has been shown to be dynamic – a constitutive recycling between peripheral endosomes and the plasma membrane (Jopling *et al*, 2011). Additionally, it has been demonstrated that VEGF binding induces VEGFR2 internalisation. It is suggested that the VEGF-VEGFR2 complex is internalised in order to prevent signalling that occurs only at the cell surface, and therefore internalisation and degradation prevents excessive signalling (Ewan *et al,* 2006; Xie *et al*, 2019).

The canonical pathway of VEGFR2 endocytosis is the clathrin-mediated endocytic pathway, where in both the presence and absence of VEGF, the receptor is directed towards degradation. Briefly, the intracellular portion of the receptor is coated with clathrin, and the receptor is 'pinched off' from the membrane to become encircled in clathrin coated vesicles. These vesicles fuse with endosomes and are eventually directed to lysosomes for degradation (Zhang *et al,* 2014) (see figure 16).

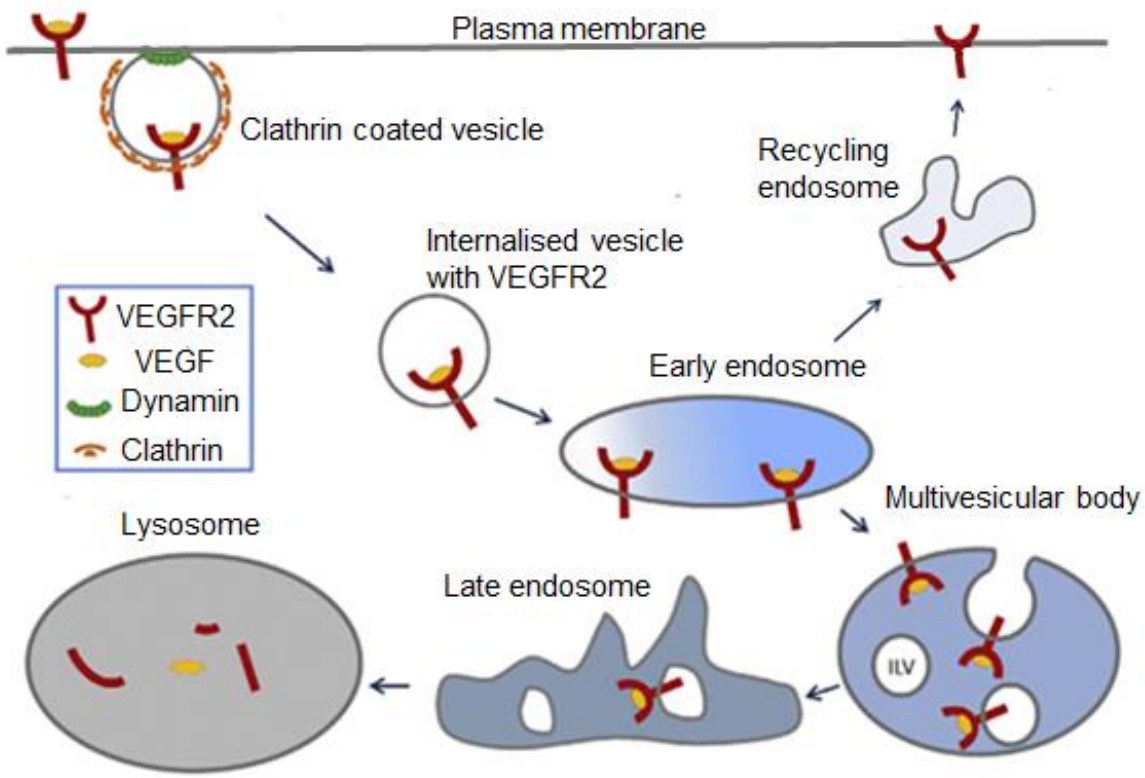

Figure 16. Clathrin-mediated endocytosis of VEGFR2. In the presence (or absence) of VEGF, VEGFR2 molecules are thought to routinely be both internalised via clathrin-mediated endocytosis and degraded by lysosomes, or recycled back to the membrane. Clathrin forms a vesicle around the intracellular portion of the receptor, which is cleaved from the membrane by the fission protein, dynamin. Internalised vesicles containing VEGFR2 fuse with early endosomes. Vesicles destined for degradation proceed to multivesicular bodies, and then to late endosomes, before eventual degradation within lysosomes by hydrolases. Receptors can also be recycled back to the membrane after leaving early endosomes (information: Zhang *et al*, 2014; Cendrowski *et al*, 2016; image adapted from Cendrowski *et al*, 2016).

Recently, experimental studies have suggested that clathrin-mediated endocytosis might not be the only endocytic pathway involved in VEGFR2 endocytosis, and that the pathway may differ depending on the presence or absence of the VEGF ligand. Upon VEGF binding to VEGFR2, an increase in VEGFR2 internalisation can be observed; however Basagiannis *et al* (2016) showed that knocking out dynamin, a protein essential for clathrin-mediated endocytosis, did not affect VEGF induced internalisation. This suggested that a different endocytic mechanism is responsible for ligand induced endocytosis. Further studies of the KO model on constitutive endocytosis also showed a decrease in VEGFR2 internalisation. Taken together, these data support the

notion that clathrin-mediated endocytosis is not the only VEGFR2 endocytic pathway. Basagiannis *et al* (2016) also observed that VEGF induced endocytosis resulted in large vesicles forming, along with areas of membrane ruffling. These are characteristics of macropinocytosis, and co-staining of VEGFR2 within the vesicles with high-molecular mass dextran (a marker of macropinocytotic vesicles) was positive.

The process of macropinocytosis involves membrane ruffling, initiated by ligand signalling induced actin polymerisation. The ruffles form invaginations into the cell, taking the receptor-ligand complex with it in a (non-clathrin) vesicle, called a macropinosome (see figure 17). Macropinosomes can measure between 0.2 and 10μm in diameter; smaller vesicles formed in this manner are called pinosomes, and the process is described as pinocytosis (or micropinocytosis).

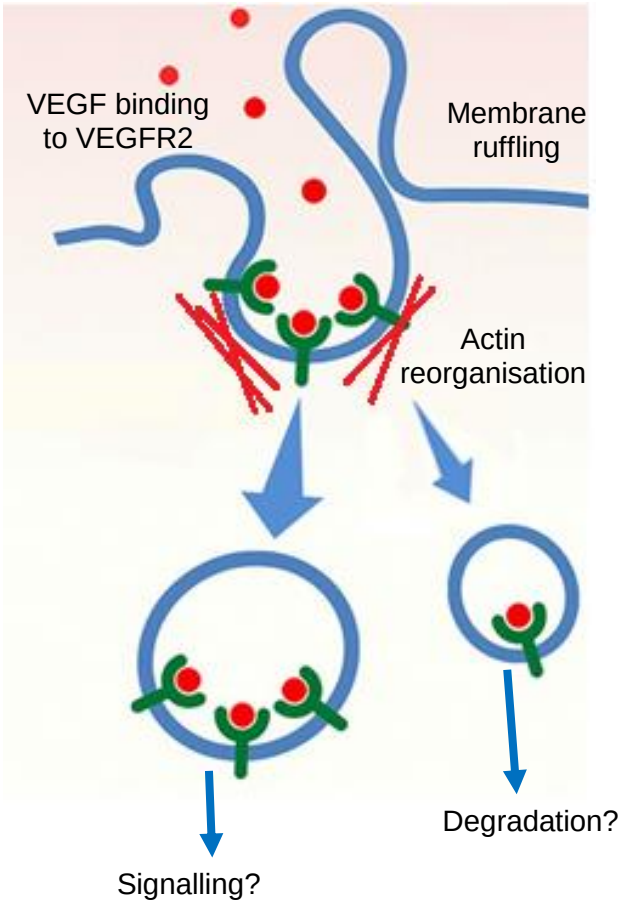

Figure 17. Ligand dependent macropinocytosis: VEGF-VEGFR2. Upon VEGF binding (red) to VEGFR2 (green), signalling pathways promote actin polymerisation, resulting in membrane ruffling, invagination, and packaging of VEGF-VEGFR2 complexes into macropinosomes (blue circles). Conflicts in the literature debate whether complexes within macropinosomes continue the VEGF signalling, or if they are solely sent down the degradation pathway (information: Gourlaouen *et al,* 2013; Lin *et al*, 2020; image adapted from Basagiannis *et al*, 2016).

1.6.3 Anti-angiogenics in treating EOC

The information presented so far within this section (1.6), shows that there are multiple pro-angiogenic factors involved in the development of EOC tumours, but that the most potent pro-angiogenic (VEGF) is heavily implicated. Furthermore, it has been discussed that VEGF signalling and regulation is complicated. The degree of tumour angiogenesis associated with EOC metastases (Masoumi Moghaddam *et al,* 2006) as well as the presence of VEGF within ascites is correlated with poorer survival, and therefore anti-angiogenic therapies for the treatment of advanced EOC have been developed. This section will therefore discuss these treatments and their effectiveness.

1.6.3.1 Bevacizumab

Bevacizumab (or Avastin) is a humanised anti-VEGF monoclonal antibody. The rationale for its use as an anti-cancer treatment is to block the pro-angiogenic effects of the VEGF ligand by preventing it from binding to VEGFR2. This would theoretically result in the inhibition of new tumour growth, potential vessel regression through decreased vessel stabilisation, and eventually tumour cell death. For instance, without VEGF pro-survival signalling, ECs may undergo apoptosis due to a reduction in B-cell lymphoma2 (Bcl-2), and potentially detach from pre-existing vessel walls (Zaitoun *et al*, 2015). Additionally, blocking VEGF could prevent the recruitment of EC progenitor cells, a tumour associated angiogenesis process described in 1.3.3.2 (Niu and Chen, 2010).

In the UK, bevacizumab is approved to treat advanced EOC, in inoperable cases of EOC or in patients with residual disease following surgery. It is administered intravenously, once every 3 weeks at 15mg/kg in advanced EOC, alongside a regimen of chemotherapeutics, notably paclitaxel and carboplatin (Hall *et al*, 2020). Whilst clinical trials have shown an effect on overall and progression free survival, the effect is modest; Burger *et al* (2011) conducted a phase III trial on 1873 patients and reported that bevacizumab given throughout a chemotherapy cycle prolonged progression free survival by 3.8 months, compared with chemotherapy alone. More recently, Tewari *et al* (2019) found no significant differences in overall survival in the final report on this trial. A phase III trial (1528 patients) of 7.5mg/kg of bevacizumab (an off-label dosage) with standard chemotherapy reported a benefit on progression free survival of only 1.5 months compared with the control chemotherapy (Perren *et al*, 2011). This off-label dosage was used in an attempt to reduce the side effects associated with the treatment (Niu and Chen, 2010). However, another phase III trial by Aghajanian *et al* (2012) found a 4 month improvement of progression free survival in the bevacizumab treatment arm, compared with control. The differences in progression free survival between these trials is likely due to the different chemotherapy regimens, as well as differences in the age and type of disease in patients recruited (inoperable cases, residual disease, or relapse). A review by Garcia and Singh (2013) discusses phase II trials in addition to the phase III trials mentioned previously, concluding that all statistically improved progression free survival in ovarian cancer. Importantly however, no

improvement in overall survival has been reported. This suggests that bevacizumab improves progression free survival, but does not enhance survival in advanced EOC. The most common side effect of treatment of advanced EOC with bevacizumab is hypertension, presenting in approximately 20% of patients from 16 clinical trials, alongside typically asymptomatic proteinuria. In EOC patients, there is an established increased risk of venous thromboembolic events from having the disease (Tateo *et al*, 2005). A potentially more serious side effect of bevacizumab is increasing the likelihood of patients experiencing an arterial thromboembolic event, although this is has not yet been fully clarified in EOC. This is associated with the increased risk of bleeding due to decreased wound healing ability – a side effect common to all anti-angiogenic therapies due to the reduction of EC stability, proliferation, and migration (Stone *et al*, 2010; Zhao *et al*, 2017).

The seemingly short-lived beneficial effects of bevacizumab on extending progression free survival but not overall survival suggest that there are compensatory pathways of angiogenesis, and/or that the tumours and their vasculature are able to develop resistance to the treatment. It is also possible that this extension of progression free survival is yielded by a completely different mechanism altogether. Indeed, data from mice and tumour imaging studies have not demonstrated remarkable decreases in the size of tumours following bevacizumab treatment (Niu and Chen, 2010).

1.6.3.2 Receptor tyrosine kinase inhibitors

Another approach to reducing VEGF signalling in EOC is to target RTKs involved in pro-angiogenic signalling. In the case of VEGF, this typically involves targeting VEGFR2 specifically, or else pan inhibition of all VEGFRs. Drugs that do this often have inhibitory effects on other RTKs as well, typically PDGF receptors (Katopodis *et al*, 2019). In EOC, no drugs targeting RTKs to inhibit angiogenesis are currently licensed for use in the UK, but some have been or are currently undergoing trials. Some of these drugs are summarised in table 5, the list taken from Yang *et al* (2020). These drugs aim to work by inhibiting the cell signalling pathways (see section 1.6.2.1) induced by VEGF binding to receptors (primarily VEGFR2). Therefore VEGF still binds to a

receptor, but the triggering of intracellular autophosphorylation and signalling pathways is inhibited.

RTK inhibitor	Trial(s) description and outcomes
Sorafenib (pan VEGFR and Raf kinase inhibitor (upstream kinase of ERK))	Phase II trial: a two arm study of 174 patients reported improvement of 2.3 months progression free survival and 7 months for overall survival with sorafenib and standard treatment versus standard treatment alone (Chekerov *et al*, 2018).
Sunitinib (pan VEGFR, PDGF receptors, and CD135 inhibitor (an RTK on haematopoietic progenitor cells))	Phase II trial: a two arm study of 73 patients where one arm received non-continuous treatment with sunitinib, the other arm received continuous sunitinib treatment. The trial reported a progression free survival of 4.8 months in the non-continuous arm, and 2.9 months in the continuous. Overall survival for non-continuous was 13.6 months and 13.7 months for continuous (Baumann *et al*, 2012).
Pazopanib (pan VEGFR, PDGF receptors, and FGF receptors)	Phase II trial: a two arm study of 940 patients reported improvement of 5.6 months progression free survival with pazopanib and standard treatment versus standard treatment alone. No significant difference in overall survival was observed (du Bois *et al*, 2014).
Nintedanib (pan VEGFR, PDGF receptors, and FGF receptors)	Phase III trial: a two arm study of 1366 patients reported improvement of 0.6 months progression free survival with nintedanib and standard treatment versus standard treatment alone (du Bois *et al*, 2016).
Cediranib (pan VEGFR inhibitor)	Phase III trial: a three arm study of 456 patients; one arm received initial placebo with standard treatment followed by placebo maintenance, the second arm received cediranib and standard treatment followed by placebo maintenance, and the third arm received cediranib and standard treatment followed by cediranib maintenance. Progression free survival in arms two and three had a progression free survival of 1.2 and 2.3 months longer than the placebo arm

	(Ledermann *et al,* 2016). Arm three demonstrated an improvement of 7.4 months in overall survival compared to the placebo arm (Ledermann *et al,* 2021).
Trebananib (Tie-2 receptor inhibitor)	Phase III trial: a two arm study of 919 patients reported improvement of 2.2 months progression free survival with trebananib and standard treatment versus standard treatment alone. No significant difference in overall survival was observed (Monk *et al*, 2014).

Table 5. A summary of the efficacy of selected anti-angiogenic receptor tyrosine kinase (RTK) inhibitors in trials to treat epithelial ovarian cancer (EOC). RTK = receptor tyrosine kinase, VEGFR = vascular endothelial growth factor receptor, Raf = rapidly accelerating fibrosarcoma, ERK = extracellular signal-related kinase, PDGF = platelet-derived growth factor, FGF = fibroblast growth factor.

Anti-angiogenic RTK inhibitors do present an interesting avenue for the treatment of advanced EOC, with some showing more promise than others. Similarly with bevacizumab, studies often report an increase in progression free survival but no significant improvement in overall survival (not in all cases). However, there are also concerns about the side effects, which seem to be more adverse when targeting the VEGF ligand. These include gastrointestinal perforation, and an increased risk of hypertension, proteinuria and impaired wound healing. Indeed, the du Bois (2016) trial for nintedanib in table 5 observed three patient deaths directly linked to nintedanib, through complications associated with gastrointestinal perforations and sepsis. There remains the challenge (including in VEGF ligand therapies) of increasing selectivity for the tumour cells and tumour associated EC cells and signalling. Furthermore, and again similarly to bevacizumab, possible resistance development is also a problem with RTK inhibitors, as demonstrated by their overall moderate successes in trial and *in vivo* (Niu and Chen, 2010; Stone *et al*, 2010).

1.6.4 Evidence for non-VEGF pathways in EOC metastasis

Taking into account the pro-angiogenic factors secreted in addition to VEGF in table 4, this appears to offer a straight forward explanation for the lack of effectiveness of therapies targeting VEGF; the other pro-angiogenic factors offer compensatory pathways to facilitate the growth of new blood vessels. However, in the case of RTK inhibitors, it appears that the inhibition of the Tie-2 receptor, FGF receptors and PDGF receptors is ineffective due to limited successes in clinical trials and observations of no significant reductions in tumour growth. Additionally, multiple *in vitro* and *in vivo* pre-clinical studies have demonstrated that inhibition of VEGF signalling alone significantly reduces angiogenic activity of ECs, and/or tumour vessel formation and development, as reviewed by Niu and Chen (2010). For example, Yu *et al* (2011) targeted VEGF in an *in vitro* model where other pro-angiogenic molecules were present in the cell media, but were not targeted. The inhibition of VEGF signalling alone with bevacizumab was sufficient to significantly reduce the proliferation and migration of bovine retinal microvascular ECs. Moreover, a mouse model of EOC demonstrated that supplementing a chemotherapy treatment (cisplatin) with a VEGF inhibitor significantly reduced ovarian tumour angiogenesis *in vivo* (Mabuchi *et al*, 2008). These studies reiterate the evidence for the potency of VEGF as a pro-angiogenic factor, and also raises questions as to why targeting VEGF signalling has had little success in treating cancers, including EOC, as discussed in sections 1.6.3.1-2.

There is growing evidence for newly known pro-angiogenic molecules playing a role in EOC metastasis to the omentum. Winiarski *et al* (2013) identified the presence of angiogenesis related proteins in the ascites of EOC patients, and demonstrated their pro-angiogenic effects on disease relevant human omental microvascular endothelial cells (HOMECs) *in vitro*. One of these molecules, cathepsin-L (CL), was shown to increase HOMEC migration and tubule formation, and interestingly, to increase the expression of *LGALS1* (the galectin-1(gal-1) gene)) in HOMECs (unpublished data).

CL is a lysosomal protease involved in the degradation of proteins. Proteolytic enzymes are known to be involved in both the progression of cancer (see section 1.5.3.1) and in angiogenesis (1.3.1) due to their involvement in degrading basement membranes and the ECM (Sudhan and Siemann, 2015).

However, in EOC omental metastasis, Pranjol *et al* (2019) demonstrated that CL exerted pro-angiogenic effects (increased HOMEC proliferation) in a non-proteolytic manner. This suggested that CL was acting as a ligand, or through another molecule. Given the observation of increased *LGALS1* expression in CL treated HOMECs, and the implication of gal-1 in tumour angiogenesis (Croci *et al*, 2012; D'Haene *et al*, 2013), this thesis investigates the hypothesis that gal-1 is a pro-angiogenic factor in EOC omental metastasis.

1.7 Galectin-1

As well as the previously identified pro-angiogenic factors in EOC omental metastasis, there is growing evidence for the involvement of other molecules, for example CL and gal-1 (discussed in 1.6.4). Gal-1 is an interesting candidate for a pro-angiogenic molecule and is currently the focus of a lot of research. Gal-1 is a small glycoprotein known to interact with glycans, posing a whole new potential avenue within angiogenesis and cancer research (Astorgues-Zerri *et al*, 2006). This shall be discussed further in this section.

1.7.1 Structure

Galectins belong to the lectin family; a large group of carbohydrate-binding proteins. The galectin subfamily share the ability to bind to β-galactosidase containing sugars. A β-galactosidase is a glycoside (a sugar bound to another functional group), where the glycosidic bond lies in the plane above a galactose (a type of sugar) residue (Camby *et al*, 2006). Galectins bind to β-galactosidase through a conserved carbohydrate recognition domain; galectin-1 is a 'proto-type' galectin, as it consists of a single polypeptide chain, has one carbohydrate recognition domain, and can dimerise. Gal-1 is expressed in most cells, and is coded for by *LGALS1*; a gene encoding four exons that can be spliced to form the 135 amino acid protein, gal-1. Human gal-1 typically exists as a homodimer, but is known to dissociate into monomers at low concentrations (Bi *et al*, 2008). As gal-1 contains six cysteine residues (an unusually high number for a small protein) this leaves it vulnerable to oxidation, but this likelihood is reduced when in the dimer form. Importantly, gal-1 can still bind to β-galactosidase in both

forms (Camby *et al*, 2006). After synthesis on free polyribosomes, gal-1 can be located both intra and extracellularly. Externalised gal-1 binds to glycans present on the cell surface. Gal-1 is known to be secreted from cells in a golgi-independent manner, owing to its lack of a recognisable secretion signal sequence. Gal-1 is also therefore not subjected to golgi mechanisms of post-translational modification. There is scope to believe that gal-1 is secreted from cells via inside-out transportation where it directly translocates across the membrane, although membrane proteins involved in this have not yet been identified (Nickel, 2005). These properties and behaviours of gal-1 occur as part of normal cell regulatory processes, but can also be influenced by external factors. For example, external stimuli can promote the synthesis of gal-1, or its cleavage from the cell surface. Additionally, the microenvironment can influence the binding partners on the surface of the cell (Girotti *et al*, 2020).

1.7.1.1 Binding partners of galectin-1

Due to the presence of a carbohydrate recognition domain and subsequent ability to bind to β-galactosidase residues, the majority of gal-1 is thought to be involved in binding to carbohydrate based molecules. These interactions are thought to primarily occur on the surface of cells, where highly glycosylated proteins are located (Chandler and Costello, 2016). This provides a high number of binding sites for gal-1, the function of which are not yet fully elucidated. Additionally, gal-1 has also been shown to have binding partners within the cell that are carbohydrate recognition domain independent; these interactions are thought to be intracellular protein-protein interactions (Camby *et al*, 2006).

Carbohydrate binding

Gal-1 binds to glycosylated proteins. Glycosylation is a post-translational modification where glycans are added to molecules, typically within the endoplasmic reticulum (ER). Glycosylation serves several functions, primarily to ensure the correct folding of proteins, and to ensure their stability (Reily *et al*, 2019). Glycan is a term used to describe molecules that consist of a large number of sugar moieties linked via glycosidic bonds. Glycans are differentially glycosylated and largely fall into two main categories, N and O-linked glycans

(usually shortened to N- and O-glycans, respectively). In N-glycans, a glycan is added to the amide nitrogen of an asparagine residue on a protein; in O-glycans, a glycan is added to the oxygen atom of a serine or threonine residue within a protein. The initial O and N-glycan structures are synthesised in the ER, with various additional modifications occurring within both the ER and the golgi apparatus, by a multitude of enzymes. Gal-1 readily binds to both N and O-glycans present on glycosylated molecules (Christiansen *et al*, 2014). The amount of gal-1 binding to these N and O-glycans will vary as there are a large number of N and O-glycan varieties that vary in their side chain modifications. Importantly for gal-1 binding, this includes galactosylation: the addition of galactose moieties (Krautter and Iqbal, 2021). The carbohydrate binding ability of gal-1 also confers an ability to bind to elements of the ECM, such as the highly N-glycosylated components laminin and fibronectin (Camby *et al*, 2006).

Carbohydrate independent binding

As previously mentioned, it is thought that there are also intracellular protein-protein interactions. Interestingly, of the proteins identified to interact in this manner in the binding of gal-1, no common domains or structural motifs are present (Camby *et al*, 2006). These proteins are gem-associated protein 4 (Gemin4), and H-ras. Gemin4 is a component of the survival of motor neuron protein complex, as well as microRNA ribonucleoprotein particle. The survival of motor neuron protein complex is involved in the splicing of small nuclear ribonucleoproteins (snRNPs). snRNPs themselves are involved in the splicing (and thus removal) of introns (Paushkin *et al*, 2002). The involvement of gal-1 with H-ras is particularly interesting in ECs, due to H-ras being downstream of VEGFR2 signalling. Gal-1 has been shown to increase membrane-associated H-ras by promoting stability in its activated form, and may contribute to cell proliferation through resultant downstream signalling pathways (Prior *et al*, 2003).

The multiple different binding capabilities of gal-1 are implicated in its ability to produce many different effects in cells. The locations of gal-1 binding are summarised in figure 18. Overall, it is the glycosylation state of the cell surface that determines how much gal-1 binds to proteins. Interestingly, there is evidence that glycan bound galectins can cross-link, potentially forming lattices

or other structures that can induce signalling events and affect the retention of receptors on the cell surface (Partridge *et al*, 2004; Liu and Rabinovich, 2005).

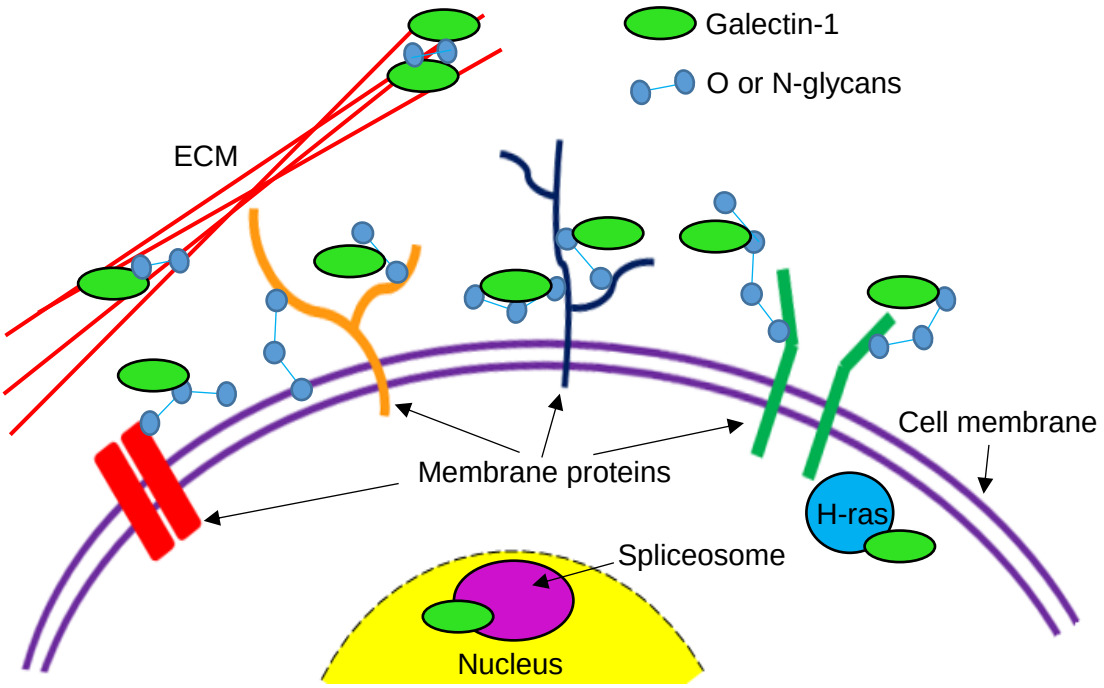

Figure 18. Cellular and extracellular locations of galectin-1 binding sites/partners. Galectin-1 (green) binds through its carbohydrate recognition domain to O and N-glycans (small blue connected circles), that are present on membrane proteins, and within the extracellular matrix (ECM; red lines). Intracellularly, gal-1 binds to the spliceosome within the nucleus, and to the small GTPase protein H-ras.

1.7.2 Functions of galectin-1

As discussed, gal-1 is expressed in most cells types, and has massive binding capabilities, both carbohydrate dependent and independent. Gal-1 is mostly known for its effects on immune cells, although there is growing evidence that implicates gal-1 in tumour development. Gal-1 is thought to mainly function by mediating cell-cell and cell-ECM interactions, which would concern carbohydrate dependent binding.

1.7.2.1 Galectin-1 and immune cells

Gal-1 is known to dampen immune responses. As discussed in section 1.1.2.1, leukocytes attach to and roll along the endothelium, in a highly studied and

documented process. However, whilst the main proteins involved in this multi-step process have been identified and studied, the glycosylation state of several proteins is also of interest. For example, it is known that both the selectins involved and intercellular adhesion molecule-1 are glycosylated. Glycan binding proteins, including gal-1, have been shown to interact with these proteins, and affect their role in leukocyte adhesion to endothelium. La *et al* (2003) showed that exogenous gal-1 inhibited leukocyte attachment, and hypothesised that this was due to gal-1 binding to glycans on selectins. Importantly, research on another galectin, galectin-3 (gal-3) has reported that its addition increases leukocyte recruitment, and indeed that a gal-3 KO *in vivo* model showed reduced leukocyte transmigration (Gittens *et al*, 2017). This is important as this suggests that despite the high binding capability shared by all galectins through the conserved carbohydrate recognition domain, that different galectins exert different effects on cells. Galectins are also implicated in leukocyte attachment through mediation of their binding to integrins; gal-1 can bind to N-glycans on α and β integrins, which are involved in leukocyte tethering. The exact effect of gal-1 is variable depending on the integrin type and elements within the ECM, and can be both pro and anti-adhesive (Camby *et al*, 2006). Gal-1 has also been shown to inhibit the recruitment and activation of neutrophils. Cooper *et al* (2008) showed that neutrophils treated with gal-1 had reduced expression of activation markers (upon stimulation), and also showed an increase in surface phosphatidylserine. This increase was associated with increased incidence of phagocytic removal of viable neutrophils.

Research has demonstrated that gal-1 plays a major role in T cell control; gal-1 can promote T cell death through binding to O and N-glycans present on various surface molecules present on various T cell subtypes. For example, T cells can be sensitised to the Fas-mediated extrinsic pathway of apoptosis by gal-1, by gal-1 interaction with Fas receptors, or the upregulation of Fas receptor surface expression (Matarrese *et al*, 2005). In terms of B cells, there is evidence suggesting that gal-1 is required for the induction of regulatory function. Indeed, Alhabbab *et al* (2018) demonstrated both *in vitro* and *in vivo* gal-1 deficiency confers impaired B cell cytokine expression.

1.7.2.2 Galectin-1 and tumour cell adhesion and extravasation

As discussed in sections 1.4.5.1 and 1.4.5.2, EOC is capable of metastasising from the primary site by both haematogenous and transcoelomic methods. The carbohydrate binding properties of gal-1 led to its implication in enhancing the adhesion of disseminated tumour cells at new sites. Gal-1 is thought to coat cancer cells by binding to the cell surface glycoprotein 90k (Grassadonia *et al*, 2002). Gal-1 has since been observed *in vitro* to enhance both prostate and ovarian cancer cell adhesion to glycoprotein components of the ECM, such as laminin and fibronectin (as reviewed by Cousin and Cloninger, 2016). During EOC metastasis to the omentum, disseminated cancer cells encounter fibronectin expressing mesothelial cells, therefore cancer cell surface bound gal-1 could enhance the adhesion of EOC cells to the omental mesothelial layer.

Similarly, there is a potential role for gal-1 in the extravasation of tumour cells at distant sites. The extravasation of tumour cells is a similar process to leukocyte adhesion and transmigration across the endothelium (described in section 1.1.2.1). Like leukocytes, it is thought that the endothelial location at which tumour cells adhere to is guided by certain chemokine signals (as reviewed by Strell and Entschladen, 2008). Interestingly, gal-1 has been shown to have contradictory effects when comparing leukocyte and tumour cell adhesion to endothelium. The adhesion of neutrophils pre-incubated with gal-1 to an activated HUEVC layer was significantly reduced (Cooper *et al*, 2008). However, Clausse *et al* (1999) observed that prostate cancer cells were more adherent to HUVECs pre-treated with gal-1. These observations suggest that the adhesive properties of gal-1 are process dependent, and that different mechanisms may be involved.

1.7.2.3 Role in angiogenesis

Normal vasculature is not associated with an increased expression of gal-1, but the tumour vasculature of multiple cancers, is. The majority of the literature of gal-1 in angiogenesis suggests that it plays a role in tumour associated angiogenesis, but some research has also suggested a role in physiological angiogenesis. It is thought that cell surface gal-1 is increased in areas of hypoxia (a feature of tumour areas, see section 1.3.3.3) as HIF-1α has been

shown to increase gal-1 mRNA (Zhao *et al*, 2010). In any case, the glycosylation on the EC surface would be a determining factor in whether extracellular gal-1 could act in a pro-angiogenic manner (Griffioen and Thijssen, 2014). The microenvironment influences cell surface glycosylation, and therefore the particular microenvironment of ECs will likely determine any involvement of gal-1 (Christiansen *et al*, 2014). This is discussed further in section 1.7.2.4.

The effect of galectin-1 on EC proliferation

Galectin-1 has been shown to be secreted by various tumour cells, as well as from other cells within the microenvironment. Current literature reports that gal-1 promotes the proliferation of tumour associated ECs, although the exact mechanism by which this happens is disputed (Griffioen and Thijssen, 2014). For example, Thijssen *et al* (2010) reported that gal-1 increased the proliferation of HUVECs in *in vitro* proliferation assays, and that a gal-1 -/- mouse model of tumour development showed decreased tumour microvessel density. Looking mechanistically, the group reported that gal-1 increased H-ras signalling in HUVECs, and therefore hypothesised this was responsible for the increase in cell proliferation. This is in line with Prior *et al* (2003), who demonstrated that gal-1 can stabilise membrane associated activated H-ras. Gal-1 induced EC proliferation via H-ras is particularly interesting, as their interaction has been shown to be carbohydrate binding independent. Paz *et al* (2001) blocked the carbohydrate recognition domain of gal-1 with an antibody, and gal-1 stabilisation and activation of H-ras was unaffected, indicating that the interaction was not through the carbohydrate recognition domain.

Another proposed mechanism for gal-1 induced EC proliferation is through its carbohydrate binding capabilities; various studies have suggested that gal-1 can act to activate VEGFR2, by binding to N-glycans on the receptor (Croci *et al*, 2014). Croci *et al* (2014) used lectin arrays to demonstrate that gal-1 could bind to tumour associated vessels from microenvironments that were associated with extensive cell surface N-glycosylation. These changes in glycosylation on the surface of ECs are thought to alter cell responses by masking or displaying ligands for lectins, and are discussed further in section 1.7.2.4. The group further demonstrated an association with high cell surface N-glycosylation in tumours that were resistant to anti-VEGF therapies, and that the

removal of these N-glycans re-sensitised the tumour associated ECs to the therapeutics.

The effect of galectin-1 on EC migration

Studies have also indicated that gal-1 exerts effects on VEGFR2 by enhancing the binding of one of its co-receptors, neuropilin-1 (NRP-1) to VEGFR2, in order to promote EC migration. Hsieh *et al* (2008) demonstrated that gal-1 increased the proliferation and migration of HUVECs, but that only the migration was associated with gal-1-NRP-1-VEGFR2 interactions. The group conducted binding studies of gal-1 on whole ECs, finding that gal-1 could only bind through its carbohydrate recognition domain to NRP-1, not VEGFR2. Importantly, the group used gal-1 in tandem with VEGF, and therefore concluded that gal-1 increases VEGF induced HUVEC proliferation and migration, but not necessarily that it is able to act in this way alone. Together with previous results on proliferation studies, it appears that pro-angiogenic effects of gal-1 are very much cell and/or microenvironment dependent, and reflect the differences in cell surface glycosylation.

In terms of cell adhesiveness, the interactions of gal-1 with integrins and subsequently, elements of the ECM, are variable. For example, gal-1 has been shown to interact with the α1β1 integrin in a manner that promotes cell motility, when the integrin is attaching the cell to laminin, but not fibronectin (Moiseeva *et al*, 2003). This implies that gal-1 mediated cell-ECM interactions are variable depending on the composition of the ECM.

The effect of galectin-1 on EC tubule formation

Ito *et al* (2011) reported that gal-1 increased HUVEC angiogenic tubule formation in Matrigel assays. The group inhibited this pro-angiogenic activity of gal-1 with thiodiagalactoside, a potent carbohydrate recognition domain inhibitor of gal-1, which successfully inhibited tubule formation. This suggested that gal-1 mediated tubule formation is dependent on carbohydrate binding through its carbohydrate recognition domain. Similarly, Laderach *et al* (2013) showed gal-1 induced tubule formation in bovine aortic endothelial cells. The group analysed conditioned media in prostate cancer cell lines, finding gal-1 to be the most abundantly overexpressed galectin. It was found that inhibition of gal-1 binding with a monoclonal antibody against the carbohydrate recognition domain

significantly reduced angiogenic tubule formation induced by the prostate cancer conditioned media. This further suggests that gal-1 can induce tubule formation through carbohydrate recognition domain binding. The molecular mechanism of this is still unclear, but D'Haeane *et al* (2013) showed that gal-1 induced tubule formation in HUVECs occurred primarily through the activation of VEGFR1, and partially VEGFR2, by differentially blocking the receptor with antibodies and adding gal-1. This is interesting as VEGFR1 is typically associated with sequestering VEGF as a regulatory mechanism, and warrants further research.

Altogether, there is evidence for pro-angiogenic effects of gal-1, although the exact effects appear to differ between both EC and disease type studied.

1.7.2.4 Galectin-1 and VEGFR2

N-glycosylation within ECs

Some of the pro-angiogenic effects of gal-1 discussed in section 1.7.2.3 result from the capability of gal-1 to bind to glycans through its carbohydrate recognition domain. These effects of gal-1 are dependent on the glycosylation state of the cell surface, and as such, need to be considered together when examining the effect of gal-1. This is particularly interesting in the case of ECs due to the presence of the glycocalyx (see section 1.2.4), which contains glycoproteins, glycolipids and proteoglycans: lipids and proteins that contain glycans. Glycans are initially synthesised in the ER before they are added to nascent proteins in subsequent enzymatic modifications in the golgi apparatus (Reily *et al*, 2019). It is thought that cytokine signalling from the microenvironment can alter glycan processing within ECs; by either up or downregulating different golgi glycosylation enzymes (Chandler *et al,* 2019a). In the context of cancer, Croci *et al* (2018) suggested that cancer cells in the tumour microenvironment can contribute to anti-angiogenic therapy resistance in late stage cancer by releasing anti-inflammatory cytokines such as interleukin-10 or TGF-β1. These cytokines were thought to affect golgi enzymes and alter the glycans on the cell surface. Scott *et al* (2013) also demonstrated that endothelial expression of N-glycans was altered in response to TNF-α (a pro-inflammatory cytokine), in five different human arterial beds. Interestingly

the group found differences in the basal cell surface N-glycosylation between the five types of EC, suggesting that this contributes to EC heterogeneity.

The relationship between N-glycans, VEGFR2 and galectin-1

The extracellular portion of VEGFR2 contains 18 potential sites where N-glycans can bind, giving it potential to be a highly N-glycosylated RTK. Depending on the number and branching of the N-glycans bound, it is thought that various combinations of these glycan epitopes are displayed, to which lectins can bind (Lau *et al*, 2007). It is thought that these N-glycans present on VEGFR2 are complex N-glycans (Patnaik *et al,* 2006; Chandler *et al*, 2019a). Croci *et al* (2018) have suggested that lectin binding to such N-glycan sites on VEGFR2 can prevent endocytosis of the receptor and therefore prolong VEGF-VEGFR2 signalling. It is currently unclear whether in VEGFR2, if these N-glycan-lectin interactions are sufficient to activate the receptor, or act by enhancing VEGF binding (Stanley, 2014).

1.7.2.5 Galectin-1 in angiogenesis during EOC metastasis

Gal-1 is overexpressed in EOC patients with metastatic disease (see table 6) and is therefore of interest as a potential prognostic biomarker. It is unclear how exactly gal-1 might contribute to EOC development, as gal-1 is thought to be involved in dampening the immune response, tumour cell adhesion, and also angiogenesis.

Group	Number of patients	Median gal-1 (ng/ml)	Range
Healthy donors	70	88	30 - 231
Benign gynaecological tumours	60	78	30 - 229
EOC stage I (non-metastatic)	44	69	30 - 163
EOC stage II	35	260	30 - 390
EOC stage III	46	352	170 - 610
EOC stage IV	15	630	480 - 950

Table 6. Levels of galectin-1 in the sera of healthy patients, and patients with non-metastatic and metastatic epithelial ovarian cancer (EOC). Metastatic disease is classified as EOC stages II-IV (see table 3). Gal-1 = galectin-1 (data taken from Chen *et al*, 2015).

Patients in this study by Chen *et al* (2015), EOC patients showed median gal-1 sera levels in the hundreds in all stages of metastatic EOC. It is important to note that these patients were identified as having established cancers that had been treated with at least one surgery. Furthermore, the sera level of gal-1 in healthy patients is known to have a large range, thus its limited use as a diagnostic biomarker (Labrie *et al*, 2017). Interestingly, a recent study by Masoodi *et al* (2021) reported a median gal-1 sera of 40.57 ± 22.2ng/ml in patients with advanced EOC, at the time of diagnosis (and therefore no surgeries). This level was still significantly higher than observed in healthy patients (9.19 ± 4.61ng/ml). This suggests that gal-1 sera levels are raised in patients with advanced EOC.

Whilst it is largely unknown if gal-1 contributes to tumour angiogenesis in EOC, there is literature on the expression of gal-1 in other types of tumour cells, as well as within EOC cells and within tumour associated vasculature (Shimada *et al*, 2020). However, there is also recent evidence that gal-1 is secreted by ECs themselves – importantly, by the microvascular ECs in the omentum (HOMECs) (Winiarski *et al*, 2013; and unpublished data). Furthermore, Pranjol *et al* (2019) showed that HOMECs produce gal-1 after treatment with CL, an EOC cell derived protease. This was interesting as this was shown to occur non-

proteolytically, suggesting that the HOMEC derived gal-1 was not simply cleaved off the cell surface. These data and literature that implicates gal-1 in certain cases of tumour associated angiogenesis suggest that gal-1 is a good candidate for study as a pro-angiogenic molecule in EOC.

As discussed earlier in section 1.5.3.2, the omentum is a key site for metastasis in most cases of advanced EOC, and offers EOC cells a particularly good site to develop secondary tumours. As discussed in section 1.2, ECs are heterogeneous, and as discussed in sections 1.7.2.3-4, potential pro-angiogenic effects of gal-1 appear dependent on the influence of the microenvironment, as well as the type of ECs used in study. In section 1.7.2.4, potential molecular mechanisms of gal-1 induced activation of VEGFR2 are discussed, including a mechanism that does not require the VEGF ligand. Therefore, this work fits into the context of advanced EOC being difficult to target with anti-angiogenics that target VEGF-VEGFR2 signalling (see section 1.6.3), and could potentially identify reasons for ineffectiveness and/or resistance. The overall aim of this thesis is to therefore examine the role of gal-1 as a potential pro-angiogenic molecule in EOC omental metastasis, using disease relevant ECs (HOMECs).

1.8 Hypothesis and aims

This thesis hypothesises that:

Galectin-1 exerts pro-angiogenic effects on HOMECs

This hypothesis will be tested with the following aims:

1. Develop an improved protocol to isolate HOMECs from patient omenta

2. Investigate functional angiogenic effects of gal-1 on HOMECs

3. Investigate molecular mechanisms behind angiogenic effects of gal-1 on HOMECs

Chapter 2. Materials and Methods

2.1 Materials

2.1.1 Consumables, reagents and cells

Alpha laboratories

Non-filter tips, Eppendorf tubes (1.5ml – 5ml)

Biolegend

Cyto-Fast Fix Perm solution, Cyto-Fast Perm wash solution, Trustain

Bio-Rad

T20 cell counter slides, Trypan blue

Biotechne

Cultrex cell migration assay kit (96-well)

CellBiologics

Human retinal endothelial cells (HRECs)

Corning

CoolCell freezing container

JFA

Woven sterile gauze swabs 10cm x 10cm

Merck

BrdU cell proliferation kit, Cathepsin L from human liver, Guava easyCheck kit, 30µm nylon net filters

Enzo Life Sciences

Collagen type I from rat tail

European Collection of Authenticated Cell Cultures

SKOV3 cells, A2780 cells, A431 cells

Peprotech

Human galectin-1 (recombinant), Human VEGF-A_{165} (recombinant)

Promocell

Endothelial cell basal medium MV2, Endothelial cell growth MV2 kit

R&D Systems

Human galectin-1 ELISA, Human VEGF-A_{165} ELISA, Human phospho-VEGFR2 ELISA kit, DuoSet ELISA ancillary reagent kit 2, Human phospho-receptor tyrosine kinase array kit, Human phosphokinase proteome profiler kit

Sarstedt

Vented T75 and T25 flasks for sensitive adherent cells

Sigma

Heat inactivated foetal calf serum (FCS), Gentamicin, Penicillin-Streptomycin, Dulbecco's Modified Eagle's Medium (DMEM), DMEM – high glucose, Roswell Park Memorial Institute (RPMI)-1640, L-glutamine, Bovine serum albumin (BSA) powder, Dimethyl sulfoxide (DMSO), (Ethylenedinitrilo)tetra-acetic (EDTA) acid, Gelatin powder (from bovine skin), Hank's balanced salt solution (HBSS) with phenol red 10x, HEPES solution, HEPES powder, Amphotericin B solution, Sodium Chloride (NaCl), Potassium chloride (KCl), HEPES powder, D-glucose, Calcium chloride ($CaCl_2$) solution, Corning sterile plastic-ware (plates, Pasteur pipettes, Cell scrapers, Petri dishes), Millicell easy slide sterile 8-well chamber slides, Trypsin, Water soluble tetrazolium salt-1 (WST-1), SU5416, Swainsonine (synthetic), Calcein-AM, 100% methanol, 4% methanol free paraformaldehyde (PFA), DAPI, Goat serum, Gold anti-fade mountant, Triton-X solution, RIPA buffer, Protease Inhibitor Cocktail (mammalian cell and tissue extracts), Phosphatase inhibitor cocktail 2, Phosphatase inhibitor cocktail 3, Accutase, Propidium iodide (PI) solution

ThermoFisher Scientific

Collagenase type I powder, Collagenase type II powder, Phosphate buffered saline without calcium/magnesium (PBS), CD31 dynabeads, Dynamag 1.5ml, Pierce bicinchoninic acid (BCA) protein assay kit

VH Bio

Human cerebral microvascular endothelial cells (hCMEC/D3 cells)

2.1.2 Primary antibodies

Antibody	Source company	Species	Conjugated probe	Working concentration /dilution
CD31	Sigma	Mouse monoclonal	-	1:100
vWF	Sigma	Rabbit polyclonal	-	1:200
Galectin-1	Abcam	Rabbit polyclonal	-	1µg/ml
VEGFR2	Abcam	Rabbit polyclonal	-	5µg/ml
VEGFR2	Thermo-Fisher Scientific	Mouse monoclonal	-	1:200
VEGFR2	Biolegend	Mouse monoclonal	AlexaFluor 488	1µl/200,000 cells
Total PLCγ1	Cell Signalling Technology	Rabbit polyclonal	-	1:50
Phos-phorylated PLCγ1	Sigma	Mouse monoclonal	AlexaFluor 488	1µl/200,000 cells

2.1.3 Secondary antibodies

Antibody	Source company	Working concentration/dilution
Goat anti-mouse AlexaFluor 488	ThermoFisher Scientific	1µg/ml
Goat anti-rabbit AlexaFluor 488	ThermoFisher Scientific	1µg/ml
Goat anti-rabbit Alexa Fluor 594	ThermoFisher Scientific	1µg/ml
Goat anti-rabbit Cy5	Abcam	1µg/ml

2.2 Cell culture solutions

2.2.1 Complete growth media for HOMEC, HREC and hCMEC/D3 cells

Endothelial cell basal medium MV2	
Heat inactivated FCS	5% (v/v)
Gentamicin	50µg/ml

Endothelial cell growth MV2 kit	
VEGF-A_{165}	0.5ng/ml
Human EGF	5ng/ml
Human bFGF	10ng/ml
IGF1	20ng/ml
Ascorbic acid	1µg/ml
Hydrocortisone	0.2µg/ml

2.2.2 Complete growth media for human brain vascular pericytes

Pericyte medium	
Heat inactivated FCS	2% (v/v)
Pericyte growth supplement	1%
Penicillin-streptomycin	1%

2.2.3 Complete growth media for HOMeso cells

DMEM	
Heat inactivated FCS	20% (v/v)
Gentamicin	50µg/ml

2.2.4 Complete growth media for A2780 cancer cells

RPMI-1640	
Heat inactivated FCS	10% (v/v)
L-glutamine	2mM
Gentamicin	50µg/ml

2.2.5 Complete growth media for SKOV3 cancer cells and human omental fibroblast (HOF) cells

DMEM	
Heat inactivated FCS	10% (v/v)
Gentamicin	50µg/ml

2.2.6 Complete growth media for A431 cells

High glucose DMEM	
Heat inactivated FCS	10%
Penicillin-streptomycin	1%
L-glutamine	4mM

2.2.7 Starvation media

Endothelial 2% starve media

Endothelial cell basal medium MV2	
Heat inactivated FCS	2% (v/v)
Gentamicin	50µg/ml

Endothelial 0.1% BSA starve media

Endothelial cell basal medium MV2	
BSA	0.1% (w/v)
Gentamicin	50µg/ml

HOMeso starve media

DMEM	
Heat inactivated FCS	5% (v/v)
Gentamicin	50µg/ml

A2780 starve media

RPMI-1640	
Heat inactivated FCS	2% (v/v)
L-glutamine	2mM
Gentamicin	50µg/ml

SKOV3 starve media

DMEM	
Heat inactivated FCS	2% (v/v)
Gentamicin	50µg/ml

2.2.8 Freezing solution for HOMEC, HREC, and hCMEC/D3 cells

Complete endothelial MV2 media	20% (v/v)
Heat inactivated FCS	70% (v/v)
DMSO	10% (v/v)

2.2.9 Freezing solution for A2780 cells

Complete RPMI-1640	70% (v/v)
Heat inactivated FCS	20% (v/v)
DMSO	10% (v/v)

2.2.10 Freezing solution for SKOV3 and HOF cells

Complete DMEM	70% (v/v)
Heat inactivated FCS	20% (v/v)
DMSO	10% (v/v)

2.2.11 Plastic/glass coating solutions for endothelial and HOMeso cells

HOMECs	2% gelatin (w/v)
HREC, HOMeso cells and hCMEC/D3s	2.5µg/ml collagen I from rat tail

Gelatin powder was dissolved in distilled water before autoclaving. Collagen I solution was prepared with PBS. Both solutions were added to plastics for a minimum of 1 hour at 37°C before aspiration just prior to cell seeding.

2.2.12 Omental sample collection medium

HBSS 10x	10% (v/v)
Autoclaved distilled water	-
HEPES	50µM
Gentamicin	50µg/ml
Amphotericin B	250µg/ml

Autoclaved distilled water was added to the final volume of 500ml.

2.2.13 Collagenase I digest solution (stored at -20°C)

Reagent	Amount	Final concentration
Collagenase type I powder	0.75g	-
NaCl	3.5g	120mM
KCl	1.87g	50mM
HEPES powder	2.98g	25mM
D-glucose	0.045g	500µM
BSA	7.5g	1.5% (w/v)
$CaCl_2$	500µl of 1M stock	1mM

Each lot of collagenase type I powder contains a mix of isoforms varying in molecular weight from 68 – 130kDa. Autoclaved distilled water was added to the final volume of 500ml (pH was adjusted to 7.4).

2.2.14 Collagenase II digest solution (stored at -20°C)

Reagent	Amount	Final concentration
Collagenase type II powder	0.75g	-
NaCl	3.5g	120mM
KCL	1.87g	50mM
HEPES powder	2.98g	25mM
D-glucose	0.045g	500µM
BSA	7.5g	1.5% (w/v)
$CaCl_2$	500µl of 1M stock	1mM

Each lot of collagenase type II powder contains a mix of isoforms varying in molecular weight from 68 – 130kDa. Autoclaved distilled water was added to the final volume of 500ml (pH was adjusted to 7.4).

2.2.15 BSA solutions (stored at -20°C)

Reagent	Mass	Final concentration
BSA	10g and 0.1g	10% and 0.1% (w/v)

BSA powder was dissolved in 100ml PBS and sterile filtered.

2.3 Cell experimentation methods

2.3.1 Cell culture

All cells were cultured in humidified incubators at 37°C, 5% CO_2 under atmospheric levels of O_2. Cells were fed every 2 - 3 days and were grown to approximately 90% confluency before either being passaged or seeded for experiments. Cells were observed using an EVOS Cell Imaging microscope (phase-contrast). Plastics and glassware for endothelial and HOMeso cells were coated with the appropriate solution (see 2.2.11) for a minimum of 1 hour at 37°C and rinsed with PBS prior to use. Cancer cells, fibroblasts and A431 cells were grown directly on plastics. For cell passaging, growth media was

aspirated, followed by two 30 second rinses with PBS. The second wash was aspirated and trypsin was added (1.5ml for T75 flasks, 750µl for T25 flasks) and spread evenly across the cell layer. The cells were placed in the incubator until sufficient detachment was observed. Trypsin was neutralised with the addition of 8ml of 5% FCS containing medium, or 4ml of 10% FCS containing medium. The cell suspension was collected, transferred to a falcon tube and centrifuged for 5 minutes at 200*g*. The supernatant was removed and cells were resuspended in either complete or serum free growth media (amount dependent on passaging ratio or seeding conditions). Cells were counted with a Bio-Rad cell counter or manually with a haemocytometer. HOMEC populations were typically expanded between passages 1 - 3 and used in experiments between passages 4 - 7. hCMEC/D3 cells were used between passages 27 - 35; HRECs between passages 3 - 10. HOFs were used between passages 3 - 7; HOMeso cells between passages 2 - 6. Human brain vascular pericytes were used between passages 4 – 13. Thawed cells were passaged at least once before being used in experiments.

2.3.1.1 Freezing cells

Cells were trypsinised and centrifuged as described in section 2.3.1. Cells were resuspended in the appropriate freezing medium, counted, and aliquoted into cryogenic storage vials at a concentration of 1,000,000 cells/ml. The vials were transferred to a CoolCell freezing container for a facilitated cooling rate of 1°C/minute in a -80°C freezer before being moved to long term storage in liquid nitrogen.

2.3.1.2 Thawing cells

Cells were defrosted with the addition of warm compete growth media and gentle pipetting. Defrosted endothelial, HOFs and HOMeso cells were transferred to a T75 flask in 20ml media (to dilute the DMSO) and left to adhere overnight. The media was changed the next day. Cancer cells were defrosted as described previously before transferral to a falcon tube containing 5ml complete growth media. Cells were pelleted at 200*g* for 5 minutes and transferred to a T75 containing 10ml complete growth media.

2.3.1.3 HOMEC isolation

Non-malignant omental tissue samples were collected from biologically female patients undergoing invasive abdominal procedures at the Royal Devon and Exeter NHS Foundation Trust, following informed written consent (SW REC2 #2003/2/26). Information on cancer diagnosis, stage, and patient ethnicities was not provided. After the tissue sample was collected during surgery, it was transferred to a pot containing the collection media described in 2.2 and kept at 4°C before commencement of the isolation protocol the following day. HOMECs were initially isolated as described by Winiarski *et al* (2011), which is summarised as follows.

Omental samples were inspected for obvious areas of fibrotic tissue and macrovessels, both of which were dissected out with scalpels. The remaining tissue was chopped into roughly 1g pieces, and added to pre-warmed collagenase II solution at a volume ratio of 1:1 collagenase:tissue for a 20 minute digestion at 37°C on a rotary mixer at 20rpm. Remaining tissue pieces were removed, dissected as small as possible, and washed 4 times with PBS. Tissue pieces were then added to collagenase I (1:1 volume ratio of collagenase:tissue) for a further 120 minutes at 37°C on a rotary mixer at 20rpm.

Digested tissue was squeezed through 2 layers of woven sterile gauze to a new tube in order to remove undigested tissue; the filtrate was centrifuged at 350*g* at 4°C to separate into layers of cell pellet, collagenase solution, and oil. The oil and collagenase were aspirated, the cell pellet was resuspended in cold 10% BSA/PBS (w/v) and re-pelleted (600*g* at 4°C). The cell pellet was resuspended in cold PBS and pelleted again at (600*g* at 4°C). The washed pellet was resuspended in cold serum free MV2 medium and filtered through a 30µm nylon swinnex filter. Microvascular fragments caught on the filter were harvested and this process was repeated 3 more times. The final cell suspension was centrifuged at 350*g* and the media was aspirated. Immunoselection using anti-CD31 dynabeads was carried out on the microvascular fragments collected from the filter to isolate HOMECs from any remaining contaminant cells. The microvascular fragment mixture was incubated with 5µl of dynabeads in 500µl of 0.1% BSA/PBS (w/v) for 20 minutes at 4°C on a roller, and then placed in a DynaMag for 2 minutes to allow magnetic separation. The 0.1% BSA/PBS (w/v)

solution (containing unbound cells) was removed by pipette and replaced with new 0.1% BSA/PBS (w/v). This was mixed with the bead/fragment mixture and magnetic separation was performed again, a total of 4 times. After the final separation, HOMECs from microvascular fragments (bound to beads) were cultured in complete endothelial medium, with repeated immunoselection if necessary at the first passage. This method was followed until the development of the newer method described in 3.3.6. Isolated HOMECs, regardless of protocol, were always characterised with immunocytochemistry (ICC), as described in section 2.3.4.4.

2.3.1.4 Removal of contaminant fibroblasts in HOMEC cultures by differential trypsinisation and manual removal

It was observed that fibroblasts typically trypsinised off from wells before HOMECs. Therefore, during passaging, trypsinisation was studied by microscopy to monitor fibroblast detachment. When this occurred (and before HOMECs started to detach) the trypsin was neutralised and the solution was aspirated. Remaining cell passaging was then carried out as described in 2.3.1. Areas identified as fibroblast clusters were marked and removed by scratching with a pipette tip.

2.3.2 Cell viability and proliferation assays

Cell viability and proliferation were assessed in response to certain molecules and conditions. Cell viability was assessed using the commercially available WST-1 reagent; the assay was typically run over 3 days (timepoints at 24, 48 and 72 hours) and therefore some results were interpreted as an indication of cell proliferation despite the metabolic basis of the assay. Cell viability was also studied on a shorter term basis when investigating toxicity of swainsonine (SW) (over 24 hours) and U73122 for 1 hour. Following the addition of WST-1, oxidoreductase enzymes externalised by the cells reduce the tetrazolium salt to a soluble formazan product (which is then measured by spectrophotometer).

For a second method, the BrdU assay was used; this assay works through horseradish peroxidase (HRP) detection of BrdU that is incorporated into cells

when DNA is replicated. This assay therefore differs from WST-1 as it indirectly measures DNA synthesis.

During cell seeding, cell viability was assessed using trypan blue. Cells were pelleted, and resuspended in either media or PBS before 10µl of suspension was mixed with 10µl of trypan blue. Cells were immediately analysed by cell counter.

2.3.2.1 WST-1 assay

HOMECs/HRECs or hCMEC/D3 cells were seeded into 96-well plates at 10,000 cells/well with a well volume of 100µl. After attachment, cells were starved overnight in 2% starve media. Controls included cells grown in complete media and wells containing only media (blank). In some experiments SU5416 (SU) was used to inhibit VEGFR2 activation (Mendel *et al*, 2000), whereas swainsonine (SW) was used to reduce gal-1 binding to the surface of the cells (Galustian *et al*, 1994; Thompson *et al,* 2012), and U73122 was used to inhibit PLCγ1 phosphorylation (Peng *et al*, 2008). Treatments were added in 2% starve media (see table 7). At each timepoint, 10µl of WST-1 was added to all wells and incubated for 2 hours. Absorbance was measured at 450nm on a PHERAstar Plus Optima plate reader. Blank values were taken away from all experimental wells.

Reagent	Concentration
Galectin-1	1, 5, 10, 25, 50, 125 ng/ml
Swainsonine	100, 500ng/ml 1, 5, 10, 20µg/ml
SU5416	10µM
U73122	0.1, 1, 2.5, 5, 7.5, 10µM

Table 7. Concentrations of all reagents tested against cell proliferation and/or toxicity.

2.3.2.2 BrdU assay

A commercially available BrdU kit was used. HOMECs/HRECs or hCMEC/D3 cells were seeded into 96-well plates at 10,000 cells/well with a well volume of

100µl. After attachment, cells were starved overnight in 2% starve media. Controls included cells grown in complete media and wells containing only media (blank). Treatments were added in 2% starve media (gal-1: 1 - 125ng/ml; see table 7). To allow time for BrdU incorporation, 20µl of working dilution BrdU reagent was added 24 hours before each experimental timepoint (meaning that BrdU was added with the 24 hour treatment, and after 24 and 48 hours for 48 and 72 hour timepoints respectively). Incorporated BrdU was detected with a monoclonal antibody followed by a peroxidase conjugate secondary with substrate reaction, carried out according to manufacturer's instructions. Plates were read at 450/540nm on a SpectraMAX plate reader.

2.3.2.3 Short-term galectin-1 treatment viability assays

To investigate whether short-term treatments of gal-1 could affect cell viability and proliferation, both WST-1 and BrdU assays were used. Cells were seeded and prepared as described in 2.3.2.1 and 2.3.2.2, except only treatments of 5 and 50ng/ml of galectin-1 were tested. The treatments were applied to cells for 10 minutes, before treatment wells were aspirated and replaced with 2% starve media. WST-1 and BrdU protocols were then carried out as described previously, after 24 hours.

2.3.3 Cell migration assays

In order to assess the effect of gal-1 on HOMEC migration, two different types of assay were used. The scratch assay was used to study cell migration on a 2D surface and to monitor migration over time. 3D cell migration, specifically chemotaxis, was studied using the Cultrex migration assay, a simplified Boyden chamber assay with an 8µm pore membrane. This assay can be used to study both chemokinesis or chemotaxis, depending on the treatment of cells and which chamber i.e. upper or lower, the treatments are added to.

2.3.3.1 Scratch assay procedure

HOMECs were seeded in 96-well plates and cultured in complete media until a confluent monolayer formed. Cells were starved overnight in 2% starve media.

Cells were scratched through the centre of the monolayer with a 200µl pipette tip and the media was aspirated. Treatments were added to wells in 2% starve media (see table 8), with 0.2ng/ml VEGF as a positive control where indicated. Wells were photographed at 0, 8, and 16 hours post scratch using a phase contrast microscope at x10; the centre of the well was positioned centrally in all photographs.

Reagent	Concentration
Galectin-1	5, 50ng/ml

Table 8. Treatments and concentrations used in scratch assays.

2.3.3.2 Scratch assay analysis

Photographs were analysed using ImageJ. The edges of the scratches were marked, before 20 evenly spaced horizontal distances across the scratch were measured and a mean distance calculated. The 0 hour timepoint was interpreted as 100% of the scratch; 8 and 16 hour timepoint mean distance measurements were expressed as a percentage of the 0 hour measurement.

2.3.3.3 Cultrex chamber migration assay

A commercially available kit was adapted for use. HOMECs starved in 2% starve media were seeded into the upper chamber of the inserts at 10,000 cells/well. Starve media containing the two gal-1 treatments was added to the bottom chamber (see table 8). 0.2ng/ml VEGF was used as a positive control; this concentration was quantified from A2780 and SKOV3 conditioned media, and had previously been shown to significantly induce angiogenic processes (proliferation, migration) in HOMECs (unpublished data from this lab). The plate was incubated for 8 hours. After incubation, the top chamber was aspirated carefully and washed with the supplied wash buffer. This was repeated for the bottom chamber. Cell dissociation buffer containing 2µM calcein-AM was added to the bottom chamber and incubated for 30 minutes. The plate was tapped to dislodge any remaining cells, and incubated for another 30 minutes. The dissociation buffer/calcein-AM solution containing labelled cells was transferred to a black plate and fluorescence was read on a SpectraMAX plate reader at 488/520nm.

2.3.4 Immunocytochemistry

HOMEC populations isolated from patient omenta were characterised with ICC before use, to confirm endothelial identity (Winiarski *et al*, 2011). CD31 and vWF were used as endothelial cell markers, necessitating both extracellular and intracellular staining. Immunocytochemistry was utilised to study extracellular and intracellular presence of gal-1, as well as the presence of extracellular VEGFR2. All staining was performed on glass 8-well chamber slides.

2.3.4.1 Intracellular fixing

For intracellular targeted staining, the media was aspirated from cells and 300µl ice-cold methanol was added to wells. The slides were incubated for 10 minutes at -20°C before being washed 4 times (2 minutes each time) with PBS.

2.3.4.2 Extracellular fixing

For extracellular targets, the media was aspirated from cells and 300µl of 4% (w/v) methanol-free PFA was added to wells. The slides were incubated for 20 minutes at room temperature (RT) before being washed 4 times (2 minutes each time) with PBS.

2.3.4.3 Staining protocol

Staining was either performed immediately after fixing/washing, or 500µl of PBS was added to wells and the slides were kept at 4°C for a maximum of 2 days. Cells were blocked to prevent non-specific binding of antibodies with a 2% BSA/5% goat serum in PBS (w/v and v/v, respectively) for 1 hour at RT. Since all secondary antibodies used were produced in goat, only goat serum was used. Primary antibodies were added in PBS at the manufacturer's recommended dilution (see 2.1.2) except for the rabbit VEGFR2 antibody; in this case the recommended concentration was 1µg/ml, but following antibody titre, concentrations of 5µg/ml were found to be optimal for staining. Primary antibodies were incubated with cells overnight at 4°C to maximise binding. The wells were washed 4 times with PBS before secondary antibodies were added. All AlexaFluor secondary antibodies were used at 1µg/ml in PBS (adding in 2%

(w/v) BSA/5% (v/v) serum was not found to be of any benefit) and were incubated in the dark for 1 hour at RT. Secondary only wells were used as a non-specific binding control. The wells were washed 4 times with PBS. Cell nuclei were counterstained with DAPI at 1µg/ml in PBS for 10 minutes at RT. The wells were washed a final 3 times with PBS and one final wash with ddH_2O. The chambers were removed and excess ddH_2O was allowed to evaporate; slides were not allowed to dry out fully. Coverslips were added to the slides using Gold Antifade Mountant and sealed with nail varnish. Cells were imaged using an EVOS fluorescent microscope.

2.3.4.4 HOMEC characterisation

For CD31 staining, HOMECs were seeded after a morphologically homologous endothelial appearing population had been cultured, typically between passages 2 - 3. The cells were grown to a confluent monolayer to allow for intercellular junction CD31 expression, before being fixed as described in 2.3.4.2 and stained. For vWF staining, cells were grown to 50% confluence and fixed as described in 2.3.4.1 (see figure 19).

A method of extracellular staining (see 2.3.4.2) followed by cell permeabilisation with 0.1% (v/v) Triton-X, to facilitate intracellular staining for vWF on the same cells, showed significant background staining and therefore CD31 and vWF staining were performed separately.

a)

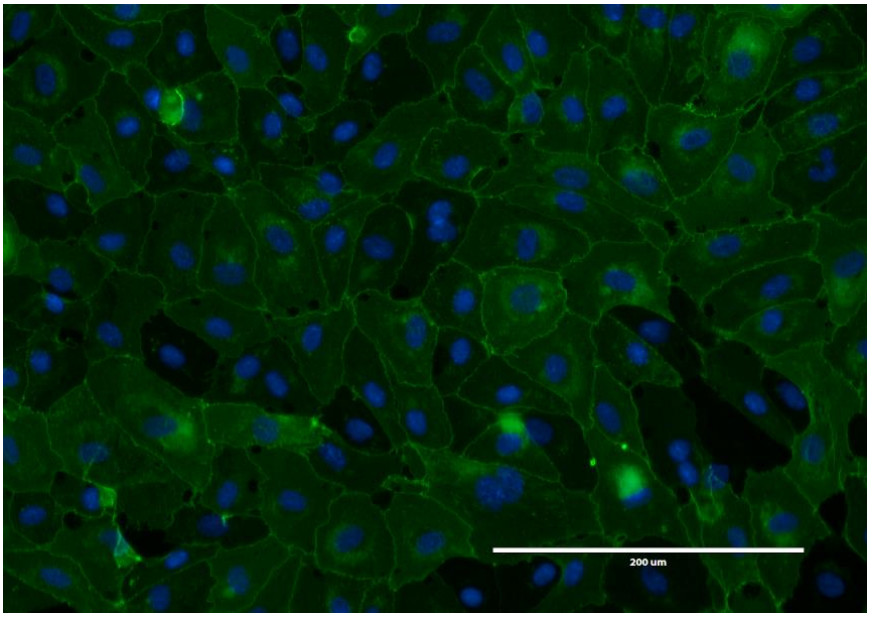

b)

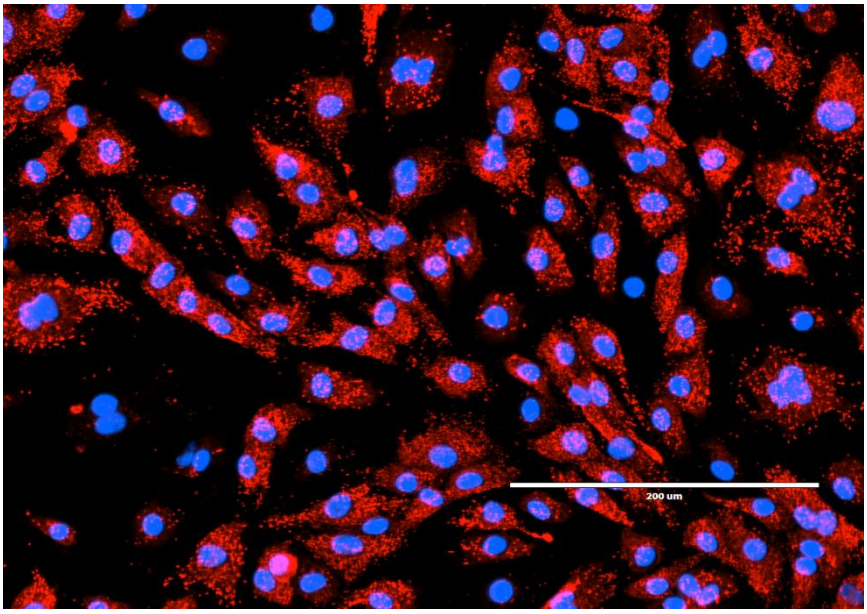

Figure 19. Characterisation of HOMECs using immunocytochemistry. a) Cells stained for extracellular CD31 (green). b) Cells stained for intracellular vWF (red). Nuclei are stained blue with DAPI. Scale bar = 200µm.

2.3.4.5 Extra and intracellular galectin-1 in HOMECs treated with cathepsin-L

To study the extra and intracellular localisation of gal-1, HOMECs were seeded at 30,000 cells/well in 8-well chamber slides. When cells reached approximately 80% confluency, cells were starved overnight in 2% starve media. 50ng/ml of CL was added in 2% starve media for various durations before the cells were fixed for either extra or intracellular staining of gal-1. The length of treatment was different for extra and intracellular staining (see table 9).

Extracellular timepoints	Intracellular timepoints
0 minutes	0 minutes
5 minutes	30 minutes
10 minutes	4 hours
30 minutes	8 hours
4 hours	24 hours

Table 9. Duration of 50ng/ml cathepsin-L (CL) treatment of HOMECs prior to galectin-1 staining.

Cells were stained for gal-1 and the nuclei counterstained with DAPI. Control cells underwent a media change to fresh 2% starve media and were fixed at identical timepoints.

2.3.4.6 Analysis of galectin-1 fluorescence in HOMECs

Immunocytochemistry images were analysed using ImageJ; fluorescence intensity (FI) was calculated by measuring fluorescence from 5 individual cells/timepoint from 3 different experiments. Cells from individual wells in the 8-well chamber slides were selected as shown in figure 20. The well was approximately divided into quadrants, with one cell from each being selected for analysis in the centre from each quadrant, as well as one from the middle of the well. Additionally, cells selected had to not be folded, or observed to be dividing.

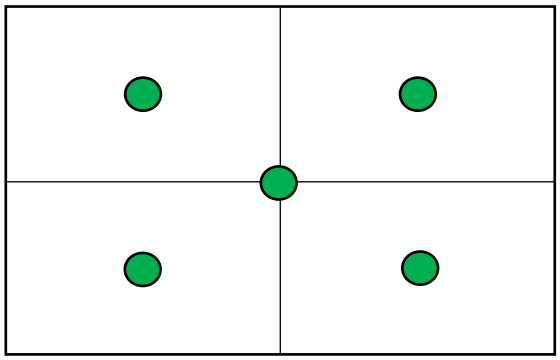

Figure 20. Schematic representation of an individual well from an 8-well chamber slide. Green circles indicate the approximate locations of cells selected for analysis.

Corrected total cell fluorescence (CTCF) was calculated with the equation:

Integrated density – (area of cell x fluorescence of background readings)

Values calculated were presented in arbitrary units and compared to values from control cells.

2.3.4.7 Determination of optimum swainsonine concentration required for reduction of extracellular galectin-1

A range of concentrations of SW in 2% starve media was examined to determine the optimum concentration to reduce gal-1 binding to the outside of HOMECs over 24 hours, without inducing cell toxicity. The effect of 24 hour treatment on HOMEC viability was assessed using WST-1 assays, as described in 2.3.2.1. Cells and SW treatments were grown/added in either 2% starve media. Cells treated only with 2% starve media or complete endothelial media were used as viability controls.

To observe the effects of SW on cell surface gal-1, HOMECs were treated with SW (see table 10) for 24 hours before 50ng/ml gal-1 was added to the media for 10 minutes. ICC to stain cell surface gal-1 was then performed as described in 2.3.4.2. Control wells with no SW treatment, as well as antibody controls were used. Cells and SW treatments were grown/added in 2% starve media.

100ng/ml	500ng/ml	1µg/ml	5µg/ml	10µg/ml	20µg/ml

Table 10. The range of swainsonine concentrations tested for reducing galectin-1 bound to the cell surface.

Fluorescence intensity was quantified as described in 2.3.4.6. The optimum concentration used for experiments was 5µg/ml; this exhibited significant reduction in extracellular gal-1 on HOMECs and was shown to be the highest concentration that did not affect HOMEC viability after 24 hours of SW treatment.

2.3.4.8 VEGFR2 staining

To confirm the presence of extracellular VEGFR2 on HOMECs, ICC staining was carried out. Two antibodies (one from rabbit, one from mouse) to the extracellular portion of the receptor were trialled. The rabbit polyclonal only showed staining when used at 5x the recommended concentration, necessitating use at 5µg/ml. The staining pattern was dissimilar to that in literature (see figure 21). The mouse monoclonal showed staining at the recommended dilution of 1:200, as well as a staining pattern observed similar to that in literature (Yamada *et al*, 2014).

a) b)

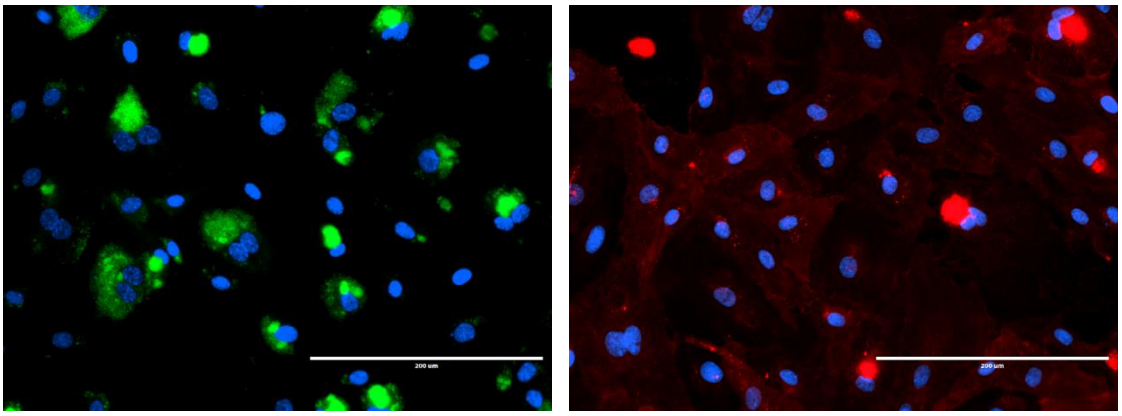

Figure 21. VEGFR2 staining patterns of HOMECs using two different primary antibodies. a) Staining using the rabbit polyclonal antibody. b) Staining using the mouse monoclonal antibody. Scale bar = 200µm.

2.3.5 ELISA protocols

Commercially available enzyme-linked immunosorbent (ELISA) kits were utilised to measure gal-1 in cell supernatants, VEGF-A_{165} in various cell media, as well as a cell lysate based ELISA to quantify the phosphorylation of VEGFR2.

2.3.5.1 Supernatant collection for galectin-1 ELISA

This ELISA was performed on HOMECs, HRECs, hCMEC/D3 cells to quantify the amount of secreted gal-1 over time in response to CL, and to quantify the naturally occurring secretion of gal-1 from A2780 and SKOV3 cancer cells. Briefly, cells were seeded at 50,000/well in 24-well plates. When cells were approximately 80% confluent, all cells were starved overnight in appropriate 2% starve media. The media was aspirated and 50ng/ml CL in 2% starve media (or just 2% starve media, for control cells) was added. At each timepoint (see table 11), the media was collected with a 1ml pipette and transferred into eppendorfs kept on ice. Eppendorfs were spun at 400*g* for 5 minutes at 4°C to pellet any cell debris. The supernatant was transferred to new eppendorfs kept on ice. The ELISA was then performed immediately, or else supernatants were stored at -80°C for a maximum of 1 month.

Supernatant collection timepoints
30 minutes
2 hours
4 hours
8 hours
24 hours

Table 11. Timepoints for supernatant collection (post cathepsin-L treatment or naturally occurring) from endothelial and cancer cells for secreted galectin-1 ELISA.

2.3.5.2 Galectin-1 ELISA

The ELISA was carried out according to manufacturer's instructions and all reagents were as supplied unless otherwise indicated. Briefly, the capture antibody was diluted in PBS to working concentration and used to coat a 96-

well plate. The plate was sealed and incubated overnight at RT. The wells were washed 4 times with wash buffer before blocking with 1% (w/v) BSA/PBS for 1 hour at RT. The wells were washed 4 times and standards were prepared in reagent diluent. The samples and standards (see table 12) were added to the plate at 100µl/well, the plate was sealed and incubated for 2 hours at RT. A sample standard curve is shown in figure 22. The wells were washed 4 times and 100µl of the detection antibody was added and incubated for 2 hours at RT. The wells were washed 4 times and 100µl of streptavidin-HRP was added and incubated for 20 minutes at RT in the dark. The wells were washed 4 times and 100µl of substrate solution was added and incubated for 20 minutes at RT in the dark. Finally 50µl of stop solution was added and the plate was read immediately using a SpectraMAX plate reader set to measure absorbance at 450/540nm.

20ng/ml	10ng/ml	5ng/ml	2.5ng/ml	1.25ng/ml	0.625ng/ml	0.313ng/ml

Table 12. Concentrations of galectin-1 standard used to generate the standard curve. Concentrations were made using serial dilution using reagent diluent.

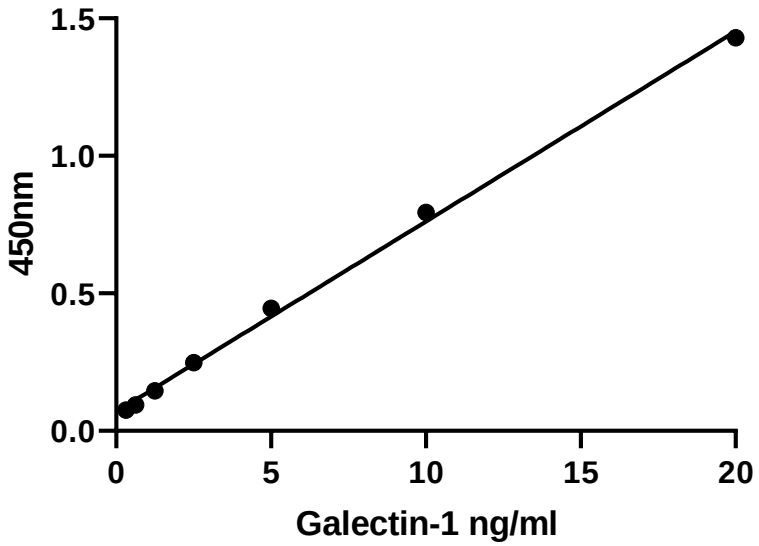

Figure 22. Example standard curve for galectin-1 generated from the commercially available kit.

2.3.5.3 VEGF-A ELISA

The ELISA was carried out according to manufacturer's instructions. The ELISA was used to quantify the level of VEGF-A_{165} secreted by HOMECs, as well as in 0.1% (w/v) BSA endothelial starve media.

Plate setup and generic ELISA protocol was followed as described in 2.3.5.2. The concentration of standards are described in (see table 13) and a sample standard curve is shown in figure 23.

2000pg/ml	1000pg/ml	500pg/ml	250pg/ml	125pg/ml	62.5pg/ml	31.3pg/ml

Table 13. Concentrations of VEGF-A_{165} standard used to generate the standard curve. Concentrations were made using serial dilution using reagent diluent.

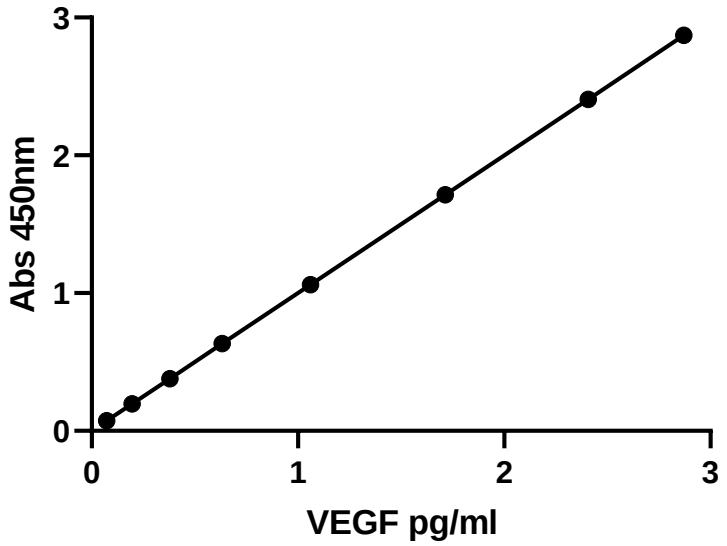

Figure 23. Example standard curve for VEGF-A_{165} generated from the commercially available kit.

2.3.5.4 Lysate collection

For lysates used in lysate based ELISAs and phosphokinase and RTK arrays, cells were lysed according to the same protocol. Lysis buffer was prepared as described in table 14, and kept on ice until use. Sufficient lysis buffer was prepared so that 600µl per treatment (2x 10cm petri dishes) was available. Minimal lysis buffer was used to increase the concentration of proteins in the lysate.

RIPA buffer	Protease Inhibitor Cocktail at 1:100 dilution	Phosphatase inhibitor cocktail 2 at 1:100 dilution	Phosphatase inhibitor cocktail 3 at 1:100 dilution

Table 14. Lysis buffer components.

Just before lysis, cells were washed with ice-cold PBS twice. Dishes were placed on ice and 600µl of lysis buffer was added per treatment. The lysis buffer was pipetted around the dish, and the dish was scraped with a sterile cell scraper. Lysate was then transferred to the second dish for that treatment and the process repeated. The resultant lysate was transferred to cold eppendorf tubes and mixed in a rotary mixer set to 20rpm at 4°C for 30 minutes. The eppendorfs were spun at 14,000*g* for 15 minutes at 4°C. The supernatant lysate was transferred to new eppendorfs and stored at -80°C until use, or kept on ice for immediate use. Care was taken to leave the cell debris pellet undisturbed.

2.3.5.5 BCA assay for protein quantification

A commercial BCA kit was used for protein quantification. The BCA assay principle relies on the reduction of copper ions by protein to produce a colorimetric change.

Briefly, 10µl of sample or BSA standard (diluted in RIPA buffer) (see table 15) was added to 200µl of working reagent (50:1 parts of reagent A: reagent B). The plate was incubated at 37°C for 30 minutes before absorbance was measured using a SpectraMAX plate reader at 562nm. A sample standard curve is shown in figure 24.

2000µg/ml	500µg/ml
1500µg/ml	250µg/ml
1000µg/ml	125µg/ml
750µg/ml	25µg/ml

Table 15. Concentration of BSA prepared in RIPA buffer for BCA assay standard curve. Standards were generated by serial dilution.

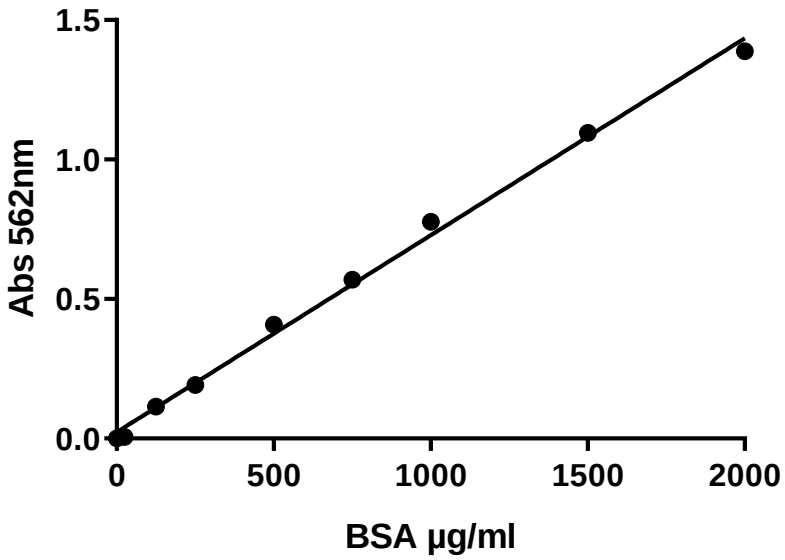

Figure 24. Example BSA standard curve generated from the commercially available BCA protein assay.

2.3.5.6 Lysate collection for phosphorylated VEGFR2 ELISA

Levels of pVEGFR2 were investigated under varying conditions in HOMECs. VEGF was used as a positive control to induce VEGFR2 phosphorylation, whereas SU was used to inhibit VEGFR2 phosphorylation where indicated. SW was used to reduce gal-1 binding to the cell surface. Cells were seeded into 10cm petri dishes, with 2 dishes/treatment (that were combined) to ensure a sufficient lysate yield. When HOMECs reached approximately 80% confluency, cells were starved overnight in 2% starve media ± SU and ± SW, followed by 4 hours in starve media supplemented only with 0.1% (w/v) BSA ± SU and ± SW. Cells were then subjected to the gal-1 and VEGF treatments shown in (see table 16) for 4 minutes. These treatments were added to the pre-treated cells so that no media change was required.

2% starve media	0.2ng/ml VEGF	5ng/ml gal-1	50ng/ml gal-1

10µM SU + 0.2ng/ml VEGF	10µM SU + 5ng/ml gal-1	10µM SU + 50ng/ml gal-1

5µg/ml SW + 0.2ng/ml VEGF	5µg/ml SW + 5ng/ml gal-1	5µg/ml SW + 50ng/ml gal-1

Table 16. HOMEC treatments for lysate used in pVEGFR2 ELISAs, all treatments were diluted in 0.1% BSA (w/v) endothelial starve media.

Cells were then lysed as described in section 2.3.5.4 and protein concentration determined by BCA assay (2.3.5.5).

2.3.5.7 Phosphorylated VEGFR2 ELISA

The pVEGFR2 ELISA was used initially to confirm results from the RTK array data. It was also used to investigate the change in pVEGFR2 in conditions described in 2.3.5.6. This ELISA was a development kit, necessitating the development of a standard curve appropriate for the assay. The kit recommended including 8000pg/ml as the highest standard concentration, which was therefore the starting point for a serial dilution. The standard curve concentrations are shown in table 17. A sample standard curve is shown in figure 25.

8000pg/ml	750pg/ml
4000pg/ml	500pg/ml
2000pg/ml	200pg/ml
1000pg/ml	100pg/ml

Table 17. Concentration of pVEGFR2 standards prepared in reagent diluent for pVEGFR2 ELISA. Standards were generated by serial dilution using reagent diluent.

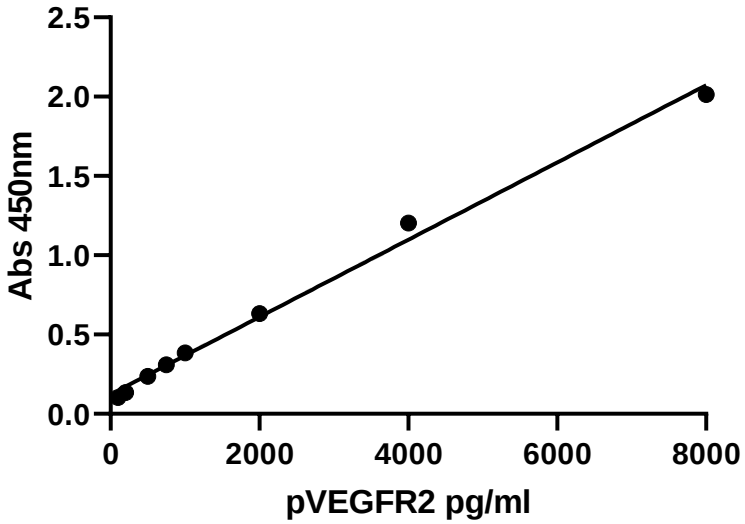

Figure 25. An example standard curve for phosphorylated VEGFR2 generated from the commercially available development ELISA kit.

The ELISA plate was setup as described in 2.3.5.2, with the exception that the detection antibody was conjugated to HRP, combining these two steps. The maximum amount of protein (from samples) that could be contained in 100µl (the ELISA well limit) was calculated from the lowest concentration of protein sample. Other samples were made up to 100µl with the appropriate reagent diluent.

2.3.6 Receptor tyrosine kinase and phosphokinase array protocols

In order to study tyrosine kinase receptor activation (phosphorylation) and downstream signalling pathway molecule phosphorylation (in response to gal-1), commercial arrays were used (see figures 26 - 27). These arrays utilise capture and control antibodies spotted in mapped areas on nitrocellulose

membranes. Cell lysates were added to membranes before detection of any binding with biotinylated detection antibodies.

2.3.6.1 Receptor tyrosine kinase array

Cells were starved overnight in 2% starve media, followed by 4 hours in 0.1% (w/v) BSA endothelial starve media to ensure receptors were in their unbound (non-activated) state prior to lysate collection. Cells were treated ± 50ng/ml gal-1 in 0.1% (w/v) BSA endothelial starve media for 4 minutes and then lysates were prepared as described in 2.3.5.4. Protein concentration was determined by BCA assay; 300µg of protein was added to each membrane as per manufacturer's instructions.

Membranes were blocked with the provided array buffer for 1 hour at RT. Blocking buffer was discarded before lysate samples were added to each membrane. Lysates were incubated with the membranes overnight at 4°C on a rocking platform shaker. Each membrane was then washed for 10 minutes on the rocking platform shaker 3 times. The anti-phospho detection antibody mix was added to each membrane for 2 hours on the shaker. The membranes were then washed as described above, excess buffer was removed, and membranes were placed in between two plastic sheets. The membranes were covered with the chemi reagent mix and the sheets were pressed to ensure complete coverage of the membrane surface area. After 1 minute incubation, excess chemi reagent mix was squeezed out between the sheets, and any remaining was blotted off. The top plastic sheet was replaced, with any air bubbles smoothed out. Membrane dots were detected via enhanced chemiluminescence and Azure software.

2.3.6.2 Array analysis

The arrays generated data in the form of dots (see figure 26) that were analysed for pixel intensity using ImageJ. A circular selection area was generated by hand and saved for use on all dots for a consistent area of analysis. Background readings were subtracted from each dot. Dots were compared to negative control dots, as well as between control and gal-1 membranes. Pixel intensity units were arbitrary, and the experiment was

performed twice. Therefore the means from these two experiments were used to identify RTKs of interest (see section 5.3.2).

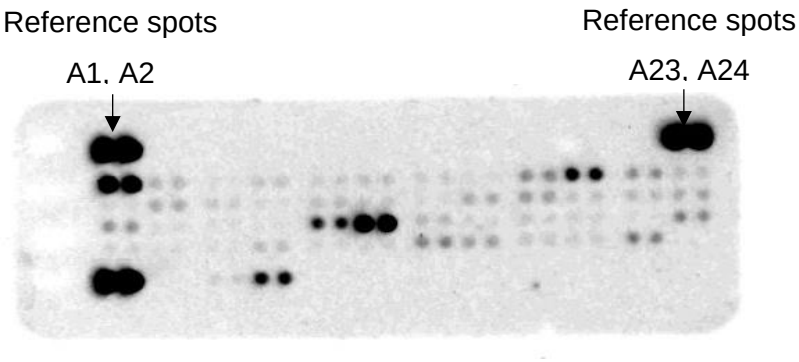

Coordinate	Receptor Family	RTK/Control	Coodinate	Receptor Family	RTK/Control
A1, A2	Reference Spots	——	D1, D2	Tie	Tie-2
A23, A24	Reference Spots	——	D3, D4	NGF R	TrkA
B1, B2	EGF R	EGF R	D5, D6	NGF R	TrkB
B3, B4	EGF R	ErbB2	D7, D8	NGF R	TrkC
B5, B6	EGF R	ErbB3	D9, D10	VEGF R	VEGF R1
B7, B8	EGF R	ErbB4	D11, D12	VEGF R	VEGF R2
B9, B10	FGF R	FGF R1	D13, D14	VEGF R	VEGF R3
B11, B12	FGF R	FGF R2α	D15, D16	MuSK	MuSK
B13, B14	FGF R	FGF R3	D17, D18	Eph R	EphA1
B15, B16	FGF R	FGF R4	D19, D20	Eph R	EphA2
B17, B18	Insulin R	Insulin R	D21, D22	Eph R	EphA3
B19, B20	Insulin R	IGF-I R	D23, D24	Eph R	EphA4
B21, B22	Axl	Axl	E1, E2	Eph R	EphA6
B23, B24	Axl	Dtk	E3, E4	Eph R	EphA7
C1, C2	Axl	Mer	E5, E6	Eph R	EphB1
C3, C4	HGF R	HGF R	E7, E8	Eph R	EphB2
C5, C6	HGF R	MSP R	E9, E10	Eph R	EphB4
C7, C8	PDGF R	PDGF Rα	E11, E12	Eph R	EphB6
C9, C10	PDGF R	PDGF Rβ	E13, E14	Insulin R	ALK
C11, C12	PDGF R	SCF R	E15, E16	——	DDR1
C13, C14	PDGF R	Flt-3	E17, E18	——	DDR2
C15, C16	PDGF R	M-CSF R	E19, E20	Eph R	EphA5
C17, C18	RET	c-Ret	E21, E22	Eph R	EphA10
C19, C20	ROR	ROR1	F1, F2	Reference Spots	——
C21, C22	ROR	ROR2	F5, F6	Eph R	EphB3
C23, C24	Tie	Tie-1	F7, F8	——	RYK
			F23, F24	Control (-)	PBS

Figure 26. Image of a developed membrane from the phosphokinase/receptor tyrosine kinase arrays and table of receptors in the human phospho-receptor tyrosine kinase array kit (R&D Systems). Dots correspond to certain receptor tyrosine kinases.

Membrane/ Coordinate	Target/Control	Phosphorylation Site
A-A1, A2	Reference Spot	——
A-A3, A4	p38α	T180/Y182
A-A5, A6	ERK1/2	T202/Y204, T185/ Y187
A-A7, A8	JNK 1/2/3	T183/Y185, T221/ Y223
A-A9, A10	GSK-3α/β	S21/S9
B-A13, A14	p53	S392
B-A17, A18	Reference Spot	——
A-B3, B4	EGF R	Y1086
A-B5, B6	MSK1/2	S376/S360
A-B7, B8	AMPKα1	T183
A-B9, B10	Akt 1/2/3	S473
B-B11, B12	Akt 1/2/3	T308
B-B13, B14	p53	S46
A-C1, C2	TOR	S2448
A-C3, C4	CREB	S133
A-C5, C6	HSP27	S78/S82
A-C7, C8	AMPKα2	T172
A-C9, C10	β-Catenin	——
B-C11, C12	p70 S6 Kinase	T389
B-C13, C14	p53	S15
B-C15, C16	c-Jun	S63
A-D1, D2	Src	Y419
A-D3, D4	Lyn	Y397
A-D5, D6	Lck	Y394
A-D7, D8	STAT2	Y689
A-D9, D10	STAT5a	Y694
B-D11, D12	p70 S6 Kinase	T421/S424
B-D13, D14	RSK1/2/3	S380/S386/S377
B-D15, D16	eNOS	S1177
A-E1, E2	Fyn	Y420
A-E3, E4	Yes	Y426
A-E5, E6	Fgr	Y412
A-E7, E8	STAT6	Y641
A-E9, E10	STAT5b	Y699
B-E11, E12	STAT3	Y705
B-E13, E14	p27	T198
B-E15, E16	PLC-γ1	Y783
A-F1, F2	Hck	Y411
A-F3, F4	Chk-2	T68
A-F5, F6	FAK	Y397
A-F7, F8	PDGF Rβ	Y751
A-F9, F10	STAT5a/b	Y694/Y699
B-F11, F12	STAT3	S727
B-F13, F14	WNK1	T60
B-F15, F16	PYK2	Y402
A-G1, G2	Reference Spot	——
A-G3, G4	PRAS40	T246
A-G9, G10	PBS (Negative Control)	——
B-G11, G12	HSP60	——
B-G17, G18	PBS (Negative Control)	——

Figure 27. Table of kinases and proteins in the human phosphokinase proteome profiler kit (R&D Systems).

2.3.6.3 Phosphokinase array

Cells were starved overnight in 2% starve media followed by 4 hours in 0.1% (w/v) BSA endothelial starve media to ensure that signalling molecules were in their basal activation state prior to lysate collection. Cells were treated ± 50ng/ml gal-1 in 0.1% (w/v) BSA endothelial starve media for 10 minutes and then lysates were prepared as described in 2.3.5.4. Protein concentration was determined by BCA assay; a maximum of 334µl of lysate was added to each membrane, to contain between 200 - 600µg of protein. For all experiments, the

lowest lysate concentration was used to determine how much protein could be added to the membranes.

The array was performed as described in 2.3.6.1, except there were two membranes and antibody mixes per treatment. Membranes were analysed as described in 2.3.6.2.

2.3.7 Experimental flow cytometry

Flow cytometry was used to confirm and investigate the phosphorylation of PLCγ1 in response to gal-1 and control treatments. Following gal-1 treatment, the internalisation of VEGFR2 was studied in response to VEGF (and pre-treatment with gal-1) and measured using flow cytometry. All flow cytometry samples were prepared at 250cells/µl, to a final volume of 500µl of 1% BSA/PBS. Blocking and staining was performed in a volume of 100µl of 1% BSA/PBS. Samples were analysed using a Guava easyCyte flow cytometer. Flow control tubes contained either unstained cells, single stain controls, or secondary antibody only samples. Unstained cells were used to set scatter controls for each cell type and were kept consistent for analyses. Compensation was set using single stain controls and automatic compensation. Positivity for each stain was determined from single stain controls and unstained cells. This gating was then applied to experimental samples. Propidium iodide (PI) was used in certain experiments to assess cell viability. Cells were incubated with 1µM PI for 15min at RT immediately prior to analysis. PFA fixed cells were used as a positive control for PI staining.

The flow cytometer was calibrated before the first use for each experiment, using the Guava easyCheck kit. Briefly, 20µl of beads were vortexed and added to 380µl of calibration buffer. The bead suspension was used in conjunction with the calibration programme on the flow cytometer; 3 runs were used to check particles/µl, scatter, and median fluorescent intensity of relevant fluorophores against ranges determined by Guava. Quick cleans of the flow cytometer were performed with de-ionised water after calibration and in between every 5 sample runs.

2.3.7.1 Measurement of PLCγ1 (total and phosphorylated)

Downstream signalling of VEGFR2 (PLCγ1) was studied after gal-1 treatments, with 0.2ng/ml VEGF treatments serving as positive controls.

HOMECs were grown in 6-well plates. When cells reached approximately 80% confluency, cells were starved overnight in 2% starve media (± any inhibitors). For 4 hours prior to gal-1/VEGF treatments, cells were further starved in endothelial media supplemented with 0.1% (w/v) BSA (± any inhibitors). Gal-1 and VEGF treatments were added to the media to avoid a media change. After 4 minutes, the media was aspirated and cells were put on ice and rinsed with cold PBS. Accutase was used to dissociate cells (5 minutes at RT), which were transferred to cold eppendorf tubes. Accutase was used as it is known to reduce cell clumping in the preparation of cells for flow cytometry (Cossarizza *et al*, 2017). Cells were pelleted and resuspended in 500µl of Cyto-Fast Fix/Perm and incubated for 10 minutes at RT to fix and permeabilise cells, with occasional vortexing. Cells were pelleted again and washed with 1x Cyto-Fast Perm Wash solution; this was repeated, and cells were resuspended in 100µl of 1% BSA (w/v) PBS. Trustain was added (3µl) to all tubes that would contain antibody to block Fc receptors, and incubated for 10 minutes at RT. Experimental controls were VEGF-VEGFR2 inhibited cells.

Total PLCγ1 was detected using a primary and secondary antibody; the primary was added at a 1:50 dilution and incubated for 30 minutes at 4°C in the BSA/PBS cell solution. Cells were pelleted and washed with PBS 3 times. The anti-rabbit Cy5 secondary antibody was added at 1µg/ml in 1% BSA (w/v) PBS and incubated for 30 minutes on ice in the dark. The cells were pelleted and washed in PBS 3 times before resuspension up to 500µl in 1% BSA (w/v) PBS, ready for flow analysis. Phosphorylated PLCγ1 (pPLCγ1) was detected using a conjugated (AlexaFluor 488) antibody at 1µl/200,000 cells, therefore only one staining incubation and subsequent wash step was required.

2.3.7.2 Measurement of PLCγ1 (phosphorylated only)

To further study the effects of gal-1 on PLCγ1 phosphorylation, the experiment described in 2.3.7.1 was performed to include pre-treatments with SW as described in table 18. 5µg/ml SW was added to the overnight starve, and 0.1µM

U73122 was added for the last hour of the 4 hour starve. Due to a discontinuation of the antibodies against PLCγ1, only the conjugated antibody against pPLCγ1 could be used. Additionally this experiment could only be run with reduced samples and as an n of 1.

0.2ng/ml VEGF	50ng/ml gal-1	0.1% BSA starve media	5µg/ml SW	
0.1µM U73122 + 0.2ng/ml VEGF	0.1µM U73122 + 50ng/ml gal-1	0.1µM U73122	5µg/ml SW + 5ng/m gal-1	5µg/ml SW + 50ng/m gal-1

Table 18. Reduced HOMEC treatments used to study phosphorylated PLCγ1.

2.3.7.3 Total and phosphorylated PLCγ1 flow analysis

Cells were analysed immediately after preparation. Cells were gated for total PLCγ1. Cells stained for phosphorylated PLCγ1 were expressed as a percentage of total PLCγ1 staining (see figure 28). Cells that could only stained for pPLCγ1 were expressed as a percentage of pPLCγ1 in control cells.

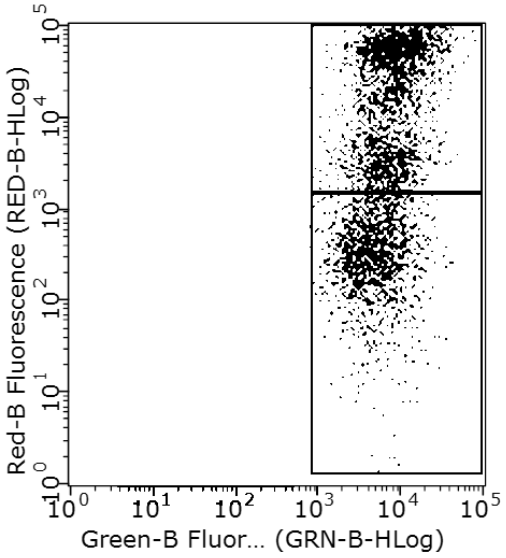

Figure 28. Gating strategy of HOMECS stained for total and phosphorylated PLCγ1. Cells in the top gate indicate the proportion of cells stained with phosphorylated PLCγ1 and total PLCγ1. The bottom gate indicates cells only stained for total PLCγ1.

2.3.7.4 Phosphorylated PLCγ1 only flow analysis

Cells were analysed immediately after preparation. The percentage of positive cells compared to whole scatter count was calculated for an indication of pPLCγ1 (n=1).

2.3.7.5 VEGFR2 internalisation

The effects of gal-1 on VEGF induced VEGFR2 removal from the cell surface were investigated using flow cytometry to detect surface levels of VEGFR2. HOMECs were pre-treated with gal-1 and some were then treated with 0.2 ng/ml VEGF in order to stimulate receptor-complex internalisation. External membrane associated VEGFR2 was quantified at four timepoints; no pre-treatment of gal-1, and no pre-treatment of gal-1 and no VEGF stimulation were used as controls. The VEGFR2 antibody was specific to the extracellular portion of the receptor; however given that the antibody would still give a fluorescent signal when internalised, receptor internalisation was halted with low temperatures (Li *et al*, 2008; Pinilla-Macua *et al*, 2015). Therefore any fluorescence was interpreted as only originating from non-internalised receptor complexes.

HOMECs were grown in 6-well plates. When cells reached approximately 80% confluency, cells were starved overnight in 2% starve media ± 5 or 50ng/ml gal-1, then starved for 4 hours prior to VEGF treatments in endothelial media supplemented with 0.1% (w/v) BSA ± 5 or 50ng/ml gal-1. VEGF was added to appropriate wells to a final concentration of 0.2ng/ml; the media was not exchanged to avoid interfering with receptor internalisation (Koch and Claesson-Welsh, 2012). VEGFR2 surface expression was monitored at 4 timepoints: 0, 5, 15, and 30 minutes, in accordance with previous literature (Ballmer-Hofer *et al*, 2011 and Basagiannis *et al*, 2016). At each timepoint, wells were aspirated and cells were washed twice with ice-cold PBS to halt further receptor internalisation. Cells were gently scraped off from the wells with a cell scraper, and pipetted slowly until a single cell suspension formed. The suspension was then transferred to eppendorf tubes on ice. Cells were not fixed as this was found to interfere with the staining. Trustain was added (3µl) to all tubes that would contain antibody to block Fc receptors. A negative control of A431 epithelial skin cells (Xu *et al*, 2016) was used due to relatively low

observable (via ICC) VEGFR2 expression on HOMECs. VEGFR2 was stained using a conjugated antibody (AlexaFluor 488) for 30 minutes on ice. Cells were washed 4 times with ice-cold PBS to remove non-bound antibody. Samples were subjected to 1µM PI staining 15 minutes before analysis so that dead cells could be excluded from analysis.

2.3.7.6 VEGFR2 flow analysis

Cells were analysed immediately after preparation. Cells showing positive VEGFR2 staining and negative PI staining were used for analysis (see figure 29). The median fluorescent intensity for stained VEGFR2 at each timepoint was used to compare treatments to controls.

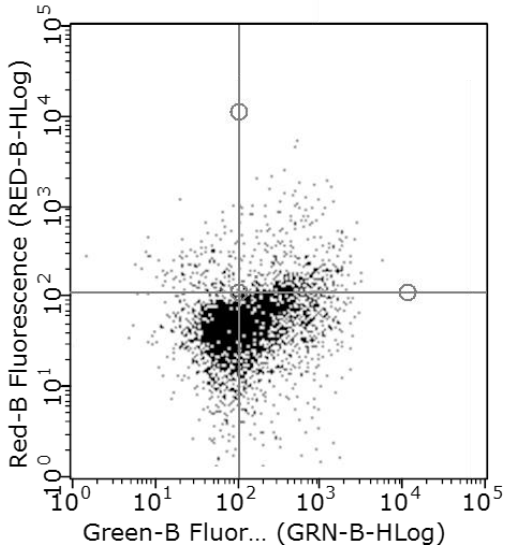

Figure 29. Gating strategy of HOMECS stained for PI and surface VEGFR2. Cells in the bottom right quadrant were used for analysis (positive for VEGFR2, negative for PI stain). Cells in the left quadrants represent cells not expressing surface VEGFR2, the top left quadrant cells also representing dead cells. The right quadrants show cells expressing surface VEGFR2, with the top right quadrant showing the dead proportion of these cells.

2.3.8 Galectin-1 HOMEC 96-well plate assays

A 96-well plate assay was used to quantify the amount of gal-1 on the cell surface. This was used to generate numerical values for stained cell surface bound gal-1. Black, clear bottom 96-well plates were used to reduce background interference. The assay was used to investigate whether additional

gal-1 could bind to cells, based on the ICC observation of high amounts of basal cell surface bound gal-1, as well as to investigate swainsonine inhibition of gal-1 binding. Gal-1 binding to HOMECs following treatment of tumour conditioned media (TCM) was also studied.

2.3.8.1 Cell surface galectin-1 plate assay

HOMECs were seeded at 10,000 cells/well and grown in 2% starve or complete media for a growth control. At approximately 80% confluency, cells grown in starve media were incubated with various treatments; 5 or 50ng/ml gal-1 for 10 minutes, or various concentrations of swainsonine (see table 10) followed by 10 minute treatments with 50ng/ml gal-1. Wells were washed with PBS prior to staining to remove any unbound gal-1.

Gal-1 plate staining was carried out as described in 2.3.4.3 without the addition of DAPI and the need to mount/coverslip the slides; plates were instead read in a SpectraMAX plate reader at 488/520nm. Control cells with no gal-1 treatments as well as secondary antibody controls were included.

2.3.8.2 Galectin-1 binding to the surface of tumour conditioned media treated HOMECs

A2780 and SKOV3 cells were grown to approximately 70% confluency in growth media described in 2.2.4 and 2.2.5. The cells were then switched to 2% endothelial starve media and allowed to adapt for 24 hours. The media was replaced with fresh 2% endothelial starve media and cells were grown for a further 24 hours in order for the tumour cells to condition the media. TCM was collected from the cells and spun at 200*g* at 4°C to pellet any debris. Media was transferred to clean tubes and stored at -80°C, or used immediately.

HOMECs were seeded at 10,000 cells/well in 96-well black plates and grown in 2% starve media. After overnight attachment, the media was aspirated from each well and replaced with the TCM media, with one plate for each cell line. Cells maintained in normal 2% FCS endothelial starve media or complete media served as basal gal-1 and growth controls respectively. Cells were incubated for 24 hours in order to allow time for any glycan synthesis and remodelling (Choi

et al, 2018). Gal-1 was then added at either 5 or 50ng/ml for 10 minutes, followed by a PBS wash. Gal-1 plate staining was then carried out as described in 2.3.8.1.

2.3.9 Cancer cell adhesion to cell monolayers

Metastasised ovarian cancer cells are known to disseminate and be able to spread transcoelomically and haematogenously (Pecot *et al*, 2011). Therefore the adhesion of gal-1 treated cancer cells to mesothelial and HOMEC monolayers was studied. The adhesion of cancer cells to a gal-1 pre-treated HOMEC monolayer was also studied. A rocking plate assay was used to quantify cancer cell adhesion to the monolayer. The assay was used to study the effect of gal-1 as a pre-treatment for cancer cells and for the HOMEC monolayer.

2.3.9.1 Adhesion of cancer cells to galectin-1 pre-treated HOMEC monolayers

HOMECs were seeded at 50,000 cells/well in black clear bottom 24-well plates and cultured until a confluent monolayer was formed. Cells were treated overnight in 2% endothelial starve media ± 5 or 50ng/ml gal-1. 2% and 5% endothelial starve media and endothelial media supplemented with 20% FCS were used as negative and positive controls respectively; FCS is known to enhance cell adhesion (Morandi *et al*, 1993).

A2780 and SKOV3 cancer cells were grown and adapted to 2% endothelial starve media as described in 2.3.8.2 prior to experimentation. Cancer cells were trypsinised and pelleted, before resuspension in 2% starve media with 2µM calcein-AM and incubated for 30 minutes at 37°C on a rotary mixer set to 20rpm. The cells were pelleted and resuspended in serum-free media; 10,000 cells in 250µl was added to the pre-treated HOMEC monolayers.

The plate was placed on a plate rocker set to lateral rocking at 60 tilts per minute (tpm). Incubation was carried out in an oven at 37°C. Due to the lack of gas control, the plates were only incubated for 2 hours. This incubation was established to not affect cell viability. Plates were removed and media/cells that

had not adhered were aspirated. Wells were washed with warm serum free endothelial cell media. The HOMEC/bound cancer cell monolayers were fixed with PFA as described in section 2.3.4.2. Fluorescence was read in a SpectraMAX plate reader at 488/520nm, and wells were imaged using an EVOS fluorescent microscope.

2.3.9.2 Adhesion of galectin-1 pre-treated cancer cells to HOMEC and mesothelial monolayers

HOMECs or HOMesos were seeded at 50,000 cells/well in 24-well plates and cultured until a confluent monolayer was formed. Prior to experimentation, cells were starved overnight in 2% endothelial starve media or 5% HOMeso starve media. A2780 and SKOV3 cancer cells were grown, trypsinised, pelleted and treated in appropriate starve media (as described in 2.3.9.1) that was treated with ± 5 or 50ng/ml of gal-1 for 10 minutes. 2% endothelial starve media and 5% HOMeso starve media served as negative controls, and 20% endothelial/HOMeso media served as positive controls. Cancer cell seeding, plate rocking and fluorescence readings were performed as described in 2.3.9.1.

2.3.9.3 Analysis of calcein-AM stained cancer cells adhering to HOMEC monolayer

These assays were performed in 24-well plates and read by plate reader to quantify fluorescence. Photographs were taken to confirm data from plate reader, an example of which is shown in figure 30.

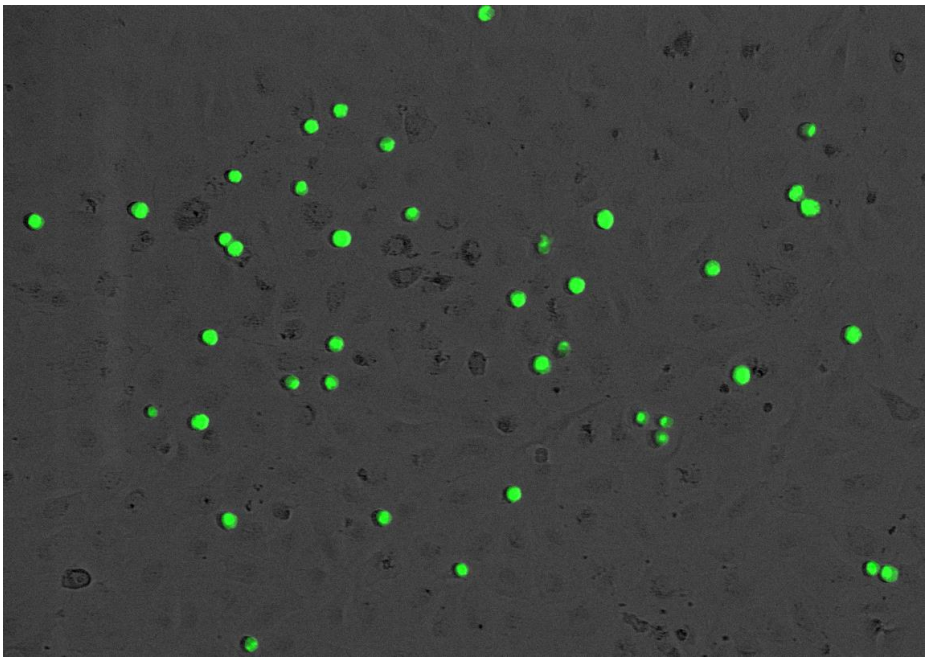

Figure 30. Representative photograph of calcein-AM stained cancer cells (green) adhered to a HOMEC monolayer (x20).

2.3.10 Statistical analysis

Statistical analyses were performed using GraphPad Prism software 8. To compare multiple groups of unpaired data, a Kruskal-Wallis test was initially employed. If the result showed significance, Mann-Whitney U tests were used as a post-hoc test between two groups where appropriate. In cases of multiple comparisons, the Dunn's test was employed for post-hoc analysis. Paired data were analysed using the Wilcoxon matched-pairs signed rank tests between two groups at a time. These non-parametric tests were chosen due to small sample sizes in these experiments, and the use of percentage data or data presented as a percentage of control (100%). $p<0.05$ was considered statistically significant. The graphical representation of data shows the mean ± standard deviation (SD).

Chapter 3. HOMEC isolation protocol development

3.1 Introduction

The concept of endothelial cell heterogeneity discussed throughout section 1.1.2 highlights the importance of using disease relevant ECs for *in vitro* research. In this case, human omental microvascular ECs (HOMECs) were required to study EOC associated angiogenesis during metastasis to the omentum. Initially, the HOMEC isolation method described in 2.3.1.3 was used. This method proved to be inefficient, and did not reliably yield HOMECs that remained at acceptable purity throughout culture. Therefore, this chapter describes the steps taken to improve the success rate of the isolation protocol. Two approaches were explored; improvement to the existing protocol (Winiarski *et al*, 2011), and developments for a fluorescence activated cell sorting (FACS) protocol.

3.2 Issues in omental microvascular endothelial cell isolation

3.2.1 Issues with initial HOMEC isolation in previous protocols

The isolation of HOMECs was first attempted by Kern *et al* (1983). The group used collagenase digestion of omental samples, and reported the successful culture of cells that exhibited characteristic cobblestone EC morphology. Anders *et al* (1987) further developed this method to improve EC yield by seeding potential HOMECs on to fibronectin coated plastics in order to increase cell attachment and growth on tissue culture plastics. Furthermore, this group addressed the problem of contamination with mesothelial cells which show a similar morphology to ECs, by staining for vWF on their isolated cells as well as mesothelial cell controls. However, Chung-Welch *et al* (1997) reported that human omental derived mesothelial cells (HOMesos) can express vWF, meaning that vWF cannot be used as an EC specific marker alone, in this case.

As a result this group developed a method that first harvested HOMesos and after further steps, HOMECs. The group also used additional markers to confirm cell identities, but crucially, their isolated 'HOMECs' did not express CD31, which is now considered a pan-endothelial cell marker, questioning the true identity of these cells. The first HOMEC isolation method to utilise immunoselection with anti-CD31 magnetic beads was described by Hutley *et al* (2001). Cells isolated with these beads would in theory, have to express surface CD31 and therefore be endothelial. It can be seen that all of the previous methods involved seeding isolated cells directly after various digestions followed by centrifugation and filtration steps. However, all of the groups discussed, including Hutley *et al* (2001), did not publish work from their isolation procedures, implying that problems were encountered and insufficient cells were obtained/could be cultured successfully.

Winiarski *et al* (2011) demonstrated the isolation and convincing characterisation of HOMECs. ECs isolated were positive for CD31 and vWF. However, the usage of this protocol in this thesis did not result in the 90% success rate described in the paper, and also encountered problems with HOMEC purity on the occasion of successful isolation.

3.2.2 Issues with HOMEC culture in previous protocols

The protocols discussed in 3.2.1 report concerns in contaminating cells present with the initial yield of HOMECs, including mesothelial cells and fibroblasts. In addition, Winiarski *et al* (2011) report contaminating pericytes as a problem. Furthermore, there has been difficulty in culturing successfully isolated HOMECs due to unknown media requirements, and variation between plastic coating procedures. In this work, successfully isolated HOMECs (from the Winiarski protocol) that had been grown and kept at -80°C as described in section 2.1.3, were initially used for experiments. These cells were observed to attach to 2% (w/v) gelatin and grow in complete endothelial media (see section 2.2.1) as described by Winiarski *et al* (2011), and therefore this aspect of HOMEC culture was not investigated or altered. However, issues remained with the purity of these HOMECs; it was observed that from passage 4 onwards (see figure 31), contaminating non-endothelial cells (based on morphological observations) would begin to outnumber HOMECs in the cultures, which would

affect experimental results. Characterisation studies indicated these contaminating cell populations largely comprised of omental mesothelial cells and fibroblasts (see figure 32). Given that HOMEC cultures had to be expanded during p1 - 3 and could only be seeded for experiments between p4 - 6, this proved to be a significant problem.

a)

b)

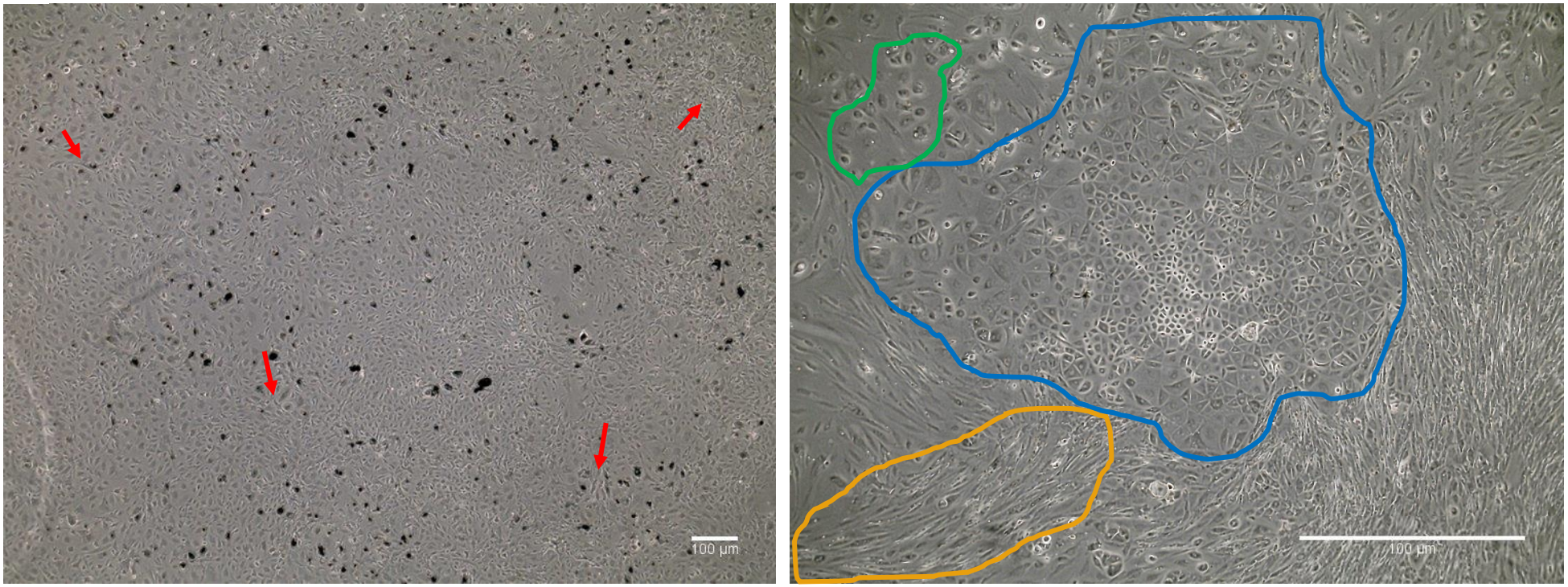

Figure 31. Representative phase contrast images of the early and late stage of HOMEC contamination with other cell types. HOMECs isolated using the protocol by Winiarski *et al* (2011) were outcompeted by contaminating cells after reaching approximately p4. a) shows HOMECs growing at p4 (dark patches are patches of dynabeads remaining bound to cells). The monolayer is somewhat uniform, but irregular patches of contaminating cells are starting to appear, as indicated with red arrows (x4 magnification). b) shows HOMECs growing at p6 (x10 magnification). The blue line encircles contaminating mesothelial cells, the orange line encircles a patch of contaminating fibroblasts (there are more present). A small patch of HOMECs are visible within the green line. Note that fibroblast contamination and overtaking of the culture was more common than mesothelial cell contamination.

a)

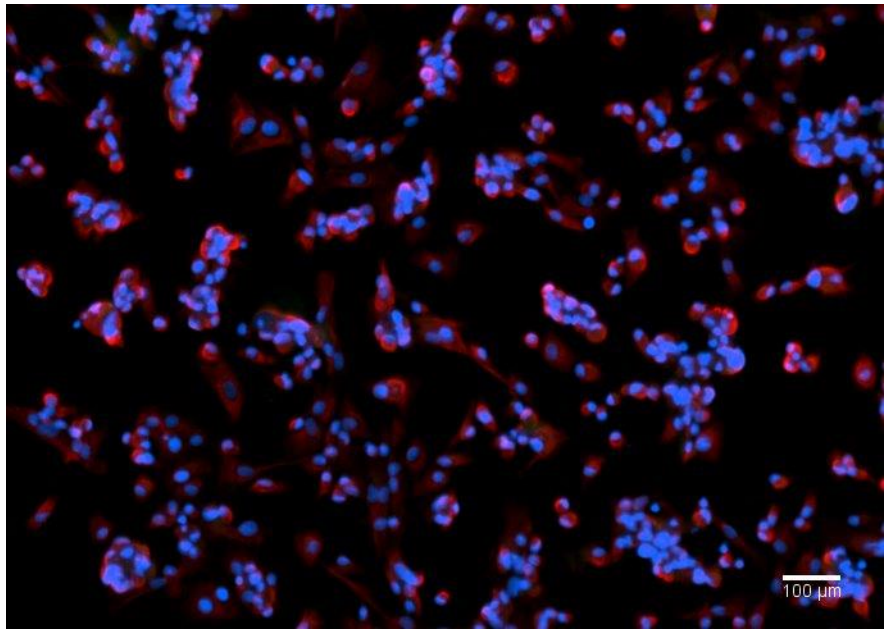

b)

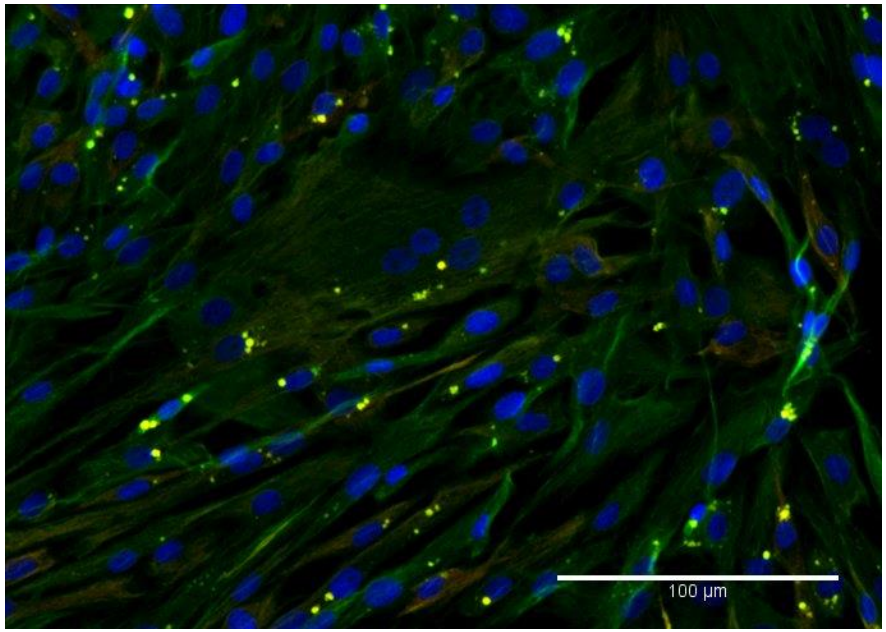

Figure 32. Characterisation of mesothelial cells and fibroblasts. Mesothelial cells and fibroblasts were stained for intracellular markers to distinguish them from HOMECs, as described in sections 2.3.4.1 and 2.3.4.4. a) mesothelial cells positive for cytokeratin-18 (red) (rabbit anti-human cytokeratin-18, Abcam), x10. b) fibroblasts positive for vimentin (green) (mouse anti-human vimentin, Abcam) x20. Staining and photos by Gillian Phua.

Although HOMesos certainly bore resemblance to HOMECs, it became possible to distinguish them by eye in most cases. This was due to other work in the lab concerning the isolation, culture and characterisation of HOMesos specifically. Additionally, isolated populations of both cell type were characterised and assessed for purity. Importantly, work from our lab also showed that HOMesos differentially expressed vWF, reiterating the need for different or additional markers of characterisation, and supporting the results from Chung-Welch *et al* (1997).

To further assess the purity of these isolated HOMECs, flow cytometry was utilised to examine the presence of different cell populations based on scatter alone. A population of passage 4 HOMECs was prepared for flow cytometry as described in section 2.3.7, albeit no particular probes were used in order to observe different populations from scatter only. The scatter is shown in figure 33.

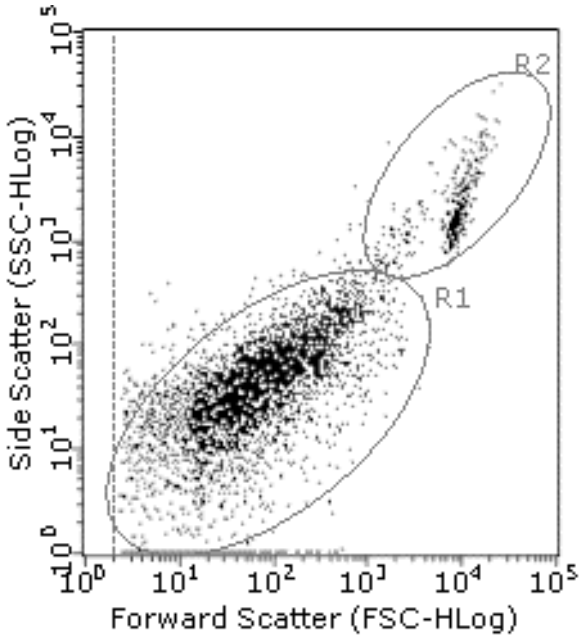

Figure 33. Scatter of a passage 4 population of HOMECs isolated using the Winiarski *et al* (2011) method. Two distinct cell populations can be seen; R1 is likely to be HOMECs. At passage 4, the majority of cells observed by microscopy appeared to be endothelial. R2 shows a smaller, yet distinct cell population that is likely comprised of either mesothelial, fibroblast or pericyte cells.

It is not possible to be certain about identities of the two populations in this scatter, but the cell counts of these two populations is useful. R2 comprises approximately 10% of the entire plot, R1, assumed to be HOMECs based on

visual examination of cell morphology prior to flow analysis, the other 90%. A cell purity of ≥95% is considered the standard in the isolation of endothelial cells (Oettel *et al*, 2016; Crouch and Doetsch, 2018), and therefore 90% is not generally considered sufficient, even though close. As shown in figure 31, monolayers of HOMECs that appear mostly homogeneous can soon be outcompeted by contaminating cultures previously present at lower numbers. It is likely that the contaminating cells were mesothelial and fibroblasts, thus a series of protocols to improve HOMEC purity were examined.

3.2.2.1 Immunoselection depletion of contaminant fibroblasts in HOMEC cultures

As discussed, contaminating fibroblasts would often overwhelm the HOMEC cultures. To reduce the number of contaminant fibroblasts, an anti-fibroblast immunoselection of growing HOMEC isolates was investigated using commercially available anti-fibroblast dynabeads and a magnetic column kit. This was trialled at all passage numbers. The growing HOMECs were trypsinised and pelleted before resuspension in 800µl 0.5% (w/v) BSA/PBS with 2mM EDTA. The cell suspension was gently syringed with a needle to ensure a single cell suspension for bead binding, and 200µl of bead solution was added. The bead solution consisted of magnetic beads coated with a specific anti-fibroblast antibody; the exact epitope was protected intellectual property. The bead/cell suspension was incubated for 30 minutes at RT. A further 5ml of buffer was added to wash the cells, then cells were pelleted by centrifuging at 300*g* at RT. The supernatant was aspirated and cells resuspended in 500µl of buffer.

The magnetic column was prepared by rinsing with buffer before the addition of cell suspension. The suspension was allowed to drip through to a clean tube. This process was repeated 4 times to maximise bead (fibroblast) attachment to the column. The cell suspension was thus separated from these retained bead-bound fibroblasts and was reseeded for further culture. It was found that fibroblasts prevailed in the HOMEC cultures as assessed by phase contrast study of culture morphology, and therefore improvements to the isolation protocol were investigated.

3.2.3 Success rate with the Winiarski protocol

As discussed in section 3.2, there were problems with both initial isolation success, as well as with maintaining subsequent HOMEC purity. The success from isolations using this protocol are summarised in table 19.

Omenta samples	Initial isolation success	Initial isolation success (%)	Culture success	Isolation and culture success (%)
10	3	30	1	10

Table 19. Initial isolation and subsequent culture success following the Winiarski protocol. Omenta samples processed using the Winiarski protocol had approximately a 30% success rate of generating HOMECs initially, and approximately a 10% success rate in successfully isolated HOMECs prevailing in culture and not being outcompeted by contaminating cells (culture success), despite fibroblast depletion with immunoselection. Percentages were calculated from the number of omenta samples and the number of initial and culture successes.

3.2.4 Analysis of original isolation protocol

After careful review, it was noted that there were several potential steps during the original isolation protocol where EC loss could be occurring (figure 34). This was important as the contamination issues discussed earlier could potentially be mitigated if a larger proportion of initial isolates were ECs. Improvements to these steps to improve HOMEC yield were therefore tested and incorporated into the final protocol if found to be effective.

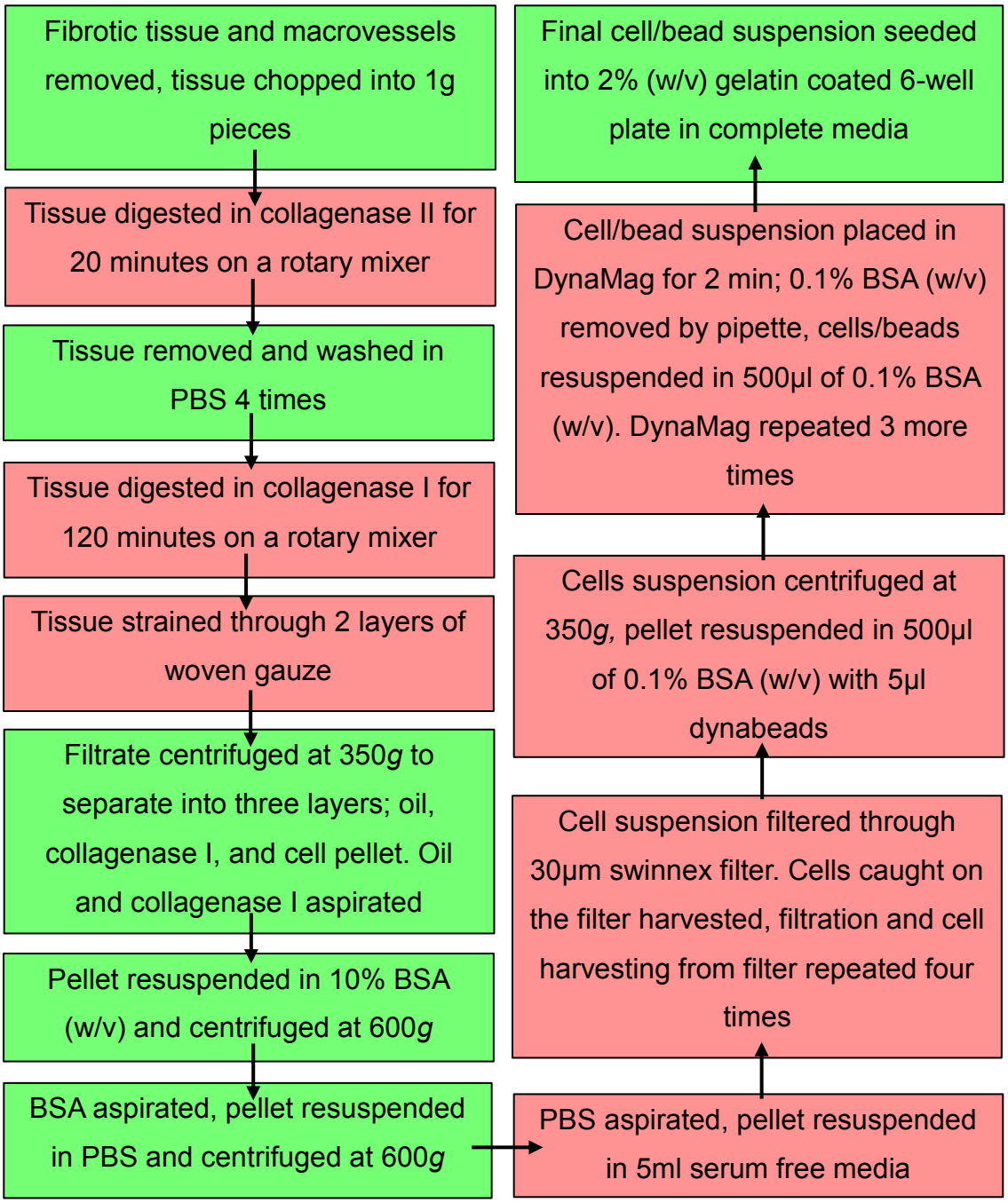

Figure 34. Identification of steps that could potentially be targeted to improve yield during the original HOMEC isolation protocol. Steps in red were identified as potential targets to improve EC yield. Steps in green were considered essential, and unlikely to contribute to low yield. Media = endothelial media.

3.2.4.1 Protocol steps not investigated

Removal of fibrotic tissue and macrovessels

The first step of the protocol required the removal of omental fibrotic areas, macrovessels, and chopping the omentum into roughly 1g pieces. Fibrotic tissues are commonly formed postoperatively. Whilst patient history was unknown, the type of operation in which omentum was sourced from was available information. It was observed that staging laparotomies (likely the first surgery a patient may have) were relatively uncommon, and it is known that many advanced EOC patients have multiple surgeries during their treatment, as it is the most effective treatment (see section 1.4.2). Therefore it is likely that most omenta came from patients who had had prior surgeries. Fibrotic tissue occurs in areas of postoperative adhesion (pathological bonds between the omentum, bowel, or abdominal wall) formation and consists of extra ECM primarily produced by mesothelial and fibroblast cells (Foster *et al*, 2020). Therefore, removal of these areas was considered beneficial as it likely removed areas dense with mesothelial cells and fibroblasts. Areas of fibrotic tissue were present in most omental samples received.

The removal of macrovessels was essential in order to improve the isolation of microvascular endothelial cells: ECs from microvessels, rather than macrovessels. This could only be performed by eye (see figure 35), and there was no reason to remove this step.

Figure 35. An example of an omental sample with visible macrovessels. Arrows indicate examples of larger and smaller macrovessels. Note that not all visible macrovessels are labelled, but all would be removed with dissection.

PBS washing between collagenase digestions

This step of the protocol was necessary in order for the collagenase I (the second digestion enzyme) to work effectively following the collagenase II digestion. Both enzymes cleave the same bond found in collagen, but collagenase type II is known to have more units/mg than collagenase type I. Therefore the PBS washes were essential in removing all collagenase type II from the tissue in order to only proceed with the gentler collagenase type I digestion.

Filtrate separated into three layers

Post enzymatic digestion and undigested tissue removal, the filtrate was centrifuged to separate it into three layers: the topmost layer of oil, a middle layer of collagenase I solution, and the cell pellet at the bottom of the tube. The oil and collagenase I are not required at this point therefore the removal was not perceived to affect the isolation of HOMECs.

10% BSA (w/v) and PBS washes of cell pellet

Although the oil and excess collagenase I were aspirated, oil droplets and a small amount of remaining enzyme solution remained in the tube. The subsequent washes and transfer of the resuspended cell pellet to a new tube was observed to remove the oil and enzyme. Furthermore, the 10% BSA (w/v) is thought to bring extra benefits, such as protection for the cells against shear forces, the scavenging of unwanted particles (like debris), and as a cell nutrient during this time with an absence of serum (Francis, 2010). Additionally, with regard to the immunoselection, both this 10% BSA (w/v) wash and the 0.1% BSA (w/v) solution used during the selection may aid in preventing non-specific binding.

Final seeding into 2% (w/v) gelatin coated well of a 6-well plate

The final cell/bead suspension was seeded into a 2% (w/v) gelatin coated well of a 6-well plate. Gelatin coated cell culture plastics was observed to promote HOMEC attachment, so this process was not changed. Moreover, the size of the well for the resultant number of cells was observed to be appropriate for the number of cells generated from the isolation protocol.

3.2.4.2 Areas identified for potential protocol improvement

Three main areas that warranted study and possible improvement were identified – the enzymatic digestion, swinnex filtration, and the immunoselection.

Enzymatic digestions

The enzymatic digestions were essential in order to break down the omental tissue and to release microvascular fragments and ECs. During the development of the Winiarski protocol, work from our lab demonstrated that sequential enzymatic digestions of collagenase II and then I, was more effective at releasing microvascular fragments over other methods, such as mechanical homogenisation. Specifically, collagenase II for a shorter digestion was shown to provide an effective first digestion. This collagenase II preparation contains more units of clostripain, making it more effective at digesting collagen; clostripain is an endopeptidase routinely used to digest tissue samples (Ståhle

et al, 2015). The following longer digestion with collagenase I offered a gentler digestion (same mechanism) but was thought to be less likely to affect cell viability. Winiarski *et al* (2011) state that the isolation protocol yielded more initial cells if the adipose tissue was completely digested. The same observations were made in this thesis, except that due to the heterogeneous nature of the omental samples, complete digestion did not always occur within the digestion timeframes in the existing protocol. Another observation was the potential limitation of the gauze filtration step; the woven gauze had a tendency to break if too much pressure was applied to squeeze the oil out of undigested tissue. This resulted in undigested tissue passing through, necessitating the repetition of this step, and also a reduction in the oil that could be collected (oil that could contain microvascular fragments and thus, ECs).

Additionally, although previous work studied cells released by enzymatic digestion every 20 minutes (during the protocol development), cells were only studied after they had been seeded. As HOMEC numbers and viability were not studied during different digestion times, it was possible that optimum digestion conditions had not been identified. This may have led to reduced efficiency of cell isolation or even loss of viability of isolated ECs. Additionally, the isolation of any HOMECs (present in microvascular fragments or as cells) released from the tissue was dependent on the intact expression of CD31. Thus, if CD31 was removed from cells during digestions, HOMEC isolation would be compromised. The effect of the collagenases on CD31 was not previously studied, and therefore it was unknown whether CD31 was being cleaved from the cell surface enzymatically.

Swinnex filtration

The swinnex filtration (through a 30µm pore nylon filter) step was originally incorporated to trap microvascular fragments on the filter, whilst contaminating single cells would be pushed through into the waste suspension below. This process was undertaken four times. Potential HOMEC loss at this step was studied by seeding all the waste suspension that passed through the filter, into wells of a 6-well plate as per the final steps in the protocol following the immunoselection. It was found that sometimes, HOMECs would be present in the suspension that the protocol instructed should be discarded (see figure 36); during investigations into potential HOMEC loss, these waste suspensions were

seeded. Of these, approximately 25% contained HOMECs, as confirmed by ICC (see section 2.3.4.4). It is important to note that these HOMEC isolation 'successes' were not factored in to the success rate discussed in section 3.2.3. Furthermore, only once did HOMECs isolated from these seeded waste suspensions became a successful culture. Regardless, their presence in these waste seeded wells confirmed that some degree of HOMEC loss occurred at this step in the protocol, namely that some HOMECs were passing through the filter. Importantly, given that the filter size was chosen so that microvascular fragments would be retained and other single cells (thought to be contaminants) would pass through, these observations suggested that at this stage in the protocol, some HOMECs were present in the suspension as single floating cells. It was noted that HOMECs isolated at this step were unlikely to become a successful culture; compared to successful initial isolations after the full protocol, fewer HOMECs were present in the wells. This suggested that insufficient HOMECs available as single cells were available at this point. It is important to note that most waste suspension seeded at this point resulted in cultures that morphologically resembled either fibroblasts or pericytes.

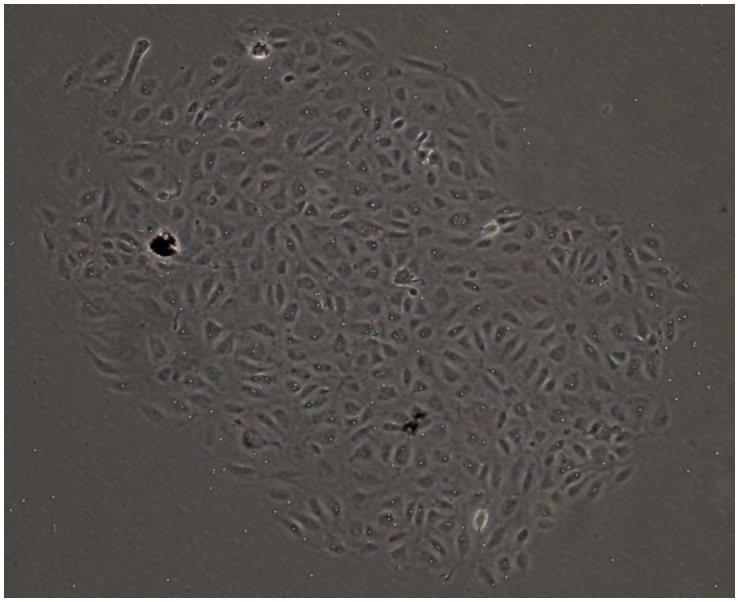

Figure 36. HOMECs growing from the waste suspension following swinnex filtration. HOMECs that passed through the swinnex filter were seeded in wells of 6-well plates (x10).

Immunoselection

It was observed that the CD31 immunoselection resulted in the isolation of cells other than HOMECs, suggesting that the selection was not specific. Furthermore, beads would persist on isolated HOMECs for several passages in culture, and the effect of this on HOMEC viability was therefore unknown.

These observations from these parts of the protocol led to the formation of hypotheses that are summarised in table 20. These steps and hypotheses were investigated with the aim to improve the protocol. These investigations are discussed in the next section.

Section of protocol	Hypotheses
Gauze filtration	• Woven gauze reduced availability of (microvascular fragment containing) oil
Enzymatic digestions	• Enzymatic digestions cleave CD31 from the surface of HOMECs • Enzymatic digestions released HOMECs but decreased HOMEC viability • Enzymatic digestions were insufficient to release sufficient numbers of HOMECs
Swinnex filtration	• HOMECs pass through the swinnex filter
Immunoselection	• The dynabeads were binding to fibroblasts • The concentration of dynabeads affected HOMEC viability

Table 20. Hypotheses for HOMEC loss during specific sections of the HOMEC isolation protocol.

3.3 HOMEC isolation protocol development

In order to potentially improve the protocol during these steps, the gauze step was modified, and the effect of the original enzymatic digestions on HOMEC viability and CD31 expression was studied. These experiments utilised pre-isolated HOMECs in order to study the effect of the digestions on single cell HOMECs. This approach was taken because it was assumed the single cell HOMECs would be more exposed to enzyme degradation than any shielded by tissue. This approach therefore would mimic the longest time that a single HOMEC could be exposed to both sequential enzymatic digestions. The enzymatic digestions were then extended, and the effect on surface CD31 and HOMEC viability were studied during the isolation protocol. From observing HOMEC culture from the waste suspension from the filtration step (see section 3.2.4.2), it had already been shown that some single cell HOMECs were able to survive the digestions. This informed the decision to not alter the concentration of the enzymes as a first line of potential improvement, instead opting for longer digestions.

3.3.1 Use of non-woven gauze

Due to the problems encountered with the woven gauze, a change to non-woven was made (sterile non-woven 10cm x 10cm swabs, Shermond). This gauze did not break, and therefore increased the amount of oil collected, and was utilised for future isolations. Representative images are shown in figure 37.

a) b)

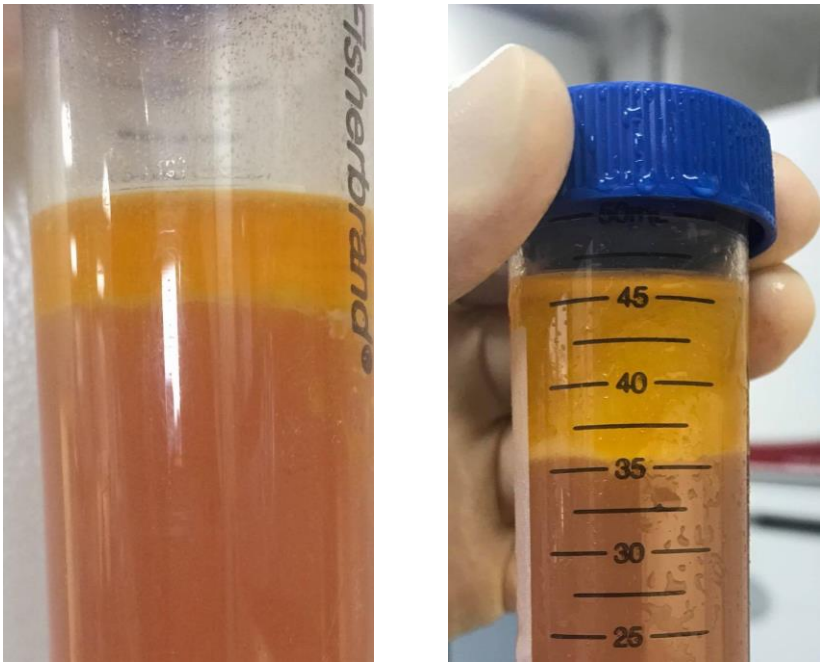

Figure 37. An increase in oil from a switch to non-woven gauze. a) oil harvested from squeezing undigested tissue through woven gauze, versus b) oil harvested from tissue squeezed through non-woven gauze. A thicker oil layer was indicative of effective tissue digestion, and more microvascular fragments may be present within the oil layer and therefore available for isolation.

3.3.2 Enzymatic digestion investigation: effects on cell viability and CD31 expression

The effect of the digestions from the original protocol on cell viability and CD31 detection were studied on single cell suspensions of HOMECs. For these experiments, initial cell dissociation from culture plastics was achieved using accutase. This was required as experiments were conducted on pre-isolated HOMECs. Thus the effect of accutase on cell viability and CD31 detection (HOMECs) was also studied in order to confirm the accutase dissociation did not affect cell viability or cleave CD31.

3.3.2.1 Study of the effect of the digestions in the original protocol on single cell HOMECs

Previously isolated and characterised populations of HOMECs were subjected to the same enzyme treatments as in the original isolation protocol. HOMECs

were dissociated from 6-well plates with accutase (see section 2.3.7), pelleted, and resuspended in 10ml of the enzyme treatment in 50ml tubes. Treatments were as follows: collagenase II only for 20 minutes, collagenase I only for 2 hours, and both collagenase II for 20 minutes followed by collagenase I for 2 hours (with PBS washing in between enzymes). The effect of accutase on cell viability and CD31 detection without any enzyme treatment was also studied at this point. All assessments were carried out by flow cytometry as described below.

Enzymatic digestions were carried out at 37°C on a rotary mixer, as per the isolation protocol. Cells were then pelleted, washed with PBS, and transferred to 500µl eppendorf tubes for staining. Flow cytometry was performed as described in section 2.3.7. Briefly, cells were dissociated using accutase and transferred to 1.5ml eppendorf tubes. Cell blocking, staining and flow analysis were carried out in 1% (w/v) BSA/PBS. Fc receptors were blocked with 3µl Trustain for 10 minutes at RT, before staining for CD31 using a conjugated antibody (mouse anti-human CD31 AlexaFluor 488, Biolegend) at 1µg/ml for 30 minutes (on ice). PI was used in order to study viability. Cells were washed 4 times with ice-cold PBS to remove non-bound antibody before resuspension in 500µl of 1% BSA/PBS. Cells were analysed immediately after preparation. The percentage of cells positive for CD31 and negative for PI (viable cells) was measured for each population of HOMECs after accutase dissociation, and the enzymatic digestion(s). A representative plot is shown in figure 38.

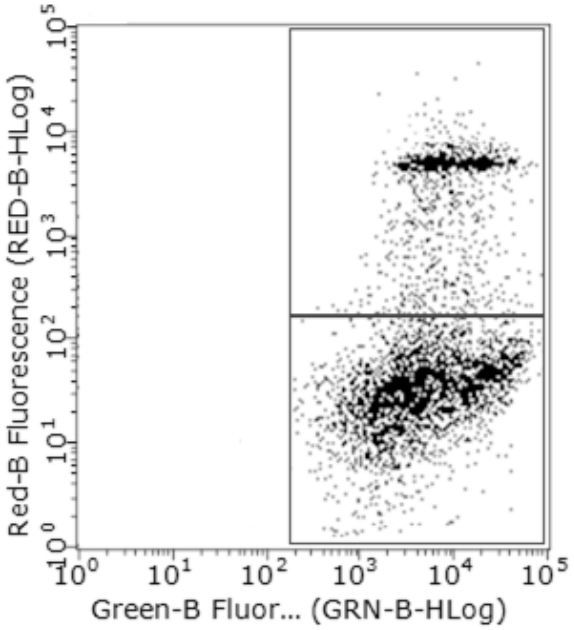

Figure 38. Gating strategy of previously isolated HOMECs stained for CD31 and PI. The top gate contains cells positive for both CD31 and PI, representing non-viable HOMECs that express CD31. The bottom gate contains cells only positive for CD31, representing live, CD31 expressing HOMECs.

Cell viability was additionally studied using trypan blue. Following digestions, cells were pelleted and resuspended in PBS before 10µl of suspension was mixed with 10µl of trypan blue. Cells were immediately analysed by cell counter.

3.3.2.2 The effect of the original protocol enzymatic digestions on single HOMECs

HOMEC viability and CD31 surface detection remained high after accutase treatment. The mean percentage of CD31+v/PI-ve cells was 98%±1, and the mean viability as assessed by trypan blue was 99%±1 (n=6). This high viability and level of CD31 detection indicated that accutase dissociated HOMECs could be used as a control for the enzymatic digestion results. It can be seen that none of the treatments altered detected levels of CD31 or HOMEC viability (see figures 39 - 40). Results are summarised in table 21.

Collagenase treatment	% CD31+ve/PI-ve
20 minutes collagenase II	99.7 ± 0.8
2 hours collagenase I	99.2 ± 1.9
Sequential digestions	98.6 ± 1.4

Table 21. HOMEC viability and surface CD31 detection of HOMECs following enzymatic digestions from the original digestion protocol. Sequential digestions consisted of the 20 minute collagenase treatment, followed by the 2 hour collagenase I treatment. Data are the mean percentage ± SD of HOMECs in the samples positive for surface CD31 and negative for PI, as detected by flow cytometry, n=6.

The trypan blue data confirmed that cell viability was not significantly affected by any of the treatments, see figure 40. Results are summarised in table 22.

Collagenase treatment	% viability
20 minutes collagenase II	99.5 ± 0.9
2 hours collagenase I	98.7 ± 1.5
Sequential digestions	98.5 ± 1.1

Table 22. HOMEC viability of single HOMECs following enzymatic digestions from the original digestion protocol. Sequential digestions consisted of the 20 minute collagenase treatment, followed by the 2 hour collagenase I treatment. Data are the mean percentage ± SD of viable HOMECs as determined by trypan blue, n=6.

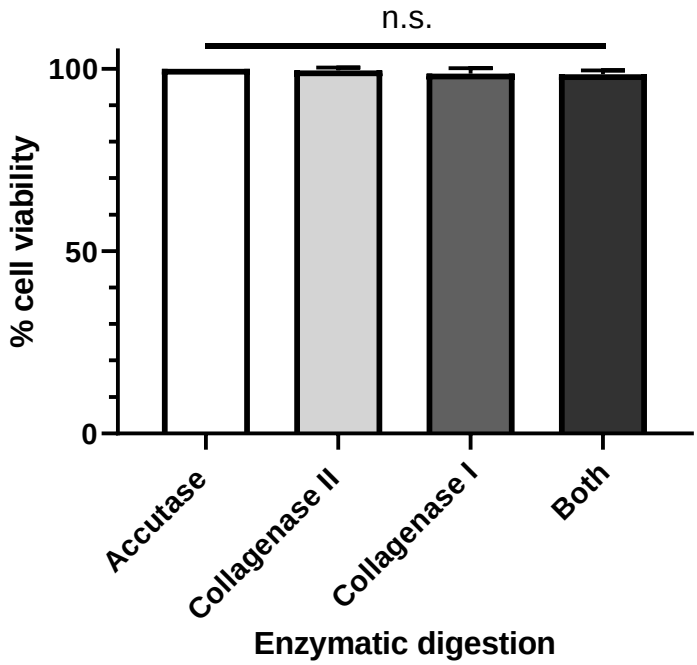

Figure 39. Collagenase enzymatic digestion conditions from the original isolation protocol do not affect surface CD31 or the viability of cell HOMECs, as assessed by flow cytometry. Previously isolated HOMECs were grown to confluence in 6-well plates before dissociation with accutase. Cells were subjected to either 20 minutes of collagenase II treatment, 2 hours of collagenase I treatment, or both treatments sequentially. Cell surface CD31 and PI positivity was analysed by flow cytometry. Data are presented as the mean ± SD and are shown as the percentage of cells in the sample positive for CD31 and negative for PI staining (n=6). Accutase dissociation was used as the 100% control. Kruskal-Wallis analysis showed no significant differences between any of the treatments (p=0.2941).

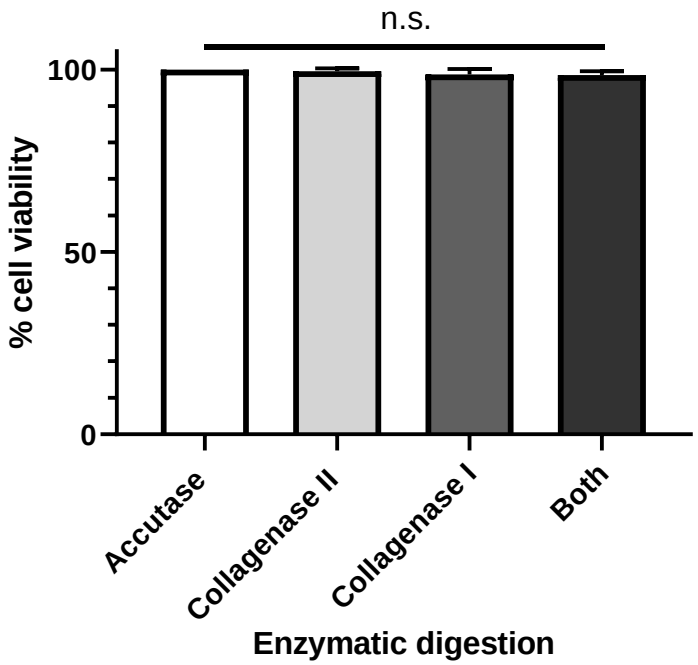

Figure 40. Collagenase enzymatic digestions from the original isolation protocol do not affect the viability of cell HOMECs, as assessed by trypan blue. Previously isolated HOMECs were grown to confluence in 6-well plates before dissociation with accutase. Cells were subjected to either 20 minutes of collagenase II treatment, 2 hours of collagenase I treatment, or both treatments sequentially. Cell viability was assessed by trypan blue exclusion and cell counting; 3 trypan blue reads were prepared and analysed separately and counted as an n=1. Data are presented as the mean ± SD and are shown as the percentage of viable cells (n=6). Accutase dissociation was used as the 100% control. Kruskal-Wallis analysis showed no significant differences between any of the treatments (p=0.0525).

3.3.2.3 Original protocol enzymatic digestions did not affect the viability or CD31 detection on HOMECs

HOMEC viability remained high after accutase treatment at 98±1 and 99±1% respectively. This was important since this removal of cells from plastic with accutase was a necessary step in all cell preparations, including cells that were then subjected to enzymatic treatments. This finding also allowed for the accutase results to be used as a control for the enzymatic digestion results. Flow cytometry analysis showed no significant effects of any of the digestion treatments on either CD31 or cell viability, and the viability data were confirmed by trypan blue analysis (see figures 39 - 40). Although the data appear to show a slight decrease in viable CD31 expressing HOMECs and trypan blue determined viable HOMECs in both the 2 hour collagenase and sequential digestions, the minimum viability reached was 98.5% (sequential treatment). These data therefore allowed the rejection of two of the hypotheses in table 20: enzymatic digestions in the original protocol did not cleave CD31, and did not decrease HOMEC viability.

It is important to note that these experiments were performed on a pure, single suspension of HOMECs that were exposed to the enzymes for the entire digest times. This is opposed to HOMECs during the isolation from tissue, where although it is possible for HOMECs to be released from tissue straight away, this is unlikely. Additionally, any HOMECs released during the first digestion would likely be lost during the PBS washing step, and so would not then be exposed to the second digestion. Importantly, none of the treatments in the original protocol were found to significantly affect CD31 detection or HOMEC viability. Indeed, Winiarski *et al* (2011) stated that isolation success and complete omental digestion were correlated. Therefore it was deemed important to then consider the third hypothesis in table: that the original enzymatic digestions were insufficient to release sufficient numbers of HOMECs.

3.3.2.4 Examination of the effect of extended enzymatic digestions on HOMEC recovery from omental tissue

Viable CD31 positive HOMECs released from the tissue at varying stages during the protocol were quantified. This method also allowed for monitoring of tissue digestion, and helped inform other potential protocol improvements.

HOMEC surface CD31 and viability were studied at different steps of the protocol: after the 20 minute collagenase II digestion, and after the 2 hour collagenase I digestion. The digestions were also extended to as follows: 20 minutes to 1 hour of collagenase II, and 2 hours to 3.5 and 5 hours of collagenase I. The 20 minute collagenase II digestion was performed before each extended collagenase I digestion.

In each case, the protocol was performed as usual until the end of the extended digestions. Any undigested tissue was removed with the gauze filtration step, and the cell pellet was generated and washed as described in 2.3.1.3. The cell pellet was resuspended and a sample was removed for staining for flow cytometry. The rest of the suspension was returned to the digestion, if there was a future timepoint. This was done so that the number of cells in cell pellets could be monitored over the digestion courses. Viable HOMECs (CD31+ve/PI-ve) were identified as described in 3.3.2.1. Three runs were performed on the flow cytometer, and collated to bring the total number of events to 15,000. This was done as the samples contained a mixed cell population and therefore analysing a higher cell number was more representative of the tissue. Previously isolated and characterised HOMECs were used for gating. A representative tissue sample scatter and viable/non-viable CD31+ve cell gating is shown in figure 41. Viable HOMECs were calculated as percentage of the cells present in the sample (the cell pellet at this point is a mixed population). The total number of cells in the cell pellet was estimated from cell counting (gated to count particles ≥6µm), and the percentage/number of possible viable HOMECs was extrapolated, in order to investigate which digestions produced the highest proportion viable HOMECs. Furthermore, the percentage/number of non-viable HOMECs (CD31+ve/PI+ve) in the cell pellet was calculated and used to calculate the percentage of viable HOMECs in all HOMECs released from the digestion(s). This was to investigate which digestions released the most HOMECs overall (viable and non-viable).

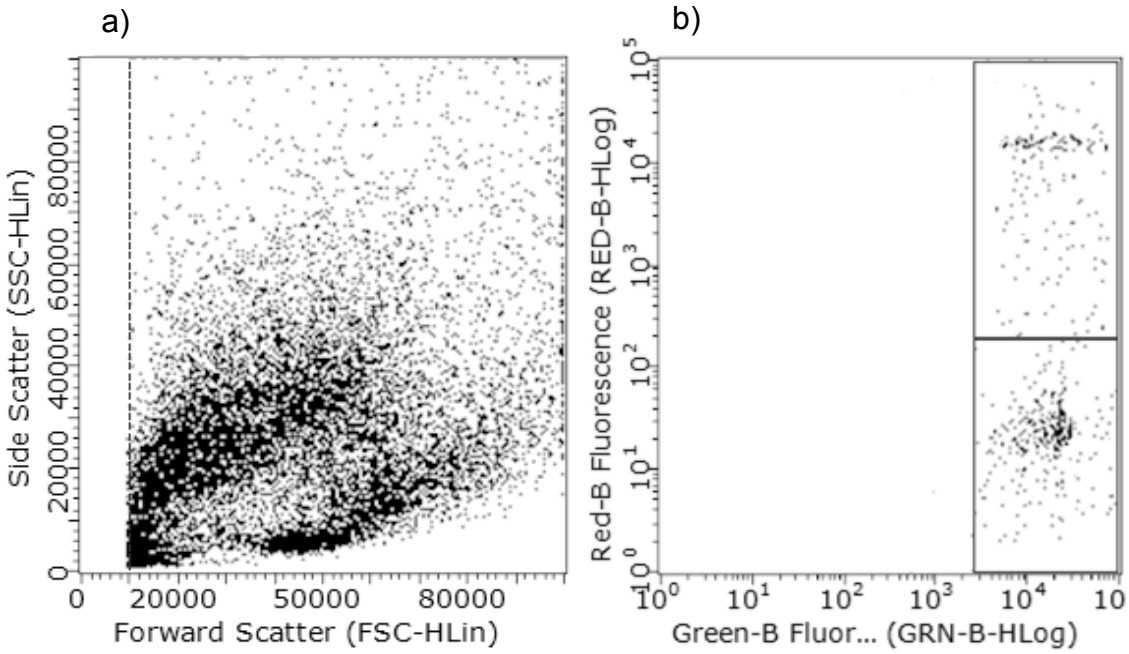

Figure 41. Representative tissue scatter plots from the mixed cell and debris pellet generated from the original isolation protocol. a) representative forward and side scatter of the mixed cell population. b) representative plot of CD31+ve cells from a tissue sample; bottom gate PI-ve (viable), top gate PI+ve (non-viable). Scatter shows 15,000 events from 3 runs from the same sample.

3.3.2.5 Examination of the effect of extended enzymatic digestions on HOMEC recovery from omental tissue

The percentage of all recovered cells identified to be viable HOMECs (CD31+ve/PI-ve) after the original and extended digestions are summarised in table 23.

Collagenase treatment	% cell pellet CD31+ve/PI-ve
20 minutes collagenase II	1.0 ± 0.5
1 hour collagenase II	0.5 ± 0.3
2 hours collagenase I	1.8 ± 0.6
3.5 hours collagenase I	3.6 ± 0.8
5 hours collagenase I	6.7 ± 1.0

Table 23. Percentage of all recovered cells identified as CD31+ve/PI-ve (HOMECs) after original and extended collagenase II and I digestions. All collagenase I digestions were preceded by the 20 minute collagenase II digestion. Data are the percentage ± SD of HOMECs in the samples positive for surface CD31 and negative for PI, as detected by flow cytometry, n=14.

Paired analysis between the two collagenase II digestions showed that there was a significant reduction in the generation of viable HOMECs out of all cells recovered if the digestion was extended to 1 hour from 20 minutes (p=0.0044, see figure 42). Paired analysis revealed that the extended 3.5 and 5 hour collagenase I digestions significantly increased the generation of viable HOMECs out of all cells recovered compared with the 2 hour digestion (p=0.0001). Moreover, the percentage of HOMECs collected after 5 hours collagenase I was significantly higher (+3.1%) than at the 3.5 hour digestion (p=0.0001) (see figure 42).

The percentage of recovered viable HOMECs out of all CD31+ve cells released by original and extended digestions are summarised in table 24.

Collagenase treatment	% viable HOMECs (out of total CD31+ve cells)
20 minutes collagenase II	44.7 ± 5.2
1 hour collagenase II	43.8 ± 6.6
2 hours collagenase I	81.5 ± 7.7
3.5 hours collagenase I	79.1 ± 7.8
5 hours collagenase I	78.6 ± 8.0

Table 24. Percentage of viable HOMECs (CD31+ve/PI-ve cells) out of all HOMECS released (CD31+ve only) after original and extended collagenase II and I digestions. All collagenase I digestions were preceded by the 20 minute collagenase II digestion. Data are the mean percentage ± SD of viable HOMECs (positive for surface CD31 and negative for PI) out of all CD31+ve cells (HOMECs), as detected by flow cytometry, n=14.

Paired analysis of the data obtained from the two collagenase II digestions showed a significant decrease with the 1 hour digestion in the percentage of viable HOMECs out of all HOMECs released (p=0.007, see figure 43). There were no significant differences in the percentage of viable HOMECS out of all HOMECs released between the 2 and 3.5 hour collagenase I digestion (p=0.3473), the 2 hour and 5 hour digestions (0.2407), or between the 3.5 and 5 hour digestions (p=0.1917) (see figure 43).

Total cells recovered after 20 minutes and an hour of collagenase II digestion ranged from approximately 400,000 - 1.6 million cells, and 954,000 - 42 million cells, respectively. Total cells recovered following 2, 3.5 and 5 hours of collagenase I digestion (after 20 minutes of collagenase II) ranged from: 1.9 – 21 million, 23 – 34 million, and 64 – 70 million cells, respectively. Paired analysis on tissues showed a significant increase in cell number (in the cell pellet) in the 1 hour collagenase II digestion compared to the 20 minute digestion (p=0.0001, see figure 44). Paired analysis on tissues showed a significant increase in cell number (in cells recovered) in both the 3.5 and 5 hour collagenase I digestions compared with the 2 hour digestion (p=0.0001). Additionally, the 5 hour digestion significantly increased the cell number collected significantly compared with the 3.5 hour digestion (p=0.0001, see figure 45).

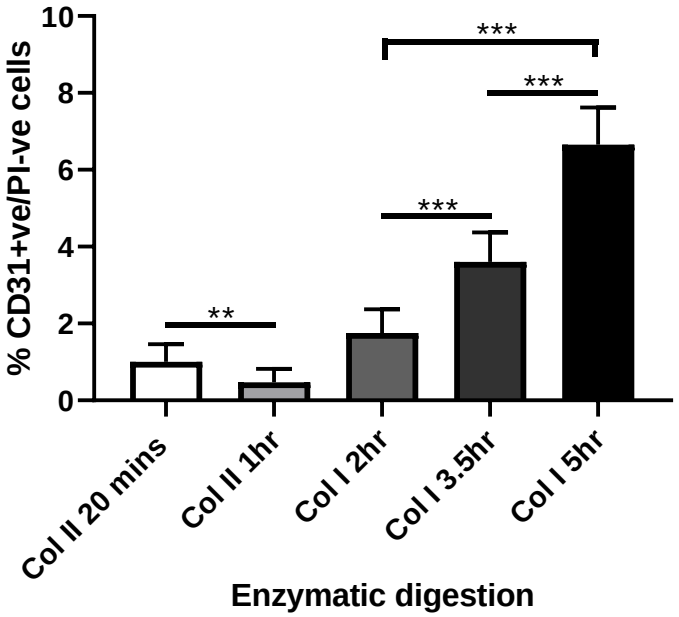

Figure 42. Mean percentage of viable HOMECs in total cells released from omental tissue following different enzymatic digestions. The isolation protocol (section 2.3.1.3) was followed as usual until the end of the extended (or normal) enzymatic digestion. Any undigested tissue was removed with gauze filtration, and a cell pellet was generated and washed as described in 2.3.1.3. Viable HOMECs (CD31+ve/PI-ve) were identified by flow cytometry of 15,000 events. HOMECs were expressed as a percentage of the total cell number recovered. Different enzyme digestions are shown (Col II = collagenase II; Col I = collagenase I). Data are the mean ± SD (n=14). **p=0.0044, ***p=0.0001 (Wilcoxon matched-pairs signed rank test).

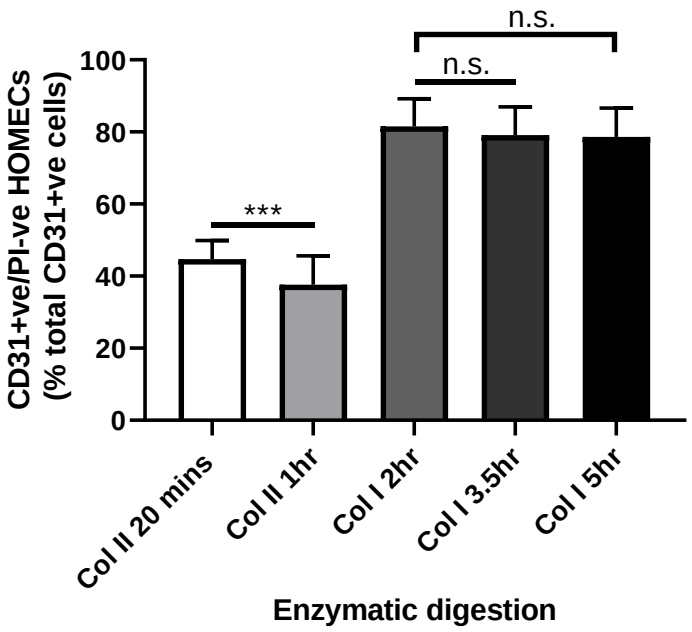

Figure 43. Mean percentage of viable HOMECs in CD31+ve cells released from omental tissue following different enzymatic digestions. The isolation protocol (section 2.3.1.3) was followed as usual until the end of the extended (or normal) enzymatic digestion. Any undigested tissue was removed with gauze filtration, and a cell pellet was generated and washed as described in 2.3.1.3. Total HOMECs (CD31+ve) and viable HOMECs (CD31+ve/PI-ve) were identified by flow cytometry of 15,000 events. Viable HOMECs are expressed as a percentage of total HOMECs (CD31+ve/PI+ve). Different enzyme digestions are shown (Col II = collagenase II; Col I = collagenase I). Data are presented as the mean ± SD (n=14). ***p=0.0007 (Wilcoxon matched-pairs signed rank test).

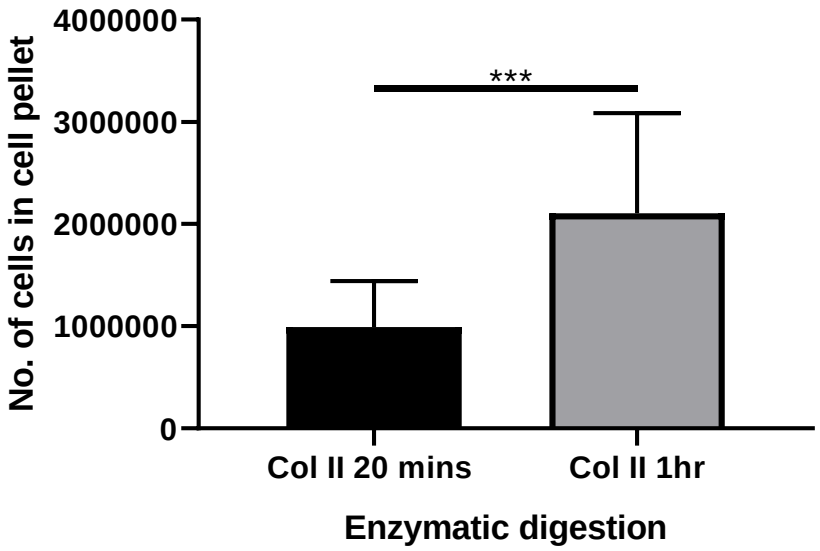

Figure 44. Number of cells present in the cell pellets generated from omental tissue after 20 minutes or 1 hour of collagenase II digestion. The isolation protocol (section 2.3.1.3) was followed as usual until the end of the extended (or normal) enzymatic digestion. Any undigested tissue was removed with gauze filtration, and a cell pellet was generated and washed as described in 2.3.1.3. The number of cells in the cell pellet was quantified using a cell counter. Different enzyme digestions are shown (Col II = collagenase II). Data are presented as the mean ± SD (n=14). ***p=0.0001 (Wilcoxon matched-pairs signed rank test).

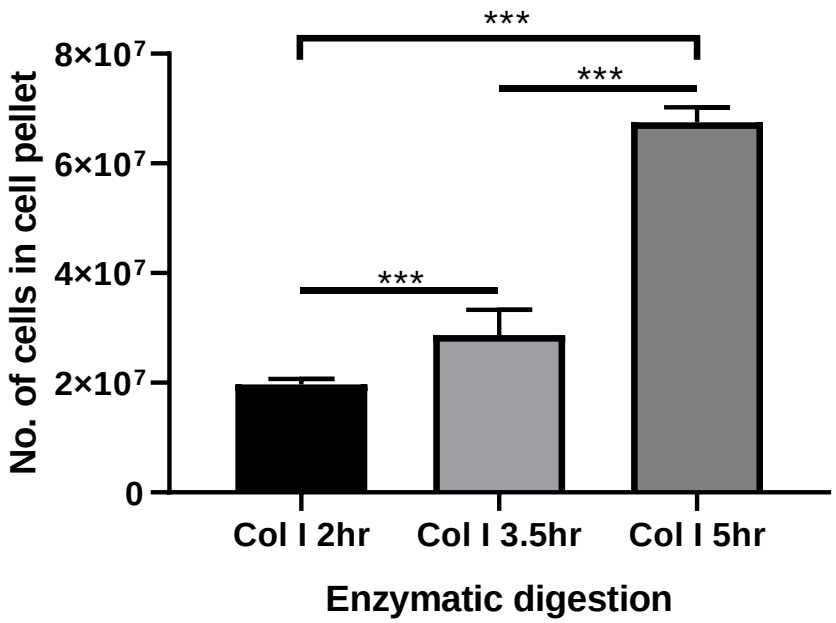

Figure 45. Number of cells present in the cell pellets generated from omental tissue after 2 hours, 3.5 hours, and 5 hours of collagenase I digestion (following 20 minutes of collagenase II digestion). The isolation protocol (section 2.3.1.3) was followed as usual until the end of the extended (or normal) enzymatic digestion. Any undigested tissue was removed with gauze filtration, and a cell pellet was generated and washed as described in 2.3.1.3. The number of cells in the cell pellet was quantified using a cell counter. Different enzyme digestions are shown (Col I = collagenase I). Data are presented as the mean ± SD (n=14). ***p values = 0.0001 (Wilcoxon matched-pairs signed rank tests).

3.3.2.6 The effect of extended enzymatic digestions on HOMEC recovery from omental tissue

This analysis allowed the hypothesis: the enzymatic digestions decreased HOMEC viability (see table 20), to be investigated. The percentage of viable HOMECs in the total cell pellet was found to decrease when the collagenase II digestion was extended to an hour from 20 minutes (see figure 42). This suggested that the extended collagenase II exposure decreased HOMEC viability. This was supported by the significant reduction in percentage of viable HOMECs in the total HOMEC population recovered after the extended digestion (see figure 43). Interestingly, the 1 hour collagenase II digestion was found to significantly increase the total number of cells released from each tissue compared to the 20 minute collagenase II digestion (see figure 44). Although this would theoretically include the release of more HOMECs, a decrease in HOMEC viability was observed, therefore these data suggest that although more HOMECs may be present in the pellet, more HOMECs are non-viable at this point. The majority of the cells released from the tissues after the 20 minute digestion were later found to be mesothelial, and this in turn led to the development of a mesothelial isolation in other work in our lab (data not shown).

The percentage of viable HOMECs recovered in the total cell pellet increased with longer collagenase I digestions (see figure 42). This suggested that viable HOMECs contributed an increasingly larger percentage of the total cell pellet as the digestion was extended. It is important to note that 5 hours was almost always enough time for the entire fat tissue to be digested, an endpoint that was found to be associated with increased isolation success in the original protocol (although this rarely occurred with the original digestion times). However, even in this scenario, the gauze step in this case was still necessary, as indigestible denser connective tissue remained. Interestingly, the percentage of viable HOMECs recovered compared with total HOMECs did not change significantly (see figure 43) with increased digestion. This suggested that although more HOMECs were being released from the tissue, some HOMECs had also become non-viable. However, as HOMECs were constituting an increasingly large percentage of the total cell pellet, and the cell pellets were significantly increasing overall (see figure 45), the data suggested that the longer the

collagenase I digestion, the greater the number of viable HOMECs that could potentially be recovered.

The range of cells generated from the tissues appeared to be related to the size of the tissue. However, the size of the tissue was not observed to be a good indicator of isolation success. This was likely due to the heterogeneity of the tissue samples received.

Ultimately, the data indicated that viable HOMECs were recovered after all digestions, including those from the original protocol. The extended digestion analysis suggested that an hour of collagenase II significantly decreased HOMEC viability, but neither the 3.5 nor 5 hour collagenase I digestions significantly reduced HOMEC viability. Analysis of the 20 minute collagenase II digestion on previously isolated HOMECs in section 3.3.2.2 showed no significant effect on HOMEC viability. This would suggest that all the HOMECs recovered during this collagenase II digestion are viable. However, this was not supported by the data on tissue digestion, where only 44.7% of recovered HOMECs were viable. It is possible that some HOMECs recovered from tissue at this early stage in the protocol are damaged during collection and storage, and that HOMECs located deeper in the tissue sample remained viable for longer prior to the isolation protocol. Importantly, the 5 hour collagenase I digestion was shown to not adversely affect HOMEC viability, and to increase the number of cells generated, as well as typically allowing for full fat tissue digestion. Therefore the 2 hour digestion was extended to 5 hours for all future isolations. This was coupled with an alteration to the swinnex filtration step, which is described below. The final results from this amended protocol are described in section 3.3.5, and address the final digestion hypothesis from table 20: the original enzymatic digestions did not recover sufficient numbers of HOMECs to generate successful cultures.

3.3.3 Omission of the swinnex filtration protocol

In the development of the original protocol (Winiarski *et al*, 2011), the swinnex step was added in order to remove single cells, as these were thought to be contaminants. However data from this thesis have suggested that HOMECs are actually lost at this stage, as single cells. The adaption of a 5 hour collagenase I

digestion as described above could result in larger numbers of viable HOMECs available as single cells after the digestion protocol. This step was therefore omitted; success would be indicated by successful HOMEC cultures that were not overtaken by contaminating cells. The filtration would have occurred after the 5 hour collagenase I digestion, and various washing steps; its omission meant that after the generation of the washed cell pellet, the immunoselection was performed immediately.

3.3.4 Optimisation of the immunoselection protocol

The proportion of ECs within the mixed cell suspension produced by the isolation protocol was previously unknown. The 5µl of dynabeads used in the immunoselection was calculated to contain 2,000,000 beads, based on manufacturer information. Data from section 3.3.2.5 indicated that the original enzymatic digestions produced cell pellets ranging from 1.9 – 21 million cells. These values suggest that the beads/cell ratio in the immunoselection ranged from approximately 1 – 11. In initial HOMEC culture, HOMECs that retained beads were observed to retain multiple beads; adherent beads were counted on 30 individual HOMECs from 5 different isolations, and ranged from 4 and 62, with an average of 44/cell. Previous work by Pezzi *et al* (2018) had reported that certain magnetic beads may reduce cell viability after isolation, and therefore the effect of beads/cell on endothelial cell viability across a range of 2 – 64 beads/cell dilutions were studied. This work was carried out on human cerebral microvascular endothelial cells (hCMEC/D3s) as HOMECs were unavailable at the time. The viability work was carried out by Georgina Westwood.

3.3.4.1 The effect of dynabeads on endothelial cell viability

Previous work demonstrated that dynabeads affect absorbance readings when cells were analysed with a spectrophotometer (data not shown). Therefore endothelial cell viability was assessed by lactate dehydrogenase (LDH) release assay (ThermoFisher). The lactate dehydrogenase enzyme is released into culture medium if there is any loss of plasma membrane integrity, which is indicative of cell death. In the assay, released LDH is added to a reaction

mixture containing lactate. LDH catalyses the conversion of lactate to pyruvate in a reduction reaction that produces NADH. This is then oxidised, which leads to the reduction of a tetrazolium salt. The red formazan product can be quantified spectrophotometrically. Since this assay uses the cell supernatant, the interference from beads is removed as a confounding variable. A positive control of 1mM hydrogen peroxide treated cells was included to confirm that cell cytotoxicity resulted in generation of LDH, and to calculate the maximum LDH activity. Samples of complete media without cells were used as a control to quantify spontaneous LDH activity.

Cells were seeded for the assay as described in section 2.3.2.1. After cells had been starved overnight in 2% FCS endothelial starve media, cells were treated with bead concentrations of 2, 4, 8, 16, 32, and 64 beads/cell, and incubated for a further 24 hours. For the assay, 50µl of medium from each sample (and control) was then transferred to a new plate, and 50µl of reaction mixture was added to each well. The plate was incubated at RT for 30 minutes in the dark, before 50µl of stop solution was added. The plate was gently tapped to ensure solutions were mixed, and absorbance was read at 490/680nm on a PHERAstar Plus Optima plate reader. The percentage of cytotoxicity was calculated with the following formula:

$$\% \text{ cytotoxicity} = \frac{\text{Bead treatment generated LDH activity} - \text{spontaneous LDH activity}}{\text{Maximum LDH activity} - \text{spontaneous activity}} \text{ x } 100$$

3.3.4.2 The different concentrations of dynabeads did not affect endothelial cell viability

None of the beads/cell ratios tested were found to result in significant levels of cell death in hCMEC/D3 cells (see figure 46), p=0.3013.

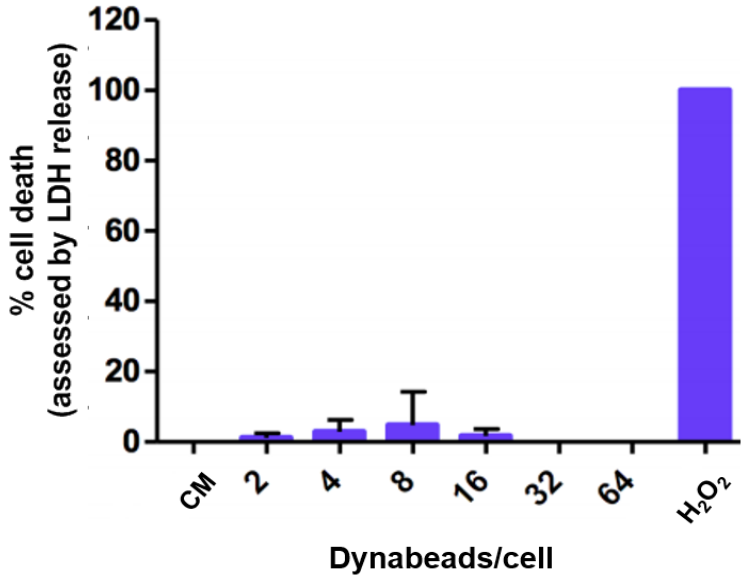

Figure 46. Anti-CD31 dynabeads (2 - 64 beads/cell) exhibited no cytotoxic effects on hCMEC/D3 cells after 24 hours. Cells were starved overnight in 2% FCS endothelial media before beads were added. After 24 hours, supernatants were removed for LDH assay and analysis. Absorbance was read at 490/680nm. Results are shown as the percentage of maximum LDH (as generated by the action of hydrogen peroxide on cells, H_2O_2). Data are the mean ± SD (n=4). Kruskal-Wallis analysis showed no significant differences in cell death between cells treated with increasing numbers of dynabeads, p=0.3013.

3.3.4.3 Dynabeads did not affect endothelial cell viability

The data indicated that the dynabeads did not significantly affect the viability of endothelial cells at any of the concentrations tested. It should be noted that although no statistical testing was able to be performed on the complete media and hydrogen peroxide controls, that the value of 0% LDH for complete media (calculated from the 100% hydrogen peroxide value) indicated that the assay worked. Overall, these data suggested that the hypothesis: the dynabeads affected HOMEC viability, could be rejected.

3.3.4.4 Potential dynabead binding to fibroblasts

The observation that fibroblasts were present in HOMEC cultures, raised the possibility that the dynabeads could be binding (and thus selecting) other cell types. However, observational study of dynabeads mixed with human omental fibroblast cultures did not observe any binding, suggesting that the hypothesis: the dynabeads were binding to fibroblasts, could be rejected.

3.3.4.5 Overall considerations for the immunoselection

The dynabeads at concentrations ranging between 2 and 64 beads/cell were not found to significantly affect EC viability. This suggests that the 5µl of dynabeads used in the original protocol (which equates to 1 – 11 beads/cell, based on cell pellet analysis in section 3.3.2.5) would not have affected HOMEC viability. From the manufacturer's protocol, the 2,000,000 beads contained in the 5µl of bead suspension would suffice for a cell suspension containing 20,000,000 cells. This was appropriate for the original isolation, as the maximum cell pellet counted was 21 million cells. However, data in section 3.2.2.5 showed that cell pellets generated from the extended digestions could be as large as 70 million cells. It was therefore decided that the final cell suspension should be counted and the volume of dynabead suspension added adjusted accordingly. For example, a pellet of 60 million cells would require 15µl of dynabeads. This step was added to the final protocol (see section 3.3.6).

Whilst the dynabeads were not observed to adhere to the fibroblasts, the fibroblast presence in culture suggested that their separation into the final purified suspension was occurring. It was possible that fibroblasts, and indeed other contaminant cells, were dragged to the wall of the tube when the beads and bead-bound cells were magnetised towards the wall. A solution to this problem could not be found, although it was noted that manufacturer guidelines instructed the magnetic separation to be undertaken in 1ml of 0.1% BSA (w/v), not 500µl. It was therefore decided to conduct the separation in 1ml of 0.1% BSA (w/v), as this would allow the suspension to spread out more and hopefully result in less isolation of non-bound cells.

3.3.5. The effect of protocol changes on isolation success rate

	Omenta samples	Initial isolation success	Initial isolation success (%)	Culture success	Isolation and culture success (%)
Original protocol	30	10	30	1	10
Protocol + changes	41	23	56	14	34

Table 25. Rates of success of initial isolation and subsequent culture following the original protocol and the amended protocol. The original protocol had an approximate 30% success rate of isolating HOMECs initially, and an approximate 10% success rate in generating a pure HOMEC culture (culture success). The initial success rate for the new protocol was approximately 56%, and 34% for culture success. Percentages were calculated from the number of omenta samples and the number of initial and initial and culture successes, to the nearest whole number.

The data suggested that the amended longer collagenase I digestion protocol and omission of the swinnex filtration steps improved both the initial and culture success rate compared to the original protocol. Initial isolation success improved by approximately 26% and overall culture success by 24%. The analysis of protocol success rate was complicated by the variation in tissue samples received; tissues varied in size and composition. However, the improvement in HOMEC isolation and culture was apparent after the analysis of 10 tissues (out of the 41 in table 25), and therefore these changes were incorporated going forward. The final protocol is summarised below in section 3.3.6.

3.3.6 The new protocol

The resulting final protocol followed the Winiarski protocol (as described in 2.3.1.3) until the collagenase I digestion step. This digestion step was extended to 5 hours. Any undigested tissue was removed by filtering through non-woven

gauze. The suspension was separated into layers, and the oil and enzyme solution discarded. The pellet was then washed with 10% BSA/PBS (w/v) followed by PBS (all as described in 2.3.1.3). The swinnex filtration step was omitted, and the washed cell pellet was re-suspended in 1ml of 0.1% BSA/PBS (w/v). At this point, the number of cells in the suspension was counted by cell counter, and the volume of dynabead suspension added adjusted accordingly (see section 3.3.4.5). The immunoselection was performed as described in section 2.3.1.3, except the 0.1% BSA/PBS (w/v) volume was increased to 1ml. HOMECs were seeded as described in section 2.3.1.3.

3.3.7 Overall discussion of the new protocol

Analysis of the extended collagenase I digestion indicated that this resulted in a higher percentage of viable HOMECs in the cell pellet. Whilst the percentage of viable HOMECs to total recovered HOMECs did not change, the greater number of overall cells released did result in a greater number of HOMECs recovered. This suggested that longer collagenase I digestion was optimal. As shown in table 25, the changes made to the original isolation protocol improved the success rate of HOMEC isolation and culture from 30% to 56%. Whilst this is a marked improvement, a 44% failure rate still leaves much room for improvement. In this particular project, this was mainly mitigated by a mostly reliable supply of omental tissues, where the 1 in 3 success rate from the new protocol was sufficient to supply HOMECs for experimental work. The previous 10% chance of success was not sufficient to provide enough HOMECs, and indeed earlier in the project, the supply of omental tissue was less reliable.

Despite the improvements there is undoubtedly HOMEC loss still occurring somewhere during the protocol. For example, data from table 23 suggests that after 20 minutes of collagenase II digestion followed by 5 hours of collagenase I digestion, viable HOMECs comprise approximately 6.7% of the cell pellet, as assessed by the percentage of CD31+ve/PI-ve cells. The lowest counted cell pellet from a tissue generated by these digestions was 67 million cells. Taken together, these data would suggest that the pellet would contain 4,489,000 viable HOMECs. However, the final bead/cell suspension seeded for culture was never observed to be close to this number. Successful isolations would often take up to three weeks to reach confluence in the well, and a confluent

layer of HOMECs would consist of approximately 1 million cells. It is possible that the initial identification of HOMECs in the pellet was inaccurate, since although CD31 is an endothelial cell marker, it is also thought to be expressed on T cells and macrophages (McKenney *et al*, 2001; Douaisi *et al*, 2017). This could mean that the HOMEC numbers were overestimated. However, with cell pellets between 64 and 70 million, it seems unlikely that the few HOMECs ultimately isolated were the only ones present in the pellets. It is therefore also possible that there were additional problems with the immunoselection. The number of beads/cell was taken from the manufacturer's instructions, and although increasing the number of beads used seems like a way of potentially improving the selection, adding more beads would contribute to the problem of non-specific physical separation other cell types. A further consideration is instances of successful isolations that appeared to remain pure, yet failed to culture successfully.

Although the plentiful supply of omental tissue generally mitigated the relative inefficiency of this protocol, there were times when tissue supply was reduced. It was therefore thought prudent to investigate the possibility of isolating cells by fluorescence activated cell sorting (FACS). This approach can utilise multiple markers for selection, and can result in sorted populations of microvascular endothelial cells of approximately 95% purity (Bernard-Patrzynski *et al*, 2019). This work is discussed in the next section.

3.4 HOMEC isolation: cell sorting approach

The immunoselection used in the original and new HOMEC isolation protocol was shown to remain inefficient, as discussed in previous sections. The number of HOMECs initially isolated was low, and contaminating cells were still present. Therefore a FACS based approach was investigated. This technique utilises the principles of flow cytometry; antibodies conjugated to fluorophores are used to identify cells of interest from within a heterogeneous cell population. In the case of cell sorting, labelled and un-labelled cells are assigned a positive or negative charge. Cells pass through an electrostatic deflection system, and are sorted into two or more containers (Almeida *et al*, 2014).

The magnetic separation based immunoselection was limited in that it was a positive selection using one marker, of only one of the cell types in the mixed cell suspension. Therefore additional markers were investigated for suitability for a cell sort, where markers could potentially be used to positively separate unwanted cell types (which would be separated from HOMECs). Markers were investigated on the cell types thought to mostly comprise the isolation cell suspension: human omental fibroblasts (HOFs), human omental mesothelial cells (HOMesos), pericytes, and HOMECs.

3.4.1 Considerations for FACS

HOMECs isolated from a cell sort would subsequently be cultured. Therefore this cell sort would require an aseptic clean of the cell sorter prior to the cell sort. Importantly, the cell sorter and collection tubes are not temperature or gas controlled, and therefore the timing of the sort would need to be as quick as possible in order to preserve cell viability. Furthermore it is advantageous to have the population of cells undergoing sorting to contain a highest possible proportion of the desired cells. In section 3.3.7, CD31+ve/PI-ve negative cells (considered to be HOMECs) were found to comprise approximately 6.7% of the cell pellets generated by the new protocol. Therefore part of the work in this section focussed on the removal of other cells from the suspension.

3.4.1.1 The removal of erythrocytes from the cell suspension

The cell suspension was known to contain erythrocytes (visualised by microscopy). The settings used for flow cytometry were chosen to eliminate debris and erythrocytes (based on forward and side scatter) and although this likely removed most of them, some would remain and register as events during flow cytometry. This necessitated their removal as the scatter would be complicated and the sort prolonged. Erythrocytes were lysed as follows, after generation of the cell pellet: 1ml of 10x ddH_2O was added and the cells resuspended. The cell suspension was gently swirled for 30 seconds, lysing the erythrocytes. Osmotic pressure was restored with 9ml of PBS, and the cells re-pelleted at 350*g* at 4°C. The previously red pellet would then turn white. The new protocol was then resumed. To confirm that the ddH_2O did not affect HOMEC viability, the treatment was carried out on pure populations of HOMECs; cells were trypsinised and subjected to trypan blue staining, as described previously. The HOMECs were then subjected to the ddH_2O treatment, before restoration of osmotic pressure with 9ml PBS. HOMECs were again assessed for viability with trypan blue. No effect on HOMEC viability was observed (data not shown).

3.4.1.2 DNase I treatment

The ddH_2O treatment was found to lead to some cell clumping, presumably due to the release of DNA. Therefore DNase I was added to a final concentration of 100µg/ml after RBC lysis. The cell pellet was resuspended gently and incubated for 15 minutes at RT. Cells were re-pelleted and washed as described in 2.3.1.3. This step was found to reduce the cell clumping and promote a single cell suspension, which is required for cell sorting.

3.4.2 Cells and cell surface markers to target with FACS

Markers on HOMECs as well as contaminating cell types in the cell suspension were investigated, as cell sorting could allow for the separation of HOMECs from other cell types by targeting markers on other cell types. All markers tested were surface markers; no permeabilisation could be performed to target any intracellular markers as this would reduce cell viability. Additional markers for

endothelial cells were tested in addition to CD31, which was previously shown to be a suitable surface marker for HOMECs for flow cytometry in section 3.3.2.2, where surface detection was shown to be 98% ± 1.This was because cell sorting could potentially be optimised based on targeting multiple markers present on one type of cell. Markers for fibroblasts, mesothelial cells and pericytes were investigated to ascertain whether suitable markers could be utilised for a separate isolation for any of these contaminating cells. Markers tested to identify certain cell types, and antibodies used are summarised in table 26.

Cell type	Marker(s)	Antibodies
HOMECs	CD31	Mouse anti-human CD31 AlexaFluor 488, Biolegend
	CD105	Mouse anti-human CD105 PE, Biolegend
	CD34 (Ribatti *et al*, 2020)	Mouse anti-human CD34 FITC, Biolegend
HOFs	-	-
HOMesos	-	-
Pericytes	CD13 (Yamakazi and Mukouyama, 2018)	Mouse anti-human CD13 APC, Biolegend

Table 26. Surface markers, cell types, and antibodies tested to develop a cell sorting antibody panel. HOMECs = human omental microvascular endothelial cells, HOFs = human omental fibroblasts, HOMesos = human omental mesothelial cells.

After investigation, no surface markers were tested for HOFs or HOMesos, as the available specific reported markers were all intracellular. Therefore these cells were only tested for surface detection of markers for other cell types in order to investigate the specificity of the antibodies, as it was important to know if antibodies could bind to more than one cell type since this would have implications in a potential cell sort.

3.4.2.1 Investigation into potential FACS markers

All cells except pericytes, were sourced from omental tissue; HOMECs were isolated as described in 3.3.6, HOMesos were gifted from Gillian Phua (isolation method not shown) and HOFs were easily sourced as by-products from failed isolations. Human brain vascular pericytes (along with their medium and associated growth supplement) were instead sourced from ScienCell. During experimentation on pericytes with the CD13 antibody, it was observed that surface detection appeared to vary depending on the age (passage number) of the pericytes used. Therefore pericytes between both passages 4 - 6 and 11 – 13 were used for these experiments. Culture materials and methods for all cell types are described in section 2.2.

Surface detection of the markers in table 26 were studied on each cell type by flow cytometry. Pure populations of the cell types were used in each case. Flow cytometry was carried out as described in 3.3.2.1 (with antibodies from table 26). The mean fluorescence intensity (MFI) for unstained and stained cells was calculated. Additionally, the percentage of cells within each population that bound the antibody was calculated (% stained cells). The MFI for unstained (control) and stained cells was compared for each cell type. Where HOMEC markers were studied, the MFI for stained HOMECs was compared to the MFI for stained cells of the other cell types. Where surface detection of a marker was strong for the associated cell type, the marker was then tested against the other cell types to assess for FACS suitability.

3.4.2.2 CD31, CD34, CD105 AND CD13 as potential markers for FACS

CD31

The surface detection of CD31 (MFI) on unstained and stained cells is shown in table 27. Representative histograms are shown in figure 47.

Cell type	Unstained MFI	Stained MFI	% stained cells
HOMECs	24.4 ± 10.3	2690.8 ± 73.4	99.3 ± 0.3
HOFs	69.3 ± 17.2	76.4 ± 13.6	0.6 ± 0.1
HOMesos	55.3 ± 27.3	59.8 ± 23.5	0.8 ± 0.2
p4 - 6 pericytes	21.6 ± 13.2	29.7 ± 9.4	0
P11 - 13 pericytes	22.6 ± 12.7	23.6 ± 9.9	0

Table 27. The median fluorescence intensity (MFI) and percentage of cells binding the conjugated CD31 antibody on different cell types. Pure populations of cells were analysed by flow cytometry. Data shown are the mean ± SD of (n=6).

It was noted that unstained HOFs and HOMeso cells displayed naturally higher autofluorescence than unstained HOMECs (see table 27 and figure 47). However, there was no overlap in the MFI values between these cell types and stained HOMECs.

CD34 and CD105

The surface detection of CD34 and CD105 (MFI) on unstained and stained HOMECs is shown in table 28. Representative histograms are shown in figure 48.

EC marker	Unstained MFI	Stained MFI	% stained cells
CD34	86.7 ± 13.4	206.5 ± 22.7	28.7 ± 26.2
CD105	16.4 ± 5.7	18.8 ± 3.2	0

Table 28. The median fluorescence intensity (MFI) and percentage of cells binding the conjugated CD34 or CD105 antibodies on HOMECs. Pure populations of HOMECs were analysed by flow cytometry. Data shown are the mean ± SD of (n=6).

CD13

The surface detection of CD13 (MFI) on unstained and stained pericytes (p4 – 6 and p11 - 13) is shown in table 29. Representative histograms are shown in figure 49.

Cell type	Unstained MFI	Stained MFI	% stained cells
p4 - 6 pericytes	6.2 ± 4.9	13.6 ± 7.5	0
P11 - 13 pericytes	26.7 ± 15.8	186.3.5 ± 25.4	36.2 ± 9.1

Table 29. The median fluorescence intensity (MFI) and percentage of cells binding the conjugated CD13 antibody on p4 - 6 and p11 – 13 pericytes. Pure populations of pericytes were analysed by flow cytometry. Data shown are the mean ± SD of (n=6).

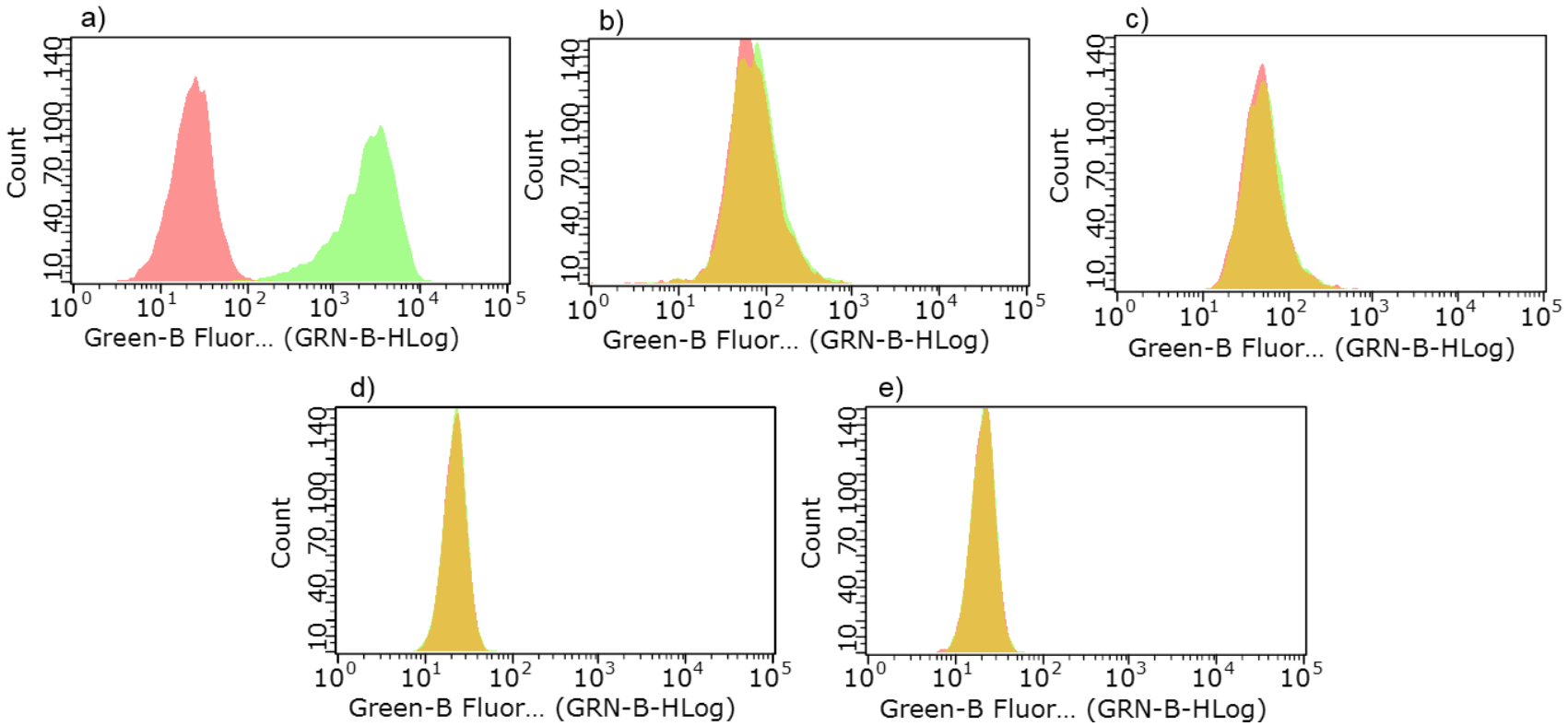

Figure 47. Representative fluorescence histograms showing surface detection of CD31 on different cell types present in the heterogeneous cell suspension generated by the revised isolation protocol. Red peaks show the median fluorescence intensity (MFI) of unstained samples, green peaks show the MFI of stained samples. Yellow areas indicate where the MFI of unstained and stained samples overlap. HOMECs are shown in a), HOFs in b), HOMEsos in c), p4 - 6 pericytes in d), and p11 - 13 pericytes in e).

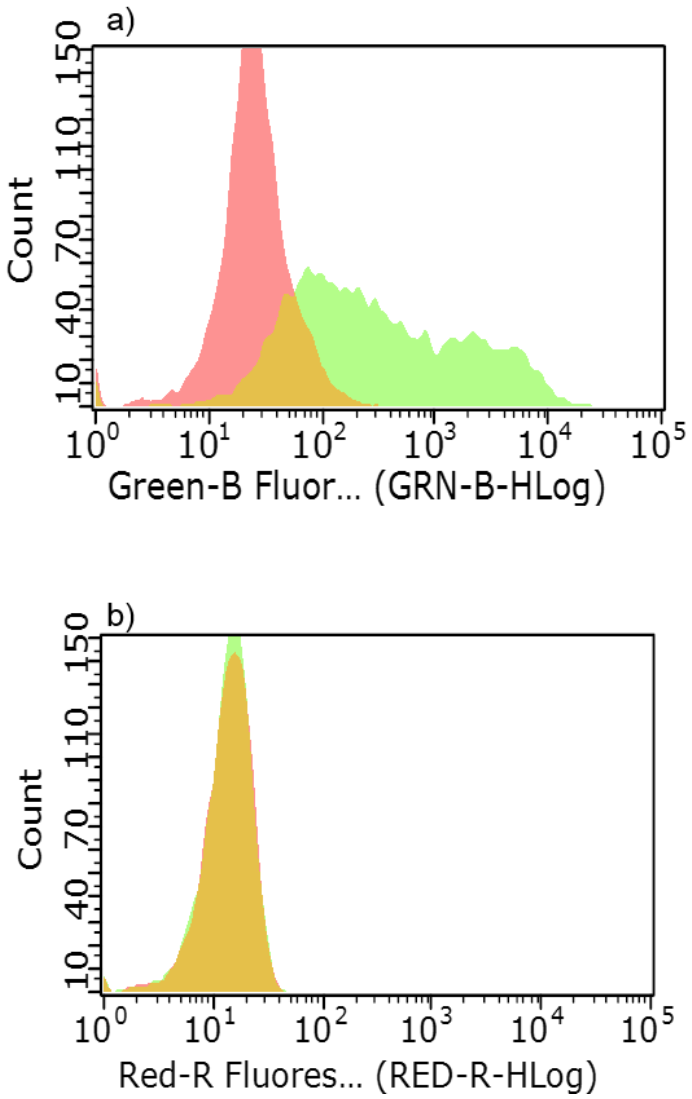

Figure 48. Representative fluorescence histograms showing surface detection of CD34 (a) and CD105 (b) on HOMECs. Red peaks show the median fluorescence intensity (MFI) of unstained samples, green peaks show the MFI of stained samples. Yellow areas indicate where the MFI of unstained and stained samples overlap.

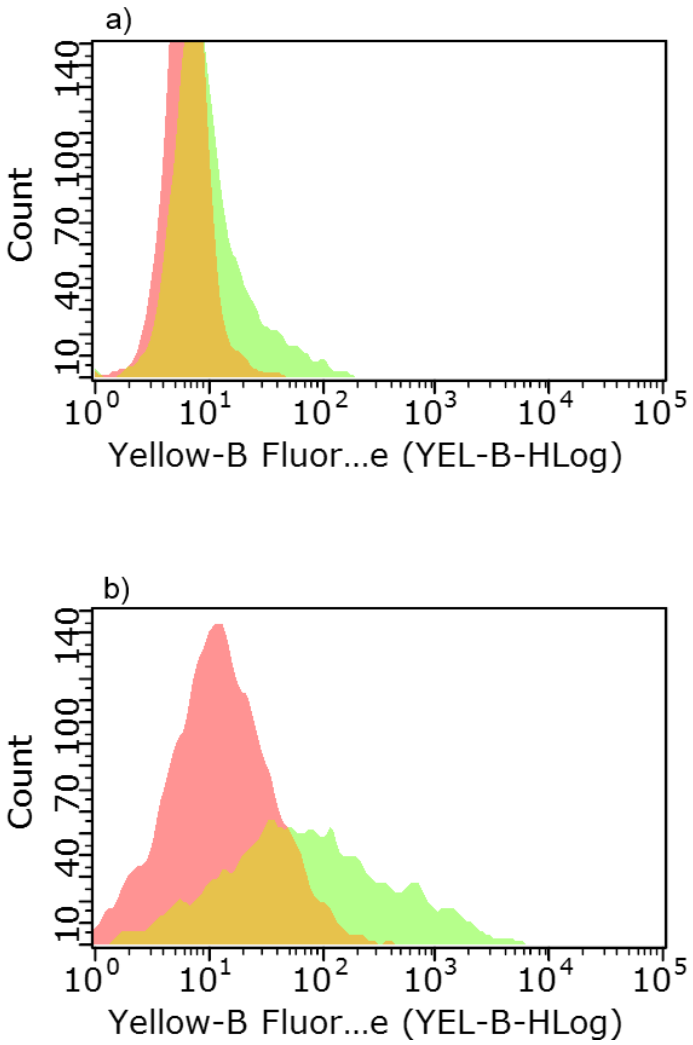

Figure 49. Representative fluorescence histograms showing surface detection of CD13 on p4 – 6 (a) and p11 – 13 pericytes (b). Red peaks show the median fluorescence intensity (MFI) of unstained samples, green peaks show the MFI of stained samples. Yellow areas indicate where the MFI of unstained and stained samples overlap.

3.4.2.3 Overall discussion for the suitability of CD31, CD34, CD105 and CD13 as FACS targets

Flow analysis of the first marker studied, CD31, suggested that 99.3% of HOMECs displayed surface CD31 (see table 27). HOFs and HOMesos showed 0.6 and 0.8% positivity for the CD31 antibody respectively, whilst neither population of pericytes studied contained any CD31 positively stained cells. These data suggest that CD31 could be a suitable EC marker, as the contaminating cells studied did not appear to express surface CD31. Furthermore, these data suggest that the specific conjugated antibody used could be a good choice for cell sorting, as assuming these cells did not express CD31, no non-specific binding was observed either. Another EC marker, CD34, appeared initially not to be as suitable; CD34 was detected on only 28.7% of HOMECs. Goncharov *et al* (2017) describe CD34 as a marker for all non-lymphatic ECs, whereas much of the literature focuses on CD34 being a classical marker for haematopoietic cells (reviewed by Sidney *et al*, 2014). The latter authors also review the idea that the presence of CD34 on ECs identifies them as endothelial progenitor cells, and that whilst these are typically isolated from blood, they exist in capillaries in larger proportions. Moreover, CD34 expressing ECs are also associated with being actively angiogenic (Siemerink *et al*, 2012). These data could explain why only 28.7 ± 26.2% of HOMECs stained positive for CD34, as these positively stained HOMECs could be either progenitor cells, or actively angiogenic. This is particularly interesting when considering the difficulty in the successful isolation and culture of HOMECs. The large standard deviation in CD34 expression (± 26.2%) suggests variability in CD34 expression between HOMEC batches, suggesting that the proportion of CD34+ve HOMECs isolated initially could be important in determining isolation and culture success. If so, this marker could be of interest for positively selecting HOMECs in tandem with CD31, as a higher proportion of these cells may contribute to the success of the isolated HOMEC culture. However, CD34 is known to be expressed on other cell types not studied in this chapter, and therefore any implications of this would have to be considered.

Interestingly, CD105 was not shown to be present on HOMECs. CD105 is known to be expressed on activated ECs that are undergoing proliferation (Dallas *et al*, 2008), and since HOMECs would typically be quiescent, this could

explain the lack of detection. It is also possible that the antibody was not suitable, as only one antibody was tested, and therefore this could be confirmed by studying another conjugated CD105 antibody. However at present, the data suggest that CD105 would not be an appropriate EC marker for cell sorting. Due to the lack of positivity of CD105 on HOMECs, it was not studied in other cell types. The analysis of CD13 on pericytes showed differential surface detection. It was not detected on p4 – 6 pericytes, but had an MFI of 36.2 ± 9.1 on p11 – 13 pericytes. These data indicate that CD13 is not a suitable target for reliably selecting pericytes by cell sorting. These particular experiments may have been limited in their suitability to study the HOMEC isolation, since the pericytes were sourced from the brain, and pericyte markers can vary depending on their location, as reviewed by Yamakazi and Mukouyama (2018). Coupled with the variable CD13 detection between lower and higher passage number pericytes, the data indicate that targeting pericytes for removal would be difficult and not an advisable strategy. Indeed, it is known that a pan-specific pericyte marker does not exist (Yamakazi and Mukouyama, 2018), and therefore multiple surface markers would have to be utilised, which would necessitate further marker study and potentially remove fluorophore options for markers for other cells.

If time had allowed, experiments to investigate the lowest percentage of HOMECs possible that could be sorted (with CD31) from a heterogeneous cell population would have been carried out, by mixing together known percentages of HOMECs, HOFs, HOMesos, and pericytes. The percentage of viable HOMECs (CD31+ve/PI-ve) out of all cells recovered from tissues following the amended protocol was approximately 6.7% (see table 23), and therefore the cell sort would be required to be able to work from at least this proportion.

Overall, there is promise in CD31 as a marker for HOMECs for a cell sort, as well as potential interest in CD34, yet further study is required. The other cell types appear difficult to target, although few markers were studied, and with only one brand of antibody each. After an antibody panel is determined, the specifics of the cell sorting protocol would have to be optimised to determine a method that would result in the isolation of the largest number of viable ECs. That is to say, a sort that could be performed quickly enough to isolate HOMECs without affecting their viability.

Chapter 4. Investigation into the functional pro-angiogenic effects of galectin-1 in epithelial ovarian cancer omental metastasis

4.1 Introduction

As outlined in the main introduction, it is well established that tumour secreted proteins interact with cells within the microenvironment, and promote the development of primary tumours and metastases. An important outcome of these interactions is tumour associated angiogenesis, which as discussed earlier, is a hallmark of cancer development (Hanahan and Weinberg, 2011). As discussed throughout sections 1.4 and 1.5, secondary tumours are often present in the omentum in advanced cases of EOC, and the omental microenvironment is good 'soil' for metastasising EOC cells (Meza-Perez and Randall, 2017). In part, the omentum is 'good soil' as it contains multiple cell types capable of producing the potent pro-angiogenic factor, VEGF (see section 1.6.1). However, anti-angiogenic drugs targeting VEGF or VEGF signalling have had little to no effect in clinical trials (section 1.6.3). Winiarski *et al* (2013) showed that the lysosomal protease cathepsin-L (CL) was secreted by ovarian cancer cell lines A2780 and SKOV3, and could induce proliferation and migration of the disease in capillary bed relevant human omental microvascular endothelial cells (HOMECs). Further study by Pranjol *et al* (2019) demonstrated that these pro-angiogenic effects were not due to proteolytic activity. Interestingly, data from our lab suggested that CL induces differential expression of gal-1 in HOMECs (Pranjol *et al*, 2019), raising the possibility that CL induced secretion of gal-1 may be a mechanism by which CL induces its effects on HOMECs.

Gal-1 is overexpressed in cases of advanced EOC, and is thought to have pro-angiogenic effects on ECs, including the promotion of EC proliferation and migration (as discussed in section 1.7.2.3). However, the secretion and subsequent localisation of gal-1 following CL treatment has not currently been described in HOMECs. In addition, the secretion of gal-1 from ovarian cancer

cells has not yet been investigated. Therefore knowledge of the role that gal-1 may play within the EOC metastatic microenvironment is currently lacking. This includes the impact of gal-1 on HOMEC proliferation, migration, and cancer cell adhesion in both haematogenous and transcoelomic metastasis. As gal-1 has previously been implicated in affecting these processes in other cellular and disease contexts, (see sections 1.7.2.2-3), the potential role that CL induced gal-1 secretion may play during the omental metastasis of EOC presents as a gap in the literature.

4.1.1 Aims

The aims of this chapter are therefore as follows:

- To investigate whether cathepsin-L induced secretion of galectin-1 from HOMECs
- To investigate the localisation of gal-1 in HOMECs in response to cathepsin-L
- To investigate whether exogenous gal-1 can bind to the surface of HOMECs
- To investigate the effect of A2780 and SKOV3 conditioned media on HOMEC surface gal-1 binding
- To investigate the secretion of gal-1 from the ovarian cancer cell lines A2780 and SKOV3
- To investigate the effect of gal-1 on A2780 and SKOV3 cell adhesiveness to mesothelial and HOMEC monolayers
- To investigate the effect of galectin-1 on HOMEC proliferation and migration

4.2 Methods

HOMEC isolation and characterisation

HOMECS were isolated as described in 3.3.6 and characterised by immunocytochemistry (2.3.4.4).

Galectin-1 secretion

Secretion of gal-1 (present in cell culture supernatant) was quantified in A2780 and SKOV3 cancer cell lines, HRECs, hCMEC/D3 cells, and HOMECs, by commercially available ELISA (as described in sections 2.3.5.1-2).

HOMEC galectin-1 localisation and expression

Intra and cell surface extracellular gal-1 in response to cathepsin-L was studied using ICC as described in 2.3.4.5 and analysed as described in 2.3.4.6.

Changes in extracellular surface bound galectin-1

The ability of HOMECs to bind exogenous galectin-1 to the cell surface was studied using 96-well plate assays as described in section 2.3.8.1.

The effect of EOC cell conditioned media on cell surface binding of exogenous galectin-1

The effect of A2780 and SKOV3 conditioned media on HOMEC binding of exogenous galectin-1 to the surface of HOMECs was studied using 96-well plate assays as described in section 2.3.8.2.

Cancer cell adhesion

The adhesion of A2780 and SKOV3 EOCs to mesothelial and HOMEC monolayers (± galectin-1) was studied using a plate rocker assay and analysed by plate reader (sections 2.3.9.1-3).

Cell proliferation

HOMEC, HREC, and hCMEC/D3 cell proliferation in response to galectin-1 and cathepsin-L was examined using both the WST-1 (2.3.2.1) and BrdU assay kits (2.3.2.2).

Cell migration

HOMEC migration in response to galectin-1 and cathepsin-L was investigated using a scratch assay (procedure 2.3.3.1, analysis 2.3.3.2), and a commercially available Cultrex chamber assay (2.3.3.3).

4.3 Results

4.3.1 Cathepsin-L induced differential secretion of galectin-1 from HOMECs, HRECs and hCMEC/D3 endothelial cells

Preliminary unpublished data from this lab suggested that CL induced differential gene expression of *LGALS1* in HOMECs. Pranjol *et al* (2019) further demonstrated that this change in *LGALS1* expression was due to non-proteolytic activity of CL, and therefore it was hypothesised that CL induces the production and secretion of gal-1 from HOMECs. To examine this, HOMECs were grown in 24-well plates, and starved overnight in 2% FCS endothelial media prior to experimentation. Cells were then treated with 50ng/ml CL for 30 minutes, 2 hours, 4 hours, 8 hours, and 24 hours and supernatants collected as described in 2.3.5.1. The concentration of 50ng/ml CL was pre-determined to be physiologically relevant by Pranjol *et al* (2019). An ELISA was carried out and analysed as described in 2.3.5.2. Preliminary experiments showed no detectable gal-1 was present in 2% FCS endothelial media (data not shown). Due to an initial shortage of HOMECs, this experiment was also conducted on primary human retinal endothelial cells (HRECs) and human cerebral microvascular endothelial cells (hCMEC/D3 cells) to assess their suitability for study in place of HOMECs, in preliminary experiments.

4.3.1.1 Cathepsin-L induced galectin-1 secretion from HOMECs

CL significantly increased secreted gal-1 compared with control cells at 30 minute, 2 hours, and 4 hour timepoints (p values = 0.0022). At 8 hours and 24 hours, CL treated HOMECs appeared to secrete more gal-1 than control cells, although not significantly (p=0.1797 and 0.2403 respectively) (see figure 50).

These data suggested that CL induced the secretion of gal-1 from HOMECs. The significant increase at 30 minutes may indicate a rapid release of readily available intracellular gal-1, or a type of non-proteolytic cleaving of cell surface gal-1. Furthermore, significant increases in secreted gal-1 at 2 and 4 hours suggest the release of pre-synthesised gal-1, although it is unclear where the gal-1 is released from. The increase in secreted gal-1 at 8 and 24 hours suggested a residual effect from the CL, or the CL could be altering

transcriptional regulation of *LGALS1,* as this could be possible after this amount of time post CL treatment. At the 24 hour timepoint, the highest levels of gal-1 in both untreated and treated HOMECs were recorded. The value for the untreated cells (3.7ng/ml) was higher than any of the values for CL treated HOMECs from the other timepoints. These data suggested that gal-1 secretion from HOMECs varies naturally, or is potentially affected by longer exposure to starve media (2% FCS). Secreted levels of gal-1 across both control and treated cells ranged from 0.8 to 6.4ng/ml (figure 50).

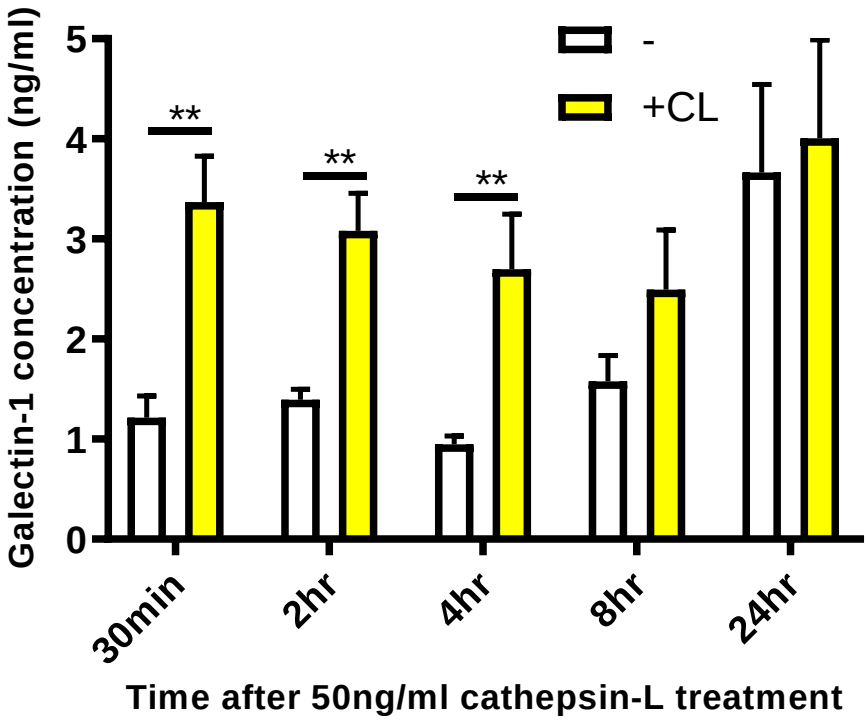

Figure 50. Cathepsin-L (CL) induced significant secretion of galectin-1 in HOMECs after 30 minutes, 2 hours and 4 hours. HOMECs were seeded in gelatin pre-coated 24-well plates at 50,000 cells/well. After an overnight starve with 2% FCS endothelial media, HOMECs were incubated with 2% endothelial media ± 50ng/ml CL and supernatants were collected after 30 minutes, 2 hours, 4 hours, 8 hours and 24 hours. Control cells received 2% FCS starve media alone. Secreted galectin-1 in the supernatants was then analysed using an ELISA kit and SpectraMax plate reader. Results are the mean ± SD, n=6 (intra-experimental n=9). HOMECs from four isolations were used. **p values = 0.0022. (Mann-Whitney U analyses between control and cells incubated with CL).

4.3.1.2 Cathepsin-L induced secretion galectin-1 from HRECs

No significant changes in the secretion of gal-1 in CL treated HRECs compared to control cells were observed at any timepoint. However, after 30 minutes of CL treatment, there was a slight increase in secreted gal-1. These data suggested that CL treatment did not induce the secretion of gal-1 from HRECs, despite the increase seen at 30 minutes ($p=0.1$). At the 24 hour timepoint, the highest levels of secreted gal-1 from both untreated and treated HRECs were recorded, similarly to HOMECs. These data suggested that gal-1 secretion from HRECs varies naturally, or is potentially affected by longer exposure to starve media (2% FCS). Secreted levels of gal-1 across both control and treated cells ranged from 3.4 to 11.2ng/ml (figure 51). These data indicated that HOMECs responded differently to CL than HRECs.

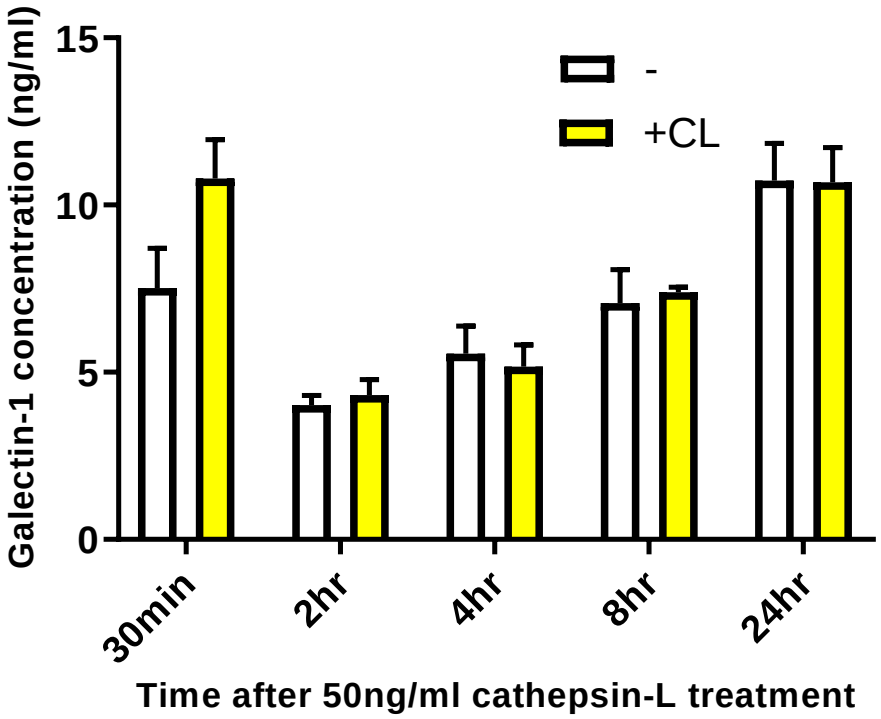

Figure 51. Cathepsin-L (CL) induced secretion of galectin-1 in HRECs. HRECs were seeded in gelatin pre-coated 24-well plates at 50,000 cells/well. After an overnight starve with 2% FCS endothelial media, HRECs were incubated with 2% endothelial media ± 50ng/ml CL and supernatants were collected after 30 minutes, 2 hours, 4 hours, 8 hours and 24 hours treatment. Control cells received 2% FCS starve media alone. Secreted galectin-1 in the supernatants were then analysed using an ELISA kit and SpectraMax plate reader. Results are the mean ± SD, n=6 (intra-experimental n=9). (Mann-Whitney U analyses between control and cells incubated with CL, all p values >0.05).

4.3.1.3 Cathepsin-L induced secreted galectin-1 from hCMEC/D3 cells

No significant changes in the secretion of gal-1 in CL treated hCMEC/D3s were observed compared to control cells. However, after 24 hours of CL treatment, there was a slight increase in secreted gal-1 ($p=0.1$). These data suggested that CL treatment does not induce the secretion of gal-1 from hCMEC/D3s. At the 24 hour timepoint, the highest levels of gal-1 in both untreated and treated hCMEC/D3s were recorded, as was observed in HOMECs and HRECs. These data suggested that gal-1 secretion from hCMEC/D3s is potentially affected by longer exposure to starve media (2% FCS). Secreted levels of gal-1 across both control and treated cells ranged from 3.0 to 12.2ng/ml (summarised in figure 52).

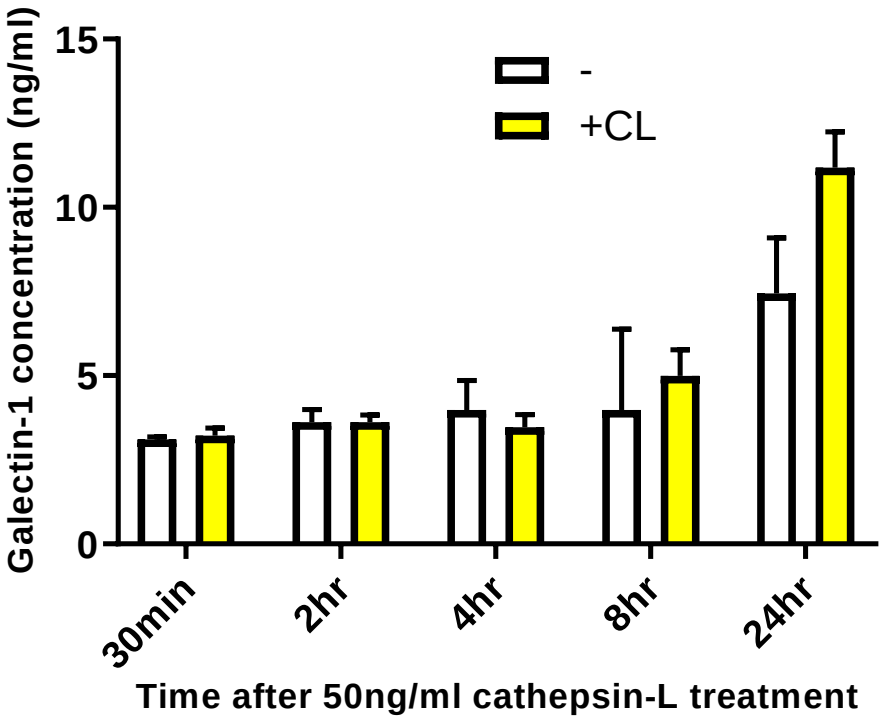

Figure 52. Cathepsin-L (CL) induced secretion of galectin-1 in hCMEC/D3 cells. hCMEC/D3 cells were seeded in gelatin pre-coated 24-well plates at 50,000 cells/well. After an overnight starve with 2% FCS endothelial media, hCMEC/D3 cells hCMEC/D3 cells were incubated with 2% endothelial media ± 50ng/ml CL and supernatants were collected after 30 minutes, 2 hours, 4 hours, 8 hours, and 24 hours treatment. Control cells received 2% FCS starve media alone. Secreted galectin-1 in the supernatants were then analysed using an ELISA kit and SpectraMax plate reader. Results are the mean ± SD, n=6 (intra-experimental n=9).

4.3.2 Levels of intra and extracellular galectin-1 in cathepsin-L treated HOMECs

The ELISA data in section 4.3.1.1 indicated that CL induced the secretion of gal-1 in HOMECs, and previous unpublished data suggested that CL also increased the expression of gal-1. However, the cellular localisation of gal-1 in HOMECs with and without CL treatment is unknown. Gal-1 is known to be found both intra and extracellularly. On the cell surface, gal-1 binding is thought to occur via its carbohydrate recognition domain (section 1.7.1.1). The localisation of gal-1 in HOMECs in response to CL was studied using ICC, in order to investigate whether gal-1 moved out of the cell and attached to the cell surface. HOMECs were grown in 8-well chamber slides and treated with 50ng/ml CL. To study cell surface associated extracellular gal-1, cells were fixed as described in 2.3.4.2 at 0 minutes, 5 minutes, 10 minutes, 30 minutes and 4 hours post CL treatment. These timepoints were chosen as they included timepoints from ELISA data in 4.3.1 where gal-1 secretion was significantly increased, as well as shorter treatment times of interest to investigate any immediate cleavage of gal-1 from the cell surface. Z stacks showed this technique demonstrated cell surface distribution (data not shown). Intracellular levels of gal-1 were examined at timepoints were 0 minutes, 30 minutes, 4 hours, 8 hours and 24 hours post CL treatment. These times were chosen to allow examination of any rapid gal-1 redistribution to the cell surface, as well as longer timepoints where HOMECs may be synthesising more gal-1 (8 hours). Cells were fixed as described in 2.3.4.1. Staining and analysis of all cells was carried out as described in sections 2.3.4.5-6. No significant staining was seen when the primary antibody was omitted (figures 54 and 56).

4.3.2.1 Changes in levels of cell surface associated extracellular galectin-1 in HOMECs in response to cathepsin-L

A significant increase in extracellular gal-1 was observed on HOMECs (in response to CL treatment) after 5 and 10 minutes ($p=0.0028$ and $p=0.04$ respectively). At 0 minutes (basal level) and 30 minutes there appeared to be more extracellular gal-1 in CL treated cells, although this was not significant ($p=0.2973$ and $p=0.2581$ respectively) (figures 53 - 54). These data suggested

that CL treated HOMECs have increased extracellular cell-surface gal-1, although this was only significant at earlier timepoints 5 and 10 minutes.

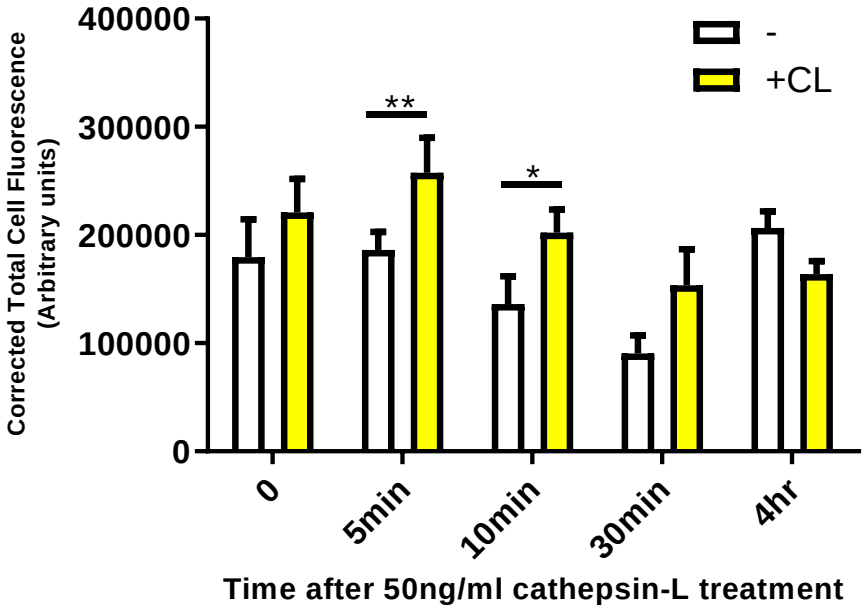

Figure 53. Cathepsin-L (CL) significantly increases cell surface extracellular galectin-1 at 5 and 10 minutes in HOMECs. HOMECs were seeded in gelatin pre-coated 8-well chamber slides at 30,000 cells/well. After an overnight starve with 2% FCS endothelial media, HOMECs were treated with 2% endothelial media ± 50ng/ml CL, for the times indicated. Cells were then fixed with paraformaldehyde and stained for galectin-1. Galectin-1 was quantified using ImageJ. Five cells from three separate images (per experiment) were analysed for an n of 1. Results shown are the mean ± SD, n=4. HOMECs from three isolations were used. *p=0.04, **p=0.0028. (Mann-Whitney U analyses between control and cells incubated with CL).

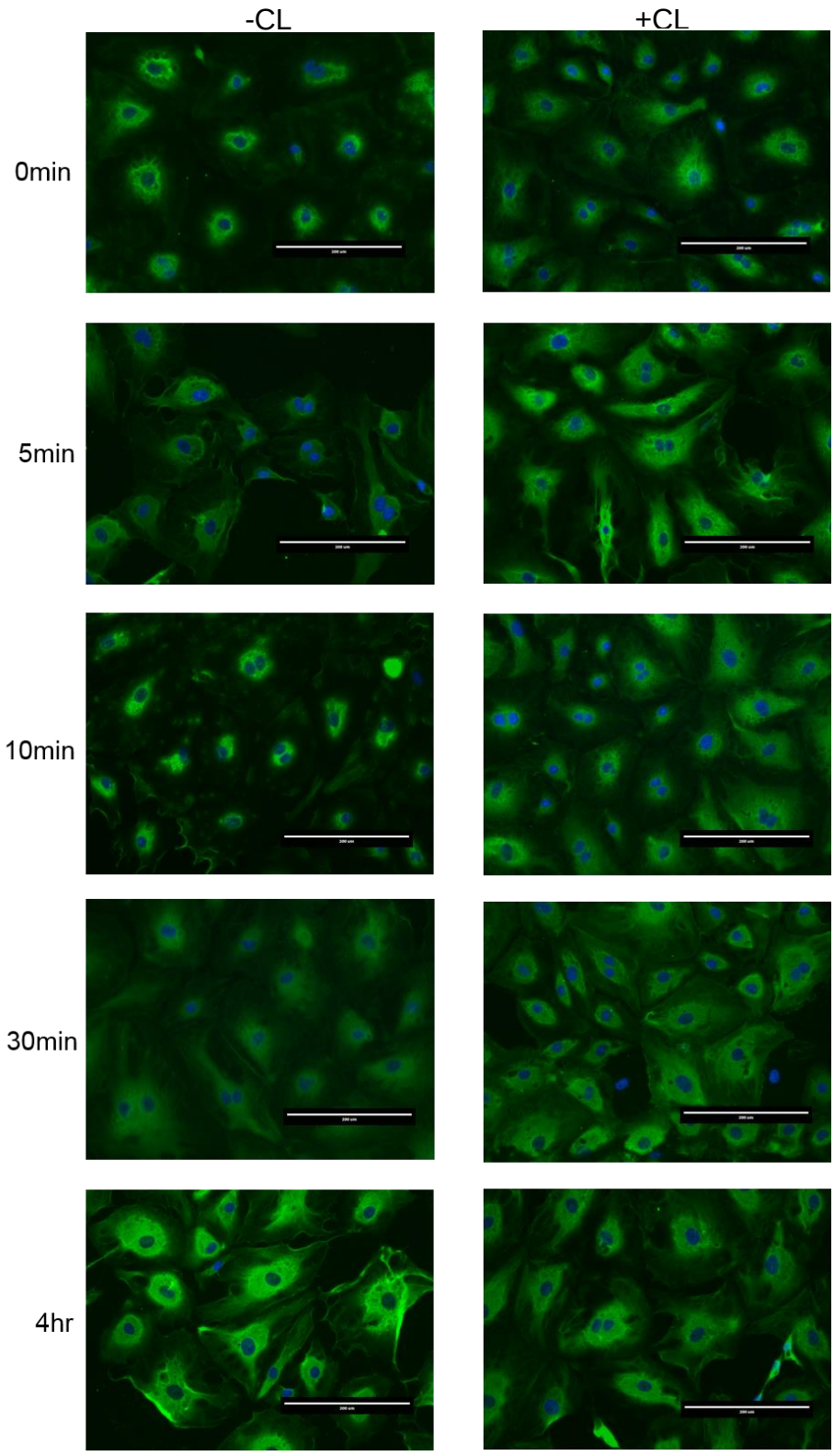

Figure 54. Representative images showing extracellular galectin-1 on cathepsin-L (CL) treated and non-treated HOMECs. HOMECs were seeded in gelatin pre-coated 8-well chamber slides at 30,000 cells/well. After an overnight starve with 2% FCS endothelial media, HOMECs were treated with 2% endothelial media ± 50ng/ml CL for the times indicated. Cells were then fixed with paraformaldehyde and stained for galectin-1 (green) and counterstained with DAPI (blue). Scale bar = 200µm.

4.3.2.2 Changes in levels of intracellular galectin-1 in HOMECs in response to cathepsin-L

A significant decrease in levels of intracellular gal-1 in HOMECs (in response to CL treatment) after 30 minutes ($p=0.0142$), and an increase in intracellular gal-1 level was seen in treated cells at 8 hours ($p=0.0028$). At 24 hours there appeared to be more intracellular gal-1 in CL treated cells, but this was not significant ($p=0.1359$). At 0 minutes (basal level) no obvious difference between intracellular gal-1 in treated and non-treated cells was observed (figures 55 - 56).

These data suggested that CL treated HOMECs have significantly less intracellular gal-1 after 30 minutes treatment, and more at 8 hours. Although data were in arbitrary units, they were able to be compared to the values calculated for extracellular gal-1. Taken together, these data suggested that there was generally more extracellular gal-1 detected than intracellular; intracellular data was only above 100,000 (arbitrary fluorescent units) in non-treated cells at 30 minutes, and treated cells at 8 and 24 hours. By comparison, in the extracellular data only non-treated cells at 30 minutes had fluorescence values <100,000.

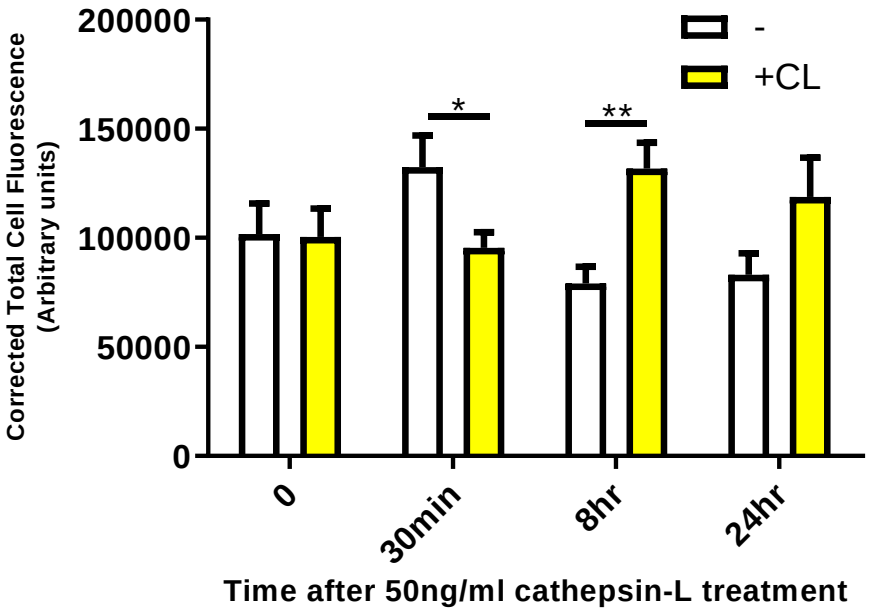

Figure 55. Cathepsin-L (CL) significantly decreases the level of intracellular galectin-1 at 30 minutes and significantly increases the intracellular galectin-1 level at 8 hours in HOMECs. HOMECs were seeded in gelatin pre-coated 8-well chamber slides at 30,000 cells/well. After an overnight starve with 2% FCS endothelial media, HOMECs were incubated in 2% endothelial media ± 50ng/ml CL for the times indicated. Cells were then fixed with methanol and stained for galectin-1. Galectin-1 was quantified using ImageJ. Five cells from three separate images (per experiment) were analysed. Results shown are the mean ± SD, n=4. HOMECs from three isolations were used. *p=0.0142, **p=0.0028 (Mann-Whitney U analyses between control and cells incubated with CL).

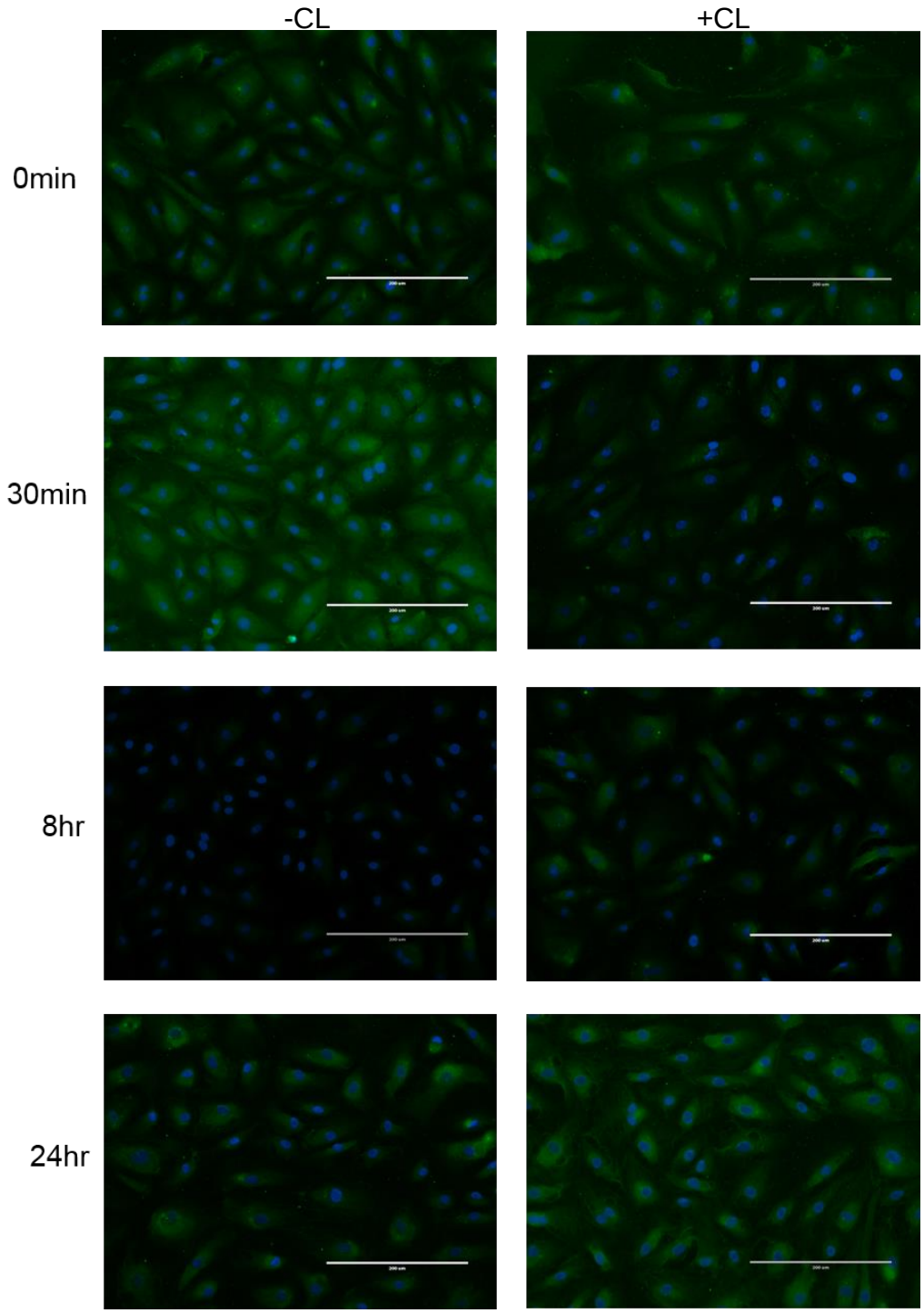

Figure 56. Representative images showing intracellular galectin-1 in cathepsin-L (CL) treated and non-treated HOMECs. HOMECs were seeded in gelatin pre-coated 8-well chamber slides at 30,000 cells/well. After an overnight starve with 2% FCS endothelial media, HOMECs were incubated with 2% endothelial media ± 50ng/ml CL for the times indicated. Cells were then fixed with methanol and stained for galectin-1 (green) and counterstained with DAPI (blue). Scale bar = 200µm.

4.3.3 Extracellular surface bound galectin-1

In section 4.3.2, the extracellular gal-1 on the surface of HOMECs was studied. This study indicated that gal-1 is present on the cell surface in unstimulated HOMECs. Furthermore this study showed that cell surface gal-1 could be present in relatively large amounts in both unstimulated and stimulated HOMECs. It was therefore investigated whether it was possible for exogenous gal-1 to adhere to the surface of HOMECs using 96-well plate assays. HOMECs were grown in 96-well black plates and starved overnight in 2% FCS endothelial media prior to experimentation. Cells were then incubated with 5 or 50ng/ml gal-1 for 10 minutes. Wells were then washed with PBS to remove any unbound gal-1, and gal-1 staining was carried out as described in 2.3.4.3 without the addition of DAPI. Fluorescence was quantified using a SpectraMAX plate reader at 488/520nm. Control cells with no gal-1 treatments as well as secondary antibody controls, and growth controls were included (described in 2.3.8.1).

The lower concentration of 5ng/ml was selected due to the ELISA data in 4.3.1.1 showing CL activated HOMECs secreting approximately 3.5ng/ml of gal-1, and ELISA data in 4.3.5 showing that SKOV3 cells secreted approximately 2ng/ml of gal-1 (SKOV3 cells secreted less gal-1 than A2780). Together, the 5ng/ml therefore was deemed a suitable lower gal-1 concentration to use in experiments. The higher concentration of 50ng/ml was selected as serum gal-1 levels in patients with metastatic EOC (post 1+ surgeries) are shown to range from 30 – 390ng/ml (Chen *et al,* 2015), and the median at time of diagnosis in patients with advanced EOC being 40.57 ± 22.1ng/ml (Masoodi *et al*, 2021). 50ng/ml was therefore deemed a suitable concentration to use as a higher concentration for experiments.

4.3.3.1 Additional galectin-1 can bind to the surface of HOMECs

A significant increase in cell surface gal-1 compared to control and HOMECs after incubation with 5 or 50ng/ml gal-1 for 10 minutes (55.5 and 96.3% respectively) (p values = 0.0022), was seen. These data suggested HOMECs incubated with exogenous gal-1 were capable of binding more gal-1 on the cell surface (figure 57).

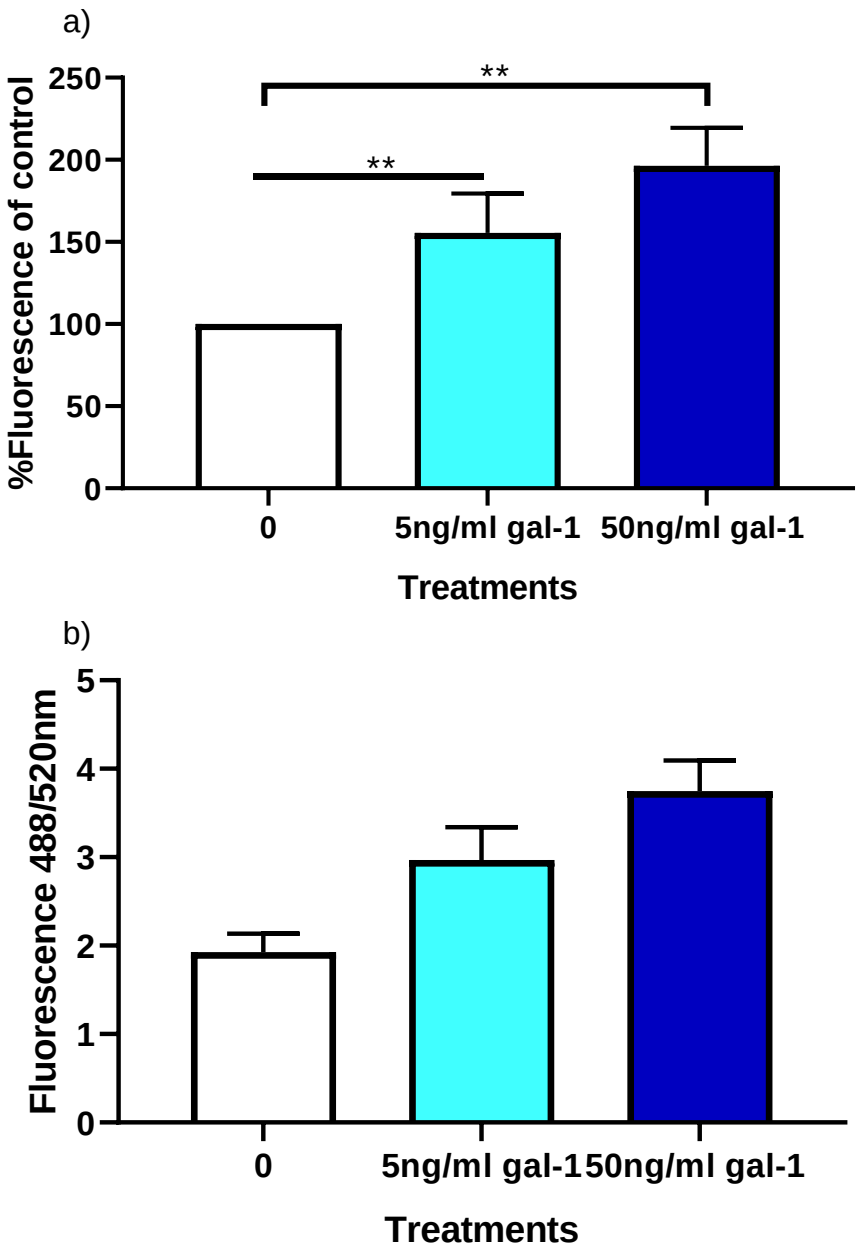

Figure 57. HOMECs can bind exogenous galectin-1. HOMECs were grown in gelatin coated 96-well black plates and starved overnight in 2% FCS endothelial media prior to experimentation. Cells were then incubated with 5 or 50ng/ml galectin-1 (gal-1) for 10 minutes. Unbound gal-1 was removed, and cells were stained for gal-1. Fluorescence was quantified using a SpectraMAX plate reader at 488/520nm. The 0 treatment represents cells not incubated with any gal-1. Results shown in a) are the mean ± SD, n=4. HOMECs from three isolations were used. **p values = 0.0022, Mann-Whitney U analyses between cells incubated with and without gal-1. b) shows raw data representative of one experiment.

4.3.4 The effect of A2780 and SKOV3 conditioned media on galectin-1 binding to the surface of HOMECs

In 4.3.3 it was indicated that HOMECs were capable of binding additional gal-1. It is thought that the tumour microenvironment can promote the binding of gal-1 to ECs by altering their cell surface glycosylation. This has previously been attributed to cytokine signals from cancer cells such as TNF-α (Scott *et al*, 2013), interleukin-10 or TGF-β1 (Croci *et al*, 2018). To investigate this, HOMECs were incubated with tumour conditioned media collected from EOC cell lines A2780 and SKOV3, and were then analysed for cell surface gal-1 in 96-well plate assays. SKOV3 cells were studied as they derive from a metastatic cancer, and A2780 cells were used as they derive from a primary ovarian tumour.

Cancer cells were adapted to 2% FCS endothelial starve media. This media was then replaced and cancer cells were incubated in this media for 24 hours, to condition the media. This tumour conditioned media (TCM) was collected and applied to HOMECs grown in black 96-well plates (HOMECs had been starved overnight in 2% FCS endothelial media). HOMECs were incubated for 24 hours in the TCM in order to allow for any glycan synthesis and remodelling (Choi *et al*, 2018). Gal-1 was then added at either 5 or 50ng/ml for 10 minutes, followed by a PBS wash. Gal-1 plate staining was then carried out as described in 2.3.8.1.

4.3.4.1 HOMECs incubated with A2780 conditioned media bind more galectin-1

A significant increase in cell surface gal-1 in HOMECs incubated with A2780 conditioned media was seen compared to control, when either 5 or 50ng/ml gal-1 was added (24.1 and 23.5% respectively) (p values = 0.0022). These data suggested HOMECs incubated with A2780 conditioned media were capable of binding more gal-1 on their cell surface (figure 58).

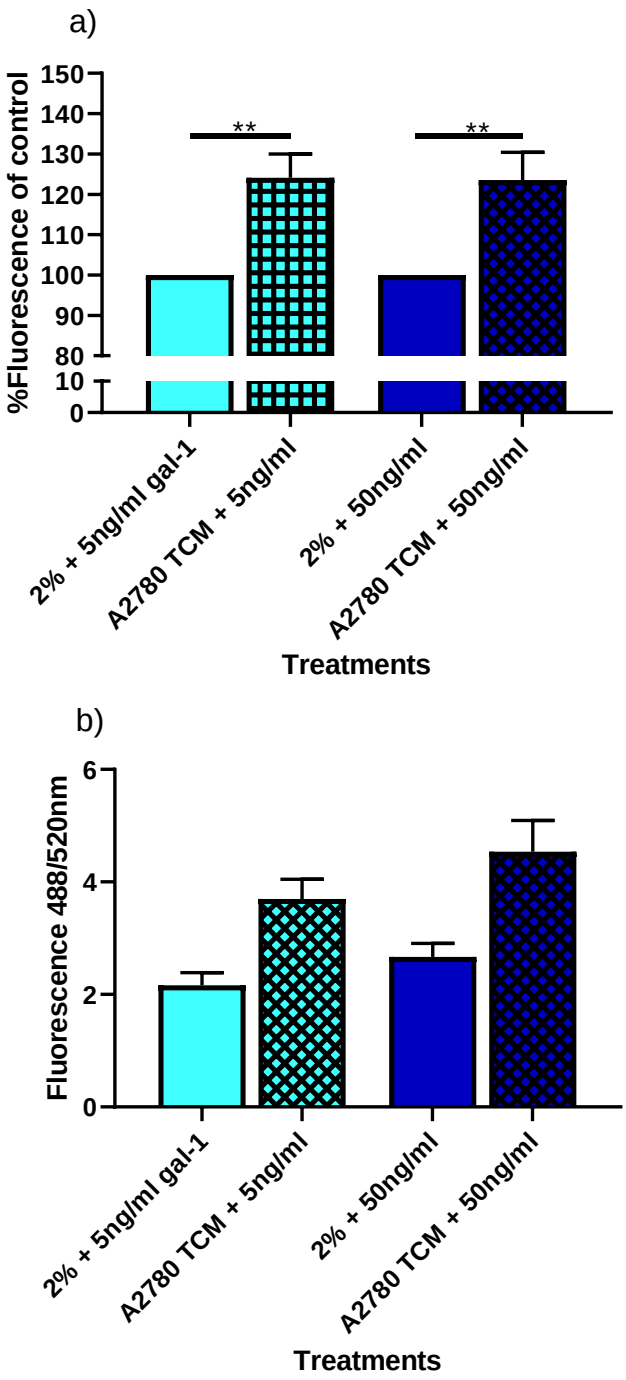

Figure 58. HOMECs incubated with A2780 conditioned media bind significantly more galectin-1. A2780 conditioned 2% FCS endothelial starve media (TCM) was collected and applied to HOMECs that had been starved overnight in 2% FCS endothelial media. After 24 hours, galectin-1 (gal-1) was then added at either 5 or 50ng/ml for 10 minutes, and unbound gal-1 was removed with PBS. Gal-1 bound to the cell surface was then stained and quantified using a SpectraMAX plate reader at 488/520nm. Results shown in a) are the mean ± SD, n=6. HOMECs from three isolations were used. **p values = 0.0022, Mann-Whitney U analyses between cells incubated with and without TCM. b) shows raw data representative of one experiment.

4.3.4.2 HOMECs incubated with SKOV3 conditioned media bind more galectin-1

A significant increase in cell surface gal-1 in HOMECs incubated with SKOV3 conditioned media was seen compared to control, when either 5 or 50ng/ml gal-1 was added (81.7 and 31.0%; p=0.0022 and p=0.0476, respectively). These data suggested HOMECs incubated with SKOV3 conditioned media were capable of binding more gal-1 on their cell surface (figure 59).

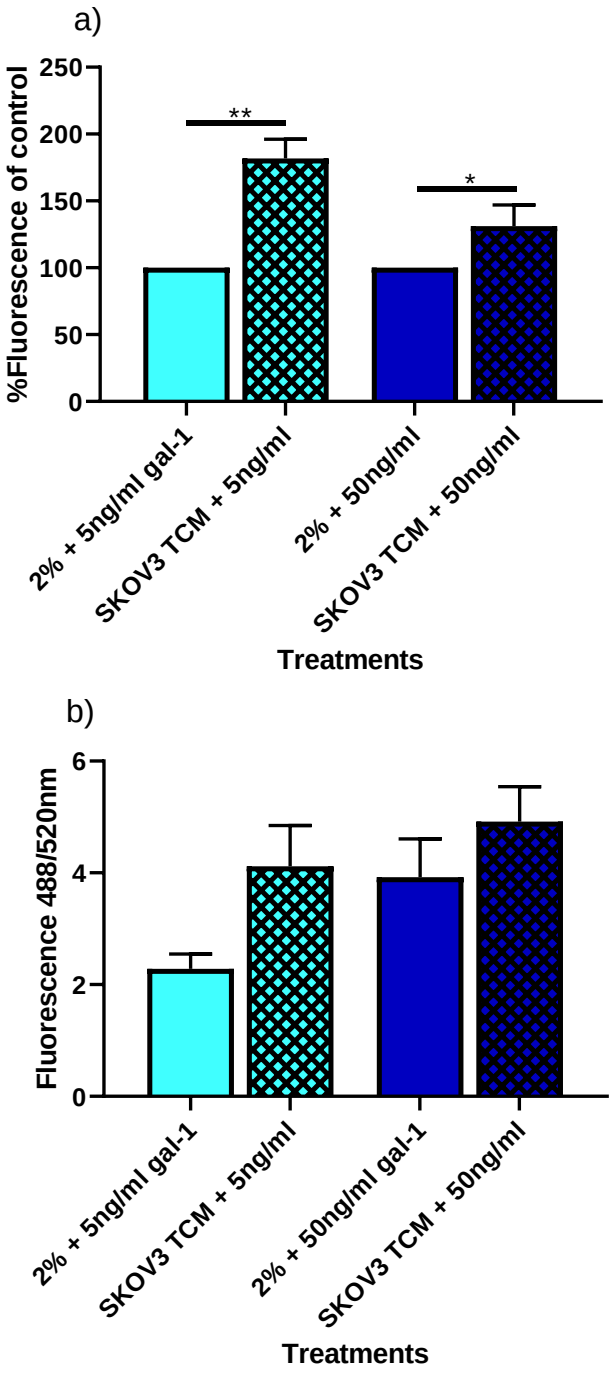

Figure 59. HOMECs incubated with SKOV3 conditioned media bind significantly more galectin-1. SKOV3 conditioned 2% FCS endothelial starve media (TCM) was collected and applied to HOMECs that had been starved overnight in 2% FCS endothelial media. After 24 hours in galectin-1 (gal-1) was then added at either 5 or 50ng/ml for 10 minutes, and unbound gal-1 was removed with PBS. Gal-1 bound to the cell surface was then stained and quantified using a SpectraMAX plate reader at 488/520nm. Results shown in a) are the mean ± SD, n=6. HOMECs from three isolations were used. **p=0.0022, *p=0.0476, Mann-Whitney U analyses between cells incubated with and without TCM. b) shows raw data representative of one experiment.

4.3.5 Secretion of galectin-1 from epithelial ovarian cancer cell lines A2780 and SKOV3

As discussed in section 1.7.2, gal-1 is expressed in most cell types. Zhang *et al* (2014) studied gal-1 expression in the EOC cell lines A2780 and SKOV3 with western blotting, confirming that both cell lines express gal-1. However, the amount of secreted gal-1 was not studied. Park *et al* (2017) quantified secreted gal-1 from SKOV3 cells by ELISA, and found that SKOV3 cells secreted gal-1 in response to lipopolysaccharide stimulation, but small amounts basally (<10pg/ml). In this study, SKOV3 cells were studied as they derive from a metastatic cancer, and A2780 cells were used as they derive from a primary ovarian tumour. In section 4.3.1 the secretion of gal-1 from HOMECs both basally and in response to CL was quantified. However, EOC cells are known to secrete factors to stimulate the microenvironment, including the omentum during EOC metastasis. Therefore more gal-1 could be present in this microenvironment than just the amount secreted from HOMECs. To study this, cancer cells were grown in their respective 2% starve media and conditioned media was collected as described in 2.3.5.1; no CL was added and media were collected after 24 hours. This timepoint was chosen as the previous ELISAs showed this to consistently be the timepoint when cells had secreted the most gal-1. Preliminary experiments showed no detectable gal-1 in either cancer cell media (data not shown). An ELISA was carried out and analysed as described in 2.3.5.2. The data indicated that A2780 cells secrete significantly more gal-1 after 24 hours compared with SKOV3 cells; 2.5 ± 0.1 and 7.3 ± 1.6ng/ml respectively, $p<0.0001$ (figure 60).

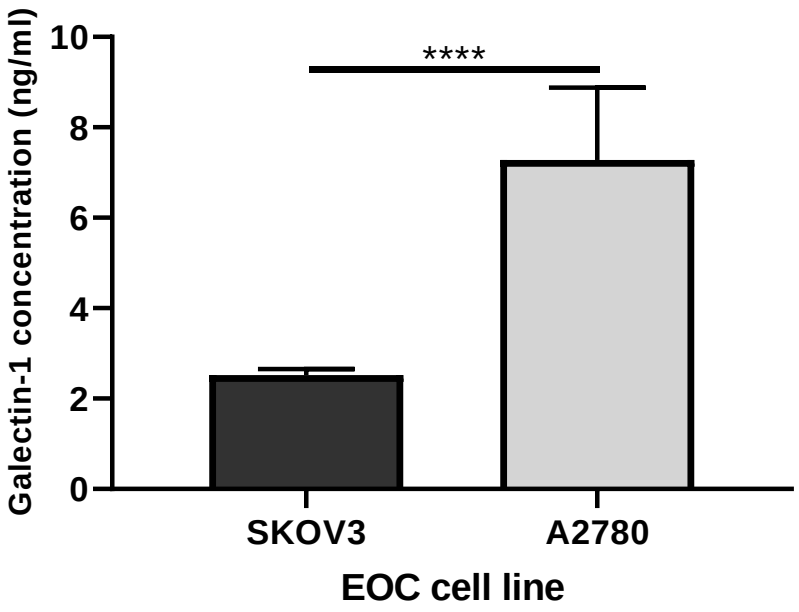

Figure 60. A2780 cells secrete more galectin-1 than SKOV3 cells. Cancer cells were seeded in 24-well plates at 50,000 cells/well. After an overnight starve with 2% FCS RPMI or DMEM media, the starve media was replaced and supernatants were collected after 24 hours. Secreted galectin-1 in the supernatants were analysed by ELISA and SpectraMax plate reader. Results are the mean ± SD, n=6 (intra-experimental n=9). ****p<0.0001. (Mann-Whitney U analysis).

4.3.6 Epithelial ovarian cancer cell adhesion to mesothelial and endothelial monolayers

Gal-1 is potentially involved in EOC cell metastasis both transcoelomically and haematogenously (sections 1.4.5.2 and 1.4.5.1). As discussed in 1.7.2.2, prostate cancer cells have been observed to bind gal-1 to the cell surface protein 90k, which enhanced their adhesion to ECM components laminin and fibronectin (Grassadonia *et al*, 2002). Furthermore, prostate cancer cells demonstrated enhanced adhesion to HUVEC monolayers pre-treated with gal-1 (Clausse *et al*, 1999). These observations have parallels in EOC omental metastasis. For instance, metastasising cancer cells in the peritoneal fluid adhere to the omental mesothelial layer (which expresses fibronectin), and during haematogenous intra/extravasation. In the latter, EOC cells spread to distant sites through the vasculature, adhere to the endothelium and transmigrate through the endothelial layer (or transmigrate through the endothelial layer into blood vessels). These processes could involve cancer cells being increasingly adherent to endothelium expressing relatively higher levels of surface gal-1, or that cancer cells themselves are coated in gal-1 and becoming innately more likely to adhere to endothelium. Given that both HOMECs, A2780, and SKOV3 cells were shown to secrete gal-1, and that gal-1 has high binding capabilities to the surface of cells, these potential pro-metastatic processes were therefore studied in the following experiments.

In order to study the effect of gal-1 on cancer cell adhesion to monolayers, either mesothelial or HOMECs were cultured in black 24-well plates until a confluent monolayer had formed. A2780 and SKOV3 ovarian cancer cells were grown and adapted to either endothelial or mesothelial cell starve media, and pre-treated with 5 and 50ng/ml gal-1 for 10 minutes (see 4.3.3). A2780 and SKOV3 cancer cells treated with 2% starve media or 20% media were used as negative and positive controls respectively, as FCS is known to enhance cell adhesion (Morandi *et al*, 1993). Cancer cells were stained with calcein-AM and their adhesion measured over 2 hours on a plate rocker system as described in section 2.3.9.1 (and analysed as in 2.3.9.3).

A2780 and SKOV3 adhesion was also studied when exposed to a 5 and 50ng/ml gal-1 pre-treated (overnight) HOMEC monolayer on a plate rocker system, as described in 2.3.9.1 (analysed as described in 2.3.9.3).

4.3.6.1 The effect of galectin-1 pre-treatment on the adhesion of A2780 and SKOV3 cells to mesothelial and endothelial monolayers

Gal-1 pre-treated A2780 cells showed no significant changes in adhesion to a HOMeso (omental mesothelial) monolayer compared to negative control (Kruskal-Wallis p=0.2684) (figure 61). Importantly, the positive control did not significantly differ from the negative control either. However, gal-1 pre-treated SKOV3 cells were significantly more adhesive than the control cells to the HOMeso layer. This was observed with pre-treatment of both 5ng/ml or 50ng/ml of gal-1 (figure 62), with approximately 75% and 70% increases in cancer cell adhesion respectively. These data suggested that gal-1 increased SKOV3 cell adhesion to a HOMeso monolayer, but had no effect on the adhesion of A2780 cells.

In the cancer cell adhesion to a HOMEC monolayer experiments, pre-treated A2780 cells were significantly more adhesive compared with control at both 5 and 50ng/ml of gal-1 (p values <0.0001), demonstrating approximately 465% and 368% increases respectively (figure 63). The increased adhesion at 50ng/ml was less than observed with 5ng/ml of gal- pre-treatment. In SKOV3 cells, both gal-1 pre-treatments were also shown to significantly increase cell adhesion compared to control, with 5 and 50ng/ml showing approximately 690% and 770% increases respectively (p values <0.0001 in both cases) (figure 64). These data indicated that 5 and 50ng/ml pre-treatment with gal-1 increased the adhesiveness of both A2780 and SKOV3 cancer cells to HOMEC monolayers.

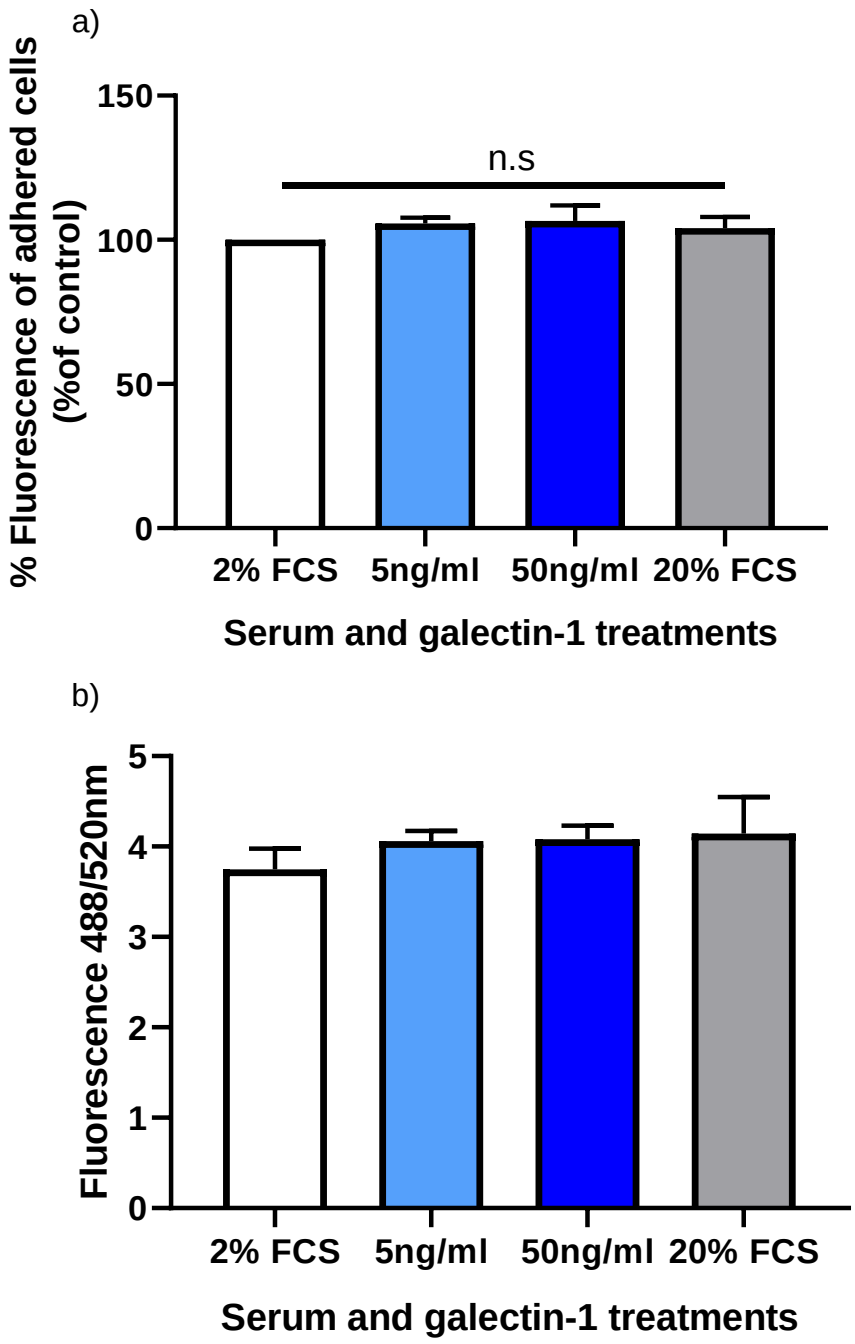

Figure 61. Galectin-1 pre-treatment of A2780 cells does not affect adhesion to an omental mesothelial (HOMeso) monolayer. A2780 cells were pre-treated with 5 or 50ng/ml galectin-1 for 10 minutes, stained with calcein-AM and added to the HOMeso monolayer. Mesothelial 2% FCS starve media was used as a 100% control; 20% FCS as a positive control. The co-culture was laterally rocked on a plate rocker at 60 tilts per minute before fluorescence of adhered cells was analysed with a plate reader at 488/540nm. a) results shown are the mean ± SD, n=4. HOMesos from three isolations were used. Kruskal-Wallis analysis showed no significant (n.s) differences between any of the treatments or positive control (p=0.2684). b) representative raw data from one experiment.

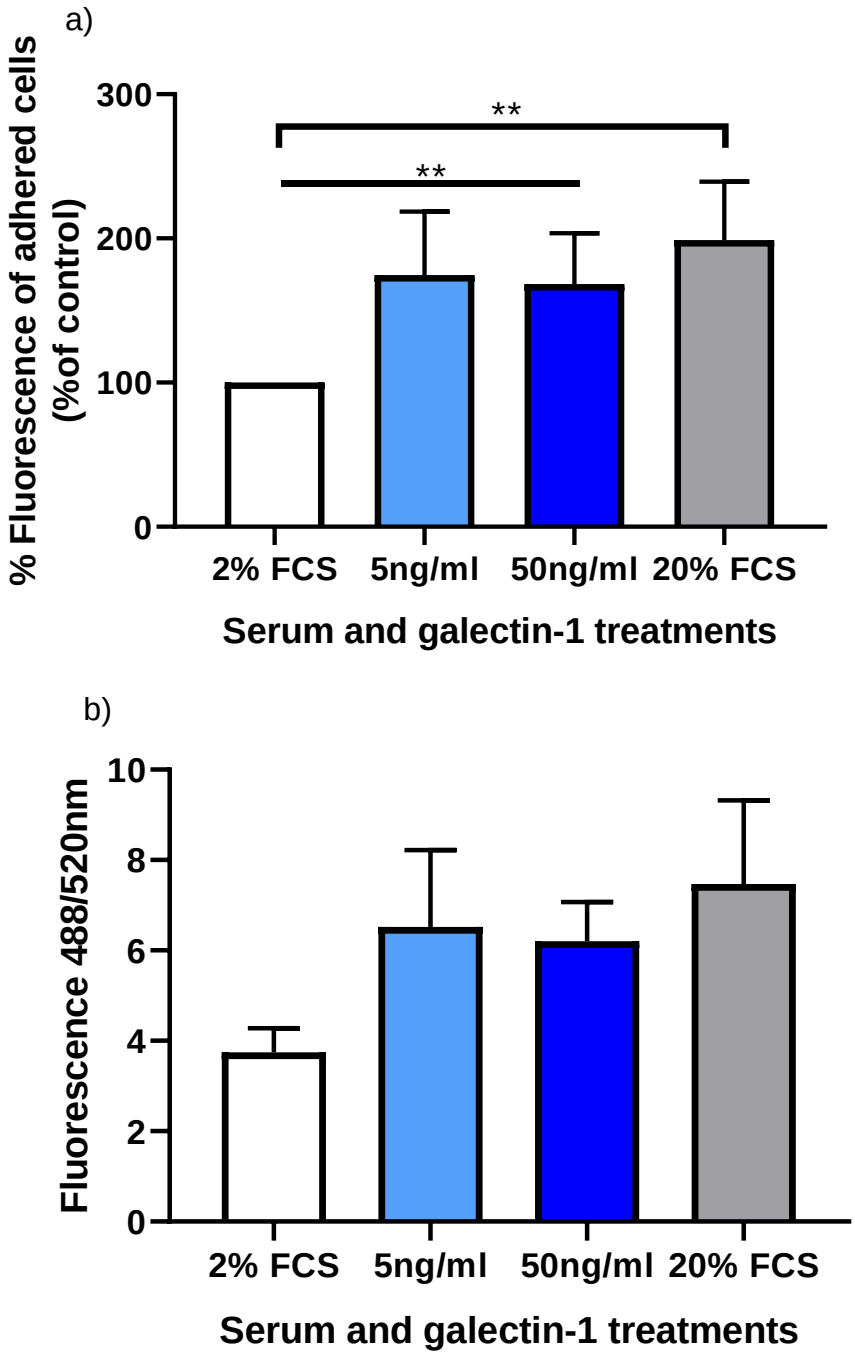

Figure 62. Galectin-1 pre-treated SKOV3 cells show increased adhesion to an omental mesothelial (HOMeso) monolayer. SKOV3 cells were pre-treated with 5 or 50ng/ml galectin-1 for 10 minutes, stained with calcein-AM and added to the HOMeso monolayer. Mesothelial 2% FCS starve media was used as a 100% control; 20% FCS as a positive control. The co-culture was laterally rocked on a plate rocker at 60 tilts per minute before fluorescence of adhered cells was analysed with a plate reader at 488/540nm. a) results shown are the mean ± SD, n=4. Kruskal-Wallis analysis, **p=0.0041. Post-hoc Mann-Whitney U analyses (shown on graph) were performed between treatments/20% FCS control and 2% control, **p values = 0.0022. HOMesos from three isolations were used. b) representative raw data from one experiment.

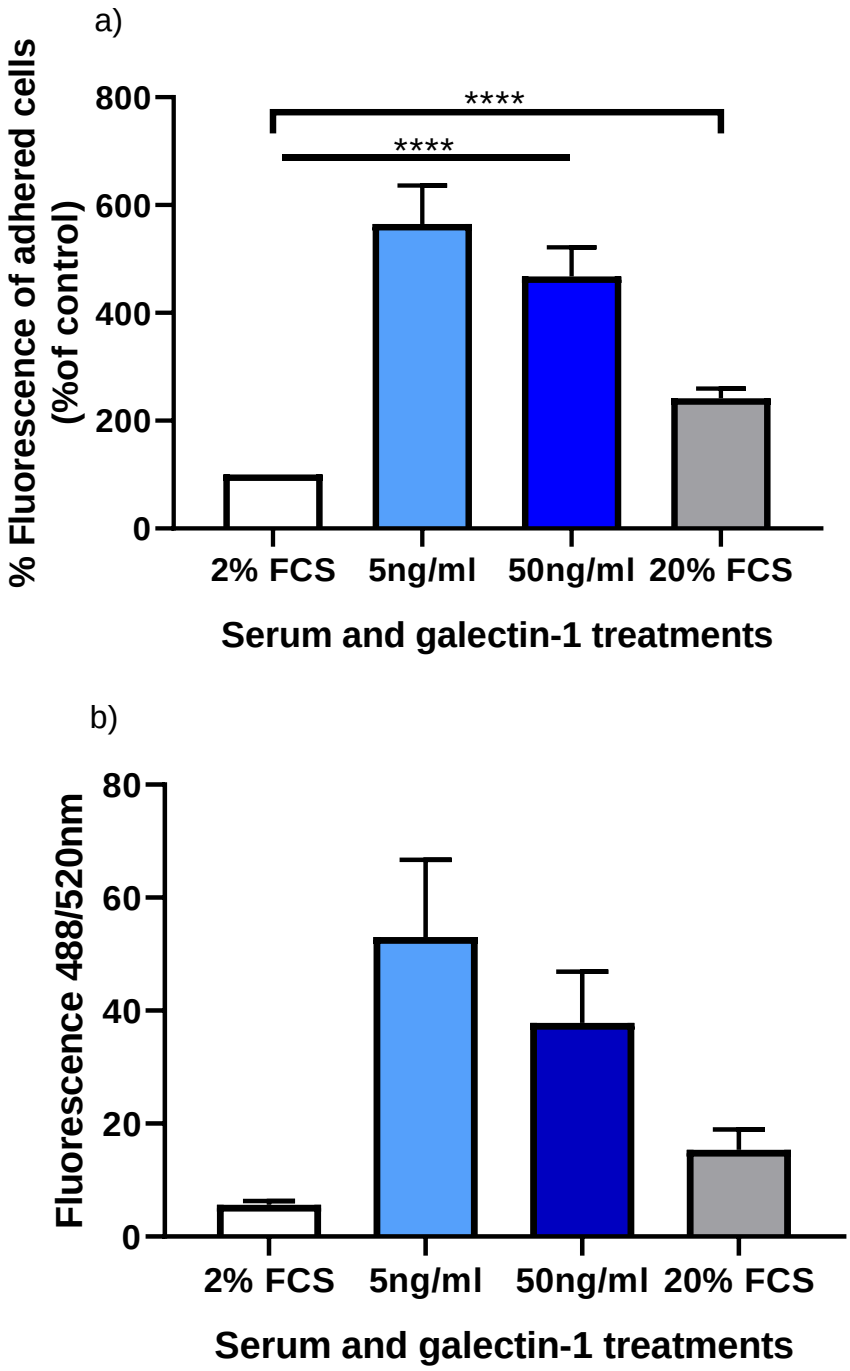

Figure 63. Galectin-1 pre-treated A2780 cells show increased adhesion to a HOMEC monolayer. A2780 cells were pre-treated with 5 or 50ng/ml galectin-1 for 10 minutes, stained with calcein-AM and added to a HOMEC monolayer. Endothelial 2% FCS starve media was used as a 100% control; 20% FCS as a positive control. The co-culture was laterally rocked on a plate rocker at 60 tilts per minute before fluorescence of adhered cells was analysed with a plate reader at 488/540nm. a) results shown are the mean ± SD, n=4. Kruskal-Wallis analysis, ****p<0.0001. Post-hoc Mann-Whitney U analyses (shown on graph) were performed between treatments/20% FCS control and 2% control, ****p values <0.0001. HOMECs from three isolations were used. b) representative raw data from one experiment.

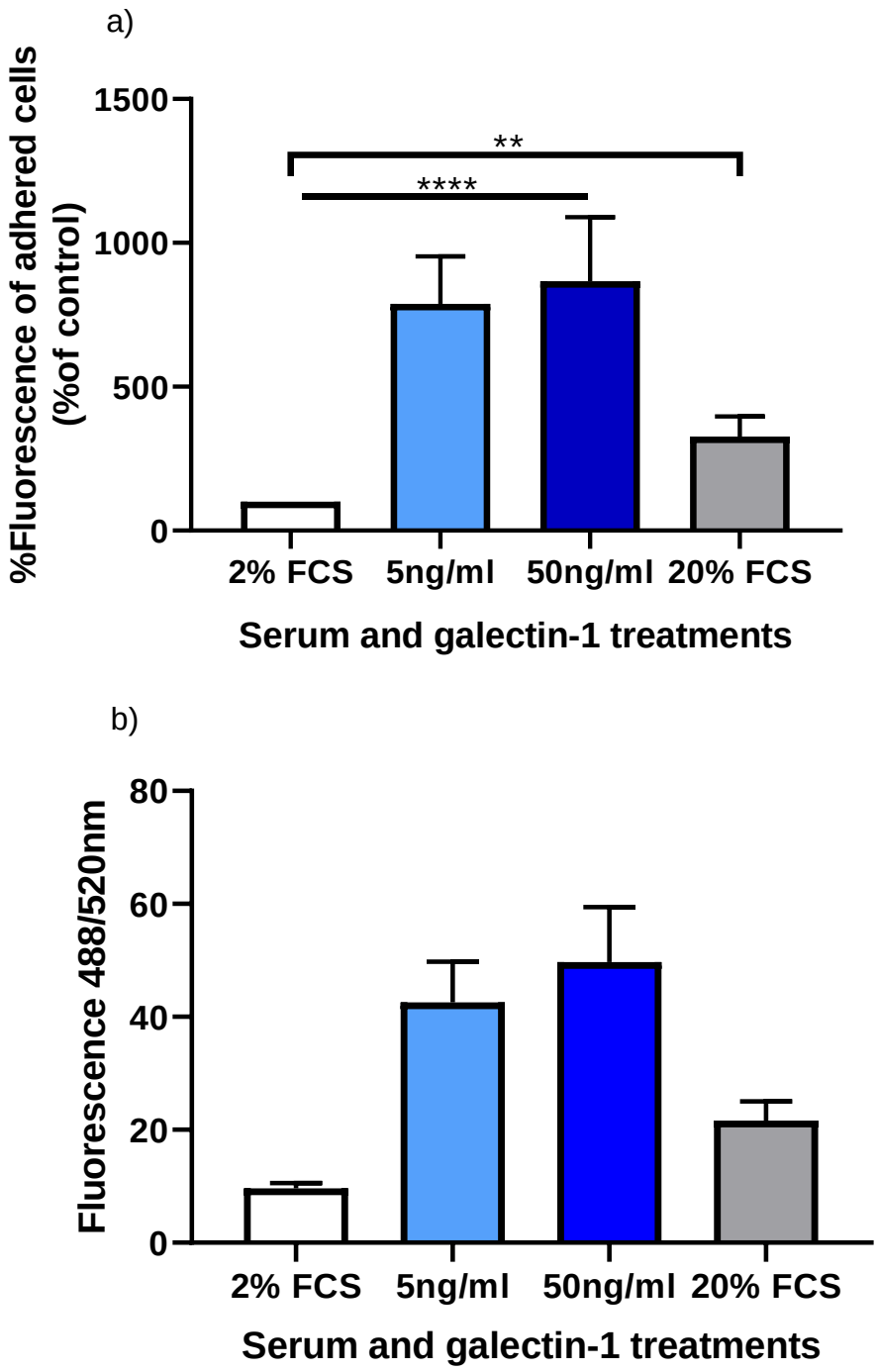

Figure 64. Galectin-1 pre-treated SKOV3 cells show increased adhesion to a HOMEC monolayer. SKOV3 cells were pre-treated with 5 or 50ng/ml galectin-1 for 10 minutes, stained with calcein-AM and added to a HOMEC monolayer. Endothelial 2% FCS starve media was used as a 100% control; 20% FCS as a positive control. The co-culture was laterally rocked on a plate rocker at 60 tilts per minute before fluorescence was analysed of adhered cells with a plate reader at 488/540nm. a) results shown are the mean ± SD, n=4. Kruskal-Wallis analysis, ****p=0.0001. Post-hoc Mann-Whitney U analyses (shown on graph) were performed between treatments/20% FCS control and 2% control, p values ****<0.0001, **p=0.0022. HOMECs from three isolations were used. b) representative raw data from one experiment.

4.3.6.2 Adhesion of A2780 and SKOV3 cells to a galectin-1 pre-treated HOMEC monolayer

Experiments on the adhesion of A2780 ovarian cancer cells to a gal-1 pre-treated HOMEC monolayer showed no significant changes compared with the negative control (Kruskal-Wallis p=0.4967) (figure 65). Importantly, the positive control did not significantly differ from the negative control either. However, SKOV3 cells were significantly more adhesive to the HOMEC monolayer pre-treated with 50ng/ml than the 2% FCS control (p=0.0079), demonstrating an approximate increase in adhesion of 117% (figure 66). These data suggested that overnight pre-treatment of the HOMEC monolayer with 50ng/ml gal-1 resulted in the increased adhesion of SKOV3 cells.

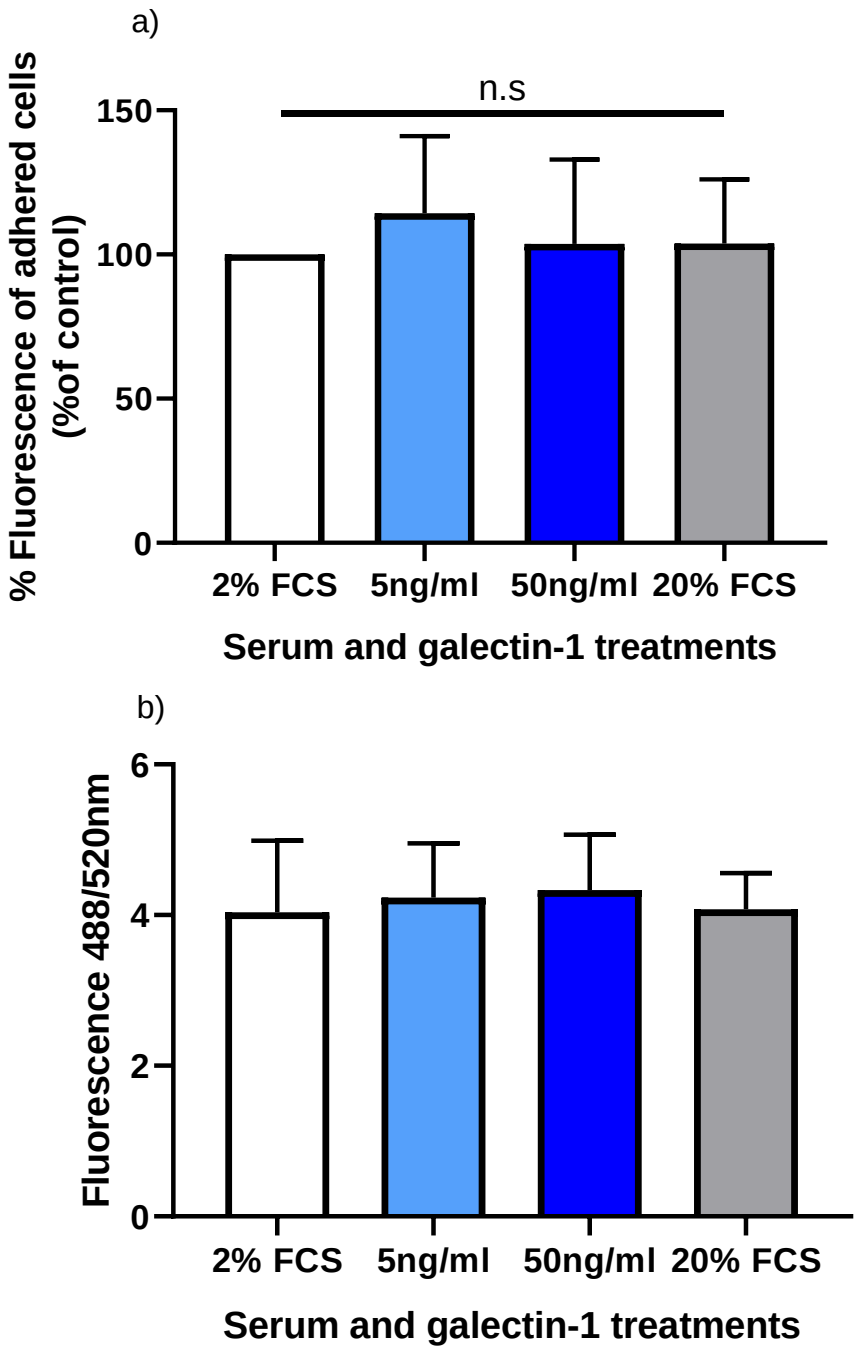

Figure 65. Galectin-1 pre-treatment of a HOMEC monolayer does not affect the adhesion of A2780 cells. A HOMEC monolayer was pre-treated with 5 or 50ng/ml galectin-1 overnight, and A2780 cells were stained with calcein-AM and added to the monolayer media. Endothelial 2% FCS starve media was used as a 100% control; 20% FCS as a positive control. The co-culture was laterally rocked on a plate rocker at 60 tilts per minute before fluorescence of adhered cells was analysed with a plate reader at 488/540nm. a) results shown are the mean ± SD, n=4. HOMECs from three isolations were used. Kruskal-Wallis analysis showed no significant (n.s) differences between any of the treatments or positive control (p=0.4967). b) representative raw data from one experiment.

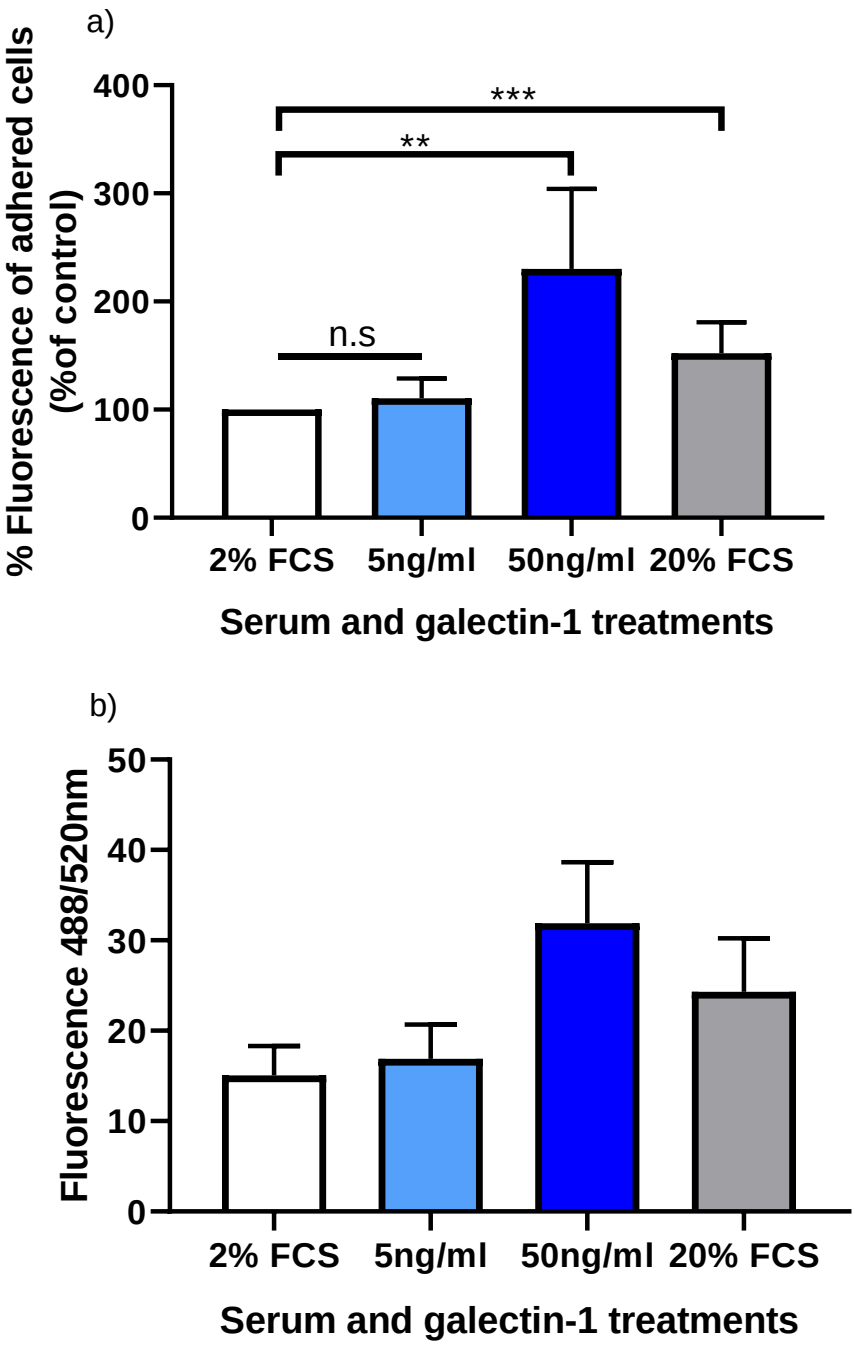

Figure 66. Increased adhesion of SKOV3 ovarian cancer cells to a galectin-1 pre-treated HOMEC monolayer. A HOMEC monolayer was pre-treated with 5 or 50ng/ml galectin-1 overnight, and SKOV3 cells were stained with calcein-AM and added to the monolayer media. Endothelial 2% FCS starve media was used as a 100% control; 20% FCS as a positive control. The co-culture was laterally rocked on a plate rocker at 60 tilts per minute before fluorescence of adhered cells was analysed with a plate reader at 488/540nm. a) results shown are the mean ± SD, n=4. HOMECs from three isolations were used. Kruskal-Wallis analysis, ****p<0.0001. Post-hoc Mann-Whitney U analyses (shown on graph) were performed between treatments/20% FCS control and 2% control, n.s denotes not significant (p=0.1270), **p=0.0079, ***p=0.004. b) representative raw data from one experiment.

4.3.7 Galectin-1 has differential effects on HOMEC, HREC, and hCMEC/D3 endothelial cell proliferation

Proliferation is a key process in angiogenesis (section 1.3.2). Increased expression of gal-1 has been observed in tumour associated vasculature, and gal-1 has been shown to promote the proliferation of endothelial cells (namely HUVECs) *in vitro* (Prior *et al*, 2003; Thijssen *et al*, 2010). Therefore the effect of galectin-1 on HOMEC proliferation was investigated. As in 4.3.1, HRECs and hCMEC/D3 cells were also studied. Proliferation was studied primarily using WST-1 assays. The BrdU assay was used as a second method for HOMECs.

For WST-1 assays, cells were seeded in 96-well plates and starved overnight in 2% endothelial starve media. Galectin-1 was added in 2% endothelial starve media at 1, 5, 10, 25, 50, and 125ng/ml. Starve media and complete endothelial media were used as negative and positive controls. At 24, 48, and 72 hours, WST-1 reagent was added and absorbance was measured (described in 2.3.2.1). BrdU assays were carried out similarly, with the same galectin-1 treatments and controls. The BrdU reagent was added 24 hours before each timepoint to allow time for incorporation. Incorporated BrdU was detected by absorbance measurement (described in 2.3.2.2).

4.3.7.1 Galectin-1 induced significant proliferation of HOMECs

Both WST-1 and BrdU data showed that galectin-1 significantly increased HOMEC proliferation as assessed indirectly by WST-1 (metabolic activity) and directly by BrdU incorporation, compared with control at all concentrations studied after 24 and 48 hours, and 72 hours (all significant except 10ng/ml BrdU data point) (figures 67 - 68). The increased proliferation was observed to be highest after 24 hours, and progressively decreased at 48 and 72 hours; this effect is shown in figure 69. For example at 24 hours, 5ng/ml increased HOMEC proliferation by 62.3%. These data suggested that gal-1 significantly increased HOMEC proliferation at 24, 48, and 72 hours, but that this effect diminishes at each timepoint.

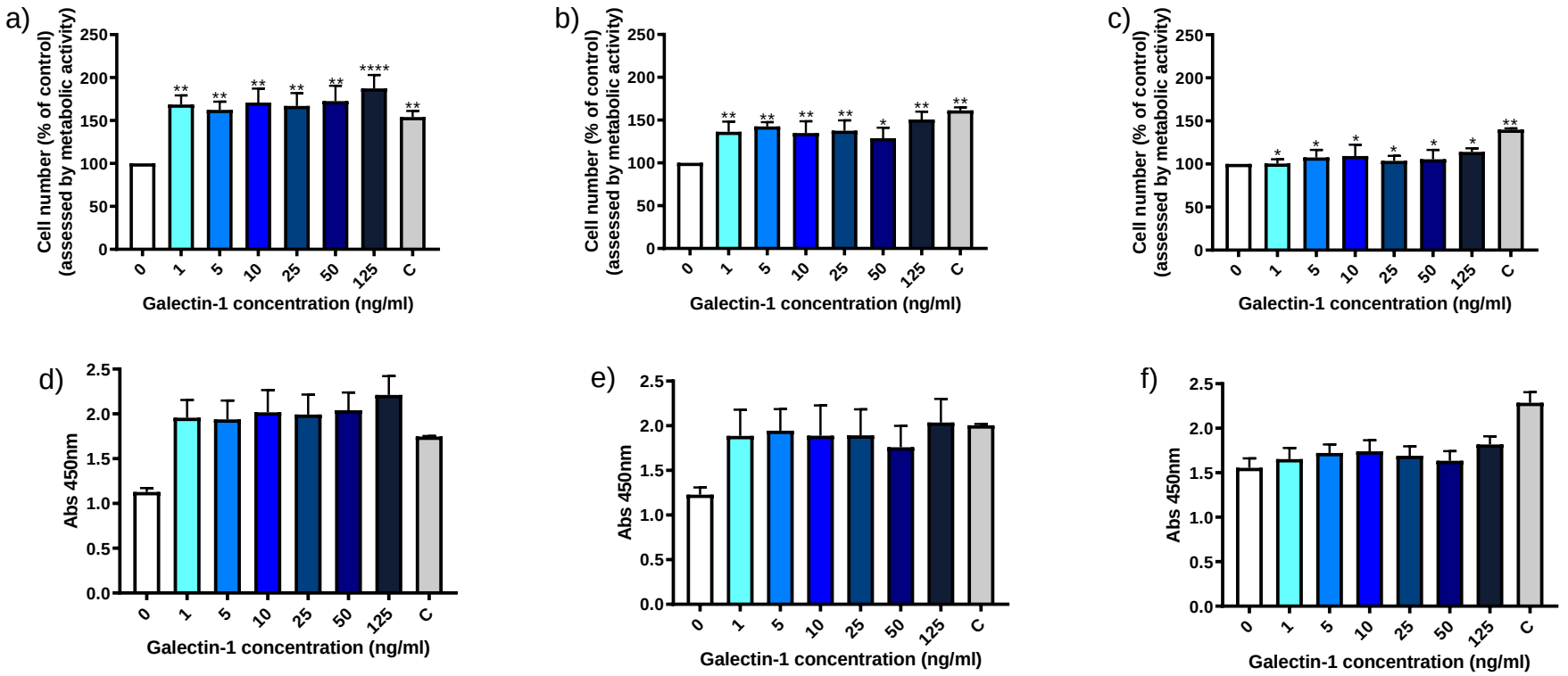

Figure 67. Galectin-1 significantly increased HOMEC proliferation at 24 (a), 48 (b), and 72 hours (c), as assessed by WST-1 metabolic assay. HOMECs were seeded in gelatin pre-coated 96-well plates at 10,000 cells/well. After overnight starve with 2% FCS endothelial media, HOMECs were incubated with 2% endothelial media ± galectin-1 or control treatments. Absorbance was read at 450nm. Results in a), b), and c) are the mean ± SD, n=6 (intra-experimental n=6). HOMECs from five isolations were used. a) Kruskal-Wallis analysis, **p=0.0015, post-hoc Dunn's test (shown on graph, p values in appendix). b) Kruskal-Wallis analysis, ***p=0.0005, post-hoc Dunn's test (shown on graph, p values in appendix). c) Kruskal-Wallis analysis, *p=0.0218, post-hoc Dunn's test (shown on graph, p values in appendix). d), e), and f) show representative raw data from one experiment for 24, 48, and 72 hours respectively. C = complete media.

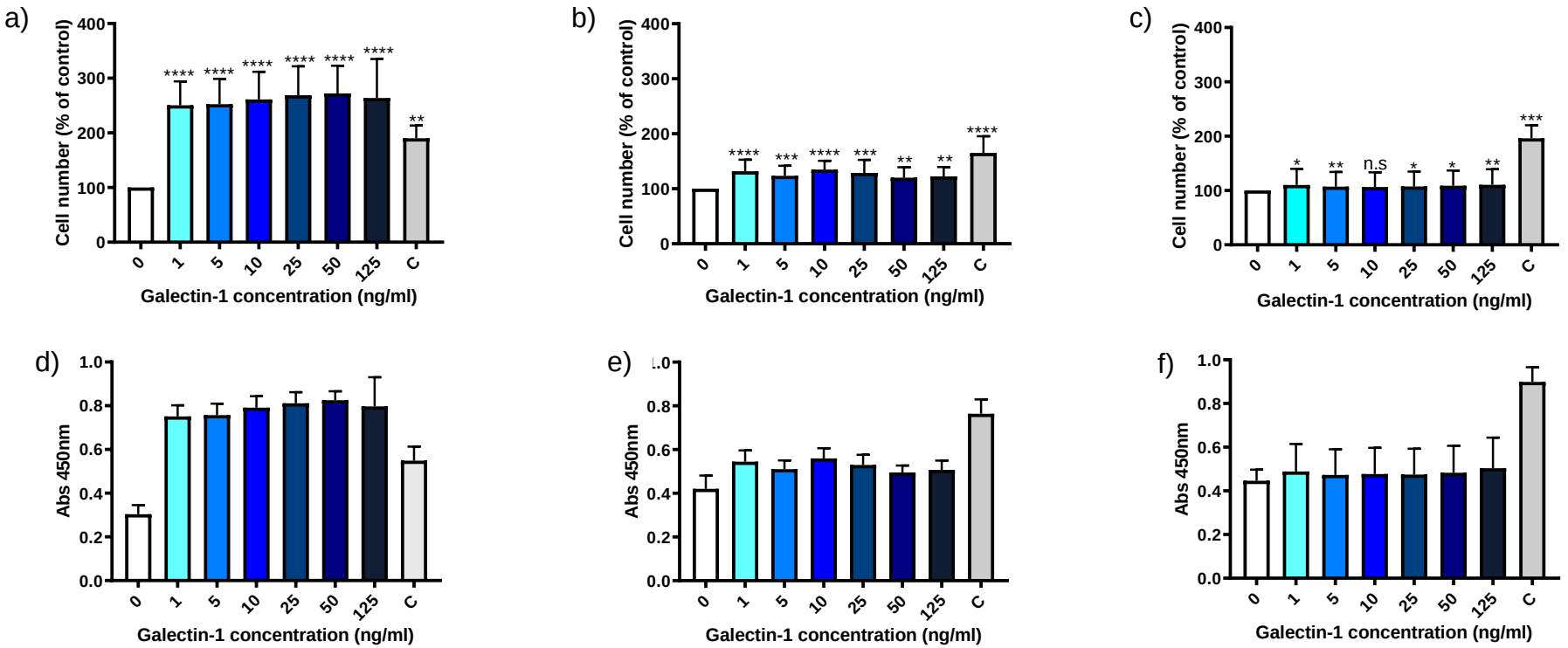

Figure 68. Galectin-1 induced significant proliferation of HOMECs is greatest after 24 hours (a), and decreased after 48 (b) and 72 hours (c) as assessed by BrdU incorporation. HOMECs were seeded in gelatin pre-coated 96-well plates at 10,000 cells/well. After overnight starve with 2% FCS endothelial media, HOMECs were treated with 2% endothelial media ± galectin-1 or control treatments. Absorbance was read at 450nm. Results are the mean ± SD, n=6 (intra-experimental n=6). HOMECs from five isolations were used. a) Kruskal-Wallis analysis, **p<0.0001, post-hoc Dunn's test (shown on graph, p values in appendix). b) Kruskal-Wallis analysis, ****p<0.0001, post-hoc Dunn's test (shown on graph, p values in appendix). c) Kruskal-Wallis analysis, *p=0.0251, post-hoc Dunn's test (shown on graph, p values in appendix). d), e), and f) show representative raw data from one experiment for 24, 48, and 72 hours respectively. C = complete media, n.s = not significant.

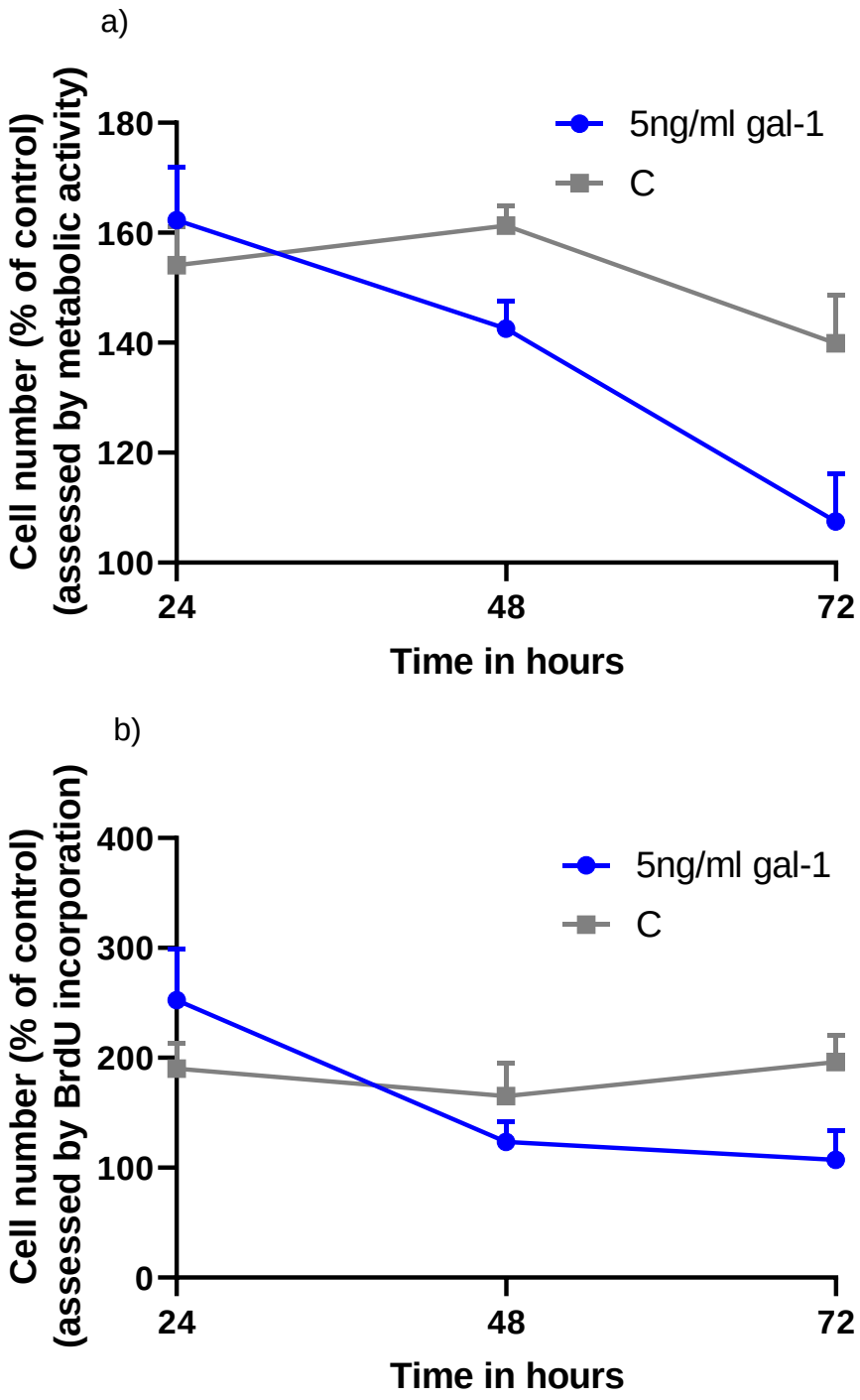

Figure 69. Galectin-1 induced significant proliferation of HOMECs is greatest after 24 hours, and decreased after 48 hours and 72 hours. HOMECs were seeded in gelatin pre-coated 96-well plates at 10,000 cells/well. After overnight starve with 2% FCS endothelial media, HOMECs were treated with 2% endothelial media ± galectin-1 (gal-1) or control treatments. Data show the effect of 5ng/ml gal-1 over 24, 48, and 72 hours as assessed by metabolic activity WST-1 assay (a) and BrdU incorporation (b). Data are the mean ± SD expressed as a percentage of 2% FCS endothelial media (0ng/ml gal-1) control (n=6). C = complete media.

4.3.7.2 Galectin-1 induced significant proliferation of HRECs

Galectin-1 significantly increased HREC proliferation compared to 2% FCS starve media at all concentrations after 24 and 72 hours, as well as at 48 hours in 1, 5, and 10ng/ml treatments, as assessed by WST-1 assay (figure 70). The increased proliferation was observed to be highest after 24 hours, and decreased at 48 and 72 hours; this effect is shown in figure 71. For example at 24 hours, 5ng/ml increased HREC proliferation by 43.1%. These data indicated that gal-1 significantly increased HREC proliferation at 24, and 72 hours at all concentrations studied, but the effect is less at 72 hours. Additionally at 48 hours, the lower concentration of gal-1, 1, 5 and 10ng/ml significantly increased HREC proliferation.

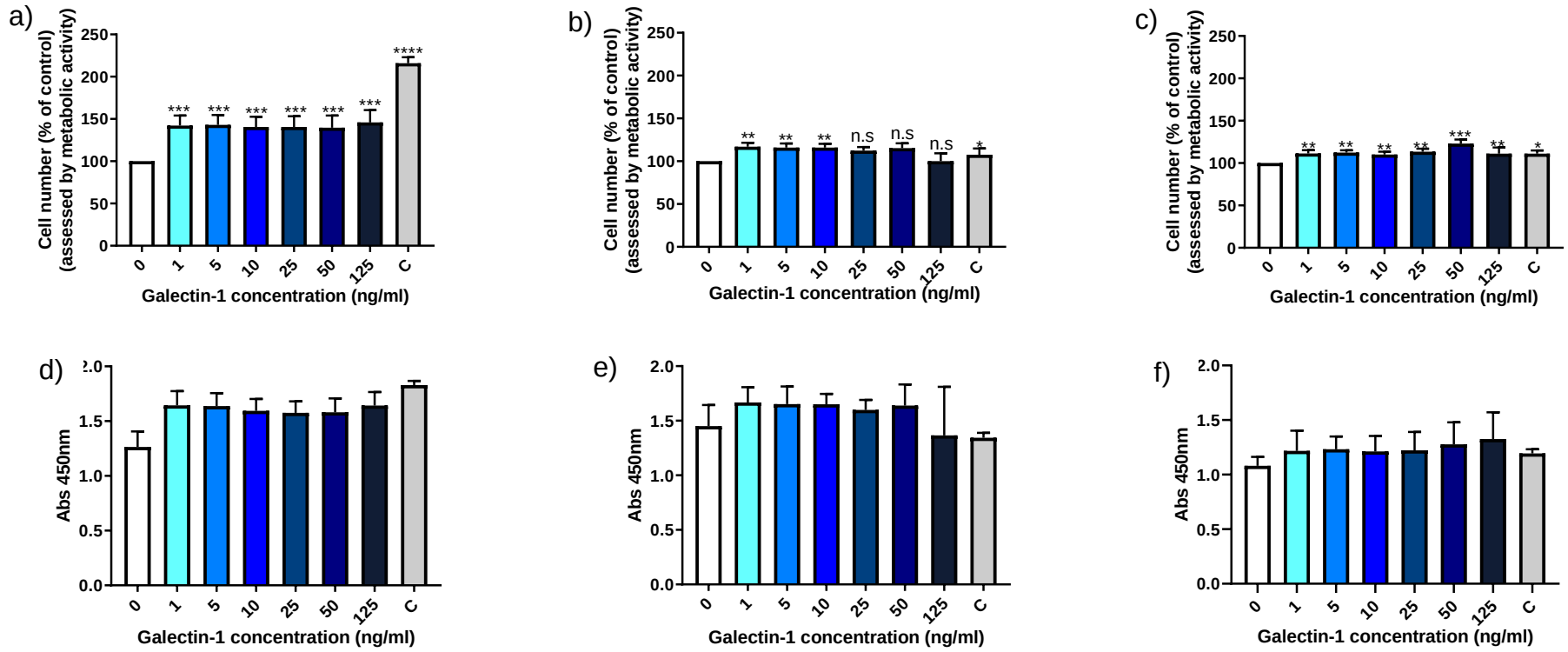

Figure 70. Galectin-1 significantly increased HREC proliferation at 24 (a), 48 (b), and 72 (c) hours, as assessed by WST-1 metabolic assay. HRECs were seeded in gelatin pre-coated 96-well plates at 10,000 cells/well. After overnight starve with 2% FCS endothelial media, HRECs were incubated with 2% endothelial media ± galectin-1 or control treatments. Absorbance was read at 450nm. Results in a), b), and c) are the mean ± SD, n=6 (intra-experimental n=6). a) Kruskal-Wallis analysis, ***p=0.0001, post-hoc Dunn's test (shown on graph, p values in appendix). b) Kruskal-Wallis analysis, **p=0.0032, post-hoc Dunn's test (shown on graph, p values in appendix). c) Kruskal-Wallis analysis, **p=0.0041, post-hoc Dunn's test (shown on graph, p values in appendix). d), e), and f) show representative raw data from one experiment for 24, 48, and 72 hours respectively. C = complete media, n.s = not significant.

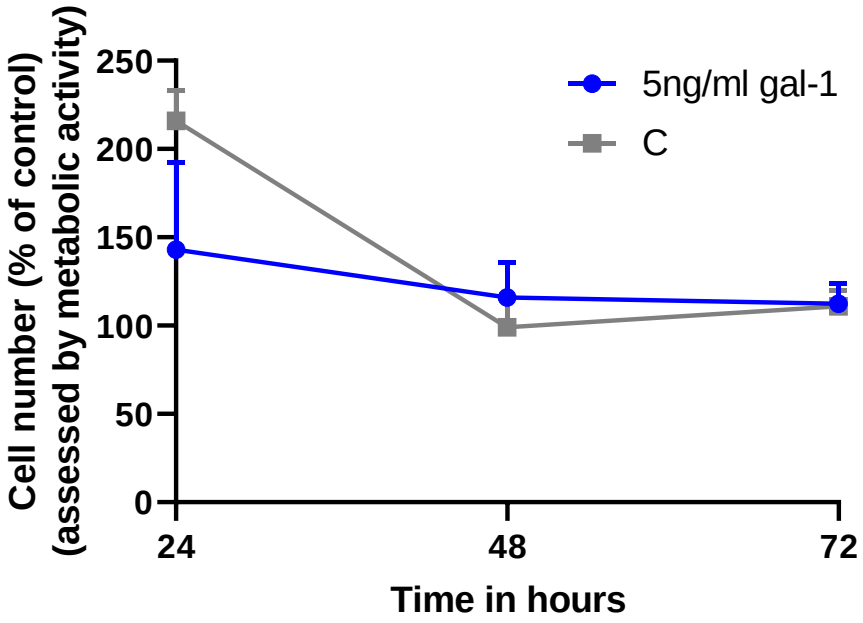

Figure 71. Galectin-1 induced significant proliferation of HRECs is greatest after 24 hours, and decreased after 48 hours and 72 hours. HRECs were seeded in gelatin pre-coated 96-well plates at 10,000 cells/well. After overnight starve with 2% FCS endothelial media, HRECs were incubated with 2% endothelial media ± galectin-1 (gal-1) or control treatments. Data show the effect of 5ng/ml gal-1 over 24, 48, and 72 hours as assessed by metabolic activity WST-1 assay. Data are the mean ± SD expressed as a percentage of 2% FCS endothelial media (0ng/ml gal-1) control (n=6). C = complete media.

4.3.7.3 Galectin-1 induced significant proliferation of hCMEC/D3 endothelial cells

Galectin-1 significantly increased hCMEC/D3 proliferation compared to 2% FCS starve media at concentrations 5 - 125 ng/ml after 72 hours, as assessed by WST-1 assay. For example 5ng/ml gal-1 increased hCMEC/D3 proliferation by 18.4%. This effect is shown in figure 73. Only 125ng/ml significantly increased hCMEC/D3 proliferation at 24 hours, (figure 72). The increased proliferation was observed to be highest in the 125ng/ml 24 hour treatment. These data suggested that 125ng/ml gal-1 significantly increased hCMEC/D3 cell proliferation after 24 hours, and at 72 hours at 5 - 125ng/ml concentrations.

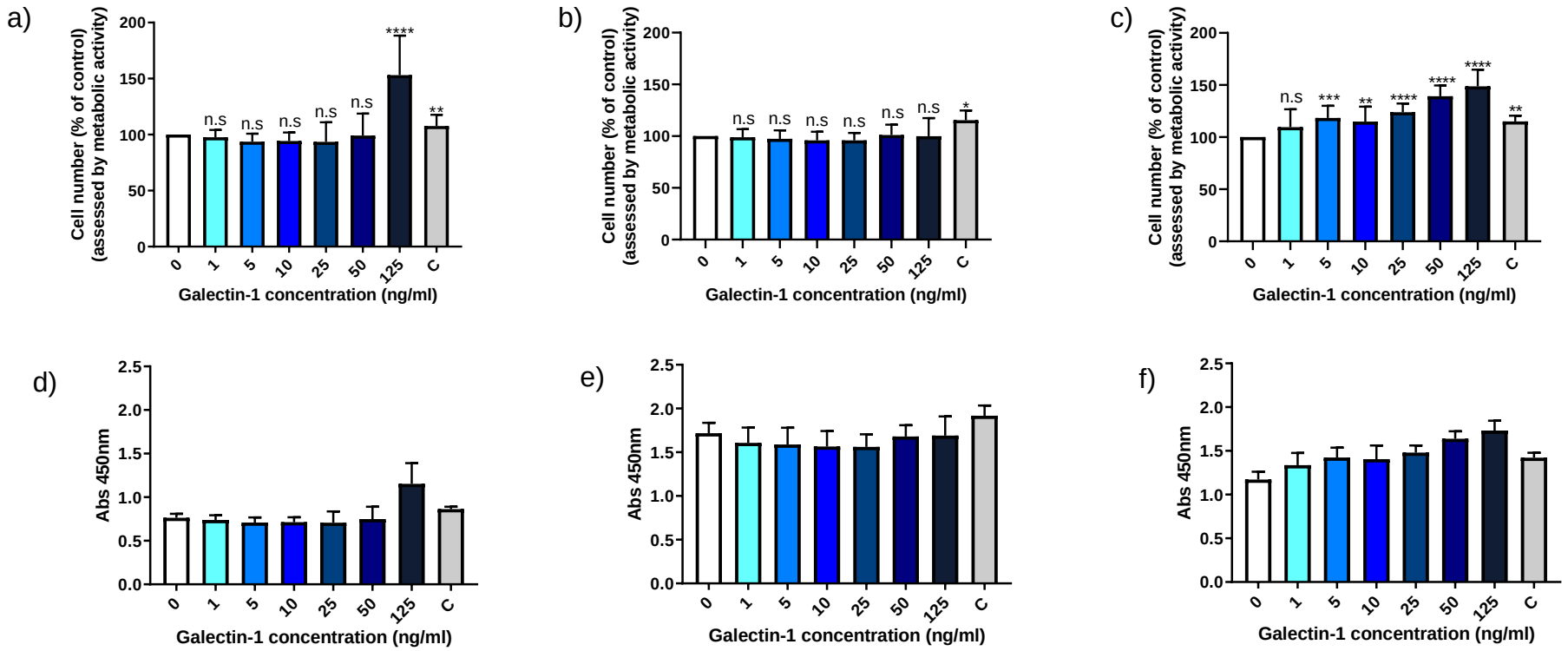

Figure 72. Galectin-1 significantly increased proliferation of hCMEC/D3 cells after 72 hours (c), and at 125ng/ml after 24 hours (a), as assessed by WST-1 metabolic assay. b) = 48 hours. hCMEC/D3s were seeded in gelatin pre-coated 96-well plates at 10,000 cells/well. After overnight starve with 2% FCS endothelial media, hCMEC/D3s were incubated with 2% endothelial media ± galectin-1 or control treatments. Absorbance was read at 450nm. Results in a), b) and c) are the mean ± SD, n=6 (intra-experimental n=6). a) Kruskal-Wallis analysis, ***p<0.0001, post-hoc Dunn's test (shown on graph, p values in appendix). b) Kruskal-Wallis analysis, **p=0.0032, post-hoc Dunn's test (shown on graph, p values in appendix). c) Kruskal-Wallis analysis, ****p<0.0001, post-hoc Dunn's test (shown on graph, p values in appendix). d), e), and f) show representative raw data from one experiment for 24, 48, and 72 hours respectively. C = complete media, n.s = not significant.

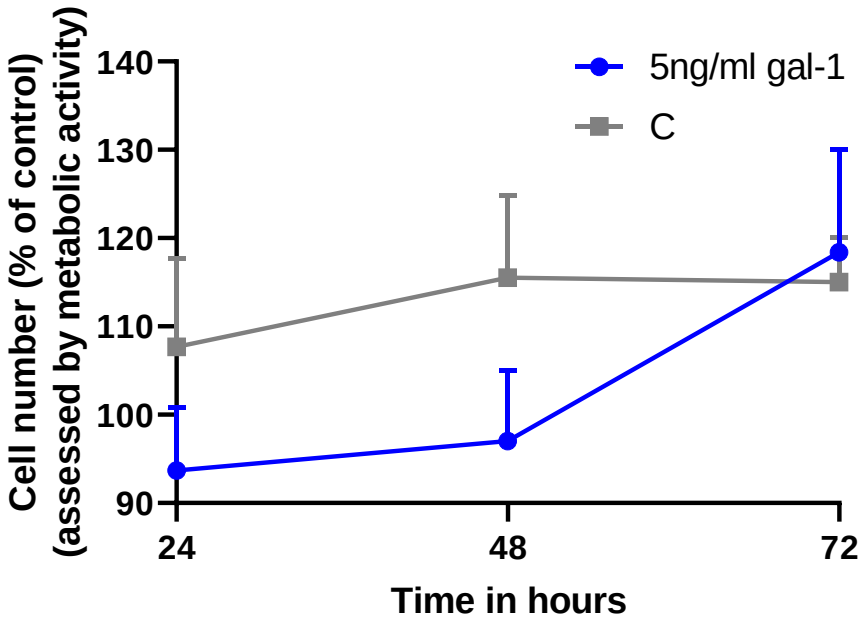

Figure 73. Galectin-1 induced significant proliferation of hCMEC/D3 cells is greatest at 72 hours. hCMEC/D3s were seeded in gelatin pre-coated 96-well plates at 10,000 cells/well. After overnight starve with 2% FCS endothelial media, hCMEC/D3s were incubated with 2% endothelial media ± galectin-1 (gal-1) or control treatments. Data show the effect of 5ng/ml gal-1 over 24, 48, and 72 hours as assessed by metabolic activity WST-1 assay. Data are the mean ± SD expressed as a percentage of 2% FCS endothelial media (0ng/ml gal-1) control (n=6). C = complete media.

4.3.8 Galectin-1 promotes HOMEC migration in Cultrex chamber assays but not scratch assays

Migration is another key step in angiogenesis (section 1.3.2). Current literature has primarily studied gal-1 and migration in HUVECs, and has reported a pro-migratory effect that is dependent on the presence of VEGF and/or the specific integrin-ECM component interaction (Moiseeva *et al*, 2003; Hsieh *et al*, 2008). The effect of gal-1 on HOMEC migration was therefore studied *in vitro* using scratch and Cultrex chamber assays (see 2.3.3).

For scratch assays, HOMECs were seeded in 96-well plates and cultured until a confluent monolayer had formed. Cells were starved overnight in 2% FCS endothelial starve media overnight. Cells were scratched using a pipette tip, the media was removed, and treatments of 5 and 50ng/ml gal-1 (see 4.3.3) were added in 2% starve media. 0.2ng/ml VEGF and 2% starve media were used as positive and negative controls respectively. Wells were photographed at 0, 8, and 16 hours post treatment (described in 2.3.3.1). Photographs were analysed to measure the percentage of scratch closure, 0% measurements were interpreted as 100% of the scratch and 8 and 16 hour timepoints were expressed as a percentage of these (2.3.3.2).

The Cultrex chamber assay kit was adapted to study chemotaxis; pre-starved (in 2% starve endothelial media) HOMECs were seeded into the upper chambers, and 2% starve media containing 5 or 50ng/ml gal-1 were added to the bottom chamber. After 8 hours, cells in the bottom chamber were dissociated and stained with calcein-AM. These cells were transferred to black plates and fluorescence was read at 488/520nm.

4.3.8.1 Galectin-1 does not promote HOMEC migration, as assessed by scratch assays

Scratch assay data showed that neither 5 nor 50ng/ml galectin-1 affected HOMEC migration compared with 2% FCS starve media after 8 and 16 hours post scratch (figure 74). The VEGF positive control showed significant HOMEC migration at both timepoints (p values <0.0001). These data suggested that gal-1 does not promote the migration of HOMECs.

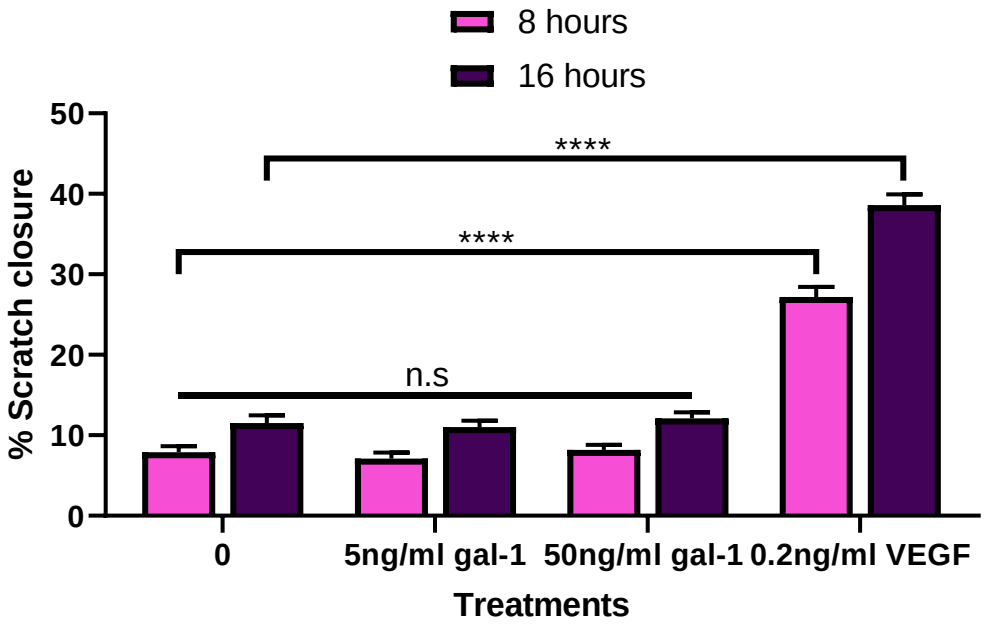

Figure 74. Galectin-1 does not affect the migration of HOMECs during scratch assays. HOMECs were seeded in gelatin pre-coated 96-well plates at 10,000 cells/well, and grown to confluence. After overnight starve with 2% FCS endothelial media, monolayers were scratched with a pipette tip down the centre of each well. The media was aspirated and replaced with 2% endothelial media ± 5 or 50ng/ml galectin-1 or 0.2ng/ml VEGF (positive control). 0 is the control treatment of 2% FCS endothelial media. Wells were photographed at 0, 8, and 16 hours after treatments. The 0 hour scratch gaps were interpreted as the 100% gap; the percentages of the scratch gaps at 8 and 16 hours were determined from the 0 hour measurements. Results are the mean ± SD, n=6 (intra-experimental n=6). HOMECs from four isolations were used. Mann-Whitney U analyses were carried out between galectin-1 treatments and 2% FCS control (0ng/ml)/0.2ngml VEGF positive control at 8 and 16 hour timepoints (****p values <0.0001). No significant differences between gal-1 treatments at either timepoint compared to control were observed (n.s).

4.3.8.2 Galectin-1 does promote HOMEC migration, as assessed by Cultrex chamber assays

Cultrex chamber assay data showed that both 5 and 50ng/ml of galectin-1 significantly increased (p values = 0.0001) chemotactic migration of HOMECs compared with control after 8 hours; 5ng/ml by 17.5% and 50ng/ml by 19.5% (figure 75). The VEGF positive control showed significant HOMEC migration ($p<0.0001$). These data suggested that gal-1 does promote HOMEC migration, as opposed to scratch assay data in 4.3.8.1.

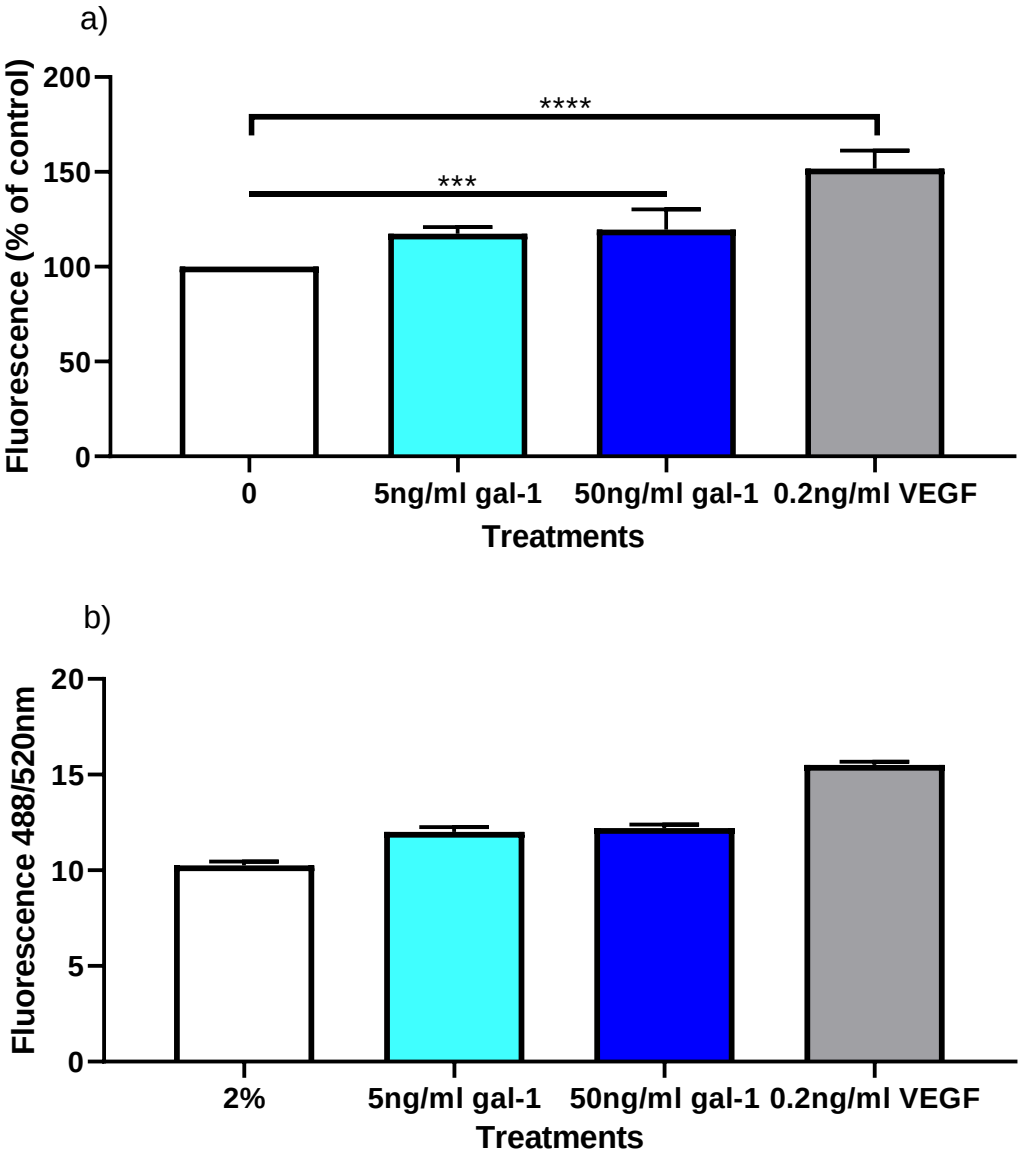

Figure 75. Galectin-1 induced HOMEC migration in Cultrex chamber assays. HOMECs pre-starved with 2% FCS endothelial media were seeded into the upper chamber of assay inserts at 10,000 cells/well. 2% starve media containing 5 or 50ng/ml galectin-1, or 0.2ng/ml of VEGF (positive control) were added to the bottom chamber. 0 is the control treatment of 2% FCS endothelial media. The plate was incubated for 8 hours. The top chamber was aspirated, and cells that had migrated to the bottom chamber were dissociated and stained with calcein-AM. The stained cells were transferred to black plates and fluorescence was read at 488/520nm. Results are the mean ± SD, n=6 (intra-experimental n=6). HOMECs from four isolations were used. Mann-Whitney U analyses were carried out between galectin-1 treatments and 2% FCS control (0ng/ml)/0.2ngml VEGF positive control (***p values = 0.0001, ****p<0.0001). Representative raw data from one experiment are shown in b).

4.4 Discussion

4.4.1 Data summary

In this chapter, gal-1 was shown to be naturally secreted by HOMECs, HRECs and hCMEC/D3 endothelial cells. HOMEC (but not HREC or hCMEC/D3) secretion of gal-1 was found to be significantly increased in response to CL after 30 minutes, 2 hours, and 4 hours. In response to CL, extracellular cell surface bound gal-1 was found to be significantly increased after 5 and 10 minutes. Interestingly, intracellular gal-1 was found to be significantly decreased after 30 minutes but increased after 8 hours. HOMECs incubated with exogenous gal-1 had significantly more cell surface bound gal-1 after 10 minutes, and pre-treatment of HOMECs with A2780 and SKOV3 conditioned media was found to significantly increase HOMEC binding of exogenous gal-1 even further.

Galectin-1 was also found to be secreted by both EOC cell lines, A2780 and SKOV3, but significantly more so by A2780 cells. Gal-1 pre-treatment of A2780 cells was not found to increase their adhesion to a HOMeso monolayer, but did significantly increase adhesion to a HOMEC monolayer. However, gal-1 pre-treatment of a HOMEC monolayer did not affect the adhesion of A2780 cells. Pre-treatment of SKOV3 cells with gal-1 significantly increased their adhesion to both a HOMeso layer and a HOMEC layer. Gal-1 pre-treatment of a HOMEC monolayer also significantly increased the subsequent adhesion of SKOV3 cells.

Galectin-1 was found to significantly increase proliferation in HOMECs, HRECs and hCMEC/D3 cells differentially over 72 hours. The increase in HOMEC proliferation compared with control was greatest after 24 hours. Interestingly, gal-1 was shown to significantly increase HOMEC migration in Cultrex chamber assays but not in scratch assays.

4.4.2 Cathepsin-L induced significant secretion of galectin-1 in HOMECs, but not HRECs and hCMEC/D3 endothelial cells

In recent literature, gal-1 has been shown to be secreted by various tumour cells (Griffioen and Thijssen, 2014). Unpublished data from this lab also found

that CL (an EOC secreted factor) induced differential expression of *LGALS1* in HOMECs. Furthermore Pranjol *et al* (2019) suggested that HOMECs produce gal-1 after treatment with CL, and therefore CL induced gal-1 secretion from these cells was studied. This was also studied in HRECs and hCMEC/D3 cells due to the initial difficulty in isolating HOMECs and their lack of availability. This was important as ECs are known to be heterogeneous (discussed throughout 1.2), and therefore a comparison of both basal and CL stimulated gal-1 secretion, as well as the effects of gal-1 on proliferation (discussed later) was necessary to examine whether the alternative microvascular ECs could substitute for HOMECs in subsequent experiments. This was shown to not be the case, since CL only induced consistent significant gal-1 secretion in HOMECs (at 30 minutes, 2 hour, and 4 hours) (figure 50). Although, both HRECs and hCMEC/D3 cells basally secreted gal-1 at higher levels than HOMECs. However, the percentage change in CL induced gal-1 secretion was less than seen in HOMECs. However, this secretion was not generally CL sensitive. These data therefore confirmed that HOMEC responses to CL were different to the other microvascular ECs studied, highlighting once again the heterogeneity of ECs from different vascular beds and the importance of studying ECs relevant for the condition/organ being studied. On the basis of these findings HOMECs were used for further gal-1 experiments.

These experiments also helped inform the concentrations of gal-1 used experimentally in subsequent work. The lower concentration of 5ng/ml was selected due to CL activated HOMECs secreting approximately 3.5ng/ml of gal-1, and ELISA data in 4.3.5 showing that SKOV3 cells secreted approximately 2ng/ml of gal-1 (SKOV3 cells secreted less gal-1 than A2780). Together, the 5ng/ml therefore was therefore deemed a suitable lower gal-1 concentration to use in experiments. Despite Chen *et al* (2015) reporting gal-1 levels in healthy patient sera as a median of 88ng/ml (range of 30 to 390ng/ml), 50ng/ml was deemed a suitable concentration to use as a higher concentration for experiments. This was due to the large range, and the fact that gal-1 is known to vary in healthy patients (Labrie *et al*, 2017; see section 1.7.2.5). 50ng/ml was considered appropriate as Masoodi *et al* (2021) specifically measured the media gal-1 sera in patients with advanced EOC, recording this as 40.57 ± 22.1ng/ml.

An important consideration for these data is the half-life of gal-1 in culture media, which has been reported as 1 hour 7 minutes (Van Ry *et al*, 2015). If true of the 2% FCS endothelial media used in these experiments, this would suggest that data from timepoints at 2 hours, 4 hours, 8 hours, and 24 hours would show an overall level of gal-1 influenced by both the secretion and degradation of gal-1. This would therefore suggest that the rate of gal-1 secretion was greater than the rate of degradation, and interestingly, all cells secreted the most gal-1 both basally and CL induced after 24 hours. This commonality suggested that the prolonged exposure to the 2% FCS starve media had altered the cell secretome. A study on HUVECs and bronchial ECs had previously shown increased secretion of cytokines involved in promoting immune cell recruitment (Püschel *et al*, 2020), a known function of gal-1 (see section 1.7.2.1). Furthermore, as reviewed by Prudovsky (2013), ECs under stress increase the availability of non-classical secreted proteins, potentially including gal-1. The prolonged exposure of the cells to the 2% FCS starve media may have had further implications on these particular experiments, as the prolonged starve may have affected the health of the glycocalyx. The glycocalyx thickness (composition) is known to vary depending on the microenvironment (Uchimido *et al*, 2019). If the starve led to a reduction in the glycocalyx, then this would have reduced the gal-1 bound to the surface of the cells, and in turn, possibly the amount of gal-1 secreted in response to CL. Therefore any effect of the starvation period on the glycocalyx (on all the cell types) would benefit from glycocalyx quantification.

The significantly increased CL induced gal-1 secretion in HOMECs that occurred at shorter timepoints suggested that not all CL enhanced gal-1 secretion was due to transcriptional changes in gal-1. Indeed, gene transcription would be expected to change over several hours which is supported by previous unpublished data from the lab indicating that increased *LGALS1* expression in HOMECs was observed after 8 hours of CL treatment. Thus, it is possible that the gal-1 measured in the culture supernatant at these earlier timepoints (30 minutes, 2 hours, and 4 hours) was either readily available in the cytoplasm and was exported out of the cell, or was lost from the cell surface. This possibility was studied further in experiments that examined whether the extra and intracellular localisation of gal-1 was altered in CL treated HOMECs.

4.4.3 Cathepsin-L significantly altered localisation of intra and extracellular galectin-1 in HOMECs

Following ELISA data in 4.3.1, gal-1 localisation, both intracellular and surface bound, was studied in response to CL with ICC. The surface levels of extracellular gal-1 showed a relatively large natural variation. However, HOMEC surface associated gal-1 was shown to be significantly higher than control after 5 and 10 minutes with CL treatment (figure 53), additionally, a non-significant increase was also observed after 30 minutes CL treatment.

Interestingly, ELISA data from the 30 minute timepoint demonstrated significant CL induced secretion of gal-1 into the culture medium. Shorter time points for CL-induced secretion were not examined, but the data do suggest a rapid response. Thus, these increases in cell surface extracellular gal-1 could be due to a proportion of the secreted gal-1 binding to the surface of HOMECs. This was therefore investigated with further experiments that are discussed in section 4.3.3. The increase in extracellular surface bound gal-1 also suggested that CL was not causing any significant cleavage of gal-1 from the cell surface, or alternatively, that any gal-1 cleaved was readily replaced by secreted gal-1.

Intracellular gal-1 was also present and the levels showed a natural variation. However, the intracellular level significantly decreased after 30 minutes in CL treated HOMECs. Taken together, these data suggested that this intracellular gal-1 was rapidly exported to the outside of the cells. This is in line with ELISA data in 4.3.1, where increased secreted gal-1 was observed at timepoints before transcriptional upregulation would be expected to occur. Interestingly, intracellular gal-1 significantly increased after 8 hours, suggesting that CL also induced *LGALS1* transcription, as shown in previous data from this lab.

Another factor to consider for these localisation and ELISA studies is the possibility that HOMECs can re-uptake gal-1. Thijssen *et al* (2010) showed that HUVECs and immortalised human vascular ECs were capable of re-uptaking gal-1 from the microenvironment. However, to date this has not been observed in primary human microvascular ECs. Further study using labelled gal-1 and HOMECs to investigate potential re-uptake would therefore be required, and would also give further insight into the origins and fate of extracellular gal-1. This would be important in order to study any effects of HOMEC released gal-1, as gal-1 is known to bind both intra and extracellularly and could exert effects

through different mechanisms. Moreover, whilst it is generally accepted that gal-1 is secreted from cells in a golgi-independent in a manner similar to bFGF (Schäfer *et al,* 2004), the exact mechanism is unknown and warrants further study.

These data demonstrated CL induced gal-1 secretion from, and localisation in HOMECs for the first time. Previous studies looking at gal-1 in other endothelial cells focussed on gal-1 expression as opposed to secretion and localisation (Baum *et al*, 1995; Thijssen *et al*, 2010). These experiments raise the possibility that effects of gal-1 secreted from HOMECs themselves influence HOMEC cellular responses in an autocrine manner. These data also show that, in general, more gal-1 (as quantified by fluorescence intensity) is present on the cell surface than within the cell in general (figures 53 - 56), as well as strong staining for gal-1 in some non-treated cells. Previous literature has focussed on gal-1 expression in activated ECs, for example Hsieh *et al* (2008) reviewed high gal-1 expression in tumour associated ECs, describing gal-1 overexpression compared to adjacent healthy cells in oral squamous cell carcinomas. Similarly, Thijssen *et al* (2006) found that tumour associated ECs expressed more gal-1 compared to ECs found within normal colon tissue. In HOMECs, ICC showed more extracellular gal-1 in non-treated cells after 4 hours, a timepoint shorter than the 24 hours previously observed to be required for increased secretion of gal-1 as an apparent response to prolonged starve media exposure. Taken together, these observations suggested a physiological role for gal-1 in HOMECs, as it was expressed, secreted and bound to the cell surface. However, further clarification of the role of gal-1 is required as these experiments demonstrated that gal-1 expression and localisation is responsive to CL stimulation.

4.4.4 Additional galectin-1 can bind to the surface of HOMECs

The expression and localisation of gal-1 was studied in section 4.3.2. Data indicated that gal-1 was present on the cell surface in both unstimulated and stimulated HOMECs (see figure 53). It was further suggested that short-term incubation with CL for 5 and 10 minutes significantly increased extracellular surface bound gal-1. This was therefore investigated further in section 4.3.3, where it was tested whether exogenous gal-1 could bind to the surface of

HOMECs. The effect of A2780 and SKOV3 TCM on gal-1 binding to the HOMEC surface was also investigated, by pre-treating HOMECs with TCM (see section 4.3.4). Previous literature has discussed that there are implications for increased cell surface gal-1 binding in both activation and regulation of cell surface receptors (Croci *et al*, 2014).

After 10 minutes incubation with gal-1, HOMECs had significantly more cell surface bound gal-1 (55.5 and 96.3% in 5 and 50ng/ml added gal-1 respectively, see figure 57). This supported data from localisation studies in 4.3.2, where more gal-1 was observed on the cell surface in response to 5 and 10 minute incubations with CL. Given that this experiment showed exogenous gal-1 added to unstimulated HOMECs could bind to the cell surface, this suggested that gal-1 from other (non-HOMEC) sources could potentially bind to HOMECs. This is important when considering different cell types within the EOC microenvironment. Localisation studies on the other hand, suggested that HOMEC induced secretion of gal-1 could bind to their own cell surface, therefore suggesting that CL induced HOMEC gal-1 secretion could have autocrine effects.

Gal-1 binding to the surface of HOMECs was also investigated after cells had been incubated with EOC cell conditioned media (see section 4.3.4). Both incubations with conditioned A2780 and SKOV3 media before the addition of gal-1 increased the amount of gal-1 on the surface of HOMECs (see figures 58 - 59). Whilst pre-treatment with A2780 TCM increased cell surface gal-1 after 5 and 50ng/ml exogenous gal-1 almost equally (24.1 and 23.5% respectively), pre-treatment with SKOV3 TCM increased cell surface gal-1 after 5ng/ml exogenous gal-1 by 81.7%, and 31.0% after 50ng/ml gal-1. The marked increase in cell surface gal-1 after SKOV3 pre-treatment (and exogenous gal-1) after 5 but not 50ng/ml was interesting, as it suggested a lower concentration of exogenous gal-1 could result in more gal-1 binding to the surface compared to adding a higher concentration. Regardless, all TCM pre-treatment and additions of exogenous gal-1 significantly increased how much gal-1 could bind to the surface of HOMECs. It is thought cytokines secreted from cancer cells can alter the gal-1 binding to the outside of the cell (by altering golgi enzymes that synthesise glycans), such as TNF-α, interleukin-10, and TGF-β1 (Scott *et al*, 2013; Croci *et al*, 2018). In the case of gal-1 binding, the enzymes affected are

thought to be those involved in N-glycan processing, where cytokine stimulation results in increased N-glycosylation. An increased number of potential N-glycan binding sites on proteins are N-glycosylated (Breitling and Aebi, 2013), or N-glycans are transported to the cell surface and can bind to N-glycosylation sites present on molecules (Patnaik *et al*, 2006). Specific N-glycosylation signatures have been shown in EOC cell lines, including A2780 and SKOV3. This is thought to affect membrane proteins in particular (Anugraham *et al*, 2014), and the glycosylation signatures of EOC tumours has been proposed as having prognostic value (Hamester *et al*, 2019; Pan *et al*, 2020). Importantly, EOC cells are thought to alter the N-glycosylation in cells in the tumour microenvironment, including ECs (Halama *et al*, 2017; Chandler *et al*, 2019b). It is therefore possible that EOC induced changes in N-glycosylation can affected amount of gal-1 that can bind to HOMECs.

As discussed earlier, HOMECs were previously shown to bind more gal-1 without any stimulus or pre-treatment. This therefore suggests that the TCM induced additional binding of gal-1 would not be required in order for HOMECs to bind additional gal-1. However, these observations may have implications when considering the EOC microenvironment.

4.4.5 Galectin-1 enhances adhesion of EOC cell lines to HOMEC and HOMeso monolayers

It had been established in the literature that cells other than ECs in the tumour microenvironment secrete gal-1, including tumour cells themselves (Shimada *et al*, 2020). However, most studies on EOC cells have primarily focussed on the level of gal-1 expressed within or bound to the surface of cells, and had not been quantified in different EOC cell lines. Therefore a metastatic EOC cell line (SKOV3) and primary EOC cell line (A2780) were studied in order to investigate their secretion of gal-1, with no external stimuli. Experiments showed that A2780 cells secreted significantly more gal-1 after 24 hours compared with SKOV3 cells (averages of 7.5ngml and 2.5ng/ml, respectively) (figure 60). These data suggest a difference in secreted gal-1 between EOC cells derived from ascites (SKOV3) and EOC cells derived from the primary tumour site (A2780). These data contrast work from Park *et al* (2017), who quantified secreted gal-1 by ELISA in SKOV3 cells after 24 hours as well as a different

primary EOC cell line, Caov-3 cells. The group found SKOV3 cells to secrete more gal-1 than Caov-3 cells; however, they found the level of SKOV3 secreted gal-1 to be approximately 10pg/ml, significantly less than the results from these experiments (2.5ng/ml). Park *et al* (2017) had an n of 2, and also reported negative values for gal-1 secretion (in pg/ml) from Caov-3 cells, suggesting that these data may have required further clarification. The data in this thesis from these experiments is interesting as higher levels of gal-1 (sera, immunohistochemistry) are known to be associated with the progression of metastasis, and indeed gal-1 is of interest as a prognostic marker in EOC (1.7.2.5). Therefore, more secretion of gal-1 from A2780 (primary tumour) cells was unexpected. However, studies have suggested that gal-1 is strongly expressed in primary ovarian tumours (Labrie *et al*, 2017), as well as in primary tumours of other cancers such as breast (Dalotto-Moreno *et al*, 2013) and pancreatic (Orozco *et al*, 2011). In these studies, gal-1 was either shown or hypothesised to be involved in growth of the primary tumour. It should be noted that SKOV3 secretion of approximately 2.5ng/ml gal-1 would be sufficient to induce HOMEC proliferation based on data in figures 57 - 58. Therefore this finding is also interesting in terms of SKOV3 being used as an *in vitro* cell model for EOC metastasis to the omentum (in terms of pro-angiogenic effects).

Data in section 4.3.5 indicated that SKOV3 and A2780 cells secreted gal-1 at levels in the ng/ml range. Since gal-1 has been implicated in cancer cell adhesion (Clausse *et al*, 1999; Cooper *et al*, 2008) experiments to assess the effect of gal-1 pre-treatment of cancer cells to a HOMEC and HOMeso monolayer was studied, as well as their adhesion to a pre-treated HOMEC layer. These experiments intended to model adhesion during haematogenous (1.4.5.1) and transcoelomic (1.4.5.2) metastasis.

Firstly, experiments were conducted using gal-1 pre-treated A2780 and SKOV3 cells and studying their adhesion to an omental mesothelial monolayer (HOMesos). SKOV3 cells pre-treated with 5 and 50ng/ml pre-treatment of gal-1 demonstrated significantly increased (+74.6 and +68.4% respectively) adhesion to the HOMesos monolayer, whereas A2780 cells did not (figures 61 - 62). The differences in adhesion between gal-1 treated SKOV3 cells and untreated SKOV3 cells suggested that gal-1 was either binding to the cancer cells (known to occur by binding to 90k (Grassadonia *et al*, 2002), or that gal-1 induced

unknown changes in the cancer cells that affected their adhesion properties. Whilst A2780 cells were not shown to be more adhesive with gal-1 pre-treatment to a HOMeso layer after gal-1 pre-treatment, they were significantly more adhesive to a HOMEC monolayer (figure 63), again suggesting gal-1 induced changes in their adhesiveness, potentially by binding to the outside of the cancer cells. As discussed earlier, SKOV3 cells are derived from ascites and are therefore metastatic cells, and A2780 cells are derived from a primary ovarian tumour. The increased adhesion to a HOMeso layer seen in SKOV3 cells is therefore interesting, as these ascites-derived cells would have been originally exposed to factors secreted in the ascites, including those from the omentum. As discussed in section 1.4.5.2, disseminated EOC cells in ascites are able to adhere to and invade the omental mesothelial layer, a process thought to be mediated through mesothelial expressed fibronectin. van den Brûle *et al* (2003) demonstrated an *in vitro* gal-1 dose-dependent increase in SKOV3 adhesion to fibronectin coated culture plastic; results which are in line with the data in this thesis, with gal-1 pre-treated SKOV3 appearing more adherent to a HOMeso layer. Alongside gal-1 secretion data in 4.3.5, these data suggested that EOC cell secreted gal-1 could increase EOC cell adhesion to the omentum during transcoelomic metastasis of EOC (section 1.4.5.2).

Gal-1 pre-treatment of both A2780 and SKOV3 cells significantly and strikingly increased their adhesion to HOMEC monolayers (figures 63 - 64); 5 and 50ng/ml pre-treatment increased A2780 cell adhesion by approximately 464.8 and 465.6% respectively, and SKOV3 cell adhesion by 687.8 and 767.0% respectively. These experiments were carried out as an investigation into the effect of gal-1 on the intra/extravasation of EOCs during haematogenous metastasis (section 1.4.5.1). They support previous reports that gal-1 may play a role in tumour cell attachment to ECs, in a manner similar to leukocyte adhesion (Clausse *et al*, 1999). The data presented a role for gal-1 in increasing EOC cell adhesion to HOMECs, an effect that could be important for intra/extravasation during haematogenous metastasis. It is unclear in EOC at what point haematogenous spread occurs, and therefore both EOC cell lines from primary and metastatic tumours were of interest.

An additional experiment to investigate the adhesion of the cancer cells to a gal-1 pre-treated HOMEC monolayer showed a significant increase only in SKOV3

adhesion at 50ng/ml (an increase of 130.3%) (figure 66). Pre-treating the monolayer this way instead of the cancer cells was done to model processes observed in leukocyte adhesion to the endothelium, where the tethering of cells is also mediated by proteins on the surface of the endothelium (see section 1.1.2.1). The increased adhesion observed in the 50ng/ml pre-treated HOMEC monolayer with SKOV3 cells but not A2780 cells is interesting, as this suggests that the metastatic SKOV3 cells are more adhesive to endothelium exposed to gal-1. The effect of gal-1 on endothelial trafficking has been better studied in an immune context, with studies interestingly suggesting a role for gal-1 in downregulating immune cell recruitment (La *et al*, 2003; Cooper *et al*, 2008).

These experiments suggested that gal-1 is an EOC secreted factor, and is implicated in EOC cell adhesion differentially, depending on the origin of the EOC cells, as well as gal-1 treatment. However, further work is required. Whilst gal-1 pre-treatment of A2780 and SKOV3 cells was shown to affect adhesion, the mechanism is unclear, and it is unknown if gal-1 was binding to the EOC cell surface, or induced other cellular changes. Furthermore the methodology used (see section 2.3.9) could be expanded upon to be better suited for physiological study. The method gave a reasonable way of modelling EOC transcoelomic metastasis (tumour cells in ascites adhering to omental mesothelial layer), but was less applicable to intra/extravasation studies as the see-saw rocking motion did not mimic unidirectional flow, as found in vessels. Therefore further work to study the effect of gal-1 on adhesion using unidirectional flow models would be useful. Furthermore, in the experiments concerning the adhesion of gal-1 pre-treatment of A2780 cells to a HOMeso monolayer, and the adhesion of A2780 cells to a gal-1 pre-treated HOMEC monolayer (figures 61 and 65 respectively), the positive controls (20% FCS) did not show a significant increase in cell adhesion compare to the negative 2% FCS control. This questions the validity of these experiments, as it both possible that the cells used were unable to increase their adhesiveness (perhaps due to viability reasons), or that under these circumstances, A2780 cells would simply not adhere to the monolayers at all. This necessitates further investigation to clarify these results, and a positive control that demonstrates an increase in cell adhesion.

4.4.6 Galectin-1 differentially increased proliferation of HOMECs, HRECs and hCMEC/D3 endothelial cells

The effect of gal-1 on EC proliferation was differential, similarly to the secretion of gal-1 in response to CL (4.3.1). HOMEC and HREC proliferation in response to gal-1 was both significant at 24, 48, and 72 hours (although not at all gal-1 concentrations or as a high as an increase in HRECs). hCMEC/D3 cells only showed significant proliferation in response to gal-1 after 72 hours. These findings supported the previous observation that HOMECs could not be substituted with other ECs, and further justified the work to improve the HOMEC isolation development discussed in chapter 3. Regardless, all the ECs studied showed significantly increased proliferation in response to gal-1, albeit at different concentrations and at different timepoints, reflecting the heterogeneity of ECs. The increase in HOMEC proliferation occurred at all gal-1 concentrations (1 - 125ng/ml) at 24, 48, and 72 hours (except 10ng/ml in 72 hour BrdU data) (figures 67 - 68), although the difference between gal-1 treatments and the control became less over time. These data suggested that gal-1 could induce HOMEC proliferation above control levels after 24, 48, and 72 hours of treatment, in a seemingly dose-independent manner. This apparent saturation effect at this range of concentrations (1 – 125ng/ml) was interesting as previous studies of the effect of gal-1 on HUVEC proliferation showed a significant increase in proliferation with a concentration of 10µg/ml (D'Haene *et al* (2013). Interestingly, Hsieh *et al* (2008) showed that lower concentrations of gal-1, 125 – 500nm) (which overlaps with the highest concentration used in this thesis) significantly increased the proliferation of tumour associated ECs. The effect of gal-1 on EC proliferation is therefore potentially heterogeneous.

Given that the largest increase compared with control occurred at 24 hours, and initial data were generated from WST-1 assays, proliferation of HOMECs was also studied using BrdU assays to confirm the results. The data from WST-1 assays reflects cellular metabolic activity and are therefore an indirect assessment of cell number. As a result these assays are a less reliable indicator of proliferation after only one timepoint, as results could be due to treatments altering metabolism and not cell proliferation (see section 2.3.2). The BrdU data showed similar results to the WST-1 data, where every concentration of gal-1 induced significant HOMEC proliferation at each timepoint (except

10ng/ml at 72 hours). Again, the pro-proliferative effect above control values was diminished at each timepoint, but BrdU data also showed this to be more prominent between 24 and 48 hours. This could suggest that the pro-proliferative effect of gal-1 is initially rapid during the first 24 hours, and then its effect diminishes over 48 and 72 hours (during which control cells start to catch up). ELISA data in 4.3.1 showed that all ECs studied secreted basal amounts of gal-1, and therefore it is possible that the gal-1 added to ECs in proliferation studies had degraded so that levels in media at 48 and 72 hours were comparable with basal levels.

Gal-1 induced HREC proliferation data was more similar to HOMECs than gal-1 induced hCMEC/D3 proliferation; data showed that gal-1 could induce HREC proliferation at 24, 48 (not 25, 50, or 125ng/ml), and 72 hours, in a seemingly dose-independent manner. Gal-1 has recently been implicated in the development of diabetic retinopathy in mice (Kanda *et al*, 2017; Yang *et al*, 2017), where gal-1 was significantly upregulated, and gal-1 inhibition decreased neovascularisation. The gal-1 induced proliferation of HRECs could therefore be of interest as a pro-angiogenic process during diabetic retinopathy, although more studies to quantify and investigate it in humans would be required. The similarities in proliferation at the 24 hour point between HRECs and HOMECs suggested these cells may be more suitable as a substitution than hCMEC/D3 cells. This was interesting as HOMECs and HRECs are primary cells, whereas hCMEC/D3 cells are a cell line. The hCMEC/D3 cells only showed significant gal-1 induced proliferation at 24 hours with 125ng/ml of gal-1, and at 72 hours (not at 1ng/ml). The significantly increased proliferation at 72 hours appeared to be dose-dependent between 5 - 125ng/ml. No significant effects were observed at 48 hours. These data indicated that gal-1 increased hCMEC/D3 proliferation after 72 hours, in contrast to the rapid effects on proliferation in both HRECs and HOMECs within 24 hours. However, it is important to consider the raw data (figure 72), as hCMEC/D3 cells after 72 hours can be seen to have decreased absorbance readings in the 0ng/ml (2% FCS endothelial starve media) control compared to those measured at 48 hours. This suggested that 72 hours in the starve media may have been affecting hCMEC/D3 cell viability, and therefore the effect of gal-1 may be more protective than pro-proliferative. Indeed, 0ng/ml control HRECs also had a lower absorbance reading at 72 hours compared to

48 hours, suggesting that a similar effect may have occurred. HOMECs were shown to grow minimally between 48 and 72 hours, suggesting that either the effect of gal-1 at this timepoint was ongoing, or that HOMECs were more viable after longer incubations in the starve media compared to HRECs and hCMEC/D3 cells.

Due to the differential effects of gal-1 on HOMEC, HREC, and hCMEC/D3 proliferation, only HOMECs were used in further studies to determine the mechanism.

4.4.7 Galectin-1 induced HOMEC migration was observed in Cultrex chamber assays but not in scratch assays

Intriguingly, a significant increase in HOMEC migration in response to gal-1 was observed in Cultrex chamber assays at both 5 and 50ng/ml, but not in scratch assays (figures 74 - 75). The gal-1 induced migration was less than that of VEGF, which was used as a positive control as VEGF is a known inducer of EC migration (Wang *et al*, 2011). These findings warranted comparison between the two techniques of migration study. Importantly, the chamber assay allowed the study of chemotactic HOMEC migration with a gal-1 gradient, whereas migration during scratch assays would be indicative of chemokinetic cell movement as there was no gal-1 gradient (Zhang *et al*, 2013). Taking this into consideration, this suggested that gal-1 could induce chemotactic HOMEC migration, but does not induce chemokinesis. However, another consideration to account for is the difference in experimental setup; scratch assays were carried out in 96-well plates pre-coated with 2% (w/v) gelatin, whereas cells were seeded into the chamber assay inserts that were not pre-coated with gelatin. As discussed in 1.7.2.3, gal-1 induced cell motility has been observed to be dependent on whether it can interact with certain integrins connecting to certain components of the ECM. For example, Moiseeva *et al* (2003) found gal-1 induced the migration of HUVECs by interacting with α1β1 integrins connected to laminin, but not fibronectin. In addition, Hsieh *et al* (2008) showed that gal-1 can interact with NRP-1, and that subsequent interaction between gal-1-NRP-1 could activate VEGFR2 and promote EC migration. Ultimately, the mechanisms of gal-1 induced EC migration are still unclear.

The study of gal-1 induced EC migration is further complicated by different results occurring under different experimental setups. For example, Thijssen *et al* (2010) found that gal-1 increased HUVEC migration in scratch assays where the culture plastics had not been coated with any ECM proteins. It is therefore possible that scratch assays on HOMECs carried out on plastics without the pre-coating with 2% (w/v) gelatin may show different results. However, HOMECs do not grow as well on uncoated plastic, and therefore it is unlikely they would be able to reach confluency and migrate unhindered during scratch assay. Further study of the effect of gal-1 on HOMEC migration using different methods would thus potentially be difficult.

4.4.8 Conclusions

The data in this chapter suggest a role for gal-1 in the adhesion of EOC cells to both HOMEC and HOMeso monolayers. These findings potentially have implications for gal-1 in both the transcoelomic and haematogenous metastasis of EOC to and from the omentum. Data also suggest that CL induces the secretion of gal-1 from HOMECs, and that intracellular gal-1 is initially exported outside of cells. The secreted gal-1 was shown to be in the ng/ml range, which was then shown to be sufficient to induce HOMEC proliferation, suggesting a possible autocrine effect of gal-1 on HOMECs, particularly as exogenous gal-1 was shown to be able to bind to HOMECs. The amount of gal-1 able to bind to HOMECs was shown to increase by pre-treating HOMECs with EOC cell conditioned media. The secretion and surface binding of gal-1 data are summarised in figure 76. Gal-1 was also shown to induce chemotactic migration of HOMECs. Overall, gal-1 was shown to induce pro-angiogenic effects on HOMECs. The mechanisms of gal-1 mediated HOMEC proliferation are investigated in chapter 5.

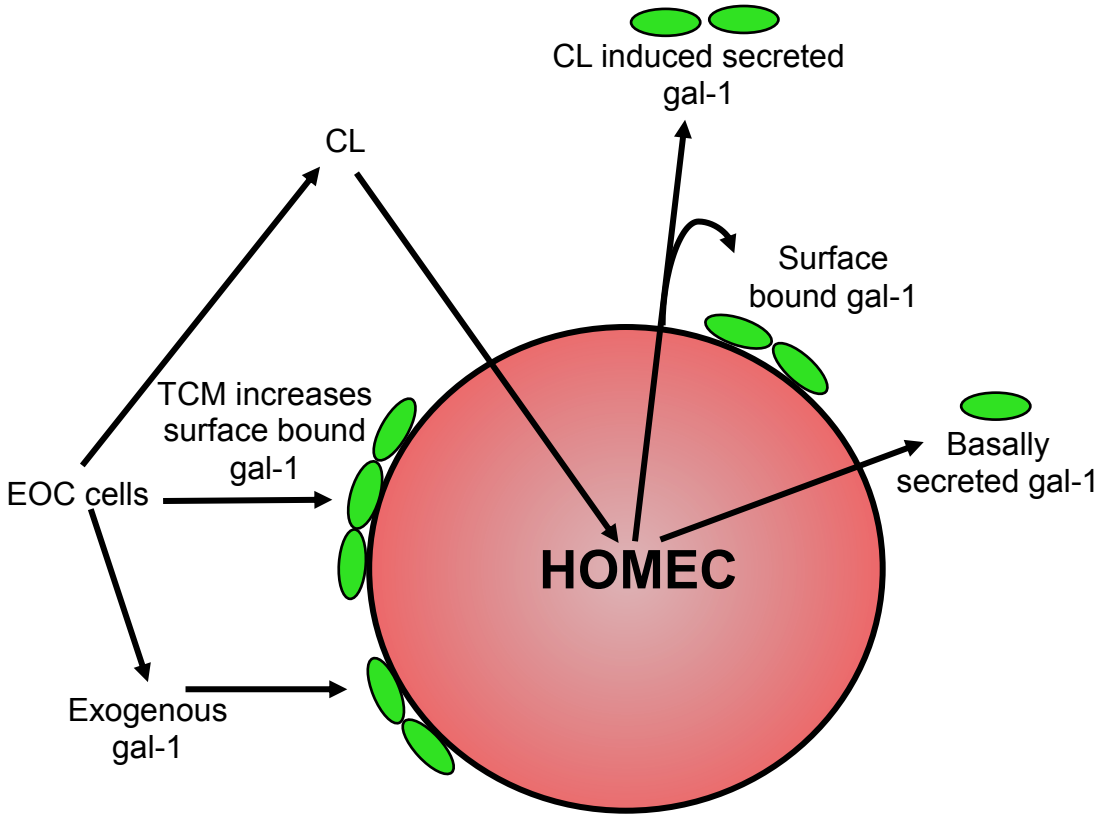

Figure 76. Summary of HOMEC galectin-1 secretion and extracellular surface binding. Cathepsin-L (CL) was previously shown to be secreted from EOC cells, which induced the secretion of galectin-1 (gal-1) from HOMECs. Incubating HOMECs with A2780 and SKOV3 conditioned media (TCM) increased HOMEC binding of surface gal-1. A2780 and SKOV3 cells secreted gal-1, and exogenous gal-1 was able to bind to HOMECs. HOMEC secreted gal-1 following incubation with CL led to increased cell surface gal-1.

Chapter 5. Investigation into the pro-proliferative mechanisms of galectin-1 in HOMECs

5.1 Introduction

In chapter 4, gal-1 was shown to significantly increase the proliferation of HOMECs (4.3.7). The mechanisms of gal-1 induced EC proliferation are currently debated in the literature and indeed, could also vary depending on the heterogeneity of ECs (1.7.2.3). As discussed in 1.7.1.1, gal-1 has high binding capabilities, both with and without its carbohydrate recognition domain, to partners both in and outside the cell. There is therefore scope for gal-1 to exert its proliferative effects through various binding partners and mechanisms. The mechanisms of the pro-proliferative effect of gal-1 in HOMECs shall be investigated in this chapter.

One proposed mechanism for gal-1 induced EC proliferation is independent of its carbohydrate binding; the ability of gal-1 to stabilise activated H-ras (Prior *et al*, 2003; Thijssen *et al*, 2010). H-ras is a GTPase, and an early stimulator of cell proliferation pathways in response to growth factors binding to their cell surface receptors. Activated H-ras can stimulate both the MAPK and PI3K pathways, and is associated with cancer cell proliferation when constitutively active (Michael *et al*, 2016). Thijssen *et al* (2010) demonstrated that gal-1 can tether activated H-ras at the membrane intracellularly, and thereby prolong pro-proliferative signalling and induce the proliferation of HUVECs. Another proposed mechanism is that gal-1 can induce EC proliferation by binding through its carbohydrate recognition domain. This is primarily thought to occur by binding extracellularly to N-glycans present on VEGFR2 and subsequently affecting receptor dimerisation and activation (Croci *et al*, 2018). This mechanism therefore depends on the gal-1 binding capabilities of surface receptors, which in turn is governed by a multitude of factors including the influence of the microenvironment (Lau *et al*, 2007). Furthermore it is currently unclear whether the effect of gal-1 binding to the extracellular portion of cell surface receptors enhances the effect of ligand-receptor binding, or if gal-1

binding and interactions alone are sufficient to induce receptor activation (Stanley, 2014).

The pro-proliferative effect of gal-1 demonstrated in section 4.3.7 is novel, and the mechanism currently unknown. Thus it is not known which signalling pathways and what (if any) receptors are activated by gal-1, or how gal-1 is exerting these effects: via non-carbohydrate binding or carbohydrate binding. An understanding of this process will provide a greater clarification of the role of gal-1 in EOC metastasis and potentially provide a target for future therapeutic interventions.

5.1.1 Aims

The aims of this chapter are therefore as follows:

- To investigate which (if any) receptors gal-1 activates on HOMECs
- To investigate what pro-proliferative signalling pathways are activated by gal-1 in HOMECs

5.2 Methods

HOMEC isolation and characterisation

HOMECS were isolated as described in 3.3.6 and characterised with immunocytochemistry (2.3.4.4).

HOMEC proliferation following short-term galectin-1 treatment

HOMECs were exposed to 10 minute gal-1 treatments and proliferation was examined by WST-1 assays as described in 2.3.2.3.

Receptor tyrosine kinase arrays

The activation of RTKs on the surface of HOMECs in response to gal-1 was studied using RTK arrays (as described and analysed in 2.3.6.1 and 2.3.6.2 respectively). Lysates were prepared as described in 2.3.5.4 and analysed for protein concentration using BCA assays (2.3.5.5).

Phosphorylated VEGFR2 ELISA

The phosphorylation of VEGF2 in response to gal-1 was confirmed with an ELISA as described in 2.3.5.7. The effect of gal-1 on the phosphorylation of VEGFR2 in the presence of various inhibitors was also assessed. Lysates were prepared as described in 2.3.5.6, and analysed for protein concentration using BCA assays (2.3.5.5).

Phosphokinase arrays

Intracellular signalling pathways in HOMECs in response to gal-1 were investigated using phosphokinase arrays (as described and analysed in 2.3.6.3 and 2.3.6.2 respectively). Lysates were prepared as described in 2.3.5.4 and analysed for protein concentration using BCA assays (2.3.5.5).

Total and phosphorylated PLCγ1 flow cytometry

The phosphorylation of PLCγ1 in response to gal-1 treatments was confirmed using flow cytometry as described in section 2.3.7.1 (analysed as described in 2.3.7.3).

VEGF ELISA

To investigate whether HOMECs secreted VEGF, a VEGF ELISA was carried out on supernatants collected from HOMECs. The ELISA was also carried out on 0.1% (w/v) BSA endothelial starve media (described in 2.3.5.3).

Confirmation of swainsonine reduction of surface complex N-glycans and prevention of gal-1 binding to the cell surface of HOMECs

Initially the toxicity of swainsonine on HOMECs was studied using WST-1 assays (2.3.4.7). The prevention of gal-1 binding to the surface of swainsonine treated HOMECs was studied using ICC as described in 2.3.4.3. This was quantified using 96-well plate assays (2.3.8.1).

Inhibition of gal-1 induced HOMEC proliferation

To confirm that the pro-proliferative effect of gal-1 occurred due to gal-1 extracellular binding and interaction with VEGFR2, WST-1 assays with swainsonine ± gal-1 treatments were utilised (2.3.2.1).

Flow cytometry to examine the phosphorylation of PLCγ1

To investigate the effects of gal-1 inhibition on PLCγ1 phosphorylation, flow cytometry was adapted as described in 2.3.7.2 (analysed as described in 2.3.7.3).

VEGFR2 internalisation

The effect of gal-1 on VEGF induced VEGFR2 internalisation was studied (with and without inhibitors) and analysed using flow cytometry as described in 2.3.7.5 and 2.3.7.6 respectively.

5.3 Results

5.3.1 Study of the effect short-term galectin-1 treatment on HOMEC proliferation

In section 4.3.7.1, data indicated that 5 and 50ng/ml gal-1 had a pro-proliferative on HOMECs (see figures 67 - 68). The treatments of 24, 48, and 72 hours were relatively long-term when considering the reported half-life of gal-1 in cell culture media, 1 hour 7 minutes (Van Ry *et al*, 2015). It is generally accepted that receptor activation occurs relatively rapidly in cells, and therefore an experiment to examine whether short-term exposure to gal-1 could also trigger subsequent proliferation in HOMECs was carried out.

Proliferation was studied using WST-1 assays. HOMECs were seeded in 96-well plates and starved overnight in 2% endothelial starve media. Gal-1 was added in 2% endothelial starve media at 5 and 50ng/ml. After 10 minutes incubation, wells were aspirated and media was replaced with 2% endothelial starve media (or complete endothelial media). Starve media and complete endothelial media were used as negative and positive controls. After 24 hours, WST-1 reagent was added and absorbance was measured (described in 2.3.2.1).

5.3.1.1 Short-term galectin-1 induced HOMEC proliferation

WST-1 data showed that 10 minute incubation with galectin-1 significantly increased HOMEC proliferation assessed after 24 hours compared with control; 5ng/ml by 49.8% and 50ng/ml by 56.2% (p values = 0.0002) (figure 77). These data suggested that 10 minutes gal-1 incubation was sufficient to induce HOMEC proliferation. The increases observed were only slightly less than seen in 4.3.7.1, where cells were incubated with gal-1 continuously for 24 hours (12.5% less than 5ng/ml 24 hours incubation, and 16.5% less than 50ng/ml 24 hours incubation).

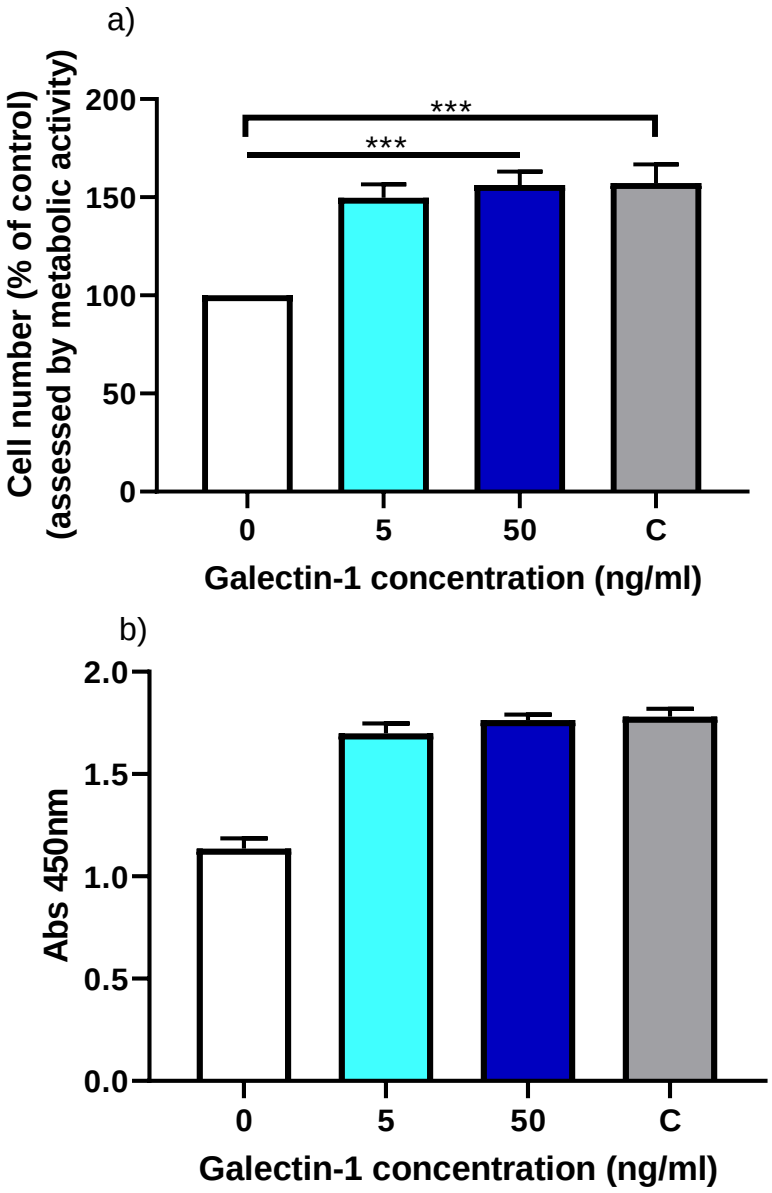

Figure 77. 10 minute incubation with galectin-1 induced significant proliferation of HOMECs after 24 hours, as assessed by WST-1 metabolic assay. HOMECs were seeded in gelatin pre-coated 96-well plates at 10,000 cells/well. After overnight starve with 2% FCS endothelial media, HOMECs were incubated with 2% endothelial media ± 5 or 50ng/ml galectin-1 or control treatments for 10 minutes. Wells were then aspirated and media replaced with 2% FCS endothelial media, or complete media (C, as a positive control). Absorbance was read at 450nm. a) results are the mean ± SD, n=3 (intra-experimental n=6). HOMECs from two isolations were used. Mann-Whitney U analyses between galectin-1 treatments/complete media positive control and 2% FCS control (0ng/ml), ***p values = 0.0002. Representative raw data from one experiment are shown in b).

5.3.2 Receptor tyrosine kinase arrays of HOMECs treated with galectin-1

The effect of gal-1 on RTK phosphorylation in ECs has not been reported. As discussed throughout section 1.2, ECs display heterogeneity. This can lead to conflicting results in the literature, and necessitates the use of disease relevant/appropriate capillary bed ECs. In this case, HOMECs. This is relevant to the study of EOC omental metastasis, due to the omentum being a highly favoured site of metastasis and the omentum being an angiogenesis supporting environment (discussed in sections 1.5 and 1.6).

To study RTK phosphorylation in response to gal-1, HOMECs were starved in 2% endothelial media overnight followed by 4 hours in 0.1% BSA (w/v) endothelial starve media. Cells were then incubated with or without 50ng/ml gal-1 for 4 minutes. An incubation of 4 minutes was chosen since previous work in this lab showed no differential receptor activation occur after 10 minutes (unpublished data). The higher concentration of gal-1 (50ng/ml) was chosen as array kits contained a limited number of membranes. These arrays served as initial identifiers of pro-angiogenic signalling pathways activated by gal-1. Lysates were collected from treated cells and applied to membranes presenting with RTK capture antibodies. Tyrosine phosphorylation was detected with an HRP-conjugated pan phospho-tyrosine antibody and visualised with chemiluminescence agents and Azure imaging software. Dots were then analysed using ImageJ (described in sections 2.3.6.1 and 2.3.6.2). This experiment was performed twice; the results presented show the mean of these two repeats. As the arrays generated values in arbitrary units in ranges that varied between the two repeats, data are presented as percentage of the control values (membranes treated with control lysates). RTKs that demonstrated a minimum of a 50% increase in activation in both arrays were considered of interest, and are summarised in table 30. Results for all RTKs are shown in figure 78.

5.3.2.1 Galectin-1 induced phosphorylation of RTKs in HOMECs

Applying a cut-off of a 50% increase in RTK phosphorylation compared to control cells in both experiments resulted in the identification of gal-1 activation of the following receptors.

Receptor tyrosine kinase
VEGFR2 (Vascular endothelial growth factor receptor 2)
Tie-2
Hepatocyte growth factor receptor (HGFR)
Insulin-like growth factor 1 receptor (IGF-1R)
Insulin receptor (IR)

Table 30. HOMEC receptor tyrosine kinases that increased in activation by 50% or more compared with control cells, in response to galectin-1.

These RTKs included multiple receptors for molecules identified in 1.3.1 as pro-angiogenic factors. However, VEGFR2 (phosphorylation increased by 70%) was selected for further initial study as its ligand VEGF, is described as the most potent pro-angiogenic factor (Harper and Bates, 2008), and due to current research implicating interactions of VEGFR2 with gal-1 (Prior *et al*, 2003; Thijssen *et al*, 2010; Croci *et al*, 2018).

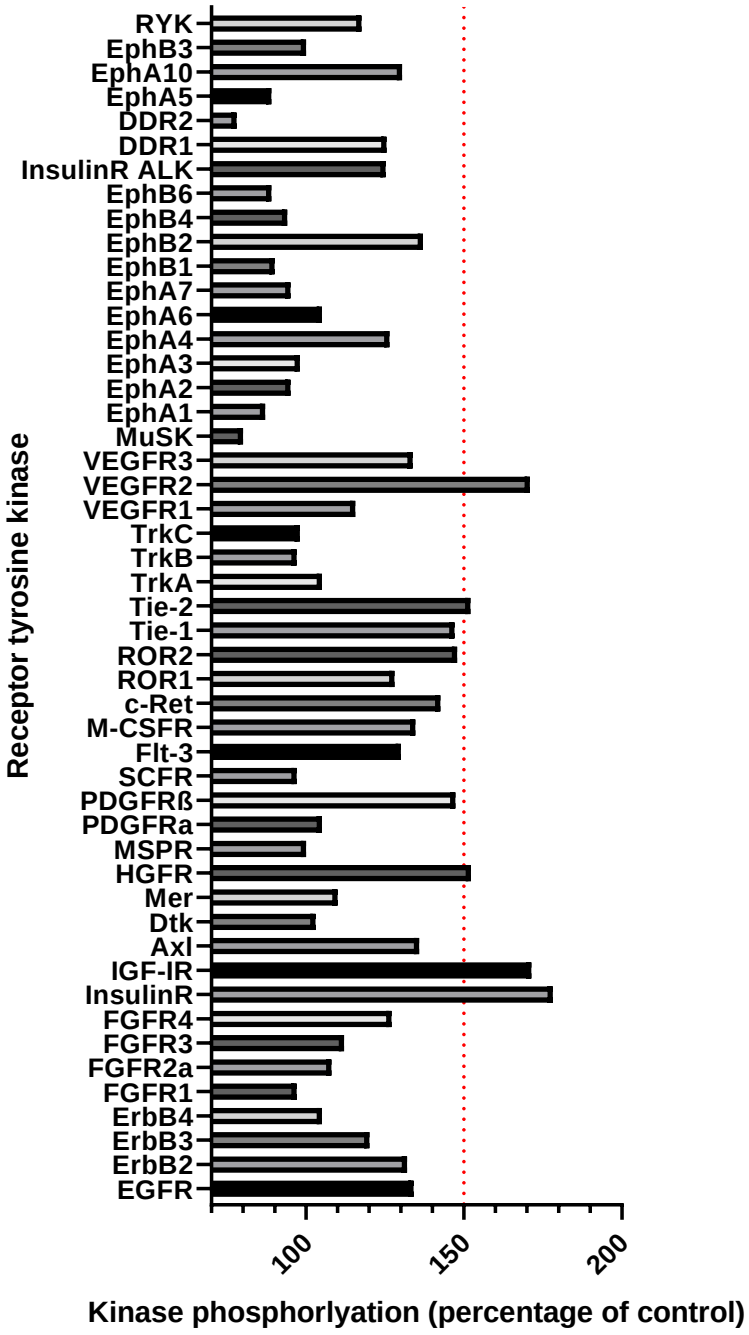

Figure 78. Activation of receptor tyrosine kinases in HOMECs in response to 4 minutes 50ng/ml galectin-1 treatment. HOMECs were starved overnight in 2% FCS endothelial media, followed by 4 hours in 0.1% BSA (w/v) endothelial starve media. Cells were then treated with 0.1% BSA starve media ± 50ng/ml gal-1 for 4 minutes. Lysates were then collected and applied to receptor tyrosine kinase (RTK) arrays and visualised using Azure software before analysis with ImageJ. Results are the mean of two separate experiments using HOMECs from two isolations. The red dotted line shows the cut-off where RTKs demonstrated a minimum of a 50% increase in activation compared to control cells. Receptor abbreviations explained in 2.3.6.2.

5.3.3 Phosphorylated VEGFR2 ELISA in HOMECs

The array data in 5.3.2.1 identified VEGFR2 as a potential RTK of interest. Therefore, the phosphorylation of VEGFR2 by gal-1 was confirmed and quantified by ELISA. The ELISA allowed the measurement of phosphorylated VEGFR2 (pVEGFR2). HOMECs were grown in petri dishes to 80% confluency, before overnight starvation in 2% FCS endothelial starve media, followed by 4 hours starvation in 0.1% BSA (w/v) endothelial starve media immediately prior to experimentation. Cells were then incubated with 5 or 50ng/ml of gal-1 for 4 minutes (see 4.3.3). 0.2ng/ml VEGF was used as a positive control, 0.1% BSA (w/v) starve media was used as negative control. Lysates were harvested as described in 2.3.5.6, and the ELISA carried out as described in 2.3.5.7.

5.3.3.1 Galectin-1 induced phosphorylation of VEGFR2 as assessed by ELISA

ELISA data indicated that incubation with both 5 and 50ng/ml gal-1 significantly increased the phosphorylation of VEGFR2 in HOMECs compared with control cells by approximately 80% (p values = 0.0268, see figure 79). These results supported the RTK array data, and further suggested that gal-1 phosphorylated VEGFR2.

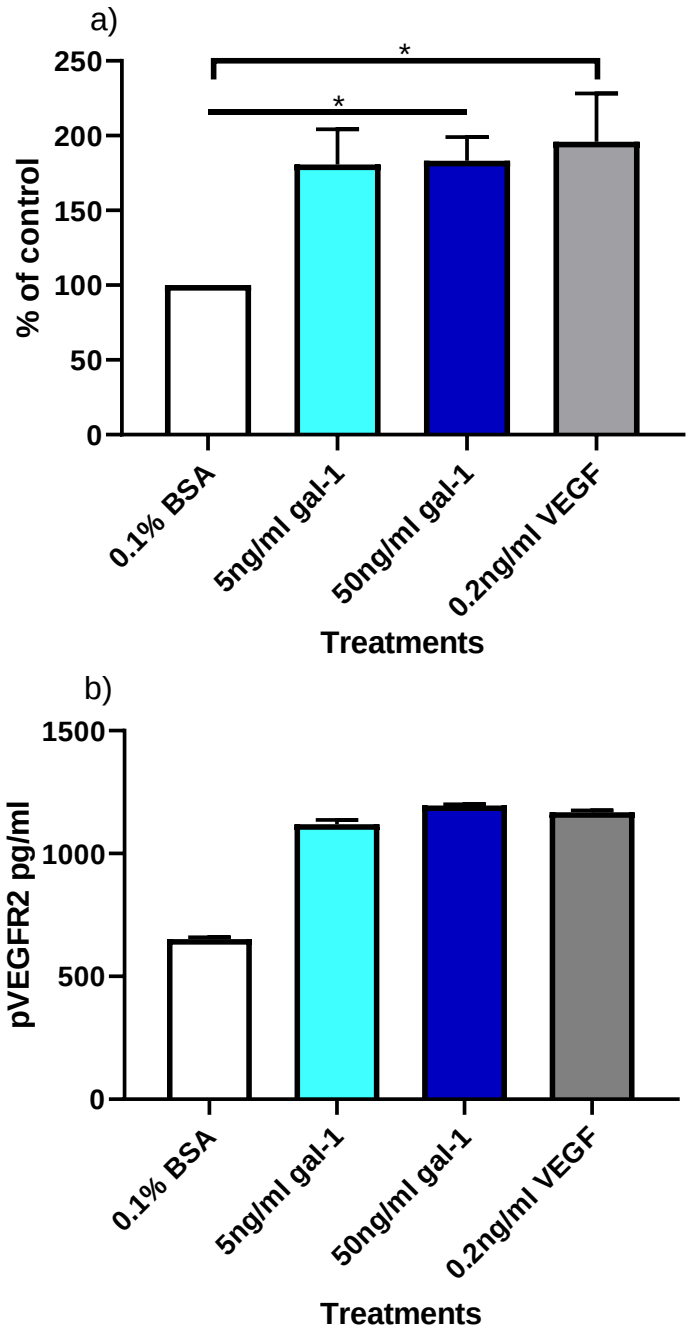

Figure 79. Galectin-1 induced significant phosphorylation of VEGFR2. HOMECs were seeded in gelatin pre-coated petri dishes and grown to 80% confluency. After overnight starve in 2% FCS endothelial starve media, cells were further starved in 0.1% BSA (w/v) endothelial starve media for 4 hours. Cells were then incubated with 5 or 50ng/ml of galectin-1 (gal-1) for 4 minutes. 0.2ng/ml VEGF was used as a positive control, 0.1% BSA (w/v) starve media was used as negative control. Lysates were collected and analysed by ELISA. a) results shown are the mean ± SD, n=6. HOMECs from four isolations were used. Mann-Whitney U analyses between gal-1 treatments/0.2ng/ml VEGF positive control and 0.1% BSA control, *p values = 0.0268. b) representative raw data from one experiment.

5.3.4 Phosphokinase arrays of HOMECs treated with galectin-1

Results from RTK arrays and ELISA (sections 5.3.2 and 5.3.3) initially identified RTKs of interest, and then confirmed that gal-1 could induce phosphorylation of VEGFR2. This suggested that exogenous gal-1 could potentially activate intracellular signalling pathways downstream of activated receptors. To further examine this, lysates generated from HOMECs incubated with 5 and 50ng/ml gal-1 were applied to phosphokinase arrays (described in 2.3.6.3, analysed as in 2.3.6.2).

HOMECs were starved in 2% endothelial media overnight followed by 4 hours in 0.1% BSA (w/v) endothelial starve media. Cells were then incubated with 50ng/ml for 10 minutes. An incubation of 10 minutes was chosen due to RTK activation being observed after 4 minutes, therefore allowing time for signal transduction. Lysates were collected and applied to membranes presenting with phosphorylated kinase capture antibodies. Kinase phosphorylation was detected with HRP-conjugated pan phospho-antibodies and visualised with chemiluminescence agents and Azure imagining software. Dots were then analysed using ImageJ (described in sections 2.3.6.1 and 2.3.6.2). This experiment was performed twice; the results presented show the mean of these two repeats. As the arrays generated values in arbitrary units in ranges that varied between the two repeats, data are presented as percentage of the control values (membranes treated with control lysates). Results for all kinases are shown in figure 80.

5.3.4.1 Galectin-1 induced phosphorylation of intracellular kinases

Galectin-1 induced phosphorylation resulted in marked increases in two particular kinases: p70 S6 kinase at phosphorylation site T389, and PLCγ1. Therefore these intracellular kinases were considered in conjunction with RTK array data in 5.3.2.1. As discussed in section 1.6.2.1, VEGFR2 phosphorylation at Y1175 induces phosphorylation of PLCγ1 (Holmqvist *et al*, 2004), and the PI3 kinase pathway (p70 S6 kinase is downstream of this pathway) (Karar and Maity, 2011). Both kinases presented as good candidates of interest downstream of VEGFR2 activation. This thesis however focussed on PLCγ1, as the associated PLCγ1 signalling pathway is more strongly associated with EC

proliferation than the PI3 kinase pathway (associated with permeability, migration and survival).

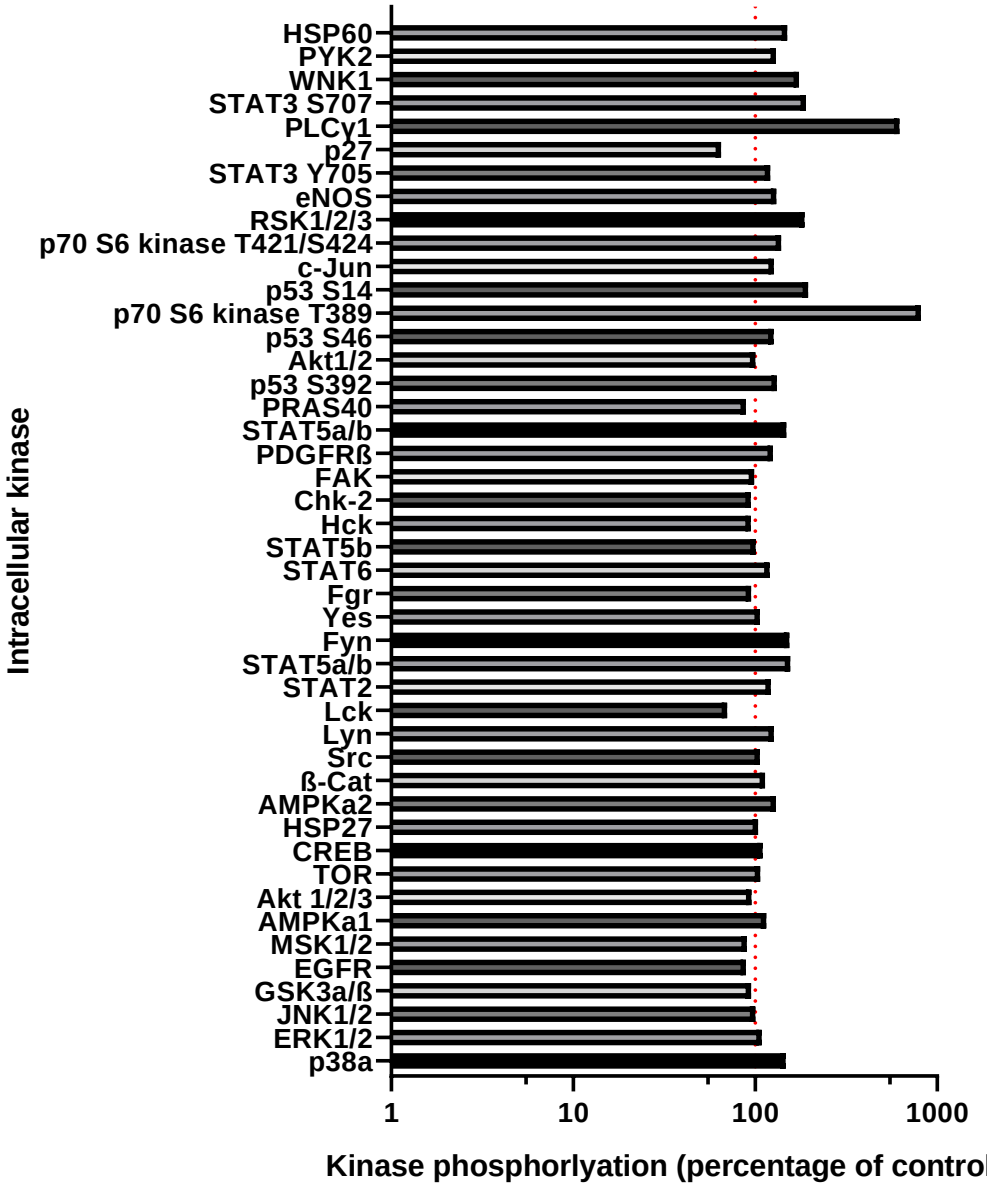

Figure 80. Activation of phosphokinases in HOMECs in response to 10 minutes 50ng/ml galectin-1 treatment. HOMECs were starved overnight in 2% FCS endothelial media, followed by 4 hours in 0.1% BSA (w/v) endothelial starve media. Cells were then treated with 0.1% BSA starve media ± 50ng/ml gal-1 for 10 minutes. Lysates were then collected and applied to phosphokinase arrays and visualised using Azure software before analysis with ImageJ. Results are the mean of two separate experiments using HOMECs from two isolations. The red dotted line shows the 100% control (x axis $\log_{10}$ scale).

5.3.5 Flow cytometry of PLCγ1 phosphorylation in HOMECs

Phosphokinase array data in 5.3.4.1 showed an increase in PLCγ1 phosphorylation in response to exogenous gal-1. This was confirmed using flow cytometry. HOMECs were grown in 6-well plates to 80% confluency, before starvation overnight in 2% FCS endothelial starve media. A further 4 hour starve in 0.1% BSA (w/v) endothelial starve media was performed immediately prior to experimentation. Cells were then incubated with 5 or 50ng/ml of gal-1 for 10 minutes (see 4.3.3). 0.2ng/ml VEGF was used as a positive control, 0.1% BSA (w/v) starve media was used as negative control. Cells were stained and prepared as described in 2.3.7 and 2.3.7.1. Total PLCγ1 was detected using a primary and fluorescent secondary antibody. Phosphorylated PLCγ1 (pPLCγ1) was detected using a conjugated (AlexaFluor 488) antibody at 1µl/200,000 cells, therefore only one staining incubation and subsequent wash step was required. Phosphorylated PLCγ1 staining was expressed as a percentage of total PLCγ1 staining as described in 2.3.7.3.

5.3.5.1 Confirmation of galectin-1 induced PLCγ1 phosphorylation in HOMECs as assessed by flow cytometry

Flow data indicated that 10 minute incubations with both 5 and 50ng/ml gal-1 significantly increased the phosphorylation of PLCγ1 in HOMECs compared to starve control by 378.4 and 539.1% respectively (p values = 0.0022, see figure 81). These results supported the phosphokinase array data, and further suggested that gal-1 phosphorylated PLCγ1.

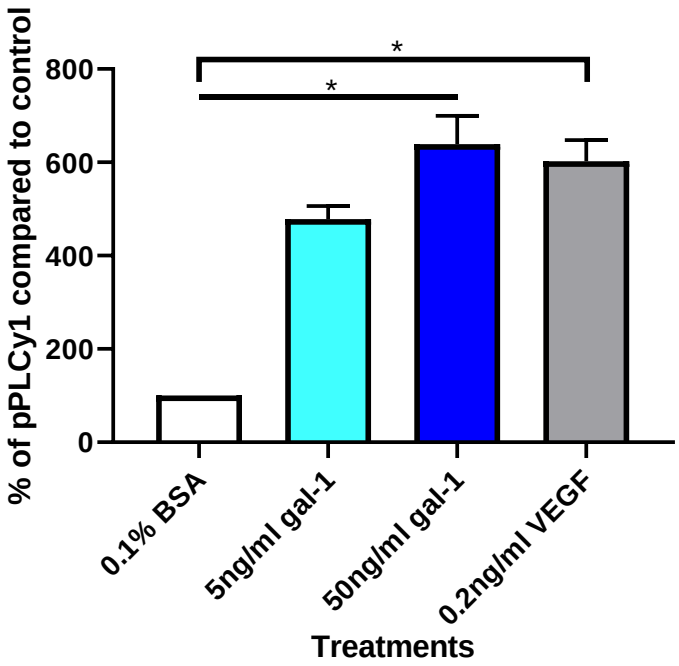

Figure 81. Galectin-1 induced significant phosphorylation of PLCγ1. HOMECs were seeded in gelatin pre-coated 6-well plates and grown to 80% confluency. After overnight starve in 2% FCS endothelial starve media, cells were further starved in 0.1% BSA (w/v) endothelial starve media for 4 hours. Cells were then incubated with 5 or 50ng/ml of galectin-1 (gal-1) for 10 minutes. 0.2ng/ml VEGF was used as a positive control, 0.1% BSA (w/v) starve media was used as negative control. Cells were dissociated and stained for total and phosphorylated PLCγ1 (pPLCγ1), and analysed with flow cytometry. pPLCγ1 was expressed as a percentage of total PLCγ1, which was then compared to the 0.1% BSA negative control (100%). Results shown are the mean ± SD, n=6. HOMECs from four isolations were used. Mann-Whitney U analyses between gal-1 treatments/0.2ng/ml VEGF positive control and 0.1% BSA control, *p values = 0.0022.

5.3.6 Investigation into HOMEC secreted VEGF, and VEGF 0.1% (w/v) BSA endothelial starve media

Due to the demonstrated activation of VEGFR2 by gal-1, it was investigated whether HOMECs in experimental starve conditions (2% FCS endothelial media starve overnight followed by 4 hours of 0.1% BSA (w/v) endothelial starve media) were secreting VEGF. This was important as it is unclear whether gal-1 can activate VEGFR2 independently of VEGF, or whether it acts by influencing the VEGF-VEGFR2 complex. The overnight starve in 2% FCS media may have introduced VEGF into the culture due to the presence of an unknown concentration of VEGF in the serum, and nutrient deprived ECs are known to secrete VEGF (Fitzgerald *et al*, 2018).

VEGF concentrations were assessed by ELISA, as described in sections 2.3.5.2 and 2.3.5.3. HOMECs were grown to 80% confluency, before overnight starve in 2% FCS endothelial starve media, followed by 4 hours starve in 0.1% BSA (w/v) endothelial starve media. At this point, the media supernatants were collected and analysed by ELISA. The 0.1% BSA (w/v) starve media was also tested. A control of known concentration, 500pg/ml VEGF, was included to ensure accuracy of the ELISA.

5.3.6.1 VEGF was not detected in HOMEC supernatant, or 0.1% (w/v) BSA endothelial starve media

No measureable VEGF was detected in either the HOMEC supernatant or in 0.1% BSA starve media (detection limit 5pg/ml). This suggested that HOMECs were not secreting VEGF under these culture conditions, and that VEGF was not present in the 0.1% BSA starve media (figure 82).

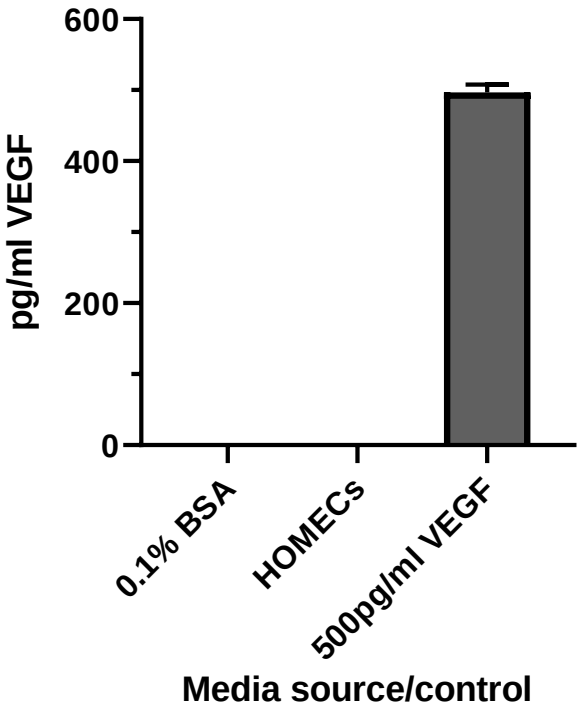

Figure 82. VEGF was not present in media from cultured HOMECs or in 0.1% BSA (w/v) endothelial starve media, as detected by ELISA. HOMECs were grown to 80% confluency, before overnight starve in 2% FCS endothelial starve media, followed by 4 hours starve in 0.1% BSA (w/v) endothelial starve media. At this point, the media was collected and analysed for VEGF concentration by ELISA. 0.1% BSA (w/v) starve media was also tested. 500pg/ml VEGF was included to ensure accuracy of the ELISA (approximately 496.6pg/ml). No VEGF was detected by the ELISA in HOMEC supernatant or the starve media. Results shown are the mean of four experiments (HOMECs from three isolations, and two bottles of 0.1% BSA starve media were used).

5.3.7 Investigation into the efficacy and toxicity of swainsonine in HOMECs

The observation that no VEGF could be detected in the HOMEC media suggested that gal-1 was directly activating VEGFR2 and inducing the observed phosphorylation. As discussed in 1.7.2, gal-1 can bind to glycans present on molecules on the surface of cells through its carbohydrate recognition domain (Lau *et al*, 2007). It has been suggested that this type of gal-1 binding may be inducing the activation (phosphorylation) of VEGFR2 shown in sections 5.3.2-3, as VEGFR2 is known to contain 18 potential N-glycosylation sites (where N-glycans can bind) (Chandler *et al*, 2019a). These N-glycans that are differentially present on VEGFR2 have been shown to be complex N-glycans (Patnaik *et al,* 2006; Chandler *et al*, 2019a), and therefore the synthesis of these glycans in particular was targeted in order to inhibit gal-1 binding to VEGFR2 on the cell surface (see section 1.7.2.4). This was achieved by inhibiting alpha2-mannosidase (AMANII), a golgi enzyme that catalyses the final hydrolytic step in the synthesis of complex N-glycans, with swainsonine. Swainsonine (SW) is a selective inhibitor of AMANII, and was therefore selected for this study (Thompson *et al,* 2012).

Initially, the optimum SW concentration to achieve significant inhibition of AMANII and reduce cell surface complex N-glycans in HOMECs had to be identified. A range of SW concentrations, as informed by literature (Chang *et al*, 2007), were tested in WST-1 assays in order to identify non-toxic concentrations, and cell surface gal-1 was assessed by ICC and 96-well plate assays to identify concentrations that significantly reduced gal-1 cell surface binding. For WST-1 assays, HOMECs were seeded in 96-well plates and starved overnight in 2% endothelial starve media ± SW (100 and 500ng/ml, and 1, 5, 10, and 20µg/ml). Starve media alone and complete endothelial media were used as controls. WST-1 reagent was added and absorbance was measured (described in 2.3.2.1). Cell surface gal-1 binding to HOMECs after SW incubation was initially investigated using ICC, and then quantified using 96-well plate assays.

For ICC assessment of gal-1 surface binding inhibition, HOMECs were grown in 8-well chamber slides and incubated with identical treatments and controls as in WST-1 assays. After 24 hours, 50ng/ml gal-1 was added to all cells. The higher

concentration of gal-1 was used as SW would subsequently be required to inhibit up to this concentration of gal-1. Cell surface gal-1 was then stained as described in sections 2.3.4.2-3. Fluorescence of cell surface bound gal-1 was quantified using plate assays; HOMECs were grown in 96-well black plates and incubated with the same SW treatments, controls, and 10 minute 50ng/ml gal-1 treatment used for the ICC. Wells were washed with PBS prior to staining to remove any unbound gal-1. Gal-1 staining was carried out as described in 2.3.4.3 without the addition of DAPI and plates were read in a SpectraMAX plate reader at 488/520nm.

5.3.7.1 Swainsonine toxicity to HOMECs

WST-1 data showed no significant difference in HOMEC viability when cells were incubated with SW concentrations of 100ng/ml, 500ng/ml, 1µg/ml, and 5µg/ml (figure 83). However, HOMEC viability was reduced by 8.5% in the 10µg/ml treatment ($p=0.0131$). At 20µg/ml, SW was shown to significantly reduce HOMEC viability by 53.2% ($p<0.0001$). These data suggested that SW starts to significantly reduce HOMEC viability after 24 hours in concentrations of 10µg/ml, and further reduces viability at 20µg/ml.

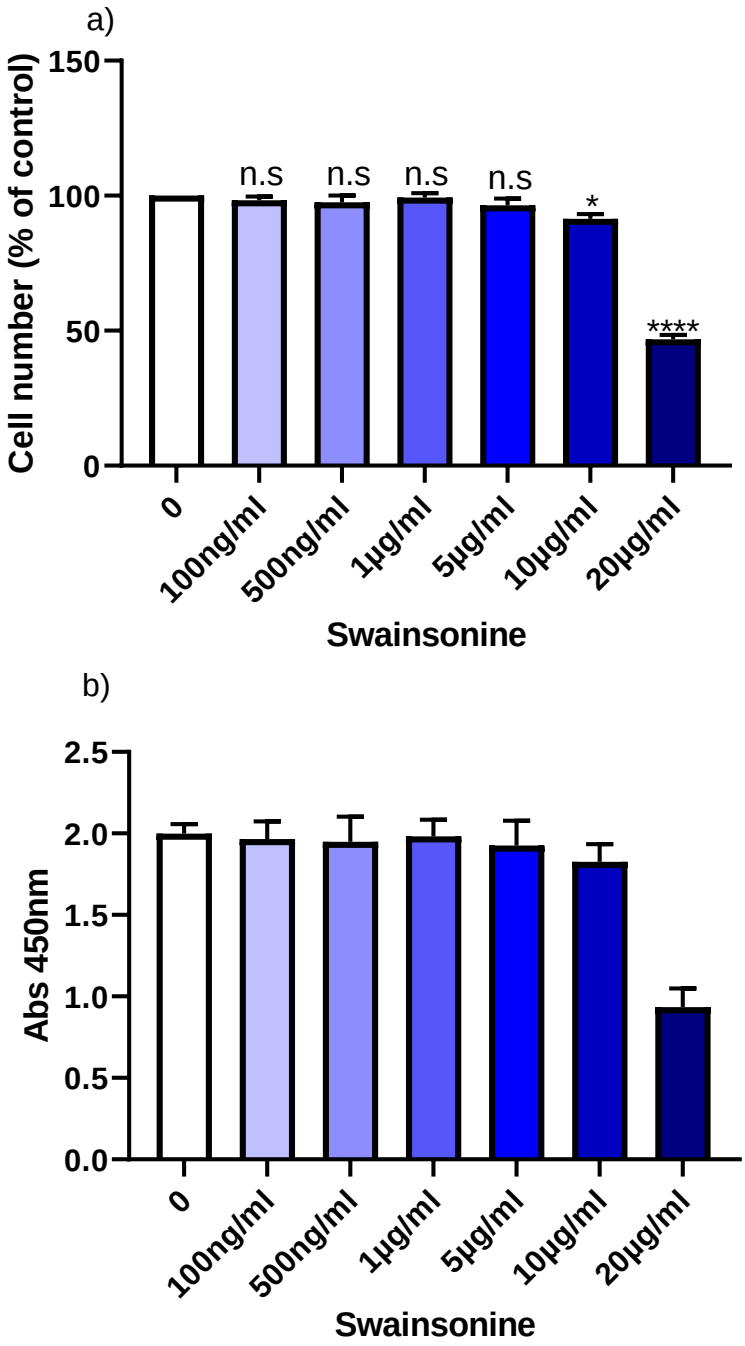

Figure 83. Toxicity of swainsonine in HOMECs after 24 hours. HOMECs were seeded in gelatin pre-coated 96-well plates at 10,000 cells/well. Cells were starved for 24 hours with 2% FCS endothelial media ± swainsonine. Absorbance was read at 450nm. a) results are the mean ± SD, n=4 (intra-experimental n=6). HOMECs from three isolations were used. Kruskal-Wallis analysis, ****p<0.0001. Post-hoc Dunn's test (shown on graph) between galectin-1 treatments and 2% FCS control (0ng/ml), *p=0.0131 and ****p<0.0001. Representative raw data from one experiment are shown in b). n.s = not significant.

5.3.7.2 Swainsonine prevention of galectin-1 binding to the surface of HOMECs as shown by immunocytochemistry

Initial ICC images (shown in figure 84) showed a reduction in cell surface gal-1 in HOMECs in response to incubation with SW. This was repeated a further two times with similar observations. However it was observed that not all cells in images displayed an equal amount of gal-1. This meant that the method of quantifying overall cell surface gal-1 utilised previously (described in 2.3.4.6) where five cells in consistent locations were analysed, was not deemed appropriate. Therefore a 96-well plate assay was used instead, where fluorescence changes in a whole population of cells in a well could be analysed by plate reader.

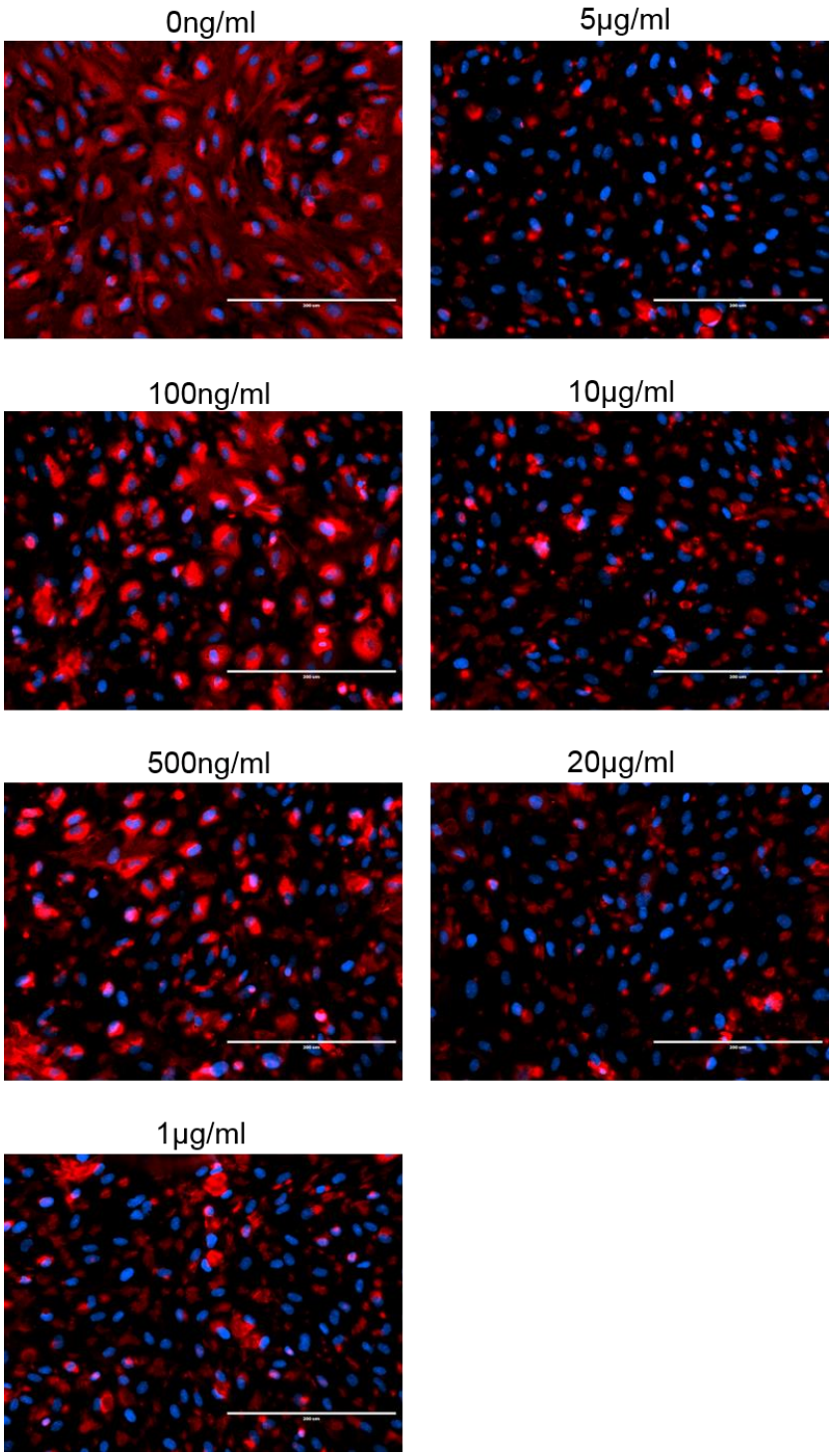

Figure 84. Representative images showing reduced cell surface galectin-1 on HOMECs after incubation with swainsonine. HOMECs were seeded in gelatin pre-coated 8-well chamber slides at 30,000 cells/well. Cells were starved overnight in 2% endothelial starve media ± swainsonine (SW) (100 and 500ng/ml, and 1, 5, 10, and 20µg/ml). Cells were then exposed to 50ng/ml gal-1 for 10 minutes, washed, and stained for cell surface galectin-1 (red) and DAPI (blue). Representative images from one experiment; the experiment was repeated 3 times with similar results. Scale bar = 200µm.

5.3.7.3 Swainsonine prevention of galectin-1 binding to the surface of HOMECs as quantified by 96-well plate assays

96-well plate fluorescence data showed that SW significantly reduced cell surface gal-1 (by 58 – 62%) across all concentrations tested (see figure 85), when compared with cell surface gal-1 on HOMECs not incubated with SW. These data suggested that any of the SW concentrations tested significantly reduced the binding of gal-1 to the surface of HOMECs by removing surface complex N-glycans, and could therefore be used for future experiments.

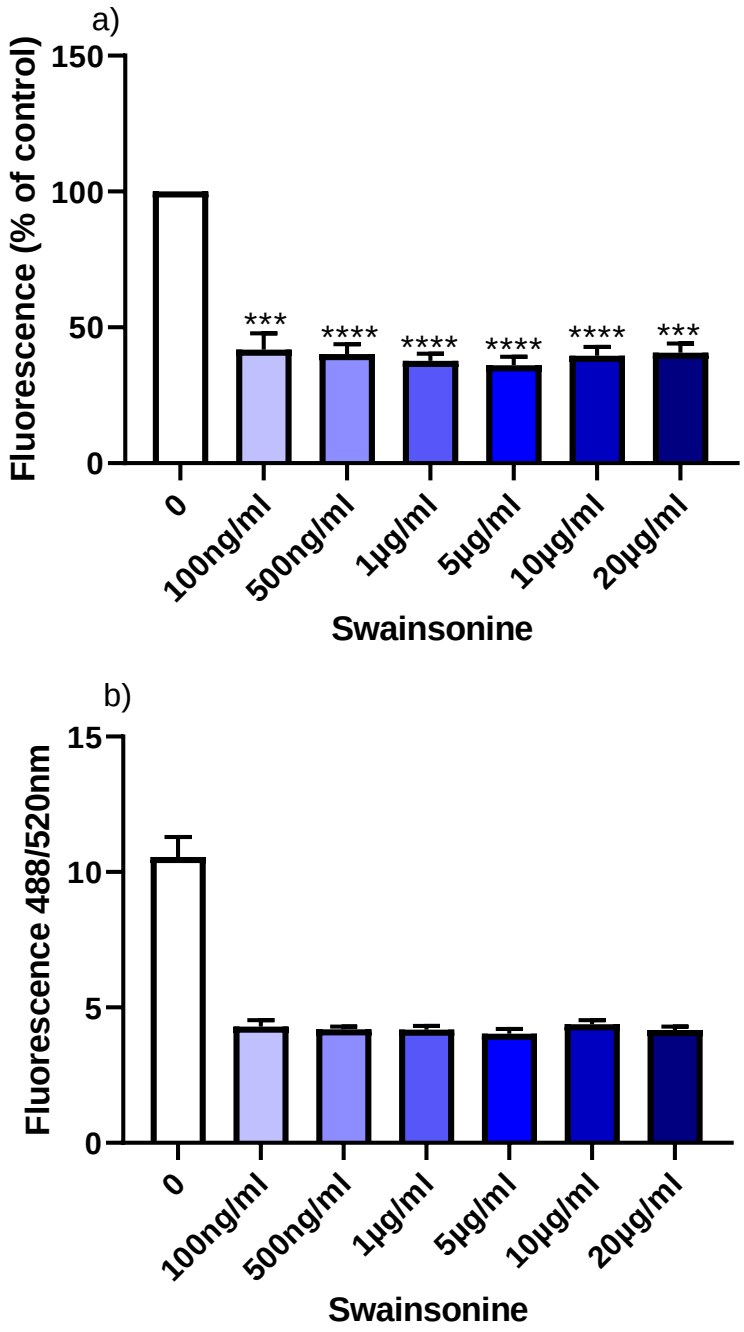

Figure 85. Swainsonine significantly reduced cell surface galectin-1 on HOMECs as assessed by 96-well plate assays. HOMECs were seeded in gelatin pre-coated black 96-well plates at 10,000 cells/well. Cells were starved overnight with 2% FCS endothelial media ± swainsonine (SW) and then incubated with 50ng/ml galectin-1 for 10 minutes. Cells were washed, and stained for cell surface galectin-1. Fluorescence was read at 488/520nm. a) results are the mean ± SD, n=4 (intra-experimental n=6). HOMECs from three isolations were used. All data were expressed as a percentage of 0 (2% starve media). Kruskal-Wallis analysis, ****p=0.0001. Post-hoc Dunn's test (shown on graph) between galectin-1 treatments and 2% FCS control (0ng/ml), 100ng/ml ***p=0.0009, ****p values <0.0001, 20µg/ml p=0.0003. Representative raw data from one experiment are shown in b).

5.3.7.4 Optimum swainsonine concentration

This set of experiments suggested that all concentrations of SW tested significantly reduced gal-1 binding to the cell surface, but that SW significantly reduced HOMEC viability at concentrations of 10 and 20µg/ml. It was therefore decided to use 5µg/ml for future experiments, as this was the highest non-toxic concentration.

5.3.8 The effect of swainsonine on galectin-1 induced HOMEC proliferation

In order to investigate whether gal-1 induced HOMEC proliferation by binding to complex N-glycans on the cell surface, WST-1 proliferation assays were repeated to include SW. A known inhibitor of VEGFR2 (Mendel *et al*, 2000), SU5416 was also used as a control for inhibition of HOMEC proliferation; previous work in this lab showed significantly decreased VEGF induced HOMEC proliferation after overnight incubation with 10µM SU5416 (as assessed by WST-assays) (Winiarski *et al*, 2013).

For the assays, HOMECs were seeded in 96-well plates and starved overnight in 2% endothelial starve media ± 5µg/ml SW or 10µM SU. These treatments were then repeated ± 5 or 50ng/ml gal-1 (see 4.3.3). Starve media alone and 0.2ng/ml VEGF were used as controls (100% and positive control, respectively). WST-1 reagent was added and absorbance was measured after 24 hours (described in 2.3.2.1).

5.3.8.1 Swainsonine inhibited galectin-1 induced HOMEC proliferation

Pre-treatment with SW significantly inhibited 5 and 50ng/ml gal-1 induced proliferation in HOMECs. Gal-1 induced proliferation was completely prevented in both cases (and reduced to below control levels by a further 15.5 and 11.9% in 5 and 50ng/ml gal-1, respectively) (p values <0.0001). Furthermore, gal-1 induced proliferation was also shown to be significantly inhibited by SU5416; completely in 5ng/ml (+ another 5.3% below control) as well as in 50ng/ml (+ another 5.9% below control). VEGF alone significantly increased HOMEC proliferation after 24 hours. This was significantly reduced to below control levels by SU5416. No significant change was observed in SW treated cells incubated with VEGF (see figure 86). These data suggested that SW and

SU5416 inhibited the pro-proliferative effect of gal-1 in HOMECs, and therefore that this effect occurred through gal-1 binding to complex N-glycans on the cell surface.

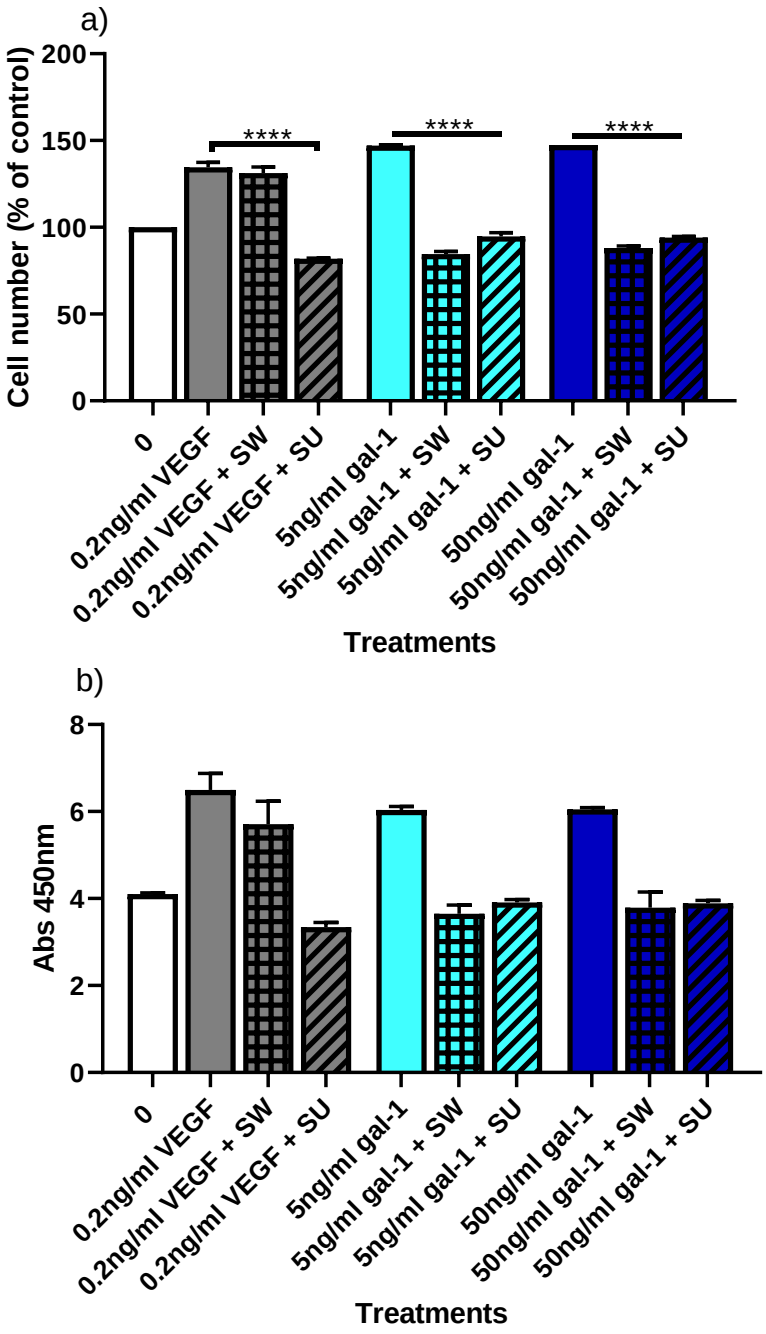

Figure 86. Swainsonine pre-treatment significantly inhibited galectin-1 induced HOMEC proliferation. HOMECs were seeded in gelatin pre-coated 96-well plates and starved overnight in 2% endothelial starve media ± 5µg/ml swainsonine (SW) or 10µM SU. These treatments were then replaced ± 5 or 50ng/ml galectin-1 (gal-1). Starve media alone and 0.2ng/ml VEGF were used as controls (100% and positive control, respectively). WST-1 reagent was added and absorbance was measured at 450nm after 24 hours. a) results are the mean ± SD, n=6 (intra-experimental n=6). HOMECs from four isolations were used. All data were expressed as a percentage of 0 (2% starve media). Mann-Whitney U analyses were performed between each treatment or control and the corresponding treatment and inhibitors, ****p values <0.0001. Representative raw data from one experiment are shown in b). SU= SU5416.

5.3.9 The effect of swainsonine on galectin-1 induced VEGFR2 phosphorylation

As observed in 5.3.8, gal-1 induced HOMEC proliferation was significantly inhibited by SW. However, these experiments could not address whether the SW inhibition of gal-1 binding to complex N-glycans was occurring on VEGFR2 or to other cell surface molecules. This was important to know in order to inform further studies on how gal-1 affects VEGFR2. Therefore the effect of SW on the gal-1 induced phosphorylation of VEGFR2 was investigated by ELISA. SU5416 was used as a control for inhibition of VEGFR2 phosphorylation. For the assays, HOMECs were grown in petri dishes to 80% confluency, before overnight starvation in 2% FCS endothelial starve media ± SW/SU, followed by 4 hours starvation in 0.1% BSA (w/v) endothelial starve media ± SW/SU immediately prior to experimentation. Cells were then incubated with 5 or 50ng/ml of gal-1 for 4 minutes (see 4.3.3). 0.2ng/ml VEGF was used as a positive control, 0.1% BSA (w/v) starve media was used as negative control. Lysates were harvested as described in 2.3.5.6, and the ELISA carried out as described in 2.3.5.7.

5.3.9.1 Swainsonine inhibited galectin-1 induced VEGFR2 phosphorylation

SW was shown to significantly inhibit both 5 and 50ng/ml gal-1 induced phosphorylation of VEGFR2; 5ng/ml phosphorylation was inhibited completely (+ another 1% below control levels), whilst 50ng/ml phosphorylation was inhibited by 91.4%. (p values = 0.0022). Furthermore, galectin-1 induced VEGFR2 phosphorylation was also shown to be significantly inhibited by SU5416; by 76.3% in 5ng/ml and by 71.3% in 50ng/ml. No significant change was observed in SW inhibited cells incubated with VEGF. VEGF alone significantly increased VEGFR2 phosphorylation after 24 hours. This was significantly reduced to below control levels by SU5416 (see figure 87). These data suggested that both SW and SU5416 inhibited gal-1 induced phosphorylation of VEGFR2.

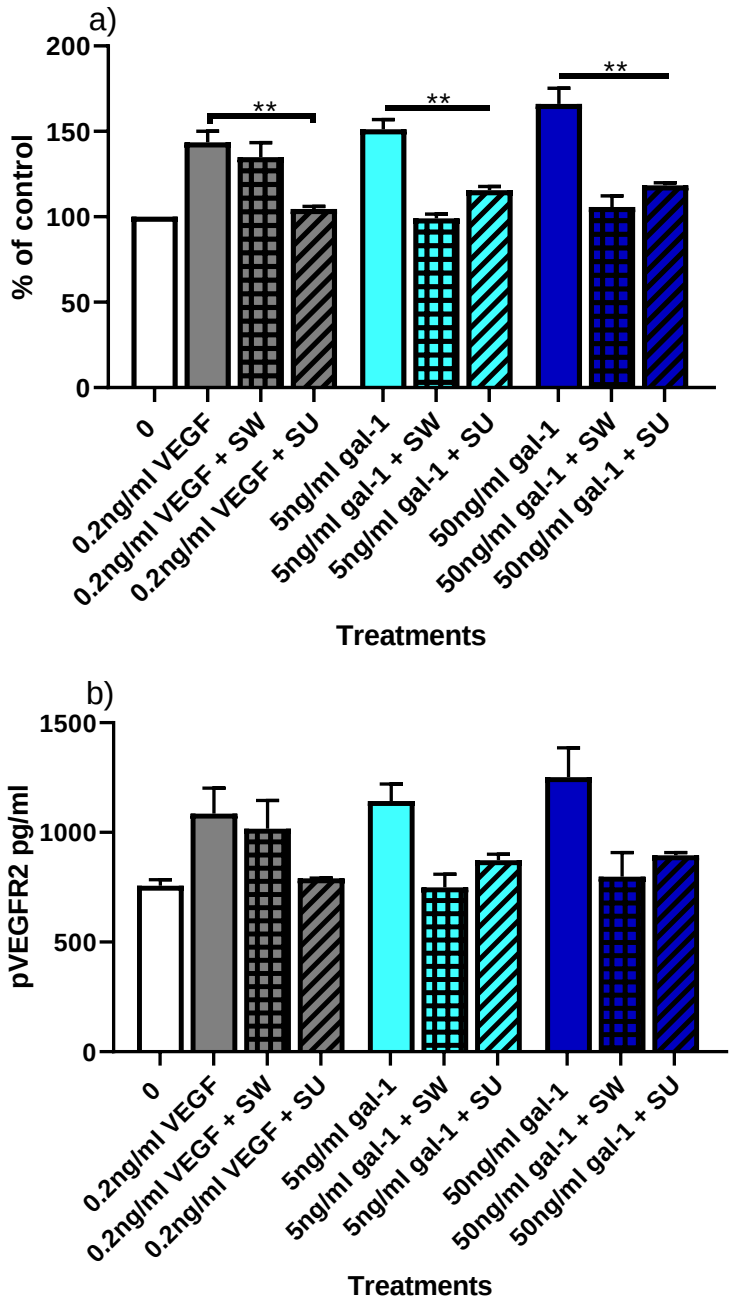

Figure 87. Swainsonine significantly inhibited galectin-1 induced VEGFR2 phosphorylation. HOMECs were seeded in gelatin pre-coated petri dishes and starved overnight in 2% endothelial starve media ± 5µg/ml swainsonine (SW) or 10µM SU, followed by 4 hours starve in 0.1% BSA (w/v) ± 5µg/ml SW/10µM SU. Cells were then incubated for 4 minutes with 5 or 50ng/ml galectin-1 (gal-1). Starve media alone and 0.2ng/ml VEGF were used as controls (100% and positive control, respectively). Lysates were harvested and an ELISA for phosphorylated VEGFR2 (pVEGFR2) was carried out a) results are the mean ± SD, n=6 (intra-experimental n=6). HOMECs from four isolations were used. All data were expressed as a percentage of 0 (0.1% BSA starve media). Mann-Whitney U analyses were performed between each treatment or control and the corresponding treatment and inhibitors, **p values = 0.0022. Representative raw data from one experiment are shown in b). SU= SU5416.

5.3.10 The effect of swainsonine on galectin-1 induced PLCγ1 phosphorylation

The data presented so far suggest that gal-1 binds to surface complex N-glycans and incudes activation (phosphorylation) of VEGFR2, and that this activation my induce HOMEC proliferation. The earlier data also indicated that gal-1 induced PLCγ1 phosphorylation possibly downstream of VEGFR2. However, it is not known if SW inhibition of gal-1 binding to complex N-glycans would affect gal-1 induced phosphorylation of PLCγ1. Therefore the effect of SW on the phosphorylation of PLCγ1 was investigated with flow cytometry, as described in section 5.3.5.1. U73122 was used as a control for inhibition of PLC phosphorylation; the toxicity of this inhibitor was first studied in HOMECs using WST-1 assays. From literature, it was known that PLCγ1 inhibition has been performed with a range of µM concentrations of U73122 at relatively short timepoints ranging from 5 minutes to 1 hour, and therefore toxicity was assessed by WST-1 assays over the course of 1 hour (Thompson *et al,* 1991).

For WST-1 assays, HOMECs were seeded in 96-well plates and starved overnight in 2% endothelial starve media, followed by a 4 hour starve in 0.1% BSA (w/v) endothelial media. Based on reports in the literature, U73122 at a range of concentrations (0.1, 1, 2.5, 5, 7.5, and 10µM) were added for the last hour of the 0.1% BSA starve. 2% starve media alone was used as a control. WST-1 reagent was added and absorbance was measured (described in 2.3.2.1).

For flow cytometry, HOMECs were grown in 6-well plates to 80% confluency, before starvation overnight in 2% FCS endothelial starve media ± 5µg/ml SW. A further 4 hour starve in 0.1% BSA (w/v) endothelial starve media ± 5µg/ml SW was performed immediately prior to experimentation. In some cells, 0.1µM U73122 was added for the last hour of this starve incubation. Cells were then incubated with 5 or 50ng/ml of gal-1 for 10 minutes (see 4.3.3). 0.2ng/ml VEGF was used as a positive control, 0.1% BSA (w/v) starve media was used as negative control. Cells were stained and prepared as described in 2.3.7 and 2.3.7.2. Phosphorylated PLCγ1 (pPLCγ1) was detected using a conjugated (AlexaFluor 488) antibody at 1µl/200,000 cells, therefore only one staining incubation and subsequent wash step was required. Phosphorylated PLCγ1 staining was expressed as a percentage of all cells in the sample as described

in 2.3.7.3. Unfortunately, this experiment could only be performed once (and without a measurement of total PLCγ1) due to a discontinuation of the PLCγ1 antibodies.

5.3.10.1 U73122 toxicity to HOMECs

WST-1 data indicated that there was a significant reduction in HOMEC viability following 1 hour incubation of U73122 at 1 ($p=0.0042$), 2.5 ($p=0.0003$), 5, 7.5 and 10μM (p values <0.0001), for example 5μM reduced HOMEC viability by 90.5%. However, there was no significant reduction in HOMEC viability when incubated with 0.1μM U73122 (see figure 88). These data suggested that U73122 starts to reduce HOMEC viability after 1 hour incubation at concentrations of 1μM. Therefore for flow cytometry experiments, a 1 hour incubation with 0.1μM U73122 was used.

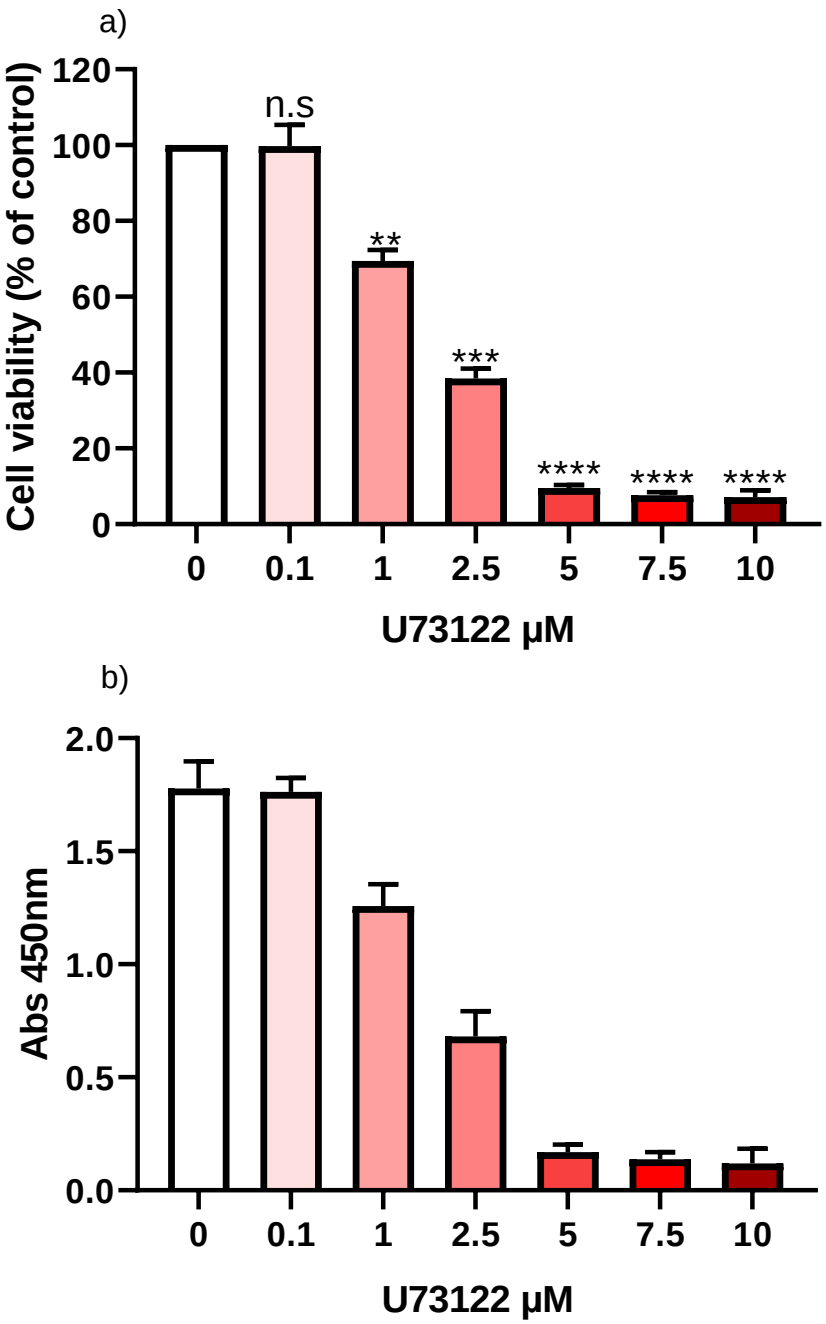

Figure 88. Toxicity induced by U73122 in HOMECs after 1 hour. HOMECs were seeded in gelatin pre-coated 96-well plates at 10,000 cells/well. Cells were starved overnight with 2% FCS endothelial media, followed by 4 hours in 0.1% BSA (w/v) endothelial stave media. U71322 was added for the last hour of this starve. Toxicity was assessed by WST-1 assay. Absorbance was read at 450nm. a) results are the mean ± SD, n=3 (intra-experimental n=6). HOMECs from two isolations were used. Kruskal-Wallis analysis, ****p<0.0001. Post-hoc Dunn's test (shown on graph) between U73122 treatments and 0.1% BSA (w/v) control (0ng/ml), **p=0.0042, ***p=0.0003, ****p values <0.0001. Representative raw data from one experiment are shown in b).

5.3.10.2 Swainsonine reduced galectin-1 induced PLCγ1 phosphorylation

The data indicated that gal-1 induced phosphorylation by approximately 400 and 616% at 5 and 50ng/ml respectively. Pre-treatment with 0.1 μM SW was observed to reduce both 5 and 50ng/ml gal-1 induced phosphorylation of PLCγ1 (by 83.3 and 85.9% respectively). Gal-1 induced pPLCγ1 was also observed to be reduced by U73122 (U7), 5ng/ml by 79.8% and 50ng/ml by 85.3% (figure 89). These data preliminarily suggest that SW and U7 inhibited gal-1 induced phosphorylation of PLCγ1. No marked change was observed in SW inhibited cells incubated with VEGF. VEGF alone significantly increased PLCγ1 phosphorylation by approximately 550%. This was significantly reduced to 42% above control levels. These data suggested that pre-treatment with U7 but not SW inhibited VEGF induced phosphorylation of PLCγ1.

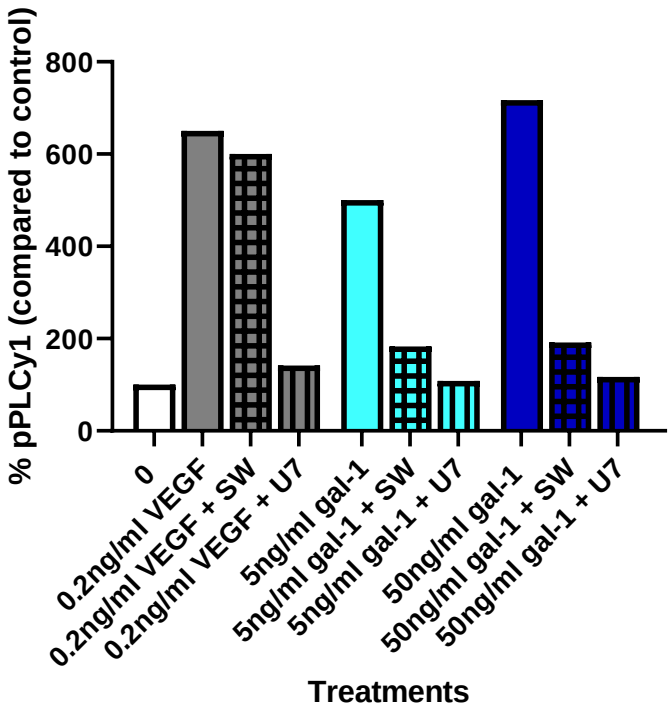

Figure 89. Swainsonine inhibited galectin-1 induced PLCγ1 phosphorylation. HOMECs were seeded in gelatin pre-coated 6-well plates and starved overnight in 2% FCS endothelial starve media ± 5µg/ml swainsonine (SW). This was followed by 4 hours starve in 0.1% BSA (w/v) endothelial starve media ± 5µg/ml SW. 0.1µM U73122 (U7) was added for the last hour of this starve incubation. Cells were then incubated with 5 or 50ng/ml of gal-1 for 10 minutes. 0.2ng/ml VEGF was used as a positive control, 0.1% BSA (w/v) starve media was used as negative control. Cells were then dissociated, stained and analysed by flow cytometry for phosphorylated PLCγ1 (pPLCγ1) n=1. pPLCγ1 was expressed as a percentage of pPLCγ1 in control cells (0).

5.3.11 The effect of galectin-1 on VEGFR2 internalisation

The data presented so far suggest that gal-1 activated VEGFR2, as well as PLCγ1. However, it is also possible that gal-1 influences VEGFR2 signalling by influencing receptor internalisation. As discussed in section 1.6.2.2, VEGFR2 signalling is regulated by internalisation processes. As a regulation mechanism, it is thought that following VEGF binding and formation of the VEGF-VEGFR2 complex, that more VEGFR2 is initially transported to the membrane, and that complexes are then internalised as a way to regulate (reduce) the activation of associated signalling pathways (Ewan *et al,* 2006; Xie *et al*, 2019). There is evidence in the literature that cell surface galectins may increase the retention of receptors at the plasma membrane, therefore prolonging their signalling when activated (Partridge *et al*, 2004; Liu and Rabinovich *et al*, 2005). The effect of gal-1 on retention of VEGFR2 at the surface was therefore investigated in HOMECs. As previous experiments suggested that gal-1 could activate VEGFR2 independently of VEGF, the effect of gal-1 alone on VEGFR2 internalisation was also initially investigated.

In order to study the effect of gal-1 on preventing internalisation of surface VEGFR2, the timepoint at which VEGF increased VEGFR2 at the cell surface with no gal-1 pre-treatment was initially identified. The 4 timepoints: 0, 5, 15, and 30 minutes, were in accordance with previous literature regarding the timeframe of VEGF induced increased surface VEGFR2, and subsequent VEGFR2 internalisation (Ballmer-Hofer *et al*, 2011 and Basagiannis *et al*, 2016), and were therefore used for this study. VEGF increased surface VEGFR2 was found to occur after 5 minutes; this was subsequently found to decrease after 15 minutes. It was then investigated whether pre-treatment with 5 or 50ng/ml gal-1 affected the increase in surface VEGFR2 after 5 minutes (see figure 90), in order to eliminate this as a variable. The effect of gal-1 on preventing VEGF induced VEGFR2 internalisation was then studied at subsequent timepoints (15 and 30 minutes), as this was when VEGFR2 was found to decrease.

HOMECs were grown in 6-well plates to 80% confluency, before overnight starve in 2% starve media ± 5 or 50ng/ml gal-1 (see 4.3.3). Cells were then starved for 4 hours prior to VEGF treatments in 0.1% (w/v) BSA starve media ± 5 or 50ng/ml gal-1. VEGF was added to appropriate wells to a final concentration of 0.2ng/ml; the media was not exchanged to avoid interfering

with receptor internalisation (Koch and Claesson-Welsh, 2012). VEGFR2 surface expression was investigated by flow cytometry by comparing median fluorescent intensities (normalised to 0.1% BSA (w/v) control). At each timepoint, internalisation was halted with ice-cold PBS before cells were dissociated and stained for surface VEGFR2 (described in section 2.3.7.5).

5.3.11.1 VEGF increased cell surface VEGFR2 after five minutes

VEGF was observed to significantly increase surface VEGFR2 compared with 0.1% BSA (w/v) starve media alone (by 14.4%) after a 5 minute incubation ($p=0.0022$). These data suggested that 5 minutes of VEGF incubation increased cell surface VEGFR2. Furthermore, neither 5 nor 50ng/ml gal-1 pre-treatment significantly altered surface VEGFR2 expression at this timepoint (figure 90a). Therefore the subsequent effect of gal-1 on the internalisation of VEGFR2 following VEGF treatment was studied at timepoints after 5 minutes. After 15 minutes of VEGF incubation, surface VEGFR2 was found to significantly decrease ($p=0.0022$) by 12.9% in HOMECs incubated with VEGF (figure 90b). The effect of the gal-1 pre-treatments on this reduction of cell surface VEGFR2 at this timepoint is explored further in 5.2.11.2.

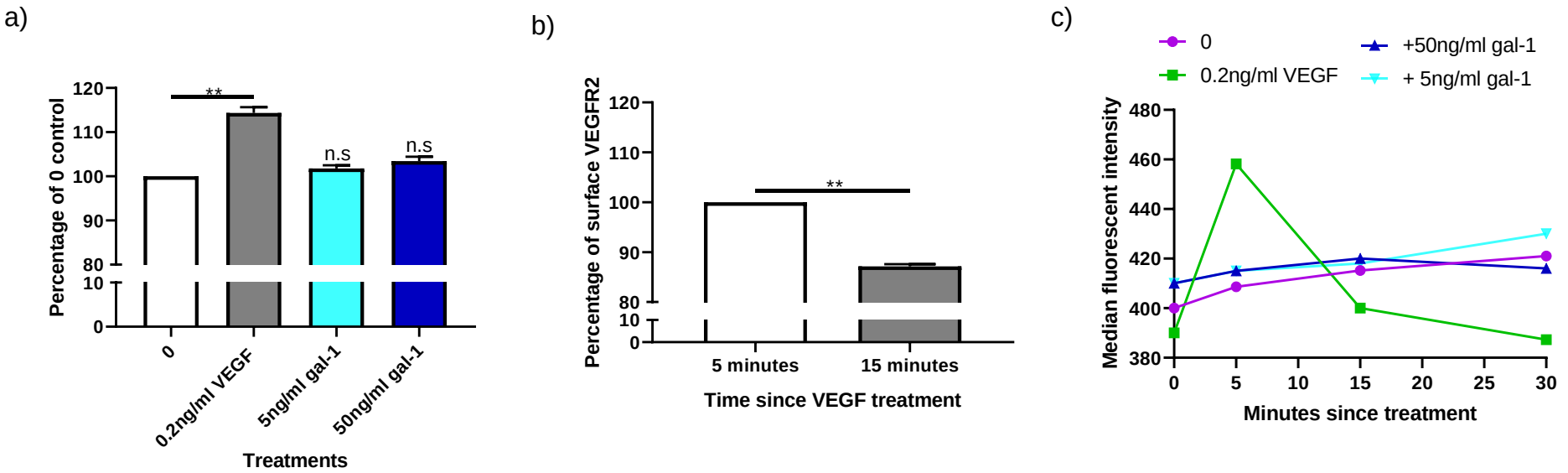

Figure 90. Surface VEGFR2 significantly increased after 5 minutes (a) and significantly decreased after 15 minutes (b) following incubation with VEGF, but not pre-treatment with galectin-1. HOMECs were grown in 6-well plates to 80% confluency, before overnight starve in 2% starve media ± 5 or 50ng/ml galectin-1 (gal-1). Cells were then starved again for 4 hours in 0.1% (w/v) BSA endothelial starve media ± 5 or 50ng/ml gal-1. 0.2ng/ml VEGF was then added to appropriate cells. At 5 minutes, VEGFR2 internalisation was halted with ice-cold PBS and cells were dissociated and stained for surface VEGFR2, and analysed with flow cytometry. Results are the mean ± SD, n=4. HOMECs from two isolations were used. a) and b) **p values = 0.0022. Mann-Whitney U analyses at each timepoint between treatments and 0.1% BSA (w/v) control (0ng/ml). c) shows raw data from one experiment, including 15 and 30 minute timepoints.

5.3.11.2 Galectin-1 significantly reduced VEGF induced internalisation of VEGFR2

After 15 minutes of VEGF stimulation, a significant reduction in surface VEGFR2 internalisation was observed in both gal-1/VEGF treatments compared to 0.2ng/ml VEGF control. (p=0.0022) (figure 91a). This effect was greatest in HOMECs treated with 50ng/ml gal-1 and VEGF, where there was 10% more surface VEGFR2. After 30 minutes of VEGF stimulation, a significant reduction in surface VEGFR2 internalisation was observed in both treatments compared to 0.2ng/ml VEGF control. (p=0.0079) (figure 91b). This effect was greatest in HOMECs treated with 50ng/ml gal-1 and 0.2ng/ml VEGF, where there was 5% more surface VEGFR2. These data suggested that gal-1 reduced the internalisation of VEGF activated VEGFR2.

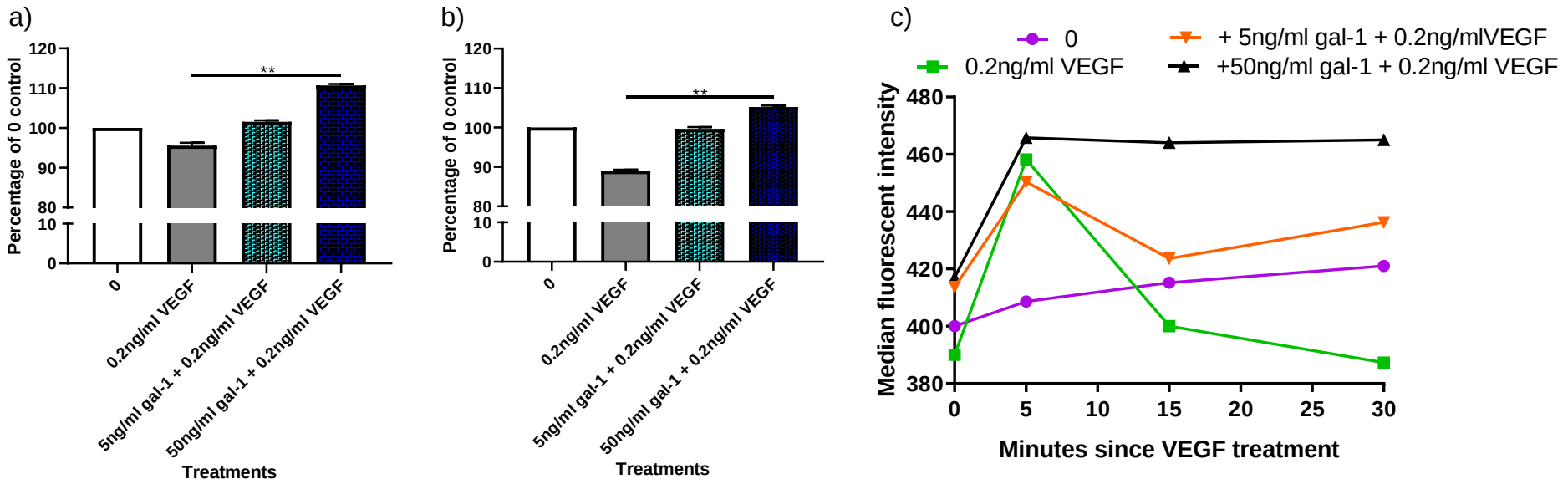

Figure 91. Galectin-1 significantly reduced internalisation of VEGFR2 after 15 minutes (a) and 30 minutes (b) HOMECs were grown in 6-well plates to 80% confluency, before overnight starve in 2% starve media ± 5 or 50ng/ml galectin-1 (gal-1). Cells were then starved again for 4 hours in 0.1% (w/v) BSA endothelial starve media ± 5 or 50ng/ml gal-1. Cells were incubated with 0.2ng/ml VEGF, or 0.1% BSA (w/v) starve media. At 15 (a) and 30 (b) minutes, VEGFR2 internalisation was halted with ice-cold PBS and cells were dissociated and stained for surface VEGFR2, and analysed with flow cytometry. Results are the mean ± SD, n=4. HOMECs from two isolations were used. a) **p values = 0.0022) b) **p values = 0.0079. Mann-Whitney U analyses were performed at each timepoint between the 0.2ng/ml VEGF treatment and gal-1/VEGF treatments. c) shows raw data from one experiment, including 0 treatment.

5.4 Discussion

5.4.1 Data summary

This chapter aimed to examine the potential mechanisms by which gal-1 induces proliferation in HOMECs. Initially, since gal-1 has a reported half-life of 1 hour 7 minutes in culture media (Van Ry *et al*, 2015), the effect of a short-term (10 minute) incubation of HOMEC proliferation after 24 hours was investigated. Proliferation was significantly increased, and since it is generally accepted that receptor activation occurs relatively rapidly in cells, RTK arrays were used to identify candidates for investigation. Several were identified: VEGFR2, Tie-2, HGFR, IGF-1R and IR. Due to the VEGF ligand being described in literature as the most potent stimulator of angiogenesis (Harper and Bates, 2008), and reports examining the relationship between gal-1 and VEGFR2 activation (see section 1.7.2.4), VEGFR2 was selected for further investigation. Initially, it was confirmed by ELISA that gal-1 could induce phosphorylation of VEGFR2. Downstream signalling pathways activated by gal-1 were also investigated by arrays. Interestingly, gal-1 induced phosphorylation (activation) of several intracellular signalling kinases was observed. These included p70 S6 kinase and PLCγ1 which are both known to be activated downstream of VEGFR2, and PLCγ1 was selected for further study due to its reported role in cell proliferation (Holmqvist *et al*, 2004; Karar and Maity, 2011). Gal-1 induced phosphorylation of PLCγ1 was subsequently confirmed with flow cytometry. As VEGF is the primary ligand for VEGFR2, and VEGFR2 signalling can induce phosphorylation of PLCγ1, it was investigated whether HOMECs in experimental conditions secreted any VEGF, or whether VEGF was present in the 0.1% BSA starve media. No VEGF was detected in either case, suggesting that the phosphorylation of VEGFR2 and PLCγ1 was due to gal-1 alone, and did not require VEGF.

In order to investigate how gal-1 was activating VEGFR2 and PLCγ1, the inhibitor SW was used to decrease the level of complex N-glycans from the cell surface and potentially prevent gal-1 cell surface binding (via its carbohydrate recognition domain). Following initial preliminary experiments to determine the optimal SW treatment conditions, it was observed that SW pre-treatment was able to inhibit gal-1 induced HOMEC proliferation. Gal-1 proliferation was also

inhibited by the known VEGFR2 inhibitor SU5416. SW did not however inhibit VEGF induced HOMEC proliferation. Similarly, the effect of SW on gal-1 induced PLCγ1 phosphorylation was investigated (alongside the effect of a known PLC inhibitor, U73122). Interestingly, gal-1 induced phosphorylation of PLCγ1 was inhibited with SW and U73122, whilst VEGF induced phosphorylation of PLCγ1 was not inhibited by SW but was inhibited by U73122. These results suggested that gal-1 induced HOMEC proliferation, and phosphorylation of VEGFR2 and PLCγ1 by interacting with cell surface complex N-glycans, potentially those present on the extracellular portion of VEGFR2.

Finally, the effect of gal-1 on the internalisation of activated VEGFR2 (a known cellular mechanism for termination of VEGFR2 signalling) was studied. It was hypothesised that the increased signalling via VEGFR2 by gal-1 could be, at least partially, due to gal-1 causing a retention of activated VEGFR2 at the cell surface, thus prolonging the activation of the signalling pathway.

In contrast, it was observed that VEGF treatment initially (within 5 minutes) enhanced surface VEGFR2 levels which then decreased (after 15 minutes) with continued exposure to VEGF, presumably as a result of internalisation as a mechanism to prevent prolonged activation. Gal-1 itself was shown to not affect surface levels of VEGFR2. Interestingly, pre-treatment with gal-1 did reduce the removal of the VEGFR2 from the cell surface following VEGF activation. Therefore, gal-1 itself did not increase or prolong VEGFR2 levels on the cells surface but did prolong the time of VEGF induced VEGFR2 surface presentation.

5.4.2 Galectin-1 activated VEGFR2 and other receptor tyrosine kinases

As discussed in section 1.7, gal-1 has huge cell surface binding capabilities owing to its carbohydrate recognition domain. Given that cell surface receptors and molecules can be differentially glycosylated depending on the cell type and microenvironment, the interaction of gal-1 with receptors is known to vary in different cell types and contexts (Elola *et al*, 2005). In this set of experiments (and with an activation threshold applied), RTK arrays suggested that gal-1 activated VEGFR2, Tie-2, HGFR, IGF-1R and IR in HOMECs (see figure 78). VEGFR2, Tie-2, and HGFR are well known receptors associated with pro-

angiogenic signalling (discussed in 1.3.1). Furthermore, both IGF-1R and IR are implicated in angiogenesis, particularly in tumour associated angiogenesis; Kondo *et al* (2003) found a significant decrease in retinal neovascularisation in an oxygen induced retinopathy mouse model in EC IGF-1R knockout animals. Interestingly, it has recently been proposed that endothelial IR signalling promotes angiogenesis. Walker *et al* (2021) found that IR knockdown in HUVECs inhibited the ability of ECs to respond to VEGF, which in turn inhibited VEGF induced sprouting angiogenesis.

Little research has connected gal-1 with Tie-2 and HGFR. However, all receptors identified above contain sites where N-glycosylation can occur (Macdonald *et al* 2006; Lau *et al*, 2007; Chen *et al,* 2013; de-Freitas-Junior *et al*, 2017), which would offer binding sites for gal-1 to interact with them. It is important to note however, that other receptors studied with these arrays also contain N-glycosylation sites and yet gal-1 did not appear to activate them, for example, FGFR1 (Duchesne *et al*, 2006). It is thought that specific N-glycosylation sites bind specific types of N-glycans, and are involved with the receptor regulation. Therefore N-glycan binding molecules such as gal-1 will not induce the same effects on every receptor (Chandler *et al*, 2019a).

The effect of gal-1 on HOMEC RTKs was also limited to study of the RTKs included in the array kits, and therefore it is possible that other RTKs and receptors may interact with gal-1. This includes neuropilin-1 (NRP-1), a co-receptor for VEGFR2. Furthermore, only very select timepoints could be studied due to the limited number of membranes in the kits. It is therefore possible that array results for activated RTKs may differ depending on the length of gal-1 incubation.

However, based on the data obtained, VEGFR2 (activation increased by 70%) was selected for further initial study, and the gal-1 induced phosphorylation of VEGFR2 was confirmed by ELISA. As VEGF is described as the most potent pro-angiogenic factor (Harper and Bates, 2008), the observation that gal-1 could directly phosphorylate the VEGF receptor (VEGFR2) in the absence of VEGF was of particular interest for elucidating the pro-proliferative effect of gal-1 on HOMECs.

5.4.3 Galectin-1 phosphorylated PLCγ1 and p70 S6 kinase

Following the identification of key RTKs of interest in 5.3.2, intracellular signalling kinases activated within HOMECs in response to gal-1 were studied using phosphokinase arrays. These arrays showed marked increases in the phosphorylation of p70 S6 kinase (T389) and PLCγ1. These kinases are associated with different signalling pathways downstream of VEGFR2, although it is important to note that these pathways are not exclusive to VEGFR2. However, both kinases exist in pathways associated with the phosphorylation of VEGFR2 at Y1175 (Holmqvist *et al*, 2004; Karar and Maity, 2011), as discussed in section 1.6.2.1.

Phosphorylation at Y1175 can activate the PI3 kinase pathway, a branch of which activates protein kinase B (Akt) and mammalian target of rapamycin (mTOR). Phosphorylation of p70 S6 kinase at site T389 is a hallmark of mTOR1 activation via this pathway (Rosner *et al*, 2012). Once activated by mTOR1, p70 S6 kinase binds to the S6 ribosomal protein and enhances the translation of mRNAs and therefore increases protein synthesis (Du *et al*, 2013). The activity of mTOR1 is frequently upregulated in many solid cancers (Tian *et al*, 2019). In most literature, this upregulation has been discussed in tumour cells, where PI3/Akt/mTOR1/p70 S6 kinase signalling has been observed to promote tumour cell survival and proliferation, as well as enable the high metabolic rate required by tumour cells (Zou *et al*, 2020). However, there is also evidence that this pathway is active in ECs. In human dermal microvascular ECs, Liu *et al* (2008) found that constitutive activation of p70 S6 kinase enhanced angiogenesis in a 3D prostate cancer co-culture sponge model, by increasing the expression of HIF-1α. This pro-angiogenic effect was inhibited with an inhibitor of p70 S6 kinase. Therefore there could potentially be a role of p70 S6 kinase in angiogenesis, although the exact mechanism still remains unclear; it is unknown whether this is due to increased EC proliferation, survival, or metabolism. However, this kinase could therefore be of interest in future study of gal-1 induced proliferation of HOMECs.

Phosphorylation of VEGR2 at Y1175 can also phosphorylate PLCγ1. This causes a release of Ca^{2+} from the ER, which in turn activates PKC and promotes EC proliferation through the ERK pathway (Wang *et al*, 2020). This branch of VEGFR2 downstream signalling is better understand than p70 S6

kinase in terms of leading to cell proliferation (Matsumoto and Mugishima, 2006; Singh *et al*, 2007). Indeed, PLCγ1 is thought to be the prime PLC isoform involved in inducing pro-angiogenic effects downstream of VEGF binding to VEGFR2 (Meyer *et al*, 2003). As discussed in section 1.6.1, tumour cells, and multiple other cell types in the tumour microenvironment, secrete VEGF. It can therefore be assumed that the phosphorylation of PLCγ1 occurs regularly in tumour associated angiogenesis (Moccia *et al*, 2019).

As discussed in 1.7.2.3, gal-1 is known to interact with membrane associated intracellular H-ras. The phosphokinase array used did not include H-ras however, and therefore these experiments could not investigate this potential mechanism. It is known that in order for H-ras to phosphorylate its target molecule Raf, it must localise to the membrane (Inouye *et al*, 2000); H-ras is downstream of PLCγ1, and therefore the phosphorylation of PLCγ1 is important for the activation and membrane localisation of H-ras (Jun *et al*, 2013). As phosphokinase array data did show an increase in PLCγ1 (which was confirmed with flow cytometry), there is potential for gal-1 to both activate and localise H-ras to the membrane, as well as then stabilise the interaction between H-ras and the membrane (Prior *et al*, 2003; Thijssen *et al*, 2010). Both of these mechanisms could contribute to a pro-proliferative effect of gal-1 in HOMECs.

As mentioned in 5.4.3, the arrays used were limited to the kinases included, as well as the limitations in studying a range of timepoints. However, the data from both RTK and phosphokinase arrays (as well as confirming ELISA and flow cytometry) suggested that gal-1 could promote HOMEC proliferation by activating VEGFR2, with the subsequent phosphorylation of VEGFR2 at Y1175 and activation of PLCγ1 associated signalling. In order to support this, further experiments were necessary to confirm that the activation of VEGFR2 was induced by gal-1 alone, and not in conjunction with VEGF. Furthermore, given that PLCγ1 signalling is not exclusive to VEGFR2 pathways, inhibitory studies were required to investigate whether the PLCγ1 phosphorylation was associated with the observed VEGFR2 activation.

5.4.4 Galectin-1 activated VEGFR2 independently of VEGF

As discussed in section 1.7.2.4, gal-1 has previously been reported to be able to bind to VEGFR2. However, the effect of gal-1 on the activation of VEGFR2 is unclear, specifically whether gal-1 alone can activate the receptor, or whether it interacts with the VEGF-VEGFR2 complex, and so this was investigated further The data described here i.e. RTK array and ELISA, were obtained from HOMECs cultured in starve media conditions (with no added VEGF). However, it was possible that the 2% FCS present in the starve media may have introduced VEGF into the culture due to the presence of an unknown concentration of VEGF in the serum. Additionally, nutrient deprived ECs are known to secrete VEGF, raising the possibility of autocrine effects which could activate VEGFR2 (Fitzgerald *et al*, 2018). Therefore it was important to ascertain whether this could be happening, and could explain the activation. Thus, the presence of VEGF in the media from HOMECs cultured in starve media was examined by ELISA. A limitation of this work was the detection level of 5pg/ml. However, previous work by Bocci *et al* (2001) reported that placental ECs secreted approximately 68.7pg/ml. Whilst this was observed in a different type of EC, this suggested that VEGF from HOMECs would likely be detectable with the ELISA.

No VEGF was detected in the experimental media, either in the supernatant collected from HOMECs after the 0.1% BSA (w/v) starve or in the 0.1% BSA (w/v) starve media itself (figure 82). This suggested that gal-1 was able to activate VEGFR2 in the absence VEGF. This is in line with work by D'Haene *et al* (2013), who showed that in HUVECs incubated with both gal-1, VEGF, and a VEGF blocking antibody, activation of VEGFR2 was not fully inhibited. Similarly, Hsieh *et al* (2008) observed gal-1 induced activation of VEGFR2 in HUVECs without the presence of VEGF. However, this group concluded gal-1 exerted this effect by binding to NRP-1, and not VEGFR2. NRP-1 can also undergo N-glycosylation and therefore in theory could bind gal-1 in a carbohydrate dependent manner (Shintani *et al*, 2006). Interestingly, Chandler *et al* (2019a) demonstrated that enzymatic removal of N-glycans from VEGFR2 in porcine aortic ECs enhanced VEGF induced VEGFR2 activation. This suggests that gal-1 binding to VEGFR2 would not enhance VEGF induced activation of VEGFR2 even if VEGF had been present, again supporting the conclusion that

gal-1 directly activates VEGFR2. It also poses the question whether N-glycans on VEGFR2, and gal-1 binding to them, can serve as a compensatory mechanism for the activation of VEGFR2 in the absence of VEGF. This question was addressed in work by Croci *et al* (2014), who described lectin-glycan interactions as highly important in the vascularisation of tumours, and suggested that abnormal glycosylation is a hallmark of neoplastic tissues. The group showed that surface glycosylation of HUVECs was altered to favourably facilitate gal-1 binding in response to anti-inflammatory cytokines such as TGF-β1, and that these ECs were not sensitive to anti-VEGF treatments, whereas cells with basal surface glycosylation were sensitive. Considering the data in this thesis, this is interesting since HOMECs were not exposed to any cytokines, yet gal-1 could bind to the cell surface and activate VEGFR2. This suggests EC heterogeneity may factor in to this mechanism, in line with observations in differential basal surface glycosylation on ECs from different vascular beds by Scott *et al* (2013).

In order to confirm that gal-1 induced the activation of VEGFR2 (and therefore HOMEC proliferation) by binding to complex N-glycans on VEGFR2, further experiments were performed using SW, an inhibitor of complex N-glycan synthesis.

5.4.5 Swainsonine inhibited galectin-1 induced HOMEC proliferation and phosphorylation of VEGFR2 and PLCγ1

Initial efficacy and toxicity studies of SW in HOMECs showed that 24 hour treatment with 5μg/ml significantly inhibited subsequent gal-1 binding to the cell surface without causing any cytotoxic effects (see figures 83 - 85). It is important to note that these data did not show a complete inhibition of cell surface gal-1 binding, but that it was instead reduced by approximately 60%. However, the reduction in synthesis of complex N-glycans by SW would not affect other N-glycan types and therefore gal-1 could still potentially bind to these N-glycans. The modification by the enzyme inhibited by SW (AMANII) occurs after previous enzyme modifications by α-glucosidase, α-mannosidase I, and β1,6-N-acetylglucosaminyltransferase I. The unimpeded actions of these enzymes maintain the generation of high mannose and hybrid type N-glycans (Goss *et al*, 1995). The use of SW therefore allowed the specific study of

potential mechanisms of gal-1 induced effects that occurred through binding to complex N-glycans. This was a useful tool since the glycosylation sites on VEGFR2 are thought to bind complex N-glycans (Patnaik *et al,* 2006; Chandler *et al*, 2019a). Other strategies commonly used to study cell surface N-glycans are enzymatic removal by peptide-N-glycosidase F, which allows analysis of the entire N-glycome with mass spectrometry (Bodnar *et al*, 2016).

The data presented in 5.3.8 showed that SW significantly reduced both 5 and 50ng/ml gal-1 induced HOMEC proliferation over 24 hours. Gal-1 induced proliferation was also significantly inhibited by the known VEGFR2 inhibitor, SU5416. It is important to note however that SU5416 is a pan VEGFR inhibitor, and would additionally inhibit VEGFR3. Indeed, gal-1 increased VEGFR3 phosphorylation by 30% compared to control in RTK arrays (see figure 78). Activated VEGFR3 can also phosphorylate PLCγ1 (Coso *et al*, 2012), and therefore the involvement of VEGFR3 cannot be ruled out with SU5416. Interestingly, in VEGF treated cells, SU5416 but not SW inhibited HOMEC proliferation, suggesting that the mechanism of gal-1 but not VEGF induced proliferation was influenced by SW. Similar observations were seen in the gal-1 induced phosphorylation of VEGFR2, and in PLCγ1 (in PLCγ1 data, the PLC inhibitor U73122 was used instead of SU5416). Collectively, these experiments therefore strongly suggested that SW inhibited gal-1 induced phosphorylation of VEGFR2 and PLCγ1, and ultimately HOMEC proliferation. The study of SW on PLCγ1 phosphorylation was however, limited to an n of 1 and therefore warrants further repeats. Additionally, these experiments showed that SW did not affect the pro-proliferative effect of VEGF, or VEGF induced phosphorylation of VEGFR2 and PLCγ1 in HOMECs. As mentioned previously, SW inhibits the synthesis of complex N-glycans. Therefore the data suggest that SW reduces N-glycosylation (by complex N-glycans) of specific sites on VEGFR2, which in turn may have prevented gal-1 from binding to these (normally glycosylated) sites on VEGFR2. Thus, it can be hypothesised that the pro-proliferative effect of gal-1 in HOMECs was due to gal-1 binding to complex N-glycans on VEGFR2 and activating the receptor.

This is in line with work by Croci *et al* (2014) (discussed in 5.4.4), who also suggested that gal-1 specifically acts on VEGFR2 by binding complex N-glycans. Importantly, this previous work suggested that gal-1 is capable of these

effects without requiring VEGF. The data presented here are in agreement with this since HOMECs (at least in these experimental conditions), interacted with gal-1 in this manner resulting in an activation of VEGFR2 under basal conditions without any exposure to cytokines that may alter the surface glycosylation of the cell. It should be noted, however, that these experiments did not address the potential pro-proliferative effects of gal-1 that were either carbohydrate binding independent, or those that occurred inside of cells (or were a combination of both). For example, this work could neither confirm nor disprove that gal-1 stabilised membrane associated H-ras as reported by Thijssen *et al* (2010). These potential other mechanisms would therefore require further study.

5.4.6 Galectin-1 inhibited internalisation of the surface VEGF-VEGFR2 complex

Initial experiments demonstrated a significant increase in surface VEGFR2 in HOMECs incubated with VEGF after 5 minutes, followed by a significant decrease, (presumably due to VEGF-VEGFR2 complex internalisation) after 15 minutes (see figure 90). These data agree with previous reports since it is known that upon VEGF stimulation of ECs, internal VEGFR2 is initially cycled to the membrane in order to increase surface VEGFR2 and VEGF-VEGFR2 complex formation. These complexes are then internalised to regulate (reduce) the activation of associated signalling pathways (Ewan *et al*, 2006; Xie *et al*, 2019). These data informed the study of the effect of gal-1 on this presumed receptor internalisation at 15 and 30 minutes; timepoints in line with previous literature (Ballmer-Hofer *et al*, 2011 and Basagiannis *et al*, 2016). Crucially, the effect of ligand-induced RTK internalisation (as described by Ewan *et al*, 2006; Xie *et al*, 2019) was assumed to be the mechanism explaining the reduction in VEGF-VEGFR2 receptor complexes after 15 minutes. In order to confirm or refute this, future work could be to adapt this experiment for study with ICC.

Additionally, the effect of gal-1 pre-treatment on the initial increase in surface VEGFR2 in response to VEGF was investigated. It was observed that neither concentration of gal-1 studied significantly affected surface levels of VEGFR2 at five minutes (see figure 90). This both allowed for this to be excluded as a variable, and suggested that gal-1 (unlike VEGF) did not increase surface

VEGFR2. This is interesting, as data in sections 5.3.2-3 suggested that gal-1 could activate VEGFR2. This observation would therefore imply that gal-1 could activate VEGFR2 but not initially increase the level of surface VEGFR2, as was observed with VEGF.

Interestingly however, pre-treatment with 5 and 50ng/ml gal-1 did significantly increase levels of VEGFR2 retained at the cell surface following 15 and 30 minute VEGF treatments compared with control (no gal-1 pre-treatment). These data suggested that gal-1 reduced the VEGF induced VEGF-VEGFR2 complex receptor internalisation. This observation suggests an additional mechanism by which gal-1 may exert pro-proliferative effects on ECs. Specifically, it may bind to complex N-glycans on VEGFR2 and then prevent internalisation of the receptor upon its activation. There is evidence in the literature that cell surface galectins may increase the retention of receptors at the membrane, and therefore prolong their signalling when activated. However, these studies attribute this as a function of gal-3 (Partridge *et al*, 2004; Liu and Rabinovich *et al*, 2005). However, studies on EGFR have showed that complex N-glycans on EGFR can bind various galectins, resulting in a reduction of ligand-EGFR complex internalisation and prolongation of EGFR signalling (Chandler *et al*, 2019a). This area of research, especially with regard to VEGFR2 and gal-1, has not yet been fully investigated but could be an important aspect to consider in the study of abnormal RTK signalling, as physiologic signalling requires strict regulation, and prolonged RTK signalling can result in cancer (Tomas *et al*, 2014).

It was interesting to note that SW prevented the initial increase in surface VEGFR2 induced by VEGF alone. Further investigation of the mechanism underlying this was outside the remit of this thesis. However, this observation did limit the experiment as the effect of SW on gal-1 inhibited VEGF-VEGFR2 complex internalisation could not be studied using this method, since SW already had an effect even before the addition of gal-1. It should also be noted that several studies have suggested that VEGF-VEGFR2 complex internalisation is required for the activation of some intracellular signalling pathways, namely ERK (Basagiannis *et al*, 2016; Walker *et al*, 2021). The results presented here suggested that gal-1 induced the phosphorylation of PLCγ1; PLCγ1 is upstream of ERK, and so it can be implied that gal-1 can

induce the activation of ERK. Therefore, if VEGF-VEGFR2 complex internalisation is necessary for the activation of ERK, this experiment should be extended to longer timepoints to study if, and when, the gal-1 induced retention of VEGF-VEGFR2 complex internalisation ends. Alternatively, gal-1 may be pro-proliferative in a manner completely independent of ERK signalling, perhaps in a manner similar to that of EGFR described by Chandler *et al* (2019a), where the maintenance of receptor-ligand complexes at the cell surface prolongs the exposure to, and binding of ligands.

5.4.7 Conclusions

The data in this chapter suggest that the pro-proliferative effect of gal-1 on HOMECs occurs by gal-1 binding to and activating VEGFR2, independently of VEGF. This in turn may induce the phosphorylation of PLCγ1, suggesting that gal-1 phosphorylated VEGFR2 at the Y1175 site in the C-terminus. This implied that the proliferation occurred through PLCγ1 signalling, suggesting involvement of ERK. Gal-1 was also shown to inhibit VEGF induced VEGFR2 internalisation, suggesting another potential pro-proliferative mechanism of gal-1. The data therefore suggests both a VEGF independent and VEGF dependent pro-proliferative role for gal-1 in HOMECs, which are summarised in figure 92.

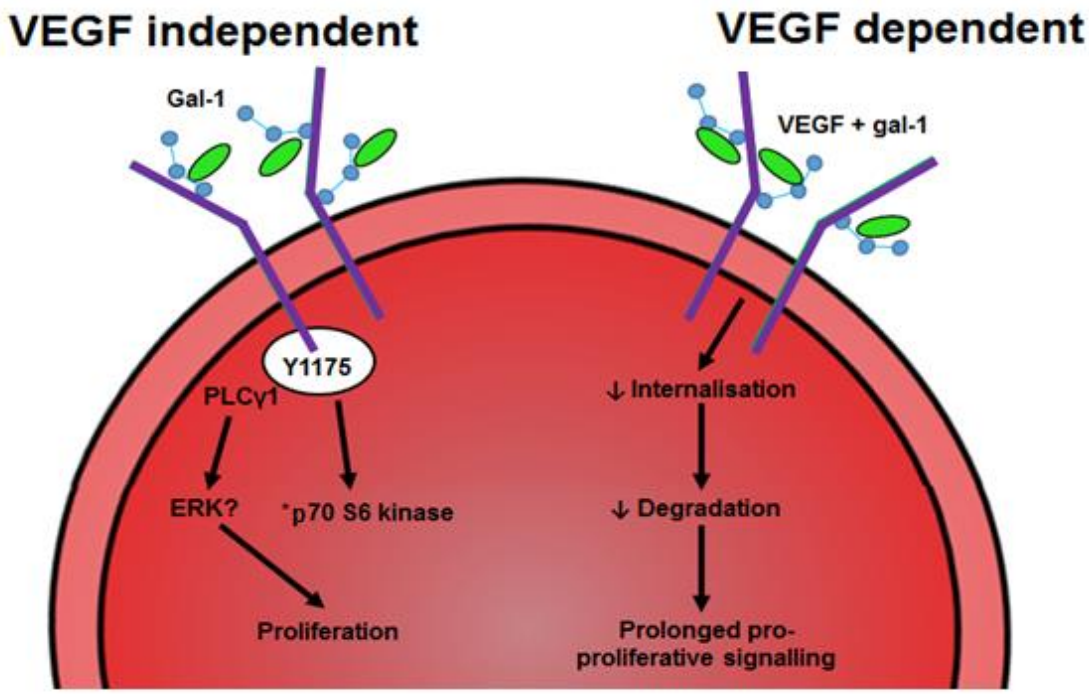

Figure 92. Summary of the potential pro-proliferative mechanisms of galectin-1 in HOMECs. Galectin-1 (gal-1) promotes HOMEC proliferation through a VEGF independent pathway (shown on the left) and a VEGF dependent pathway (shown on the right). The VEGF independent pathway involves gal-1 (green) directly activating VEGFR2 (purple) via binding to complex N-glycans on the extracellular portion of VEGFR2 (blue). This in turn leads to the phosphorylation of PLCγ1, which can regulate proliferation through ERK. The VEGF dependent pathway involves gal-1 binding to complex N-glycans on the extracellular portion of VEGF activated VEGFR2, and preventing the complex from internalisation and degradation, resulting in prolonged pro-proliferative signalling. *gal-1 may also induce phosphorylation of p70 S6 kinase.

Chapter 6. Overall discussion and future work

The ability of tumours to induce angiogenesis is a required process for tumour growth, and is considered a hallmark of cancer development (Hanahan and Weinberg, 2011). Angiogenesis is a process typically suppressed in physiological conditions by a balance of pro and anti-angiogenic factors secreted from cells in the local microenvironment. Within the tumour microenvironment, this balance is altered in favour of pro-angiogenic factors, as tumour cells (and other cells) secrete pro-angiogenic factors such as VEGF and MMP9 (Bouïs *et al*, 2006; Burrell and Zadeh, 2012). These pro-angiogenic factors trigger the activation of typically proliferatively quiescent ECs from local pre-existing vasculature; growth factors such as VEGF induce EC proliferation, migration and increase vascular permeability. Other pro-angiogenic factors such as MMP9 contribute to ECM/basement membrane degradation, and as such create a path for newly forming vessels (Pepper, 2001).

EOC is often diagnosed at an advanced stage when the disease has already progressed and metastasised, and a common site of metastasis is the omentum (Doufekas and Olaitan, 2014). The omentum confers some local immune responses to the abdominal and pelvic cavity, but it is not itself an essential organ (Di Nicola, 2019). However, its fatty composition is known as a good 'soil' for metastasising EOC cells, and can actively facilitate cancer cell binding and growth (Meza-Perez and Randall, 2017). Crucially, the omental environment enhances tumour associated angiogenesis. In addition to EOC cells, adipocytes, mesothelial cells, and immune cells all secrete pro-angiogenic factors in response to EOC cell signalling, including VEGF (Gavalas *et al*, 2013). Secondary tumours can therefore readily establish, and this correlates to a poorer prognosis; whilst the omentum is not essential, it overlies abdominal organs and is itself highly vascularised. This can facilitate further metastases through both transcoelomic and haematogenous routes (Yoo *et al*, 2007; Yousefi *et al*, 2020).

As poorer prognoses are correlated with higher levels of VEGF, the targeting of VEGF with anti-angiogenic therapies has been an area of therapeutic research for treating advanced EOC. This has primarily involved the anti-VEGF

monoclonal antibody therapy, bevacizumab. However, the benefits to patients with advanced EOC are minimal. The drug modestly prolongs disease free survival (Burger *et al*, 2011), but has little to no effect on overall survival (Tewan *et al*, 2019), and is associated with severe side effects (Perren *et al*, 2011). Current anti-angiogenic therapy for the treatment of advanced EOC therefore is not particularly effective, and subsequent work has sought to understand why. In the context of omental metastasis, previous work form this lab reported that blocking VEGF was not enough to prevent angiogenic processes in disease relevant HOMECs that had been incubated with EOC cell conditioned media (Winiarski *et al*, 2013). CL, a protease, was subsequently identified in the EOC cell conditioned media and shown to induce the proliferation and migration of HOMECs in a non-proteolytic manner. Interestingly, HOMECs incubated with CL were found to secrete gal-1. Gal-1 is a small glycoprotein that is upregulated in EOC, and corresponds to a poorer prognosis (Chen *et al*, 2015). Gal-1 has been implicated in the proliferation (Prior *et al*, 2003; Thijssen *et al*, 2010) and migration (Hsieh *et al*, 2008; D'Haeane *et al*, 2013) of ECs during angiogenesis. This thesis therefore hypothesised that gal-1, secreted either from HOMECs themselves in response to CL or by other cells in the tumour microenvironment, could contribute to the pro-proliferative and migratory effects induced in HOMECs by EOC.

Initially, to investigate this hypothesis, a protocol to isolate disease relevant HOMECs from omental tissue was improved (chapter 3). This was achieved by extending enzymatic digestions and confirming that this did not affect EC viability or surface CD31. The possibility of a FACS based protocol was also investigated, with preliminary results suggesting that CD31 would be a suitable marker for HOMECs, and that other cell types may be difficult to target. Whilst the protocol used for this thesis was based on immunoselection, the development of a FACS approach would be useful for future work, as overall isolation success rate remained relatively low at 34% (improved from 10%). This improved (but persistently low) success rate was mitigated during this project due to fortunately receiving regular omental samples. However, higher success rates with FACS (and higher cell purities) have been reported (Cossarizza *et al*, 2017), and therefore this alternative presents as an opportunity for future work. Initially this would involve trialling a cell sort using a

CD31 antibody, and potentially expanding the antibody panel to optimise the cell sort.

The effect of gal-1 on HOMEC proliferation and migration was studied in chapter 4, as well as CL induced gal-1 secretion in HOMECs, and the CL induced expression and localisation of extracellular cell surface bound and intracellular gal-1. CL increased gal-1 secretion, which corresponded to an initial decrease in intracellular gal-1 and increase in extracellular surface bound gal-1. This suggested that intracellular gal-1 was exported out of the cell, and that some of this gal-1 became bound to the cell surface, raising the possibility that HOMEC secreted gal-1 could be a molecule with autocrine effects. HOMECs incubated with exogenous gal-1 also bound more cell surface gal-1, and pre-treatment of HOMECs with A2780 and SKOV3 conditioned media increased bound exogenous gal-1 even further. This suggested that exogenous gal-1 could also bind to the surface of HOMECs which was interesting as both A2780 and SKOV3 cells were found to secrete gal-1 (see figure 76).

Pre-treatment of A2780 and SKOV3 cells with gal-1 was shown to increase their adhesiveness to HOMEC monolayers, as well as SKOV3 cell adhesion to a HOMeso monolayer. Pre-treatment of a HOMEC monolayer also increased the adhesion of SKOV3 cells, but not A2780 cells. These data suggested that gal-1 may increase EOC cell adhesion during transcoelomic and haematogenous metastases processes. In particular, increased adhesion of gal-1 pre-treated SKOV3 cells to a HOMeso monolayer has implications in transcoelomic metastasis where cancer cells present in ascites adhere to, and subsequently, invade the omental mesothelial layer. The increased adhesion of both gal-1 pre-treated A2780 and SKOV3 cells to HOMEC monolayers (and SKOV3 to a gal-1 pre-treated HOMEC monolayer) suggested a potential role during intra and extravasation during haematogenous metastasis. These experiments offered an interesting preliminary look at the effect of gal-1 on EOC cell adhesion to different, disease relevant cell monolayers, but require further study due their limitations. The experiments used bi-directional flow, which was only relevant for modelling cell adhesion to the mesothelial omental layer (from ascites), and did not effectively model the unidirectional flow at the correct flow rate required for studying intra and extravasation processes. Therefore future work using

these cell types and gal-1 pre-treatment in an appropriate model of blood vessel flow (within the omentum) would be beneficial.

Importantly, gal-1 was shown to increase HOMEC proliferation. The increase in proliferation was highest after 24 hours, although gal-1 treated cells still showed increased proliferation, compared with control, after 48 and 72 hours. Interestingly, gal-1 induced HOMEC migration in chamber assays but not scratch assays. Previous literature of gal-1 induced migration of ECs has reported that results vary depending on the experimental setup, as gal-1 is thought to mediate cell binding to surfaces (which can be coated with various ECM components during experiments) (Moiseeva *et al*, 2003; Thijssen *et al*, 2010). The pro-migratory effect, or indeed the lack of this effect in scratch assays, was not addressed in this thesis but presents an interesting avenue for future work, as gal-1 associated pro-migratory signalling largely remains under investigated.

The mechanisms of gal-1 induced HOMEC proliferation were investigated in chapter 5. Short-term exposure to gal-1 was sufficient to induce the proliferation of HOMECs, which prompted the investigation of RTKs that are potentially activated by gal-1. Several RTKs associated with angiogenesis were identified using RTK arrays, including VEGFR2, which was selected for further study as VEGF is described as the most potent stimulator of angiogenesis (Harper and Bates, 2008). This was also interesting, as previous literature had reported potential interactions between gal-1 and VEGFR2 (Lau *et al*, 2007; Croci *et al*, 2014). The activation of VEGFR2 by gal-1 was confirmed by ELISA, and phosphokinase arrays suggested that gal-1 induced phosphorylation of PLCγ1 and p70 S6 kinase, suggesting phosphorylation of VEGFR2 by gal-1 at site Y1175. PLCγ1 was selected for further study due to its association with cell proliferation (Holmqvist *et al*, 2004; Karar and Maity, 2011), and gal-1 induced PLCγ1 phosphorylation was subsequently confirmed with flow cytometry. However, p70 S6 kinase implicated activation of the PI3 kinase/mTOR1 pathway, which itself is associated with cell survival, increased vascular permeability and increased protein synthesis (Du *et al*, 2013). This therefore presents as another pathway of interest in gal-1 induced HOMEC proliferation and another line of future work.

The activation of VEGFR2 by gal-1 and associated downstream signalling was interesting, as cells had been starved in media devoid of VEGF four hours prior to experimentation. This indicated that gal-1 activated VEGFR2 in the absence of VEGF, a capability disputed in current literature (Stanley, 2014). However, before experimentation, cells were starved, and ECs are known to produce VEGF in these conditions (Fitzgerald *et al*, 2018). However, no VEGF was detected in starve media alone, or in HOMEC conditioned starve media, suggesting that no VEGF was in the experimental system. These data suggested that gal-1 could directly activate VEGFR2 and downstream signalling pathways independently of VEGFR2.

The data presented had so far demonstrated the proliferation of HOMECs in response to gal-1, and had implicated the activation of VEGFR2 and associated downstream signalling, notably in the absence of VEGF. However, further investigation of how gal-1 interacted with VEGFR2 was undertaken using SW, an inhibitor of complex N-glycan synthesis, in experiments to investigate the possibility that gal-1 directly interacts with glycan moieties on VEGFR2. The receptor has 18 extracellular sites where it is potentially N-glycosylated, primarily by complex N-glycans (Patnaik *et al,* 2006; Chandler *et al*, 2019a). Gal-1 can bind to these complex N-glycans through its carbohydrate recognition site, and interactions between these N-glycans and gal-1 are implicated in VEGFR2 activation (Croci *et al*, 2014). Pre-treating HOMECs with SW was shown to inhibit gal-1 induced proliferation, phosphorylation of VEGFR2, and phosphorylation of PLCγ1. The study of SW on gal-1 induced phosphorylation of PLCγ1 was only performed once however (due to antibody discontinuation) and therefore this work requires further repeats, potentially with a different method such as western blotting if no suitable conjugated antibodies can be sourced. Interestingly, SW pre-treatment did not inhibit VEGF induced proliferation or VEGFR2/PLCγ1 phosphorylation. These data suggested that gal-1 induced these pro-proliferative effects and signalling by binding to complex N-glycans on VEGFR2, and activating the receptor, and that VEGF activation of VEGFR2 was not dependent on the presence of these complex N-glycans. This was in line with work by Croci *et al* (2014) and Chandler *et al* (2019a). However, a limitation of the experiments in this thesis include the omission of studying the VEGFR2 co-receptor, NRP-1. NRP-1 also contains

sites for potential N-glycosylation, and has been implicated in interacting simultaneously with both gal-1 and VEGFR2 (Hsieh *et al*, 2008). Future work to investigate whether gal-1 therefore activates VEGFR2 by interacting with N-glycans on VEGFR2, or NRP-1 (or indeed, both) is therefore required.

Lastly, gal-1 was shown to reduce the assumed internalisation of activated VEGFR2 from the membrane. The incubation of HOMECs with VEGF showed an initial increase in surface VEGFR2, followed by a decrease (where it was assumed that complexes were being internalised to terminate signalling). Gal-1 itself did not affect surface levels of VEGFR2. However, pre-treatment of HOMECs with gal-1 was shown to reduce VEGF activated VEGFR2 internalisation, and this prolongation of ligand-receptor complex at the cell membrane is thought to prolong activation of associated signalling pathways (Partridge *et al*, 2004; Liu and Rabinovich *et al*, 2005). Thus, these data suggested a potential VEGF dependent mechanism by which gal-1 can promote pro-proliferative signalling which is in addition to the direct gal-1 (and VEGF independent) activation of pro-angiogenic responses. Specifically, gal-1 in the tumour microenvironment might act in both an autocrine and paracrine manner to induce angiogenic responses that are both independent of VEGF and also enhance VEGF induced outcomes. As mentioned, the decrease in surface VEGFR2 was assumed to be as a result from complex internalisation, as this is a process well studied in the literature (Basagiannis *et al*, 2016; Walker *et al*, 2021). However, this was not demonstrated in these experiments. Future work where this is investigated is required; for example, the experiment could be adapted for an ICC approach where VEGF-VEGFR2 complexes could be visualised as internalised after VEGF treatment (or not).

Overall, the work in this thesis highlights the complexity of the tumour microenvironment in the omentum and how this complexity may contribute to the relative ineffectiveness of anti-angiogenics in treating advanced EOC. It is important to note that these studies were all carried out on ECs isolated from a vascular bed relevant to the disease being studied. This is critical since, as discussed in the introduction, ECs demonstrate considerable phenotypic heterogeneity across different vascular beds and so responses are likely to differ between cell types. Indeed, this may partially explain why pre-clinical *in vitro* data does not always translate into clinical success.

The main findings of this thesis are collated in figure 93. In summary, the data indicate, for the first time, that gal-1 has direct pro-metastatic effects on EOC cells, and a pro-angiogenic role in disease relevant HOMECs that are both independent and dependent of VEGF, which therefore presents gal-1 as a non-VEGF pro-angiogenic signalling molecule (see figures 92 - 93). This could also partially explain why targeting VEGF with treatments such as bevacizumab, does not prolong overall survival in patients, and presents gal-1 as a potential therapeutic target. As experimental work with inhibitors SU and SW in this thesis shows, it may be more prudent to target VEGFR2 intracellular signalling pathways in order to prevent VEGFR2 signalling (as opposed to targeting VEGF). Several RTK inhibitors have been trialled with limited success (see table 5), and therefore further work in this area is warranted. Furthermore, gal-1 is presented as a potential ligand to target, as well as the complex N-glycans on VEGFR2. Further work to examine these as pharmacological possibilities is required, as both gal-1 and complex N-glycans are ubiquitous. There is also potential to target the enzymes that produce the complex N-glycans, either directly in HOMECs themselves, or by targeting cancer cell derived signals that may influence these enzymes and promote aberrant complex N-glycosylation.

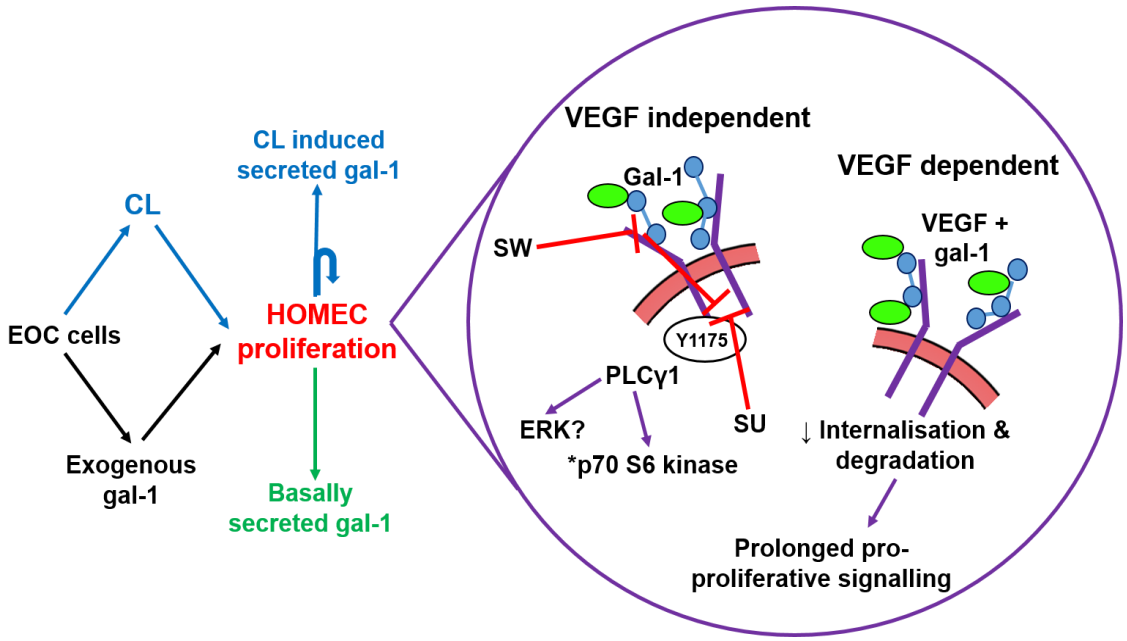

Figure 93. Summary of main thesis findings: EOC and HOMEC derived sources of galetin-1, and the potential pro-angiogenic pathways in HOMECs. Cathepsin-L (CL) was previously shown to be secreted from epithelial ovarian cancer (EOC) cells, which induced the secretion of galectin-1 (gal-1) from HOMECs. EOC cell lines A2780 and SKOV3 also secreted gal-1. HOMEC secreted gal-1 following incubation with CL led to increased cell surface gal-1 (indicated by the curved blue arrow), and HOMECs also secreted gal-1 without any CL activation. Gal-1 potentially promotes HOMEC proliferation through a VEGF independent pathway and a VEGF dependent pathway. The VEGF independent pathway involves gal-1 (green) directly activating VEGFR2 (purple) via binding to complex N-glycans on the extracellular portion of VEGFR2 (blue). This in turn may lead to the phosphorylation of PLCγ1 (via phosphorylation site Y1175), which can regulate proliferation through ERK. The VEGF dependent pathway involves gal-1 binding to complex N-glycans on the extracellular portion of VEGF activated VEGFR2, and preventing the complex from internalisation and degradation, resulting in prolonged pro-proliferative signalling. *gal-1 may also induce phosphorylation of p70 S6 kinase. Gal-1 induced proliferation was inhibited by both the pan-VEGFR inhibitor SU5416 (SU) which inhibits intracellular signalling, as well as swainsonine (SW) which inhibits the production of complex N-glycans (and subsequently, gal-1 induced VEGFR2 signalling).

Appendix

Tabulated data for figures 50 - 52

Time after CL treatment	- CL (control cells)	+ CL treated cells	Significance
30 minutes	1.2 ± 0.5	3.4 ± 1.1	↑**
2 hours	1.4 ± 0.2	3.0 ± 0.9	↑**
4 hours	1.0 ± 0.2	2.7 ± 1.3	↑**
8 hours	1.6 ± 0.6	2.5 ± 1.5	n.s
24 hours	3.7 ± 2.2	4.0 ± 2.4	n.s

Measurement of secreted galectin-1 from control and cathepsin-L (CL) treated HOMECs. Values shown are the mean ± SD, and units are ng/ml. ↑** indicates a significant increase in secreted gal-1 (p=0.0022), and n.s denotes no significant changes. (Mann-Whitney U analyses).

Time after CL treatment	- CL (control cells)	+ CL treated cells	Significance
30 minutes	7.6 ± 0.9	10.8 ± 0.5	n.s
2 hours	3.7 ± 0.3	3.9 ± 0.4	n.s
4 hours	5.2 ± 0.9	5.1 ± 0.2	n.s
8 hours	6.8 ± 0.6	7.0 ± 0.2	n.s
24 hours	10.6 ± 0.6	10.5 ± 0.5	n.s

Measurement of secreted galectin-1 from control and cathepsin-L (CL) treated HRECs. Values shown are the mean ± SD, and units are ng/ml. n.s denotes not significant (Mann-Whitney U analyses).

Time after CL treatment	- CL (control cells)	+ CL treated cells	Significance
30 minutes	3.1 ± 0.1	3.2 ± 0.2	n.s
2 hours	3.6 ± 0.2	3.6 ± 0.2	n.s
4 hours	4.0 ± 0.4	3.5 ± 0.4	n.s
8 hours	4.0 ± 1.0	5.0 ± 1.0	n.s
24 hours	7.4 ± 0.7	11.2 ± 1.0	n.s

Measurement of galectin-1 from control and cathepsin-L (CL) treated hCMEC/D3 cells. Values shown are the mean ± SD, and units are ng/ml. n.s denotes no significant changes. (Mann-Whitney U analyses).

Tabulated data for figures 67 - 73

	1ng/ml	5ng/ml	10ng/ml	25ng/ml	50ng/ml	125ng/ml	C
24 hours	168.6 ± 10.7 **p=0.0049	162.3 ± 9.7 **p=0.0038	171.0 ± 16.3 **p=0.0016	167.1 ± 14.9 **p=0.0074	172.7 ±15.5 **p=0.0015	187.5 ± 15.5 ****p<0.0001	154.1 ± 7.0 **p=0.0039
48 hours	136.3 ± 11.9 **p=0.0012	146.6 ± 5.1 **p=0.0010	134.9 ± 13.7 **p=0.0012	137.7 ± 12.1 **p=0.0060	128.9 ± 12.2 *p=0.0718	150.8 ± 9.15 **p=0.0010	161.3 ± 3.5 **p=0.002
72 hours	100.5 ± 5.0 *p=0.0492	107.5 ± 8.7 *p=0.0110	109.2 ± 13.2 *p=0.0233	103.6 ± 5.9 *p=0.0464	105.5 ± 10.84 *p=0.00265	114.1 ± 4.2 *p=0.0430	139.9 ± 1.4 **p=0.0042

Summary of the pro-proliferative effect of 1 - 125ng/ml galectin-1 on HOMECs after 24, 48, and 72 hours as assessed by WST-1 assay.

Results are the mean ± SD, n=6 (intra-experimental n=6), and shown as the percentage of the 0ng/ml gal-1 2% FCS media control. P values from post-hoc Dunn's test (all vs 100% control). C = complete media.

	1ng/ml	5ng/ml	10ng/ml	25ng/ml	50ng/ml	125ng/ml	C
24 hours	250.6 ± 43.5 ****p<0.0001	252.5 ± 46.5 ****p<0.0001	261.3 ± 50.5 ****p<0.0001	268.7 ± 53.3 ****p<0.0001	272.0 ± 50.7 ****p<0.0001	263.7 ± 71.5 ****p<0.0001	190.1 ± 23.23 **p=0.0042
48 hours	131.8 ± 21.0 ****p<0.0001	123.5 ± 18.4 ***p=0.0001	134.8 ± 16.0 **** p<0.0001	128.9 ± 23.7 ***p=0.0002	120.3 ± 18.7 **p=0.0047	122.4 ± 17.2 **p=0.0054	165.1 ± 30.40 **** p<0.0001
72 hours	110.2 ± 29.5 *p=0.0222	107.3 ± 26.8 **p=0.0026	106.5 ± 26.9 p=0.0867	107.5 ± 27.5 **p=0.0052	108.7 ± 28.2 *p=0.0026	196.0 ± 24.3 **0.0022	196.0 ±24.31 ***p=0.0002

Summary of the pro-proliferative effect of 1 - 125ng/ml galectin-1 on HOMECs after 24, 48, and 72 hours as assessed by BrdU incorporation. Results are the mean ± SD, n=6 (intra-experimental n=6), and shown as the percentage of the 0ng/ml gal-1 2% FCS media control. P values from post-hoc Dunn's test (all vs 100% control). C = complete media.

	1ng/ml	5ng/ml	10ng/ml	25ng/ml	50ng/ml	125ng/ml	C
24 hours	142.2 ± 50.2 ***p=0.0002	143.1 ± 49.2 ***p=0.0004	140.6 ± 50.7 ***p=0.0005	140.4 ± 54.1 ***p=0.0008	139.7 ± 60.8 ***p=0.0005	146.0 ± 61.8 ***p=0.004	215.9 ± 17.24 ****p<0.0001
48 hours	117.0 ± 19.8 **p=0.0015	116.0 ± 20.2 **p=0.0018	115.9 ± 18.2 **p=0.0014	112.3 ± 17.9 p=0.0825	115.4 ± 23.6 p=0.0718	100.1 ± 38.6 p=0.0054	99 ± 16.32 *p=0.014
72 hours	111.4 ± 16.9 **p=0.0040	112.3 ± 11.8 **p=0.0023	110.1 ± 14.4 **p=0.0012	113.5 ± 15.2 **p=0.0090	123.0 ± 20.2 ***p=0.0009	111.2 ± 9.3 **0.0010	111.2 ± 9.27 *p=0.0373

Summary of the pro-proliferative effect of 1 - 125ng/ml galectin-1 on HRECs after 24, 48, and 72 hours as assessed by WST-1 assay. Results are the mean ± SD, n=6 (intra-experimental n=6), and shown as the percentage of the 0ng/ml gal-1 2% FCS media control. P values from post-hoc Dunn's test (all vs 100% control). C = complete media.

	1ng/ml	5ng/ml	10ng/ml	25ng/ml	50ng/ml	125ng/ml	C
24 hours	97.6 ± 6.6 p=0.3486	93.7 ± 7.1 p=0.0800	94.4 ± 7.6 p=0.0863	93.5 ± 17.6 p=0.1892	99.2 ± 19.5 p=0.8195	153.1 ± 35.3 ****p=0.0005	107.7 ± 10.0 *p=0.0369
48 hours	98.9 ± 7.8 p=0.0817	97.4 ± 8.1 p=0.4600	95.9 ± 8.4 p=0.6344	95.9 ± 7.1 p=0.0672	101.2 ± 9.9 p=0.0652	99.9 ± 17.5 p=0.1420	115.5 ± 9.3 *p=0.0110
72 hours	109.6 ± 17.1	118.4 ± 11.6 ***p=0.0007	114.9 ± 14.3 **p=0.0033	123.8 ± 8.4 **** p<0.0001	139.2 ± 10.3 **** p<0.0001	148.7 ± 16.0 ****p<0.0001	115.0 ± 5.5 **p=0.0036

Summary of the pro-proliferative effect of 1 - 125ng/ml galectin-1 on hCMEC/D3 cells after 24, 48, and 72 hours (WST-1). Results are the mean ± SD, n=6 (intra-experimental n=6), and shown as the percentage of the 0ng/ml gal-1 2% FCS media control. P values from post-hoc Dunn's test (all vs 100% control). C = complete media.

Published journal article

- Pranjol, M., Zinovkin, D. A., Maskell, A., Stephens, L. J., Achinovich, S. L., Los', D. M., Nadyrov, E. A., Hannemann, M., Gutowski, N. J., & Whatmore, J. L. (2019). Cathepsin L-induced galectin-1 may act as a proangiogenic factor in the metastasis of high-grade serous carcinoma. *Journal of translational medicine*, *17*(1), 216.

Published conference abstracts

- Maskell, A., Staton, S. Vorinostat Demonstrates Anti-Angiogenic Activity *In Vitro* [abstract]. In: British Microcirculation Society meeting, 2017.
- Maskell, A., Gutowski, N., Hannemann, M., Whatmore, J. Does Galectin-1 Play A Pro-Angiogenic Role In The Metastasis Of Epithelial Ovarian Cancer (EOC) To The Omentum? [abstract]. In: British Microcirculation Society meeting, 2018.
- Maskell, A., Gutowski, N., Hannemann, M., Whatmore, J. Microvascular Endothelial Cells From Different Vascular Beds Show Heterogeneous Secretion Of Galectin-1 In Response To Cathepsin L [abstract]. In: British Microcirculation Society meeting, 2019.
- Maskell, A., Gutowski, N., Hannemann, M., Whatmore, J. Galectin-1 Induces VEGFR2 Phosphorylation And Downstream Signalling In Human Omental Microvascular Endothelial Cells [abstract]. In: European Association for Cancer Research Society meeting, 2019.
- Maskell, A., Gutowski, N., Hannemann, M., Whatmore, J. The Role Of Galectin-1 Secreted From Epithelial Ovarian Cancer Cells In Angiogenesis During Omental Metastasis [abstract]. In: British Microcirculation Society meeting, 2018.

References

Abcouwer, S. F. (2013) 'Angiogenic Factors and Cytokines in Diabetic Retinopathy', *J Clin Cell Immunol,* Suppl 1(11), pp. 1-12.

Aghajanian, C., Blank, S. V., Goff, B. A., Judson, P. L., Teneriello, M. G., Husain, A., Sovak, M. A., Yi, J. and Nycum, L. R. (2012) 'OCEANS: a randomized, double-blind, placebo-controlled phase III trial of chemotherapy with or without bevacizumab in patients with platinum-sensitive recurrent epithelial ovarian, primary peritoneal, or fallopian tube cancer', *J Clin Oncol,* 30(17), pp. 2039-45.

Aird, W. C. (2007a) 'Phenotypic heterogeneity of the endothelium: I. Structure, function, and mechanisms', *Circ Res,* 100(2), pp. 158-73.

Aird, W. C. (2007b) 'Phenotypic heterogeneity of the endothelium: II. Representative vascular beds', *Circ Res,* 100(2), pp. 174-90.

Al Habyan, S., Kalos, C., Szymborski, J. and McCaffrey, L. (2018) 'Multicellular detachment generates metastatic spheroids during intra-abdominal dissemination in epithelial ovarian cancer', *Oncogene,* 37(37), pp. 5127-5135.

Alhabbab, R., Blair, P., Smyth, L. A., Ratnasothy, K., Peng, Q., Moreau, A., Lechler, R., Elgueta, R. and Lombardi, G. (2018) 'Galectin-1 is required for the regulatory function of B cells', *Sci Rep,* 8(1), pp. 2725.

Almeida, M., García-Montero, A. C. and Orfao, A. (2014) 'Cell purification: a new challenge for biobanks', *Pathobiology,* 81(5-6), pp. 261-75.

Anders, E., Alles, J. U., Delvos, U., Pötzsch, B., Preissner, K. T. and Müller-Berghaus, G. (1987) 'Microvascular endothelial cells from human omental tissue: modified method for long-term cultivation and new aspects of characterization', *Microvasc Res,* 34(2), pp. 239-49.

Anugraham, M., Jacob, F., Nixdorf, S., Everest-Dass, A. V., Heinzelmann-Schwarz, V. and Packer, N. H. (2014) 'Specific glycosylation of membrane proteins in epithelial ovarian cancer cell lines: glycan structures reflect gene expression and DNA methylation status', *Mol Cell Proteomics,* 13(9), pp. 2213-32.

Astorgues-Xerri, L., Riveiro, M. E., Tijeras-Raballand, A., Serova, M., Neuzillet, C., Albert, S., Raymond, E. and Faivre, S. (2014) 'Unraveling galectin-1 as a novel therapeutic target for cancer', *Cancer Treat Rev,* 40(2), pp. 307-19.

Auguste, P., Lemiere, S., Larrieu-Lahargue, F. and Bikfalvi, A. (2005) 'Molecular mechanisms of tumor vascularization', *Crit Rev Oncol Hematol,* 54(1), pp. 53-61.

Bachmann, R., Brucker, S., Stäbler, A., Krämer, B., Ladurner, R., Königsrainer, A., Wallwiener, D. and Bachmann, C. (2021) 'Prognostic relevance of high pretreatment CA125 levels in primary serous ovarian cancer', *Mol Clin Oncol,* 14(1), pp. 8.

Ballmer-Hofer, K., Andersson, A. E., Ratcliffe, L. E. and Berger, P. (2011) 'Neuropilin-1 promotes VEGFR-2 trafficking through Rab11 vesicles thereby specifying signal output', *Blood,* 118(3), pp. 816-26.

Barreiro, O. and Sánchez-Madrid, F. (2009) 'Molecular basis of leukocyte-endothelium interactions during the inflammatory response', *Rev Esp Cardiol,* 62(5), pp. 552-62.

Basagiannis, D., Zografou, S., Murphy, C., Fotsis, T., Morbidelli, L., Ziche, M., Bleck, C., Mercer, J. and Christoforidis, S. (2016) 'VEGF induces signalling and angiogenesis by directing VEGFR2 internalisation through macropinocytosis', *J Cell Sci,* 129(21), pp. 4091-4104.

Bates, D. O., Hillman, N. J., Williams, B., Neal, C. R. and Pocock, T. M. (2002) 'Regulation of microvascular permeability by vascular endothelial growth factors', *J Anat,* 200(6), pp. 581-97.

Baum, L. G., Seilhamer, J. J., Pang, M., Levine, W. B., Beynon, D. and Berliner, J. A. (1995) 'Synthesis of an endogeneous lectin, galectin-1, by human endothelial cells is up-regulated by endothelial cell activation', *Glycoconj J,* 12(1), pp. 63-8.

Baumann, K. H., du Bois, A., Meier, W., Rau, J., Wimberger, P., Sehouli, J., Kurzeder, C., Hilpert, F., Hasenburg, A., Canzler, U., Hanker, L. C., Hillemanns, P., Richter, B., Wollschlaeger, K., Dewitz, T., Bauerschlag, D. and Wagner, U. (2012) 'A phase II trial (AGO 2.11) in platinum-resistant ovarian cancer: a randomized multicenter trial with sunitinib (SU11248) to evaluate dosage, schedule, tolerability, toxicity and effectiveness of a multitargeted receptor tyrosine kinase inhibitor monotherapy', *Ann Oncol,* 23(9), pp. 2265-2271.

Beral, V., Bull, D., Green, J. and Reeves, G. (2007) 'Ovarian cancer and hormone replacement therapy in the Million Women Study', *Lancet,* 369(9574), pp. 1703-10.

Bernard-Patrzynski, F., Lécuyer, M. A., Puscas, I., Boukhatem, I., Charabati, M., Bourbonnière, L., Ramassamy, C., Leclair, G., Prat, A. and Roullin, V. G. (2019) 'Isolation of endothelial cells, pericytes and astrocytes from mouse brain', *PLoS One,* 14(12), pp. e0226302.

Bi, S., Earl, L. A., Jacobs, L. and Baum, L. G. (2008) 'Structural features of galectin-9 and galectin-1 that determine distinct T cell death pathways', *J Biol Chem,* 283(18), pp. 12248-58.

Bocci, G., Fasciani, A., Danesi, R., Viacava, P., Genazzani, A. R. and Del Tacca, M. (2001) 'In-vitro evidence of autocrine secretion of vascular endothelial growth factor by endothelial cells from human placental blood vessels', *Mol Hum Reprod,* 7(8), pp. 771-7.

Bodnar, J., Szekrenyes, A., Szigeti, M., Jarvas, G., Krenkova, J., Foret, F. and Guttman, A. (2016) 'Enzymatic removal of N-glycans by PNGase F coated magnetic microparticles', *Electrophoresis,* 37(10), pp. 1264-9.

Bouïs, D., Kusumanto, Y., Meijer, C., Mulder, N. H. and Hospers, G. A. (2006) 'A review on pro- and anti-angiogenic factors as targets of clinical intervention', *Pharmacol Res,* 53(2), pp. 89-103.

Bray, F., Ferlay, J., Soerjomataram, I., Siegel, R. L., Torre, L. A. and Jemal, A. (2018) 'Global cancer statistics 2018: GLOBOCAN estimates of incidence and mortality worldwide for 36 cancers in 185 countries', *CA Cancer J Clin,* 68(6), pp. 394-424.

Bredholt, G., Mannelqvist, M., Stefansson, I. M., Birkeland, E., Bø, T. H., Øyan, A. M., Trovik, J., Kalland, K. H., Jonassen, I., Salvesen, H. B., Wik, E. and Akslen, L. A. (2015) 'Tumor necrosis is an important hallmark of aggressive endometrial cancer and associates with hypoxia, angiogenesis and inflammation responses', *Oncotarget,* 6(37), pp. 39676-91.

Breitling, J. and Aebi, M. (2013) 'N-linked protein glycosylation in the endoplasmic reticulum', *Cold Spring Harb Perspect Biol,* 5(8), pp. a013359.

British Gynaecological Cancer Society. (2014) *British Gynaecological Cancer Society (BGCS) Epithelial Ovarian / Fallopian Tube / Primary Peritoneal Cancer Guidelines: Recommendations for Practice.* Available from: https://www.bgcs.org.uk/wp-content/uploads/2019/05/BGCS-Guidelines-Ovarian-Guidelines-2017.pdf. Accessed: May 2021.

Burger, R. A., Brady, M. F., Bookman, M. A., Fleming, G. F., Monk, B. J., Huang, H., Mannel, R. S., Homesley, H. D., Fowler, J., Greer, B. E., Boente, M., Birrer, M. J. and Liang, S. X. (2011) 'Incorporation of bevacizumab in the primary treatment of ovarian cancer', *N Engl J Med,* 365(26), pp. 2473-83.

Burrell, K., Gelareh, Z. (2012) Molecular Mechanisms of Tumor Angiogenesis, IntechOpen. Available from: https://www.intechopen.com/chapters/28610.

Butler, M. J., Down, C. J., Foster, R. R. and Satchell, S. C. (2020) 'The Pathological Relevance of Increased Endothelial Glycocalyx Permeability', *Am J Pathol,* 190(4), pp. 742-751.

Camby, I., Le Mercier, M., Lefranc, F. and Kiss, R. (2006) 'Galectin-1: a small protein with major functions', *Glycobiology,* 16(11), pp. 137r-157r.

Campbell, H. K., Maiers, J. L. and DeMali, K. A. (2017) 'Interplay between tight junctions & adherens junctions', *Exp Cell Res,* 358(1), pp. 39-44.

Cantatore, F. P., Maruotti, N., Corrado, A. and Ribatti, D. (2017) 'Angiogenesis Dysregulation in the Pathogenesis of Systemic Sclerosis', *Biomed Res Int,* 2017, pp. 5345673.

Cardenas, C., Alvero, A. B., Yun, B. S. and Mor, G. (2016) 'Redefining the origin and evolution of ovarian cancer: a hormonal connection', *Endocr Relat Cancer,* 23(9), pp. R411-22.

Casey, R. C. and Skubitz, A. P. (2000) 'CD44 and beta1 integrins mediate ovarian carcinoma cell migration toward extracellular matrix proteins', *Clin Exp Metastasis,* 18(1), pp. 67-75.

Cendrowski, J., Mamińska, A. and Miaczynska, M. (2016) 'Endocytic regulation of cytokine receptor signaling', *Cytokine Growth Factor Rev,* 32, pp. 63-73.

Chandler, K. B. and Costello, C. E. (2016) 'Glycomics and glycoproteomics of membrane proteins and cell-surface receptors: Present trends and future opportunities', *Electrophoresis,* 37(11), pp. 1407-19.

Chandler, K. B., Costello, C. E. and Rahimi, N. (2019) 'Glycosylation in the Tumor Microenvironment: Implications for Tumor Angiogenesis and Metastasis', *Cells,* 8(6).

Chandler, K. B., Leon, D. R., Kuang, J., Meyer, R. D., Rahimi, N. and Costello, C. E. (2019) 'N-Glycosylation regulates ligand-dependent activation and signaling of vascular endothelial growth factor receptor 2 (VEGFR2)', *J Biol Chem,* 294(35), pp. 13117-13130.

Chang, V. T., Crispin, M., Aricescu, A. R., Harvey, D. J., Nettleship, J. E., Fennelly, J. A., Yu, C., Boles, K. S., Evans, E. J., Stuart, D. I., Dwek, R. A., Jones, E. Y., Owens, R. J. and Davis, S. J. (2007) 'Glycoprotein structural genomics: solving the glycosylation problem', *Structure,* 15(3), pp. 267-73.

Chang, Y. S., di Tomaso, E., McDonald, D. M., Jones, R., Jain, R. K. and Munn, L. L. (2000) 'Mosaic blood vessels in tumors: frequency of cancer cells in contact with flowing blood', *Proc Natl Acad Sci U S A,* 97(26), pp. 14608-13.

Chekerov, R., Hilpert, F., Mahner, S., El-Balat, A., Harter, P., De Gregorio, N., Fridrich, C., Markmann, S., Potenberg, J., Lorenz, R., Oskay-Oezcelik, G., Schmidt, M., Krabisch, P., Lueck, H. J., Richter, R., Braicu, E. I., du Bois, A. and Sehouli, J. (2018) 'Sorafenib plus topotecan versus placebo plus topotecan for platinum-resistant ovarian cancer (TRIAS): a multicentre, randomised, double-blind, placebo-controlled, phase 2 trial', *Lancet Oncol,* 19(9), pp. 1247-1258.

Chen, H. (2018) 'Role of thromboxane A(2) signaling in endothelium-dependent contractions of arteries', *Prostaglandins Other Lipid Mediat,* 134, pp. 32-37.

Chen, H. F. and Wu, K. J. (2016) 'Endothelial Transdifferentiation of Tumor Cells Triggered by the Twist1-Jagged1-KLF4 Axis: Relationship between Cancer Stemness and Angiogenesis', *Stem Cells Int,* 2016, pp. 6439864.

Chen, L., Yao, Y., Sun, L., Zhou, J., Liu, J., Wang, J., Li, J. and Tang, J. (2015) 'Clinical implication of the serum galectin-1 expression in epithelial ovarian cancer patients', *J Ovarian Res,* 8, pp. 78.

Chen, R., Li, J., Feng, C. H., Chen, S. K., Liu, Y. P., Duan, C. Y., Li, H., Xia, X. M., He, T., Wei, M. and Dai, R. Y. (2013) 'c-Met function requires N-linked glycosylation modification of pro-Met', *J Cell Biochem,* 114(4), pp. 816-22.

Cheng, K. W., Lahad, J. P., Kuo, W. L., Lapuk, A., Yamada, K., Auersperg, N., Liu, J., Smith-McCune, K., Lu, K. H., Fishman, D., Gray, J. W. and Mills, G. B. (2004) 'The RAB25 small GTPase determines aggressiveness of ovarian and breast cancers', *Nat Med,* 10(11), pp. 1251-6.

Chistiakov, D. A., Orekhov, A. N. and Bobryshev, Y. V. (2017) 'Effects of shear stress on endothelial cells: go with the flow', *Acta Physiol (Oxf),* 219(2), pp. 382-408.

Cho, J. A., Park, H., Lim, E. H., Kim, K. H., Choi, J. S., Lee, J. H., Shin, J. W. and Lee, K. W. (2011) 'Exosomes from ovarian cancer cells induce adipose tissue-derived mesenchymal stem cells to acquire the physical and functional characteristics of tumor-supporting myofibroblasts', *Gynecol Oncol,* 123(2), pp. 379-86.

Choi, H. Y., Park, H., Hong, J. K., Kim, S. D., Kwon, J. Y., You, S., Do, J., Lee, D. Y., Kim, H. H. and Kim, D. I. (2018) 'N-glycan Remodeling Using Mannosidase Inhibitors to Increase High-mannose Glycans on Acid α-Glucosidase in Transgenic Rice Cell Cultures', *Sci Rep,* 8(1), pp. 16130.

Choi, J. H., Wong, A. S., Huang, H. F. and Leung, P. C. (2007) 'Gonadotropins and ovarian cancer', *Endocr Rev,* 28(4), pp. 440-61.

Christiansen, M. N., Chik, J., Lee, L., Anugraham, M., Abrahams, J. L. and Packer, N. H. (2014) 'Cell surface protein glycosylation in cancer', *Proteomics,* 14(4-5), pp. 525-46.

Chua, R. A. and Arbiser, J. L. (2009) 'The role of angiogenesis in the pathogenesis of psoriasis', *Autoimmunity,* 42(7), pp. 574-9.

Chung-Welch, N., Patton, W. F., Shepro, D. and Cambria, R. P. (1997) 'Two-stage isolation procedure for obtaining homogenous populations of microvascular endothelial and mesothelial cells from human omentum', *Microvasc Res,* 54(2), pp. 121-34.

Clausse, N., van den Brûle, F., Waltregny, D., Garnier, F. and Castronovo, V. (1999) 'Galectin-1 expression in prostate tumor-associated capillary endothelial cells is increased by prostate carcinoma cells and modulates heterotypic cell-cell adhesion', *Angiogenesis,* 3(4), pp. 317-25.

Coenen, D. M., Mastenbroek, T. G. and Cosemans, J. (2017) 'Platelet interaction with activated endothelium: mechanistic insights from microfluidics', *Blood,* 130(26), pp. 2819-2828.

Collins, D., Hogan, A. M., O'Shea, D. and Winter, D. C. (2009) 'The omentum: anatomical, metabolic, and surgical aspects', *J Gastrointest Surg,* 13(6), pp. 1138-46.

Cooper, D., Norling, L. V. and Perretti, M. (2008) 'Novel insights into the inhibitory effects of Galectin-1 on neutrophil recruitment under flow', *J Leukoc Biol,* 83(6), pp. 1459-66.

Coso, S., Zeng, Y., Opeskin, K. and Williams, E. D. (2012) 'Vascular endothelial growth factor receptor-3 directly interacts with phosphatidylinositol 3-kinase to regulate lymphangiogenesis', *PLoS One,* 7(6), pp. e39558.

Cossarizza, A. and Chang, H.-D. and Radbruch, A. and Akdis, M. and Andrä, I. and Annunziato, F. and Bacher, P. and Barnaba, V. and Battistini, L. and Bauer, W. M. and Baumgart, S. and Becher, B. and Beisker, W. and Berek, C. and Blanco, A. and Borsellino, G. and Boulais, P. E. and Brinkman, R. R. and Büscher, M. and Busch, D. H. and Bushnell, T. P. and Cao, X. and Cavani, A. and Chattopadhyay, P. K. and Cheng, Q. and Chow, S. and Clerici, M. and Cooke, A. and Cosma, A. and Cosmi, L. and Cumano, A. and Dang, V. D. and Davies, D. and De Biasi, S. and Del Zotto, G. and Della Bella, S. and Dellabona, P. and Deniz, G. and Dessing, M. and Diefenbach, A. and Di Santo, J. and Dieli, F. and Dolf, A. and Donnenberg, V. S. and Dörner, T. and Ehrhardt, G. R. A. and Endl, E. and Engel, P. and Engelhardt, B. and Esser, C. and Everts, B. and Dreher, A. and Falk, C. S. and Fehniger, T. A. and Filby, A. and Fillatreau, S. and Follo, M. and Förster, I. and Foster, J. and Foulds, G. A. and Frenette, P. S. and Galbraith, D. and Garbi, N. and García-Godoy, M. D. and Geginat, J. and Ghoreschi, K. and Gibellini, L. and Goettlinger, C. and Goodyear, C. S. and Gori, A. and Grogan, J. and Gross, M. and Grützkau, A. and Grummitt, D. and Hahn, J. and Hammer, Q. and Hauser, A. E. and Haviland, D. L. and Hedley, D. and Herrera, G. and Herrmann, M. and Hiepe, F. and Holland, T. and Hombrink, P. and Houston, J. P. and Hoyer, B. F. and Huang, B. and Hunter, C. A. and Iannone, A. and Jäck, H.-M. and Jávega, B. and Jonjic, S. and Juelke, K. and Jung, S. and Kaiser, T. and Kalina, T. and Keller, B. and Khan, S. and Kienhöfer, D. and Kroneis, T. and Kunkel, D. and Kurts, C. and Kvistborg, P. and Lannigan, J. and Lantz, O. and Larbi, A. and LeibundGut-Landmann, S. and Leipold, M. D. and Levings, M. K. and Litwin, V. and Liu, Y. and Lohoff, M. and Lombardi, G. and Lopez, L. and Lovett-Racke, A. and Lubberts, E. and Ludewig, B. and Lugli, E. and Maecker, H. T. and Martrus, G. and Matarese, G. and Maueröder, C. and McGrath, M. and McInnes, I. and Mei, H. E. and Melchers, F. and Melzer, S. and Mielenz, D. and Mills, K. and Mirrer, D. and Mjösberg, J. and Moore, J. and Moran, B. and Moretta, A. and Moretta, L. and Mosmann, T. R. and Müller, S. and Müller, W. and Münz, C. and Multhoff, G. and Munoz, L. E. and Murphy, K. M. and Nakayama, T. and Nasi, M. and Neudörfl, C. and Nolan, J. and Nourshargh, S. and O'Connor, J.-E. and Ouyang, W. and Oxenius, A. and Palankar, R. and Panse, I. and Peterson, P. and Peth, C. and Petriz, J. and Philips, D. and Pickl, W. and Piconese, S. and Pinti, M. and Pockley, A. G. and Podolska, M. J. and Pucillo, C. and Quataert, S. A. and Radstake, T. R. D. J. and Rajwa, B.

and Rebhahn, J. A. and Recktenwald, D. and Remmerswaal, E. B. M. and Rezvani, K. and Rico, L. G. and Robinson, J. P. and Romagnani, C. and Rubartelli, A. and Ruckert, B. and Ruland, J. and Sakaguchi, S. and Sala-de-Oyanguren, F. and Samstag, Y. and Sanderson, S. and Sawitzki, B. and Scheffold, A. and Schiemann, M. and Schildberg, F. and Schimisky, E. and Schmid, S. A. and Schmitt, S. and Schober, K. and Schüler, T. and Schulz, A. R. and Schumacher, T. and Scotta, C. and Shankey, T. V. and Shemer, A. and Simon, A.-K. and Spidlen, J. and Stall, A. M. and Stark, R. and Stehle, C. and Stein, M. and Steinmetz, T. and Stockinger, H. and Takahama, Y. and Tarnok, A. and Tian, Z. and Toldi, G. and Tornack, J. and Traggiai, E. and Trotter, J. and Ulrich, H. and van der Braber, M. and van Lier, R. A. W. and Veldhoen, M. and Vento-Asturias, S. and Vieira, P. and Voehringer, D. and Volk, H.-D. and von Volkmann, K. and Waisman, A. and Walker, R. and Ward, M. D. and Warnatz, K. and Warth, S. and Watson, J. V. and Watzl, C. and Wegener, L. and Wiedemann, A. and Wienands, J. and Willimsky, G. and Wing, J. and Wurst, P. and Yu, L. and Yue, A. and Zhang, Q. and Zhao, Y. and Ziegler, S. and Zimmermann, J. (2017) 'Guidelines for the use of flow cytometry and cell sorting in immunological studies', *European Journal of Immunology,* 47(10), pp. 1584-1797.

Cousin, J. M. and Cloninger, M. J. (2016) 'The Role of Galectin-1 in Cancer Progression, and Synthetic Multivalent Systems for the Study of Galectin-1', *Int J Mol Sci,* 17(9).

Croci, D. O., Cerliani, J. P., Dalotto-Moreno, T., Méndez-Huergo, S. P., Mascanfroni, I. D., Dergan-Dylon, S., Toscano, M. A., Caramelo, J. J., García-Vallejo, J. J., Ouyang, J., Mesri, E. A., Junttila, M. R., Bais, C., Shipp, M. A., Salatino, M. and Rabinovich, G. A. (2014) 'Glycosylation-dependent lectin-receptor interactions preserve angiogenesis in anti-VEGF refractory tumors', *Cell,* 156(4), pp. 744-58.

Croci, D. O., Mendez-Huergo, S. P., Cerliani, J. P. and Rabinovich, G. A. (2018) 'Immune-Mediated and Hypoxia-Regulated Programs: Accomplices in Resistance to Anti-angiogenic Therapies', *Handb Exp Pharmacol,* 249, pp. 31-61.

Croci, D. O., Salatino, M., Rubinstein, N., Cerliani, J. P., Cavallin, L. E., Leung, H. J., Ouyang, J., Ilarregui, J. M., Toscano, M. A., Domaica, C. I., Croci, M. C., Shipp, M. A., Mesri, E. A., Albini, A. and Rabinovich, G. A. (2012) 'Disrupting galectin-1 interactions with N-glycans suppresses hypoxia-driven angiogenesis and tumorigenesis in Kaposi's sarcoma', *J Exp Med,* 209(11), pp. 1985-2000.

Crouch, E. E. and Doetsch, F. (2018) 'FACS isolation of endothelial cells and pericytes from mouse brain microregions', *Nat Protoc,* 13(4), pp. 738-751.

Cui, L., Kwong, J. and Wang, C. C. (2015) 'Prognostic value of circulating tumor cells and disseminated tumor cells in patients with ovarian cancer: a systematic review and meta-analysis', *J Ovarian Res,* 8, pp. 38.

D'Amico, G., Muñoz-Félix, J. M., Pedrosa, A. R. and Hodivala-Dilke, K. M. (2020) '"Splitting the matrix": intussusceptive angiogenesis meets MT1-MMP', *EMBO Mol Med,* 12(2), pp. e11663.

D'Haene, N., Sauvage, S., Maris, C., Adanja, I., Le Mercier, M., Decaestecker, C., Baum, L. and Salmon, I. (2013) 'VEGFR1 and VEGFR2 involvement in extracellular galectin-1- and galectin-3-induced angiogenesis', *PLoS One,* 8(6), pp. e67029.

Dai, L., Song, K. and Di, W. (2020) 'Adipocytes: active facilitators in epithelial ovarian cancer progression?', *J Ovarian Res,* 13(1), pp. 115.

Dallas, N. A., Samuel, S., Xia, L., Fan, F., Gray, M. J., Lim, S. J. and Ellis, L. M. (2008) 'Endoglin (CD105): a marker of tumor vasculature and potential target for therapy', *Clin Cancer Res,* 14(7), pp. 1931-7.

Dalotto-Moreno, T., Croci, D. O., Cerliani, J. P., Martinez-Allo, V. C., Dergan-Dylon, S., Méndez-Huergo, S. P., Stupirski, J. C., Mazal, D., Osinaga, E., Toscano, M. A., Sundblad, V., Rabinovich, G. A. and Salatino, M. (2013) 'Targeting galectin-1 overcomes breast cancer-associated immunosuppression and prevents metastatic disease', *Cancer Res,* 73(3), pp. 1107-17.

Daniilidis, A. and Karagiannis, V. (2007) 'Epithelial ovarian cancer. Risk factors, screening and the role of prophylactic oophorectomy', *Hippokratia,* 11(2), pp. 63-6.

de-Freitas-Junior, J. C. M., Andrade-da-Costa, J., Silva, M. C. and Pinho, S. S. (2017) 'Glycans as Regulatory Elements of the Insulin/IGF System: Impact in Cancer Progression', *Int J Mol Sci,* 18(9).

Deng, K., Yang, C., Tan, Q., Song, W., Lu, M., Zhao, W., Lou, G., Li, Z., Li, K. and Hou, Y. (2018) 'Sites of distant metastases and overall survival in ovarian cancer: A study of 1481 patients', *Gynecol Oncol,* 150(3), pp. 460-465.

Di Nicola, V. (2019) 'Omentum a powerful biological source in regenerative surgery', *Regen Ther,* 11, pp. 182-191.

Ding, D. C., Chen, W., Wang, J. H. and Lin, S. Z. (2018) 'Association between polycystic ovarian syndrome and endometrial, ovarian, and breast cancer: A population-based cohort study in Taiwan', *Medicine (Baltimore),* 97(39), pp. e12608.

Dixon-Suen, S. C. and Nagle, C. M. and Thrift, A. P. and Pharoah, P. D. P. and Ewing, A. and Pearce, C. L. and Zheng, W. and Chenevix-Trench, G. and Fasching, P. A. and Beckmann, M. W. and Lambrechts, D. and Vergote, I. and Lambrechts, S. and Van Nieuwenhuysen, E. and Rossing, M. A. and Doherty, J. A. and Wicklund, K. G. and Chang-Claude, J. and Jung, A. Y. and Moysich, K. B. and Odunsi, K. and Goodman, M. T. and Wilkens, L. R. and Thompson, P. J. and Shvetsov, Y. B. and Dörk, T. and Park-Simon, T. W. and Hillemanns, P. and Bogdanova, N. and Butzow, R. and Nevanlinna, H. and Pelttari, L. M. and Leminen, A. and Modugno, F. and Ness, R. B. and Edwards, R. P. and

Kelley, J. L. and Heitz, F. and du Bois, A. and Harter, P. and Schwaab, I. and Karlan, B. Y. and Lester, J. and Orsulic, S. and Rimel, B. J. and Kjær, S. K. and Høgdall, E. and Jensen, A. and Goode, E. L. and Fridley, B. L. and Cunningham, J. M. and Winham, S. J. and Giles, G. G. and Bruinsma, F. and Milne, R. L. and Southey, M. C. and Hildebrandt, M. A. T. and Wu, X. and Lu, K. H. and Liang, D. and Levine, D. A. and Bisogna, M. and Schildkraut, J. M. and Berchuck, A. and Cramer, D. W. and Terry, K. L. and Bandera, E. V. and Olson, S. H. and Salvesen, H. B. and Thomsen, L. C. V. and Kopperud, R. K. and Bjorge, L. and Kiemeney, L. A. and Massuger, L. and Pejovic, T. and Bruegl, A. and Cook, L. S. and Le, N. D. and Swenerton, K. D. and Brooks-Wilson, A. and Kelemen, L. E. and Lubiński, J. and Huzarski, T. and Gronwald, J. and Menkiszak, J. and Wentzensen, N. and Brinton, L. and Yang, H. and Lissowska, J. and Høgdall, C. K. and Lundvall, L. and Song, H. and Tyrer, J. P. and Campbell, I. and Eccles, D. and Paul, J. and Glasspool, R. and Siddiqui, N. and Whittemore, A. S. and Sieh, W. and McGuire, V. and Rothstein, J. H. and Narod, S. A. and Phelan, C. and Risch, H. A. and McLaughlin, J. R. and Anton-Culver, H. and Ziogas, A. and Menon, U. and Gayther, S. A. and Ramus, S. J. and Gentry-Maharaj, A. and Wu, A. H. and Pike, M. C. and Tseng, C. C. and Kupryjanczyk, J. and Dansonka-Mieszkowska, A. and Budzilowska, A. and Rzepecka, I. K. and Webb, P. M. (2018) 'Adult height is associated with increased risk of ovarian cancer: a Mendelian randomisation study', *Br J Cancer,* 118(8), pp. 1123-1129.

Douaisi, M., Resop, R. S., Nagasawa, M., Craft, J., Jamieson, B. D., Blom, B. and Uittenbogaart, C. H. (2017) 'CD31, a Valuable Marker to Identify Early and Late Stages of T Cell Differentiation in the Human Thymus', *J Immunol,* 198(6), pp. 2310-2319.

Doufekas, K. and Olaitan, A. (2014) 'Clinical epidemiology of epithelial ovarian cancer in the UK', *Int J Womens Health,* 6, pp. 537-45.

Dougher, M. and Terman, B. I. (1999) 'Autophosphorylation of KDR in the kinase domain is required for maximal VEGF-stimulated kinase activity and receptor internalization', *Oncogene,* 18(8), pp. 1619-27.

du Bois, A., Floquet, A., Kim, J. W., Rau, J., del Campo, J. M., Friedlander, M., Pignata, S., Fujiwara, K., Vergote, I., Colombo, N., Mirza, M. R., Monk, B. J., Kimmig, R., Ray-Coquard, I., Zang, R., Diaz-Padilla, I., Baumann, K. H., Mouret-Reynier, M. A., Kim, J. H., Kurzeder, C., Lesoin, A., Vasey, P., Marth, C., Canzler, U., Scambia, G., Shimada, M., Calvert, P., Pujade-Lauraine, E., Kim, B. G., Herzog, T. J., Mitrica, I., Schade-Brittinger, C., Wang, Q., Crescenzo, R. and Harter, P. (2014) 'Incorporation of pazopanib in maintenance therapy of ovarian cancer', *J Clin Oncol,* 32(30), pp. 3374-82.

du Bois, A., Kristensen, G., Ray-Coquard, I., Reuss, A., Pignata, S., Colombo, N., Denison, U., Vergote, I., Del Campo, J. M., Ottevanger, P., Heubner, M., Minarik, T., Sevin, E., de Gregorio, N., Bidziński, M., Pfisterer, J., Malander, S., Hilpert, F., Mirza, M. R., Scambia, G., Meier, W., Nicoletto, M. O., Bjørge, L., Lortholary, A., Sailer, M. O., Merger, M. and Harter, P. (2016) 'Standard first-line chemotherapy with or without nintedanib for advanced ovarian cancer (AGO-OVAR 12): a randomised, double-blind, placebo-controlled phase 3 trial', *Lancet Oncol,* 17(1), pp. 78-89.

Du, W., Gerald, D., Perruzzi, C. A., Rodriguez-Waitkus, P., Enayati, L., Krishnan, B., Edmonds, J., Hochman, M. L., Lev, D. C. and Phung, T. L. (2013) 'Vascular tumors have increased p70 S6-kinase activation and are inhibited by topical rapamycin', *Lab Invest,* 93(10), pp. 1115-27.

Duchesne, L., Tissot, B., Rudd, T. R., Dell, A. and Fernig, D. G. (2006) 'N-glycosylation of fibroblast growth factor receptor 1 regulates ligand and heparan sulfate co-receptor binding', *J Biol Chem,* 281(37), pp. 27178-89.

Duluc, D., Delneste, Y., Tan, F., Moles, M. P., Grimaud, L., Lenoir, J., Preisser, L., Anegon, I., Catala, L., Ifrah, N., Descamps, P., Gamelin, E., Gascan, H., Hebbar, M. and Jeannin, P. (2007) 'Tumor-associated leukemia inhibitory factor and IL-6 skew monocyte differentiation into tumor-associated macrophage-like cells', *Blood,* 110(13), pp. 4319-30.

Elola, M. T., Chiesa, M. E., Alberti, A. F., Mordoh, J. and Fink, N. E. (2005) 'Galectin-1 receptors in different cell types', *J Biomed Sci,* 12(1), pp. 13-29.

Elshabrawy, H. A., Chen, Z., Volin, M. V., Ravella, S., Virupannavar, S. and Shahrara, S. (2015) 'The pathogenic role of angiogenesis in rheumatoid arthritis', *Angiogenesis,* 18(4), pp. 433-48.

Ewan, L. C., Jopling, H. M., Jia, H., Mittar, S., Bagherzadeh, A., Howell, G. J., Walker, J. H., Zachary, I. C. and Ponnambalam, S. (2006) 'Intrinsic tyrosine kinase activity is required for vascular endothelial growth factor receptor 2 ubiquitination, sorting and degradation in endothelial cells', *Traffic,* 7(9), pp. 1270-82.

Fadini, G. P., Albiero, M., Bonora, B. M. and Avogaro, A. (2019) 'Angiogenic Abnormalities in Diabetes Mellitus: Mechanistic and Clinical Aspects', *J Clin Endocrinol Metab,* 104(11), pp. 5431-5444.

Fathalla, M. F. (2013) 'Incessant ovulation and ovarian cancer - a hypothesis re-visited', *Facts Views Vis Obgyn,* 5(4), pp. 292-7.

Fernández-Cortés, M., Delgado-Bellido, D. and Oliver, F. J. (2019) 'Vasculogenic Mimicry: Become an Endothelial Cell "But Not So Much"', *Front Oncol,* 9, pp. 803.

Figueroa, X. F. and Duling, B. R. (2009) 'Gap junctions in the control of vascular function', *Antioxid Redox Signal,* 11(2), pp. 251-66.

Fitzgerald, G., Soro-Arnaiz, I. and De Bock, K. (2018) 'The Warburg Effect in Endothelial Cells and its Potential as an Anti-angiogenic Target in Cancer', *Front Cell Dev Biol,* 6, pp. 100.

Fleming, J. S., Beaugié, C. R., Haviv, I., Chenevix-Trench, G. and Tan, O. L. (2006) 'Incessant ovulation, inflammation and epithelial ovarian carcinogenesis: revisiting old hypotheses', *Mol Cell Endocrinol,* 247(1-2), pp. 4-21.

Foster, D. S., Marshall, C. D., Gulati, G. S., Chinta, M. S., Nguyen, A., Salhotra, A., Jones, R. E., Burcham, A., Lerbs, T., Cui, L., King, M. E., Titan, A. L., Ransom, R. C., Manjunath, A., Hu, M. S., Blackshear, C. P., Mascharak, S., Moore, A. L., Norton, J. A., Kin, C. J., Shelton, A. A., Januszyk, M., Gurtner, G. C., Wernig, G. and Longaker, M. T. (2020) 'Elucidating the fundamental fibrotic processes driving abdominal adhesion formation', *Nat Commun,* 11(1), pp. 4061.

Francis, G. L. (2010) 'Albumin and mammalian cell culture: implications for biotechnology applications', *Cytotechnology,* 62(1), pp. 1-16.

Fujimoto, N., He, Y., D'Addio, M., Tacconi, C., Detmar, M. and Dieterich, L. C. (2020) 'Single-cell mapping reveals new markers and functions of lymphatic endothelial cells in lymph nodes', *PLoS Biol,* 18(4), pp. e3000704.

Fung, K. Y. Y., Fairn, G. D. and Lee, W. L. (2018) 'Transcellular vesicular transport in epithelial and endothelial cells: Challenges and opportunities', *Traffic,* 19(1), pp. 5-18.

Funston, G., Hamilton, W., Abel, G., Crosbie, E. J., Rous, B. and Walter, F. M. (2020) 'The diagnostic performance of CA125 for the detection of ovarian and non-ovarian cancer in primary care: A population-based cohort study', *PLoS Med,* 17(10), pp. e1003295.

Galley, H. F. and Webster, N. R. (2004) 'Physiology of the endothelium', *Br J Anaesth,* 93(1), pp. 105-13.

Galustian, C., Foulds, S., Dye, J. F. and Guillou, P. J. (1994) 'Swainsonine, a glycosylation inhibitor, enhances both lymphocyte efficacy and tumour susceptibility in LAK and NK cytotoxicity', *Immunopharmacology,* 27(2), pp. 165-72.

Garcia, A. and Singh, H. (2013) 'Bevacizumab and ovarian cancer', *Ther Adv Med Oncol,* 5(2), pp. 133-41.

Gavalas, N. G., Liontos, M., Trachana, S. P., Bagratuni, T., Arapinis, C., Liacos, C., Dimopoulos, M. A. and Bamias, A. (2013) 'Angiogenesis-related pathways in the pathogenesis of ovarian cancer', *Int J Mol Sci,* 14(8), pp. 15885-909.

Girotti, M. R., Salatino, M., Dalotto-Moreno, T. and Rabinovich, G. A. (2020) 'Sweetening the hallmarks of cancer: Galectins as multifunctional mediators of tumor progression', *J Exp Med,* 217(2).

Gittens, B. R., Bodkin, J. V., Nourshargh, S., Perretti, M. and Cooper, D. (2017) 'Galectin-3: A Positive Regulator of Leukocyte Recruitment in the Inflamed Microcirculation', *J Immunol,* 198(11), pp. 4458-4469.

Goncharov, N. V., Nadeev, A. D., Jenkins, R. O. and Avdonin, P. V. (2017) 'Markers and Biomarkers of Endothelium: When Something Is Rotten in the State', *Oxid Med Cell Longev,* 2017, pp. 9759735.

Gordon, E. J., Fukuhara, D., Weström, S., Padhan, N., Sjöström, E. O., van Meeteren, L., He, L., Orsenigo, F., Dejana, E., Bentley, K., Spurkland, A. and Claesson-Welsh, L. (2016) 'The endothelial adaptor molecule TSAd is required for VEGF-induced angiogenic sprouting through junctional c-Src activation', *Sci Signal,* 9(437), pp. ra72.

Goss, P. E., Baker, M. A., Carver, J. P. and Dennis, J. W. (1995) 'Inhibitors of carbohydrate processing: A new class of anticancer agents', *Clin Cancer Res,* 1(9), pp. 935-44.

Gourlaouen, M., Welti, J. C., Vasudev, N. S. and Reynolds, A. R. (2013) 'Essential role for endocytosis in the growth factor-stimulated activation of ERK1/2 in endothelial cells', *J Biol Chem,* 288(11), pp. 7467-7480.

Grassadonia, A., Tinari, N., Iurisci, I., Piccolo, E., Cumashi, A., Innominato, P., D'Egidio, M., Natoli, C., Piantelli, M. and Iacobelli, S. (2002) '90K (Mac-2 BP) and galectins in tumor progression and metastasis', *Glycoconj J,* 19(7-9), pp. 551-6.

Griffioen, A. W. and Thijssen, V. L. (2014) 'Galectins in tumor angiogenesis', *Ann Transl Med,* 2(9), pp. 90.

Guven, G., Hilty, M. P. and Ince, C. 'Microcirculation: Physiology, Pathophysiology, and Clinical Application'.

Hadjipanayi, E., Kuhn, P. H., Moog, P., Bauer, A. T., Kuekrek, H., Mirzoyan, L., Hummel, A., Kirchhoff, K., Salgin, B., Isenburg, S., Dornseifer, U., Ninkovic, M., Machens, H. G. and Schilling, A. F. (2015) 'The Fibrin Matrix Regulates Angiogenic Responses within the Hemostatic Microenvironment through Biochemical Control', *PLoS One,* 10(8), pp. e0135618.

Halama, A., Guerrouahen, B. S., Pasquier, J., Satheesh, N. J., Suhre, K. and Rafii, A. (2017) 'Nesting of colon and ovarian cancer cells in the endothelial niche is associated with alterations in glycan and lipid metabolism', *Scientific Reports,* 7(1), pp. 39999.

Hall, M., Bertelli, G., Li, L., Green, C., Chan, S., Yeoh, C. C., Hasan, J., Jones, R., Ograbek, A. and Perren, T. J. (2020) 'Role of front-line bevacizumab in advanced ovarian cancer: the OSCAR study', *Int J Gynecol Cancer,* 30(2), pp. 213-220.

Hamester, F., Legler, K., Wichert, B., Kelle, N., Eylmann, K., Rossberg, M., Ding, Y., Kürti, S., Schmalfeldt, B., Milde-Langosch, K. and Oliveira-Ferrer, L. (2019) 'Prognostic relevance of the Golgi mannosidase MAN1A1 in ovarian cancer: impact of N-glycosylation on tumour cell aggregation', *British Journal of Cancer,* 121(11), pp. 944-953.

Hamilos, M., Petousis, S. and Parthenakis, F. (2018) 'Interaction between platelets and endothelium: from pathophysiology to new therapeutic options', *Cardiovasc Diagn Ther,* 8(5), pp. 568-580.

Han, B., Li, X. and Yu, T. (2014) 'Cruciferous vegetables consumption and the risk of ovarian cancer: a meta-analysis of observational studies', *Diagn Pathol,* 9, pp. 7.

Hanahan, D. and Weinberg, R. A. (2011) 'Hallmarks of cancer: the next generation', *Cell,* 144(5), pp. 646-74.

Harper, S. J. and Bates, D. O. (2008) 'VEGF-A splicing: the key to anti-angiogenic therapeutics?', *Nat Rev Cancer,* 8(11), pp. 880-7.

Heerboth, S., Housman, G., Leary, M., Longacre, M., Byler, S., Lapinska, K., Willbanks, A. and Sarkar, S. (2015) 'EMT and tumor metastasis', *Clin Transl Med,* 4, pp. 6.

Heredia-Soto, V., López-Guerrero, J. A., Redondo, A. and Mendiola, M. (2020) 'The hallmarks of ovarian cancer: Focus on angiogenesis and micro-environment and new models for their characterisation', *EJC Suppl,* 15, pp. 49-55.

Hillen, F. and Griffioen, A. W. (2007) 'Tumour vascularization: sprouting angiogenesis and beyond', *Cancer Metastasis Rev,* 26(3-4), pp. 489-502.

Holmqvist, K., Cross, M. J., Rolny, C., Hägerkvist, R., Rahimi, N., Matsumoto, T., Claesson-Welsh, L. and Welsh, M. (2004) 'The adaptor protein shb binds to tyrosine 1175 in vascular endothelial growth factor (VEGF) receptor-2 and regulates VEGF-dependent cellular migration', *J Biol Chem,* 279(21), pp. 22267-75.

Hsieh, S. H., Ying, N. W., Wu, M. H., Chiang, W. F., Hsu, C. L., Wong, T. Y., Jin, Y. T., Hong, T. M. and Chen, Y. L. (2008) 'Galectin-1, a novel ligand of neuropilin-1, activates VEGFR-2 signaling and modulates the migration of vascular endothelial cells', *Oncogene,* 27(26), pp. 3746-53.

Huang, Z. and Bao, S. D. (2004) 'Roles of main pro- and anti-angiogenic factors in tumor angiogenesis', *World J Gastroenterol,* 10(4), pp. 463-70.

Huang, Z., Wu, T., Liu, A. Y. and Ouyang, G. (2015) 'Differentiation and transdifferentiation potentials of cancer stem cells', *Oncotarget,* 6(37), pp. 39550-63.

Hutley, L. J., Herington, A. C., Shurety, W., Cheung, C., Vesey, D. A., Cameron, D. P. and Prins, J. B. (2001) 'Human adipose tissue endothelial cells promote preadipocyte proliferation', *Am J Physiol Endocrinol Metab,* 281(5), pp. E1037-44.

Inouye, K., Mizutani, S., Koide, H. and Kaziro, Y. (2000) 'Formation of the Ras dimer is essential for Raf-1 activation', *J Biol Chem,* 275(6), pp. 3737-40.

Ito, K., Scott, S. A., Cutler, S., Dong, L. F., Neuzil, J., Blanchard, H. and Ralph, S. J. (2011) 'Thiodigalactoside inhibits murine cancers by concurrently blocking effects of galectin-1 on immune dysregulation, angiogenesis and protection against oxidative stress', *Angiogenesis,* 14(3), pp. 293-307.

Iwagoi, Y., Motohara, T., Hwang, S., Fujimoto, K., Ikeda, T. and Katabuchi, H. (2021) 'Omental metastasis as a predictive risk factor for unfavorable prognosis in patients with stage III-IV epithelial ovarian cancer', *Int J Clin Oncol*.

Jambusaria, A., Hong, Z., Zhang, L., Srivastava, S., Jana, A., Toth, P. T., Dai, Y., Malik, A. B. and Rehman, J. (2020) 'Endothelial heterogeneity across distinct vascular beds during homeostasis and inflammation', *Elife,* 9.

Jeltsch, M., Leppänen, V. M., Saharinen, P. and Alitalo, K. (2013) 'Receptor tyrosine kinase-mediated angiogenesis', *Cold Spring Harb Perspect Biol,* 5(9).

Jeon, E. S., Moon, H. J., Lee, M. J., Song, H. Y., Kim, Y. M., Cho, M., Suh, D. S., Yoon, M. S., Chang, C. L., Jung, J. S. and Kim, J. H. (2008) 'Cancer-derived lysophosphatidic acid stimulates differentiation of human mesenchymal stem cells to myofibroblast-like cells', *Stem Cells,* 26(3), pp. 789-97.

Jopling, H. M., Howell, G. J., Gamper, N. and Ponnambalam, S. (2011) 'The VEGFR2 receptor tyrosine kinase undergoes constitutive endosome-to-plasma membrane recycling', *Biochem Biophys Res Commun,* 410(2), pp. 170-6.

Jopling, H. M., Odell, A. F., Pellet-Many, C., Latham, A. M., Frankel, P., Sivaprasadarao, A., Walker, J. H., Zachary, I. C. and Ponnambalam, S. (2014) 'Endosome-to-Plasma Membrane Recycling of VEGFR2 Receptor Tyrosine Kinase Regulates Endothelial Function and Blood Vessel Formation', *Cells,* 3(2), pp. 363-85.

Jun, J. E., Rubio, I. and Roose, J. P. (2013) 'Regulation of ras exchange factors and cellular localization of ras activation by lipid messengers in T cells', *Front Immunol,* 4, pp. 239.

Kanda, A., Dong, Y., Noda, K., Saito, W. and Ishida, S. (2017) 'Advanced glycation endproducts link inflammatory cues to upregulation of galectin-1 in diabetic retinopathy', *Scientific Reports,* 7(1), pp. 16168.

Karar, J. and Maity, A. (2011) 'PI3K/AKT/mTOR Pathway in Angiogenesis', *Front Mol Neurosci,* 4, pp. 51.

Katopodis, P., Chudasama, D., Wander, G., Sales, L., Kumar, J., Pandhal, M., Anikin, V., Chatterjee, J., Hall, M. and Karteris, E. (2019) 'Kinase Inhibitors and Ovarian Cancer', *Cancers (Basel),* 11(9).

Kazerounian, S. and Lawler, J. (2018) 'Integration of pro- and anti-angiogenic signals by endothelial cells', *J Cell Commun Signal,* 12(1), pp. 171-179.

Kenny, H. A., Chiang, C. Y., White, E. A., Schryver, E. M., Habis, M., Romero, I. L., Ladanyi, A., Penicka, C. V., George, J., Matlin, K., Montag, A., Wroblewski, K., Yamada, S. D., Mazar, A. P., Bowtell, D. and Lengyel, E. (2014) 'Mesothelial cells promote early ovarian cancer metastasis through fibronectin secretion', *J Clin Invest,* 124(10), pp. 4614-28.

Kern, P. A., Knedler, A. and Eckel, R. H. (1983) 'Isolation and culture of microvascular endothelium from human adipose tissue', *J Clin Invest,* 71(6), pp. 1822-9.

Kim, J., Park, E. Y., Kim, O., Schilder, J. M., Coffey, D. M., Cho, C. H. and Bast, R. C., Jr. (2018) 'Cell Origins of High-Grade Serous Ovarian Cancer', *Cancers (Basel),* 10(11).

Kim, Y. H., Nijst, P., Kiefer, K. and Tang, W. H. (2017) 'Endothelial Glycocalyx as Biomarker for Cardiovascular Diseases: Mechanistic and Clinical Implications', *Curr Heart Fail Rep,* 14(2), pp. 117-126.

Koch, S. and Claesson-Welsh, L. (2012) 'Signal transduction by vascular endothelial growth factor receptors', *Cold Spring Harb Perspect Med,* 2(7), pp. a006502.

Komarova, Y. and Malik, A. B. (2010) 'Regulation of endothelial permeability via paracellular and transcellular transport pathways', *Annu Rev Physiol,* 72, pp. 463-93.

Kondo, T., Vicent, D., Suzuma, K., Yanagisawa, M., King, G. L., Holzenberger, M. and Kahn, C. R. (2003) 'Knockout of insulin and IGF-1 receptors on vascular endothelial cells protects against retinal neovascularization', *J Clin Invest,* 111(12), pp. 1835-42.

Kowalczyk, A., Kleniewska, P., Kolodziejczyk, M., Skibska, B. and Goraca, A. (2015) 'The role of endothelin-1 and endothelin receptor antagonists in inflammatory response and sepsis', *Arch Immunol Ther Exp (Warsz),* 63(1), pp. 41-52.

Kowanetz, M. and Ferrara, N. (2006) 'Vascular endothelial growth factor signaling pathways: therapeutic perspective', *Clin Cancer Res,* 12(17), pp. 5018-22.

Krautter, F. and Iqbal, A. J. (2021) 'Glycans and Glycan-Binding Proteins as Regulators and Potential Targets in Leukocyte Recruitment', *Front Cell Dev Biol,* 9, pp. 624082.

Krishnan, V., Clark, R., Chekmareva, M., Johnson, A., George, S., Shaw, P., Seewaldt, V. and Rinker-Schaeffer, C. (2015) 'In Vivo and Ex Vivo Approaches to Study Ovarian Cancer Metastatic Colonization of Milky Spot Structures in Peritoneal Adipose', *J Vis Exp,* (105), pp. e52721.

Krishnan, V., Tallapragada, S., Schaar, B., Kamat, K., Chanana, A. M., Zhang, Y., Patel, S., Parkash, V., Rinker-Schaeffer, C., Folkins, A. K., Rankin, E. B. and Dorigo, O. (2020) 'Omental macrophages secrete chemokine ligands that promote ovarian cancer colonization of the omentum via CCR1', *Commun Biol,* 3(1), pp. 524.

Kuczynski, E. A., Vermeulen, P. B., Pezzella, F., Kerbel, R. S. and Reynolds, A. R. (2019) 'Vessel co-option in cancer', *Nat Rev Clin Oncol,* 16(8), pp. 469-493.

Kuroki, L. and Guntupalli, S. R. (2020) 'Treatment of epithelial ovarian cancer', *Bmj,* 371, pp. m3773.

La, M., Cao, T. V., Cerchiaro, G., Chilton, K., Hirabayashi, J., Kasai, K., Oliani, S. M., Chernajovsky, Y. and Perretti, M. (2003) 'A novel biological activity for galectin-1: inhibition of leukocyte-endothelial cell interactions in experimental inflammation', *Am J Pathol,* 163(4), pp. 1505-15.

Labrie, M., De Araujo, L. O. F., Communal, L., Mes-Masson, A.-M. and St-Pierre, Y. (2017) 'Tissue and plasma levels of galectins in patients with high grade serous ovarian carcinoma as new predictive biomarkers', *Scientific Reports,* 7(1), pp. 13244.

Laderach, D. J., Gentilini, L. D., Giribaldi, L., Delgado, V. C., Nugnes, L., Croci, D. O., Al Nakouzi, N., Sacca, P., Casas, G., Mazza, O., Shipp, M. A., Vazquez, E., Chauchereau, A., Kutok, J. L., Rodig, S. J., Elola, M. T., Compagno, D. and Rabinovich, G. A. (2013) 'A unique galectin signature in human prostate cancer progression suggests galectin-1 as a key target for treatment of advanced disease', *Cancer Res,* 73(1), pp. 86-96.

Lampugnani, M. G. (2010) 'Endothelial adherens junctions and the actin cytoskeleton: an 'infinity net'?', *J Biol,* 9(3), pp. 16.

Langer, H. F. and Chavakis, T. (2009) 'Leukocyte-endothelial interactions in inflammation', *J Cell Mol Med,* 13(7), pp. 1211-20.

Langley, R. R. and Fidler, I. J. (2011) 'The seed and soil hypothesis revisited--the role of tumor-stroma interactions in metastasis to different organs', *Int J Cancer,* 128(11), pp. 2527-35.

Lau, K. S., Partridge, E. A., Grigorian, A., Silvescu, C. I., Reinhold, V. N., Demetriou, M. and Dennis, J. W. (2007) 'Complex N-glycan number and degree of branching cooperate to regulate cell proliferation and differentiation', *Cell,* 129(1), pp. 123-34.

Lau, T. S., Chan, L. K., Wong, E. C., Hui, C. W., Sneddon, K., Cheung, T. H., Yim, S. F., Lee, J. H., Yeung, C. S., Chung, T. K. and Kwong, J. (2017) 'A loop of cancer-stroma-cancer interaction promotes peritoneal metastasis of ovarian cancer via TNFα-TGFα-EGFR', *Oncogene,* 36(25), pp. 3576-3587.

Ledermann, J. A., Embleton, A. C., Raja, F., Perren, T. J., Jayson, G. C., Rustin, G. J. S., Kaye, S. B., Hirte, H., Eisenhauer, E., Vaughan, M., Friedlander, M., González-Martín, A., Stark, D., Clark, E., Farrelly, L., Swart, A. M., Cook, A., Kaplan, R. S. and Parmar, M. K. B. (2016) 'Cediranib in patients with relapsed platinum-sensitive ovarian cancer (ICON6): a randomised, double-blind, placebo-controlled phase 3 trial', *Lancet,* 387(10023), pp. 1066-1074.

Ledermann, J. A., Embleton-Thirsk, A. C., Perren, T. J., Jayson, G. C., Rustin, G. J. S., Kaye, S. B., Hirte, H., Oza, A., Vaughan, M., Friedlander, M., González-Martín, A., Deane, E., Popoola, B., Farrelly, L., Swart, A. M., Kaplan, R. S. and Parmar, M. K. B. (2021) 'Cediranib in addition to chemotherapy for women with relapsed platinum-sensitive ovarian cancer (ICON6): overall survival results of a phase III randomised trial', *ESMO Open,* 6(2), pp. 100043.

Ledermann, J. A., Raja, F. A., Fotopoulou, C., Gonzalez-Martin, A., Colombo, N. and Sessa, C. (2013) 'Newly diagnosed and relapsed epithelial ovarian carcinoma: ESMO Clinical Practice Guidelines for diagnosis, treatment and follow-up', *Ann Oncol,* 24 Suppl 6, pp. vi24-32.

Li, N., Hill, K. S. and Elferink, L. A. (2008) 'Analysis of receptor tyrosine kinase internalization using flow cytometry', *Methods Mol Biol,* 457, pp. 305-17.

Li, Q., Xie, Y., Wong, M. and Lebrilla, C. B. (2019) 'Characterization of Cell Glycocalyx with Mass Spectrometry Methods', *Cells,* 8(8).

Liao, J. K. (2013) 'Linking endothelial dysfunction with endothelial cell activation', *J Clin Invest,* 123(2), pp. 540-1.

Lin, X. P., Mintern, J. D. and Gleeson, P. A. (2020) 'Macropinocytosis in Different Cell Types: Similarities and Differences', *Membranes (Basel),* 10(8).

Lis, R., Touboul, C., Raynaud, C. M., Malek, J. A., Suhre, K., Mirshahi, M. and Rafii, A. (2012) 'Mesenchymal cell interaction with ovarian cancer cells triggers pro-metastatic properties', *PLoS One,* 7(5), pp. e38340.

Liu, F. T. and Rabinovich, G. A. (2005) 'Galectins as modulators of tumour progression', *Nat Rev Cancer,* 5(1), pp. 29-41.

Liu, L. and Shi, G. P. (2012) 'CD31: beyond a marker for endothelial cells', *Cardiovasc Res: Vol. 1*. England, pp. 3-5.

Liu, L. Z., Zheng, J. Z., Wang, X. R. and Jiang, B. H. (2008) 'Endothelial p70 S6 kinase 1 in regulating tumor angiogenesis', *Cancer Res,* 68(19), pp. 8183-8.

Lugano, R., Ramachandran, M. and Dimberg, A. (2020) 'Tumor angiogenesis: causes, consequences, challenges and opportunities', *Cell Mol Life Sci,* 77(9), pp. 1745-1770.

Lynch, H. T., Casey, M. J., Snyder, C. L., Bewtra, C., Lynch, J. F., Butts, M. and Godwin, A. K. (2009) 'Hereditary ovarian carcinoma: heterogeneity, molecular genetics, pathology, and management', *Mol Oncol,* 3(2), pp. 97-137.

Lähteenvuo, J. and Rosenzweig, A. (2012) 'Effects of aging on angiogenesis', *Circ Res,* 110(9), pp. 1252-64.

Mabuchi, S., Terai, Y., Morishige, K., Tanabe-Kimura, A., Sasaki, H., Kanemura, M., Tsunetoh, S., Tanaka, Y., Sakata, M., Burger, R. A., Kimura, T. and Ohmichi, M. (2008) 'Maintenance treatment with bevacizumab prolongs survival in an in vivo ovarian cancer model', *Clin Cancer Res,* 14(23), pp. 7781-9.

Macdonald, P. R., Progias, P., Ciani, B., Patel, S., Mayer, U., Steinmetz, M. O. and Kammerer, R. A. (2006) 'Structure of the extracellular domain of Tie receptor tyrosine kinases and localization of the angiopoietin-binding epitope', *J Biol Chem,* 281(38), pp. 28408-14.

Maeshima, Y. and Makino, H. (2010) 'Angiogenesis and chronic kidney disease', *Fibrogenesis Tissue Repair,* 3, pp. 13.

Manetti, M., Guiducci, S., Ibba-Manneschi, L. and Matucci-Cerinic, M. (2011) 'Impaired angiogenesis in systemic sclerosis: the emerging role of the antiangiogenic VEGF(165)b splice variant', *Trends Cardiovasc Med,* 21(7), pp. 204-10.

Marcelo, K. L., Goldie, L. C. and Hirschi, K. K. (2013) 'Regulation of endothelial cell differentiation and specification', *Circ Res,* 112(9), pp. 1272-87.

Martin-Padura, I. and Bertolini, F. (2009) 'Circulating endothelial cells as biomarkers for angiogenesis in tumor progression', *Front Biosci (Schol Ed),* 1, pp. 304-18.

Martinou, J. C., Le Van Thai, A., Cassar, G., Roubinet, F. and Weber, M. J. (1989) 'Characterization of two factors enhancing choline acetyltransferase activity in cultures of purified rat motoneurons', *J Neurosci,* 9(10), pp. 3645-56.

Masoodi, M., Shah, Z. A., Beigh, A. H., Ahmad, S. Z., Mir, A. W., Yasin, B., Rasool, R., Masoodi, K. Z. and Bhat, G. M. (2021) 'Galectin-1 as a predictive biomarker in ovarian cancer', *J Ovarian Res,* 14(1), pp. 123.

Masoumi Moghaddam, S., Amini, A., Morris, D. L. and Pourgholami, M. H. (2012) 'Significance of vascular endothelial growth factor in growth and peritoneal dissemination of ovarian cancer', *Cancer Metastasis Rev,* 31(1-2), pp. 143-62.

Matarrese, P., Tinari, A., Mormone, E., Bianco, G. A., Toscano, M. A., Ascione, B., Rabinovich, G. A. and Malorni, W. (2005) 'Galectin-1 sensitizes resting human T lymphocytes to Fas (CD95)-mediated cell death via mitochondrial hyperpolarization, budding, and fission', *J Biol Chem,* 280(8), pp. 6969-85.

Matsumoto, T. and Mugishima, H. (2006) 'Signal transduction via vascular endothelial growth factor (VEGF) receptors and their roles in atherogenesis', *J Atheroscler Thromb,* 13(3), pp. 130-5.

McKenney, J. K., Weiss, S. W. and Folpe, A. L. (2001) 'CD31 expression in intratumoral macrophages: a potential diagnostic pitfall', *Am J Surg Pathol,* 25(9), pp. 1167-73.

McLean, K., Gong, Y., Choi, Y., Deng, N., Yang, K., Bai, S., Cabrera, L., Keller, E., McCauley, L., Cho, K. R. and Buckanovich, R. J. (2011) 'Human ovarian carcinoma–associated mesenchymal stem cells regulate cancer stem cells and tumorigenesis via altered BMP production', *J Clin Invest,* 121(8), pp. 3206-19.

Mehta, P. K. and Griendling, K. K. (2007) 'Angiotensin II cell signaling: physiological and pathological effects in the cardiovascular system', *Am J Physiol Cell Physiol,* 292(1), pp. C82-97.

Mendel, D. B., Schreck, R. E., West, D. C., Li, G., Strawn, L. M., Tanciongco, S. S., Vasile, S., Shawver, L. K. and Cherrington, J. M. (2000) 'The angiogenesis inhibitor SU5416 has long-lasting effects on vascular endothelial growth factor receptor phosphorylation and function', *Clin Cancer Res,* 6(12), pp. 4848-58.

Meyer, R. D., Latz, C. and Rahimi, N. (2003) 'Recruitment and activation of phospholipase Cgamma1 by vascular endothelial growth factor receptor-2 are required for tubulogenesis and differentiation of endothelial cells', *J Biol Chem,* 278(18), pp. 16347-55.

Meza-Perez, S. and Randall, T. D. (2017) 'Immunological Functions of the Omentum', *Trends Immunol,* 38(7), pp. 526-536.

Michael, J. V., Wurtzel, J. G. and Goldfinger, L. E. (2016) 'Inhibition of Galectin-1 Sensitizes HRAS-driven Tumor Growth to Rapamycin Treatment', *Anticancer Res,* 36(10), pp. 5053-5061.

Miranda, F., Mannion, D., Liu, S., Zheng, Y., Mangala, L. S., Redondo, C., Herrero-Gonzalez, S., Xu, R., Taylor, C., Chedom, D. F., Karaminejadranjbar, M., Albukhari, A., Jiang, D., Pradeep, S., Rodriguez-Aguayo, C., Lopez-Berestein, G., Salah, E., Abdul Azeez, K. R., Elkins, J. M., Campo, L., Myers, K. A., Klotz, D., Bivona, S., Dhar, S., Bast, R. C., Jr., Saya, H., Choi, H. G., Gray, N. S., Fischer, R., Kessler, B. M., Yau, C., Sood, A. K., Motohara, T., Knapp, S. and Ahmed, A. A. (2016) 'Salt-Inducible Kinase 2 Couples Ovarian Cancer Cell Metabolism with Survival at the Adipocyte-Rich Metastatic Niche', *Cancer Cell,* 30(2), pp. 273-289.

Mitra, A. K., Zillhardt, M., Hua, Y., Tiwari, P., Murmann, A. E., Peter, M. E. and Lengyel, E. (2012) 'MicroRNAs reprogram normal fibroblasts into cancer-associated fibroblasts in ovarian cancer', *Cancer Discov,* 2(12), pp. 1100-8.

Moccia, F., Negri, S., Shekha, M., Faris, P. and Guerra, G. (2019) 'Endothelial Ca(2+) Signaling, Angiogenesis and Vasculogenesis: just What It Takes to Make a Blood Vessel', *Int J Mol Sci,* 20(16).

Moiseeva, E. P., Williams, B. and Samani, N. J. (2003) 'Galectin 1 inhibits incorporation of vitronectin and chondroitin sulfate B into the extracellular matrix of human vascular smooth muscle cells', *Biochim Biophys Acta,* 1619(2), pp. 125-32.

Monk, B. J., Poveda, A., Vergote, I., Raspagliesi, F., Fujiwara, K., Bae, D. S., Oaknin, A., Ray-Coquard, I., Provencher, D. M., Karlan, B. Y., Lhommé, C., Richardson, G., Rincón, D. G., Coleman, R. L., Herzog, T. J., Marth, C., Brize, A., Fabbro, M., Redondo, A., Bamias, A., Tassoudji, M., Navale, L., Warner, D. J. and Oza, A. M. (2014) 'Anti-angiopoietin therapy with trebananib for recurrent ovarian cancer (TRINOVA-1): a randomised, multicentre, double-blind, placebo-controlled phase 3 trial', *Lancet Oncol,* 15(8), pp. 799-808.

Morandi, V., Fauvel-Lafeve, F., Legrand, C. and Legrand, Y. J. (1993) 'Role of thrombospondin in the adhesion of human endothelial cells in primary culture', *In Vitro Cell Dev Biol Anim,* 29a(7), pp. 585-91.

Moro, F., Leombroni, M., Pasciuto, T., Trivellizzi, I. N., Mascilini, F., Ciccarone, F., Zannoni, G. F., Fanfani, F., Scambia, G. and Testa, A. C. (2019) 'Synchronous primary cancers of endometrium and ovary vs endometrial cancer with ovarian metastasis: an observational study', *Ultrasound Obstet Gynecol,* 53(6), pp. 827-835.

Motohara, T., Masuda, K., Morotti, M., Zheng, Y., El-Sahhar, S., Chong, K. Y., Wietek, N., Alsaadi, A., Karaminejadranjbar, M., Hu, Z., Artibani, M., Gonzalez, L. S., Katabuchi, H., Saya, H. and Ahmed, A. A. (2019) 'An evolving story of the metastatic voyage of ovarian cancer cells: cellular and molecular orchestration of the adipose-rich metastatic microenvironment', *Oncogene,* 38(16), pp. 2885-2898.

Muller, W. A. (2011) 'Mechanisms of leukocyte transendothelial migration', *Annu Rev Pathol,* 6, pp. 323-44.

Márquez-Rosado, L., Solan, J. L., Dunn, C. A., Norris, R. P. and Lampe, P. D. (2012) 'Connexin43 phosphorylation in brain, cardiac, endothelial and epithelial tissues', *Biochim Biophys Acta,* 1818(8), pp. 1985-92.

Nakagawa, T., Kosugi, T., Haneda, M., Rivard, C. J. and Long, D. A. (2009) 'Abnormal angiogenesis in diabetic nephropathy', *Diabetes,* 58(7), pp. 1471-8.

Nakamura, K., Sawada, K., Kobayashi, M., Miyamoto, M., Shimizu, A., Yamamoto, M., Kinose, Y. and Kimura, T. (2019) 'Role of the Exosome in Ovarian Cancer Progression and Its Potential as a Therapeutic Target', *Cancers (Basel),* 11(8).

Neesham, D., Richards, A. and McGauran, M. (2020) 'Advances in epithelial ovarian cancer', *Aust J Gen Pract,* 49(10), pp. 665-669.

Nickel, W. (2005) 'Unconventional secretory routes: direct protein export across the plasma membrane of mammalian cells', *Traffic,* 6(8), pp. 607-14.

Nieman, K. M., Kenny, H. A., Penicka, C. V., Ladanyi, A., Buell-Gutbrod, R., Zillhardt, M. R., Romero, I. L., Carey, M. S., Mills, G. B., Hotamisligil, G. S., Yamada, S. D., Peter, M. E., Gwin, K. and Lengyel, E. (2011) 'Adipocytes promote ovarian cancer metastasis and provide energy for rapid tumor growth', *Nat Med,* 17(11), pp. 1498-503.

Niu, G. and Chen, X. (2010) 'Vascular endothelial growth factor as an anti-angiogenic target for cancer therapy', *Curr Drug Targets,* 11(8), pp. 1000-17.

Obgyn Key. (2016) *Normal Morphology of the Female Genital Tract.* Available from: https://obgynkey.com/normal-morphology-of-the-female-genital-tract/. Accessed: August 2021.

Oettel, A., Lorenz, M., Stangl, V., Costa, S. D., Zenclussen, A. C. and Schumacher, A. (2016) 'Human Umbilical Vein Endothelial Cells foster conversion of CD4+CD25-Foxp3- T cells into CD4+Foxp3+ Regulatory T Cells via Transforming Growth Factor-β', *Sci Rep,* 6, pp. 23278.

Okamoto, T., Usuda, H., Tanaka, T., Wada, K. and Shimaoka, M. (2019) 'The Functional Implications of Endothelial Gap Junctions and Cellular Mechanics in Vascular Angiogenesis', *Cancers (Basel),* 11(2).

Orozco, C. A., Martinez-Bosch, N., Guerrero, P. E., Vinaixa, J., Dalotto-Moreno, T., Iglesias, M., Moreno, M., Djurec, M., Poirier, F., Gabius, H. J., Fernandez-Zapico, M. E., Hwang, R. F., Guerra, C., Rabinovich, G. A. and Navarro, P. (2018) 'Targeting galectin-1 inhibits pancreatic cancer progression by modulating tumor-stroma crosstalk', *Proc Natl Acad Sci U S A,* 115(16), pp. E3769-e3778.

Ozkor, M. A. and Quyyumi, A. A. (2011) 'Endothelium-derived hyperpolarizing factor and vascular function', *Cardiol Res Pract,* 2011, pp. 156146.

Pakuła, M., Uruski, P., Niklas, A., Woźniak, A., Szpurek, D., Tykarski, A., Mikuła-Pietrasik, J. and Książek, K. (2019) 'A Unique Pattern of Mesothelial-Mesenchymal Transition Induced in the Normal Peritoneal Mesothelium by High-Grade Serous Ovarian Cancer', *Cancers (Basel),* 11(5).

Pan, J., Hu, Y., Sun, S., Chen, L., Schnaubelt, M., Clark, D., Ao, M., Zhang, Z., Chan, D., Qian, J. and Zhang, H. (2020) 'Glycoproteomics-based signatures for tumor subtyping and clinical outcome prediction of high-grade serous ovarian cancer', *Nat Commun,* 11(1), pp. 6139.

Park, G. B., Chung, Y. H. and Kim, D. (2017) 'Induction of galectin-1 by TLR-dependent PI3K activation enhances epithelial-mesenchymal transition of metastatic ovarian cancer cells', *Oncol Rep,* 37(5), pp. 3137-3145.

Partridge, E. A., Le Roy, C., Di Guglielmo, G. M., Pawling, J., Cheung, P., Granovsky, M., Nabi, I. R., Wrana, J. L. and Dennis, J. W. (2004) 'Regulation of cytokine receptors by Golgi N-glycan processing and endocytosis', *Science,* 306(5693), pp. 120-4.

Patnaik, S. K., Potvin, B., Carlsson, S., Sturm, D., Leffler, H. and Stanley, P. (2006) 'Complex N-glycans are the major ligands for galectin-1, -3, and -8 on Chinese hamster ovary cells', *Glycobiology,* 16(4), pp. 305-17.

Paushkin, S., Gubitz, A. K., Massenet, S. and Dreyfuss, G. (2002) 'The SMN complex, an assemblyosome of ribonucleoproteins', *Curr Opin Cell Biol,* 14(3), pp. 305-12.

Paz, A., Haklai, R., Elad-Sfadia, G., Ballan, E. and Kloog, Y. (2001) 'Galectin-1 binds oncogenic H-Ras to mediate Ras membrane anchorage and cell transformation', *Oncogene,* 20(51), pp. 7486-93.

Pecot, C. V., Bischoff, F. Z., Mayer, J. A., Wong, K. L., Pham, T., Bottsford-Miller, J., Stone, R. L., Lin, Y. G., Jaladurgam, P., Roh, J. W., Goodman, B. W., Merritt, W. M., Pircher, T. J., Mikolajczyk, S. D., Nick, A. M., Celestino, J., Eng, C., Ellis, L. M., Deavers, M. T. and Sood, A. K. (2011) 'A novel platform for detection of CK+ and CK- CTCs', *Cancer Discov,* 1(7), pp. 580-6.

Peng, T., Shen, E., Fan, J., Zhang, Y., Arnold, J. M. and Feng, Q. (2008) 'Disruption of phospholipase Cgamma1 signalling attenuates cardiac tumor necrosis factor-alpha expression and improves myocardial function during endotoxemia', *Cardiovasc Res,* 78(1), pp. 90-7.

Pepper, M. S. (2001) 'Role of the matrix metalloproteinase and plasminogen activator-plasmin systems in angiogenesis', *Arterioscler Thromb Vasc Biol,* 21(7), pp. 1104-17.

Perren, T. J., Swart, A. M., Pfisterer, J., Ledermann, J. A., Pujade-Lauraine, E., Kristensen, G., Carey, M. S., Beale, P., Cervantes, A., Kurzeder, C., du Bois, A., Sehouli, J., Kimmig, R., Stähle, A., Collinson, F., Essapen, S., Gourley, C., Lortholary, A., Selle, F., Mirza, M. R., Leminen, A., Plante, M., Stark, D., Qian, W., Parmar, M. K. and Oza, A. M. (2011) 'A phase 3 trial of bevacizumab in ovarian cancer', *N Engl J Med,* 365(26), pp. 2484-96.

Pezzi, H. M., Niles, D. J., Schehr, J. L., Beebe, D. J. and Lang, J. M. (2018) 'Integration of Magnetic Bead-Based Cell Selection into Complex Isolations', *ACS Omega,* 3(4), pp. 3908-3917.

Piatek, S., Panek, G., Lewandowski, Z., Bidzinski, M., Piatek, D., Kosinski, P. and Wielgos, M. (2020) 'Rising serum CA-125 levels within the normal range is strongly associated recurrence risk and survival of ovarian cancer', *Journal of Ovarian Research,* 13(1), pp. 102.

Pinilla-Macua, I. and Sorkin, A. (2015) 'Methods to study endocytic trafficking of the EGF receptor', *Methods Cell Biol,* 130, pp. 347-67.

Plagens-Rotman, K., Chmaj-Wierzchowska, K., Pięta, B. and Bojar, I. (2018) 'Modifiable lifestyle factors and ovarian cancer incidence in women', *Ann Agric Environ Med,* 25(1), pp. 36-40.

Platell, C., Cooper, D., Papadimitriou, J. M. and Hall, J. C. (2000) 'The omentum', *World J Gastroenterol,* 6(2), pp. 169-176.

Pober, J. S. and Sessa, W. C. (2007) 'Evolving functions of endothelial cells in inflammation', *Nat Rev Immunol,* 7(10), pp. 803-15.

Popel, A. S. and Johnson, P. C. (2005) 'Microcirculation and Hemorheology', *Annu Rev Fluid Mech,* 37, pp. 43-69.

Pradeep, S., Kim, S. W., Wu, S. Y., Nishimura, M., Chaluvally-Raghavan, P., Miyake, T., Pecot, C. V., Kim, S. J., Choi, H. J., Bischoff, F. Z., Mayer, J. A., Huang, L., Nick, A. M., Hall, C. S., Rodriguez-Aguayo, C., Zand, B., Dalton, H. J., Arumugam, T., Lee, H. J., Han, H. D., Cho, M. S., Rupaimoole, R., Mangala, L. S., Sehgal, V., Oh, S. C., Liu, J., Lee, J. S., Coleman, R. L., Ram, P., Lopez-Berestein, G., Fidler, I. J. and Sood, A. K. (2014) 'Hematogenous metastasis of ovarian cancer: rethinking mode of spread', *Cancer Cell,* 26(1), pp. 77-91.

Pranjol, M. Z. I., Gutowski, N. J., Hannemann, M. and Whatmore, J. L. (2019) 'Cathepsin L Induces Proangiogenic Changes in Human Omental Microvascular Endothelial Cells via Activation of the ERK1/2 Pathway', *Curr Cancer Drug Targets: Vol. 3*. Netherlands: Copyright© Bentham Science Publishers; For any queries, please email at epub@benthamscience.net., pp. 231-242.

Prior, I. A., Muncke, C., Parton, R. G. and Hancock, J. F. (2003) 'Direct visualization of Ras proteins in spatially distinct cell surface microdomains', *J Cell Biol,* 160(2), pp. 165-70.

Prudovsky, I. (2013) 'Nonclassically Secreted Regulators of Angiogenesis', *Angiol Open Access,* 1(1), pp. 1000101.

Püschel, F., Favaro, F., Redondo-Pedraza, J., Lucendo, E., Iurlaro, R., Marchetti, S., Majem, B., Eldering, E., Nadal, E., Ricci, J. E., Chevet, E. and Muñoz-Pinedo, C. (2020) 'Starvation and antimetabolic therapy promote cytokine release and recruitment of immune cells', *Proc Natl Acad Sci U S A,* 117(18), pp. 9932-9941.

Rafikov, R., Fonseca, F. V., Kumar, S., Pardo, D., Darragh, C., Elms, S., Fulton, D. and Black, S. M. (2011) 'eNOS activation and NO function: structural motifs responsible for the posttranslational control of endothelial nitric oxide synthase activity', *J Endocrinol,* 210(3), pp. 271-84.

Rahimi, N. (2017) 'Defenders and Challengers of Endothelial Barrier Function', *Front Immunol,* 8, pp. 1847.

Rajendran, P., Rengarajan, T., Thangavel, J., Nishigaki, Y., Sakthisekaran, D., Sethi, G. and Nishigaki, I. (2013) 'The vascular endothelium and human diseases', *Int J Biol Sci,* 9(10), pp. 1057-69.

Rasmussen, C. B., Kjaer, S. K., Albieri, V., Bandera, E. V., Doherty, J. A., Høgdall, E., Webb, P. M., Jordan, S. J., Rossing, M. A., Wicklund, K. G., Goodman, M. T., Modugno, F., Moysich, K. B., Ness, R. B., Edwards, R. P., Schildkraut, J. M., Berchuck, A., Olson, S. H., Kiemeney, L. A., Massuger, L. F., Narod, S. A., Phelan, C. M., Anton-Culver, H., Ziogas, A., Wu, A. H., Pearce, C. L., Risch, H. A. and Jensen, A. (2017) 'Pelvic Inflammatory Disease and the Risk of Ovarian Cancer and Borderline Ovarian Tumors: A Pooled Analysis of 13 Case-Control Studies', *Am J Epidemiol,* 185(1), pp. 8-20.

Ray, A., Fornsaglio, J., Dogan, S., Hedau, S., Naik, D. and De, A. (2018) 'Gynaecological cancers and leptin: A focus on the endometrium and ovary', *Facts Views Vis Obgyn,* 10(1), pp. 5-18.

Reid, B. M., Permuth, J. B. and Sellers, T. A. (2017) 'Epidemiology of ovarian cancer: a review', *Cancer Biol Med,* 14(1), pp. 9-32.

Reily, C., Stewart, T. J., Renfrow, M. B. and Novak, J. (2019) 'Glycosylation in health and disease', *Nat Rev Nephrol,* 15(6), pp. 346-366.

Ribatti, D., Nico, B., Crivellato, E., Roccaro, A. M. and Vacca, A. (2007) 'The history of the angiogenic switch concept', *Leukemia,* 21(1), pp. 44-52.

Ribatti, D., Tamma, R., Ruggieri, S., Annese, T. and Crivellato, E. (2020) 'Surface markers: An identity card of endothelial cells', *Microcirculation,* 27(1), pp. e12587.

Rodriguez, C., Calle, E. E., Fakhrabadi-Shokoohi, D., Jacobs, E. J. and Thun, M. J. (2002) 'Body mass index, height, and the risk of ovarian cancer mortality in a prospective cohort of postmenopausal women', *Cancer Epidemiol Biomarkers Prev,* 11(9), pp. 822-8.

Rosner, M., Schipany, K. and Hengstschläger, M. (2012) 'p70 S6K1 nuclear localization depends on its mTOR-mediated phosphorylation at T389, but not on its kinase activity towards S6', *Amino Acids,* 42(6), pp. 2251-6.

Rossaint, J., Margraf, A. and Zarbock, A. (2018) 'Role of Platelets in Leukocyte Recruitment and Resolution of Inflammation', *Front Immunol,* 9, pp. 2712.

Roy, R., Chun, J. and Powell, S. N. (2011) 'BRCA1 and BRCA2: different roles in a common pathway of genome protection', *Nat Rev Cancer,* 12(1), pp. 68-78.

Rudno-Rudzińska, J., Kielan, W., Frejlich, E., Kotulski, K., Hap, W., Kurnol, K., Dzierżek, P., Zawadzki, M. and Hałoń, A. (2017) 'A review on Eph/ephrin, angiogenesis and lymphangiogenesis in gastric, colorectal and pancreatic cancers', *Chin J Cancer Res,* 29(4), pp. 303-312.

Rump, A., Morikawa, Y., Tanaka, M., Minami, S., Umesaki, N., Takeuchi, M. and Miyajima, A. (2004) 'Binding of ovarian cancer antigen CA125/MUC16 to mesothelin mediates cell adhesion', *J Biol Chem,* 279(10), pp. 9190-8.

Ruoslahti, E. (2002) 'Specialization of tumour vasculature', *Nat Rev Cancer,* 2(2), pp. 83-90.

Sako, A., Kitayama, J., Yamaguchi, H., Kaisaki, S., Suzuki, H., Fukatsu, K., Fujii, S. and Nagawa, H. (2003) 'Vascular endothelial growth factor synthesis by human omental mesothelial cells is augmented by fibroblast growth factor-2: possible role of mesothelial cell on the development of peritoneal metastasis', *J Surg Res,* 115(1), pp. 113-20.

Salceda, S., Tang, T., Kmet, M., Munteanu, A., Ghosh, M., Macina, R., Liu, W., Pilkington, G. and Papkoff, J. (2005) 'The immunomodulatory protein B7-H4 is overexpressed in breast and ovarian cancers and promotes epithelial cell transformation', *Exp Cell Res,* 306(1), pp. 128-41.

Salimian Rizi, B., Caneba, C., Nowicka, A., Nabiyar, A. W., Liu, X., Chen, K., Klopp, A. and Nagrath, D. (2015) 'Nitric oxide mediates metabolic coupling of omentum-derived adipose stroma to ovarian and endometrial cancer cells', *Cancer Res,* 75(2), pp. 456-71.

Sandoo, A., van Zanten, J. J., Metsios, G. S., Carroll, D. and Kitas, G. D. (2010) 'The endothelium and its role in regulating vascular tone', *Open Cardiovasc Med J,* 4, pp. 302-12.

Santos-Oliveira, P., Correia, A., Rodrigues, T., Ribeiro-Rodrigues, T. M., Matafome, P., Rodríguez-Manzaneque, J. C., Seiça, R., Girão, H. and Travasso, R. D. (2015) 'The Force at the Tip--Modelling Tension and Proliferation in Sprouting Angiogenesis', *PLoS Comput Biol,* 11(8), pp. e1004436.

Satchell, S. C. and Braet, F. (2009) 'Glomerular endothelial cell fenestrations: an integral component of the glomerular filtration barrier', *Am J Physiol Renal Physiol,* 296(5), pp. F947-56.

Sawada, K., Mitra, A. K., Radjabi, A. R., Bhaskar, V., Kistner, E. O., Tretiakova, M., Jagadeeswaran, S., Montag, A., Becker, A., Kenny, H. A., Peter, M. E., Ramakrishnan, V., Yamada, S. D. and Lengyel, E. (2008) 'Loss of E-cadherin promotes ovarian cancer metastasis via alpha 5-integrin, which is a therapeutic target', *Cancer Res,* 68(7), pp. 2329-39.

Schildkraut, J. M., Cooper, G. S., Halabi, S., Calingaert, B., Hartge, P. and Whittemore, A. S. (2001) 'Age at natural menopause and the risk of epithelial ovarian cancer', *Obstet Gynecol,* 98(1), pp. 85-90.

Scholler, N. and Urban, N. (2007) 'CA125 in ovarian cancer', *Biomark Med,* 1(4), pp. 513-23.

Schäfer, T., Zentgraf, H., Zehe, C., Brügger, B., Bernhagen, J. and Nickel, W. (2004) 'Unconventional secretion of fibroblast growth factor 2 is mediated by direct translocation across the plasma membrane of mammalian cells', *J Biol Chem,* 279(8), pp. 6244-51.

Scott, D. W., Vallejo, M. O. and Patel, R. P. (2013) 'Heterogenic endothelial responses to inflammation: role for differential N-glycosylation and vascular bed of origin', *J Am Heart Assoc,* 2(4), pp. e000263.

Sheng, J. and Xu, Z. (2016) 'Three decades of research on angiogenin: a review and perspective', *Acta Biochim Biophys Sin (Shanghai),* 48(5), pp. 399-410.

Shi, Y. and Vanhoutte, P. M. (2017) 'Macro- and microvascular endothelial dysfunction in diabetes', *J Diabetes,* 9(5), pp. 434-449.

Shimada, C., Xu, R., Al-Alem, L., Stasenko, M., Spriggs, D. R. and Rueda, B. R. (2020) 'Galectins and Ovarian Cancer', *Cancers (Basel),* 12(6).

Shintani, Y., Takashima, S., Asano, Y., Kato, H., Liao, Y., Yamazaki, S., Tsukamoto, O., Seguchi, O., Yamamoto, H., Fukushima, T., Sugahara, K., Kitakaze, M. and Hori, M. (2006) 'Glycosaminoglycan modification of neuropilin-1 modulates VEGFR2 signaling', *Embo j,* 25(13), pp. 3045-55.

Sidney, L. E., Branch, M. J., Dunphy, S. E., Dua, H. S. and Hopkinson, A. (2014) 'Concise review: evidence for CD34 as a common marker for diverse progenitors', *Stem Cells,* 32(6), pp. 1380-9.

Siemerink, M. J., Klaassen, I., Vogels, I. M., Griffioen, A. W., Van Noorden, C. J. and Schlingemann, R. O. (2012) 'CD34 marks angiogenic tip cells in human vascular endothelial cell cultures', *Angiogenesis,* 15(1), pp. 151-63.

Singh, A. J., Meyer, R. D., Navruzbekov, G., Shelke, R., Duan, L., Band, H., Leeman, S. E. and Rahimi, N. (2007) 'A critical role for the E3-ligase activity of c-Cbl in VEGFR-2-mediated PLCγ1 activation and angiogenesis', *Proceedings of the National Academy of Sciences,* 104(13), pp. 5413-5418.

Soegaard, M., Frederiksen, K., Jensen, A., Høgdall, E., Høgdall, C., Blaakaer, J., Ramus, S. J., Gayther, S. A. and Kjaer, S. K. (2009) 'Risk of ovarian cancer in women with first-degree relatives with cancer', *Acta Obstet Gynecol Scand,* 88(4), pp. 449-56.

Soga, N., Namba, N., McAllister, S., Cornelius, L., Teitelbaum, S. L., Dowdy, S. F., Kawamura, J. and Hruska, K. A. (2001) 'Rho family GTPases regulate VEGF-stimulated endothelial cell motility', *Exp Cell Res,* 269(1), pp. 73-87.

Stanley, P. (2014) 'Galectin-1 Pulls the Strings on VEGFR2', *Cell,* 156(4), pp. 625-626.

Staton, C. A., Reed, M. W. and Brown, N. J. (2009) 'A critical analysis of current in vitro and in vivo angiogenesis assays', *Int J Exp Pathol,* 90(3), pp. 195-221.

Stone, R. L., Sood, A. K. and Coleman, R. L. (2010) 'Collateral damage: toxic effects of targeted antiangiogenic therapies in ovarian cancer', *Lancet Oncol,* 11(5), pp. 465-75.

Strell, C. and Entschladen, F. (2008) 'Extravasation of leukocytes in comparison to tumor cells', *Cell Commun Signal,* 6, pp. 10.

Ståhle, M., Foss, A., Gustafsson, B., Lempinen, M., Lundgren, T., Rafael, E., Tufveson, G., Korsgren, O. and Friberg, A. (2015) 'Clostripain, the Missing Link in the Enzyme Blend for Efficient Human Islet Isolation', *Transplant Direct,* 1(5), pp. e19.

Sudhan, D. R. and Siemann, D. W. (2015) 'Cathepsin L targeting in cancer treatment', *Pharmacol Ther,* 155, pp. 105-16.

Swisher, E. M., Garcia, R. L., Kilgore, M. R. and Norquist, B. M. (2016) 'Culprit or Bystander? The Role of the Fallopian Tube in "Ovarian" High-Grade Serous Carcinoma', *Cancer Discov,* 6(12), pp. 1309-1311.

Takahashi, T., Yamaguchi, S., Chida, K. and Shibuya, M. (2001) 'A single autophosphorylation site on KDR/Flk-1 is essential for VEGF-A-dependent activation of PLC-gamma and DNA synthesis in vascular endothelial cells', *Embo j,* 20(11), pp. 2768-78.

Tarin, D., Price, J. E., Kettlewell, M. G., Souter, R. G., Vass, A. C. and Crossley, B. (1984) 'Mechanisms of human tumor metastasis studied in patients with peritoneovenous shunts', *Cancer Res,* 44(8), pp. 3584-92.

Tateo, S., Mereu, L., Salamano, S., Klersy, C., Barone, M., Spyropoulos, A. C. and Piovella, F. (2005) 'Ovarian cancer and venous thromboembolic risk', *Gynecol Oncol,* 99(1), pp. 119-25.

Tewari, K. S., Burger, R. A., Enserro, D., Norquist, B. M., Swisher, E. M., Brady, M. F., Bookman, M. A., Fleming, G. F., Huang, H., Homesley, H. D., Fowler, J. M., Greer, B. E., Boente, M., Liang, S. X., Ye, C., Bais, C., Randall, L. M., Chan, J. K., Ferriss, J. S., Coleman, R. L., Aghajanian, C., Herzog, T. J., DiSaia, P. J., Copeland, L. J., Mannel, R. S., Birrer, M. J. and Monk, B. J. (2019) 'Final Overall Survival of a Randomized Trial of Bevacizumab for Primary Treatment of Ovarian Cancer', *J Clin Oncol,* 37(26), pp. 2317-2328.

Thijssen, V. L., Barkan, B., Shoji, H., Aries, I. M., Mathieu, V., Deltour, L., Hackeng, T. M., Kiss, R., Kloog, Y., Poirier, F. and Griffioen, A. W. (2010) 'Tumor cells secrete galectin-1 to enhance endothelial cell activity', *Cancer Res,* 70(15), pp. 6216-24.

Thijssen, V. L., Postel, R., Brandwijk, R. J., Dings, R. P., Nesmelova, I., Satijn, S., Verhofstad, N., Nakabeppu, Y., Baum, L. G., Bakkers, J., Mayo, K. H., Poirier, F. and Griffioen, A. W. (2006) 'Galectin-1 is essential in tumor angiogenesis and is a target for antiangiogenesis therapy', *Proc Natl Acad Sci U S A,* 103(43), pp. 15975-80.

Thompson, A. J., Williams, R. J., Hakki, Z., Alonzi, D. S., Wennekes, T., Gloster, T. M., Songsrirote, K., Thomas-Oates, J. E., Wrodnigg, T. M., Spreitz, J., Stütz, A. E., Butters, T. D., Williams, S. J. and Davies, G. J. (2012) 'Structural and mechanistic insight into N-glycan processing by endo-α-mannosidase', *Proceedings of the National Academy of Sciences,* 109(3), pp. 781.

Thompson, A. K., Mostafapour, S. P., Denlinger, L. C., Bleasdale, J. E. and Fisher, S. K. (1991) 'The aminosteroid U-73122 inhibits muscarinic receptor sequestration and phosphoinositide hydrolysis in SK-N-SH neuroblastoma cells. A role for Gp in receptor compartmentation', *J Biol Chem,* 266(35), pp. 23856-62.

Tian, T., Li, X. and Zhang, J. (2019) 'mTOR Signaling in Cancer and mTOR Inhibitors in Solid Tumor Targeting Therapy', *Int J Mol Sci,* 20(3).

Tomas, A., Futter, C. E. and Eden, E. R. (2014) 'EGF receptor trafficking: consequences for signaling and cancer', *Trends Cell Biol,* 24(1), pp. 26-34.

Tortora, G., Derrickson, B. (2011) *Principles of Anatomy and Physiology*, 13th edition. John Wiley & Sons, New York.

Toss, A., Tomasello, C., Razzaboni, E., Contu, G., Grandi, G., Cagnacci, A., Schilder, R. J. and Cortesi, L. (2015) 'Hereditary ovarian cancer: not only BRCA 1 and 2 genes', *Biomed Res Int,* 2015, pp. 341723.

Tran, T. H., Steffen, J. E., Clancy, K. M., Bird, T. and Egilman, D. S. (2019) 'Talc, Asbestos, and Epidemiology: Corporate Influence and Scientific Incognizance', *Epidemiology,* 30(6), pp. 783-788.

Tworoger, S. S. and Huang, T. (2016) 'Obesity and Ovarian Cancer', *Recent Results Cancer Res,* 208, pp. 155-176.

Tzima, E. (2006) 'Role of small GTPases in endothelial cytoskeletal dynamics and the shear stress response', *Circ Res,* 98(2), pp. 176-85.

Uchimido, R., Schmidt, E. P. and Shapiro, N. I. (2019) 'The glycocalyx: a novel diagnostic and therapeutic target in sepsis', *Critical Care,* 23(1), pp. 16.

Ungvari, Z., Tarantini, S., Kiss, T., Wren, J. D., Giles, C. B., Griffin, C. T., Murfee, W. L., Pacher, P. and Csiszar, A. (2018) 'Endothelial dysfunction and angiogenesis impairment in the ageing vasculature', *Nat Rev Cardiol,* 15(9), pp. 555-565.

Vailhé, B., Vittet, D. and Feige, J. J. (2001) 'In vitro models of vasculogenesis and angiogenesis', *Lab Invest,* 81(4), pp. 439-52.

van den Brûle, F., Califice, S., Garnier, F., Fernandez, P. L., Berchuck, A. and Castronovo, V. (2003) 'Galectin-1 accumulation in the ovary carcinoma peritumoral stroma is induced by ovary carcinoma cells and affects both cancer cell proliferation and adhesion to laminin-1 and fibronectin', *Lab Invest,* 83(3), pp. 377-86.

Van Ry, P. M., Wuebbles, R. D., Key, M. and Burkin, D. J. (2015) 'Galectin-1 Protein Therapy Prevents Pathology and Improves Muscle Function in the mdx Mouse Model of Duchenne Muscular Dystrophy', *Mol Ther,* 23(8), pp. 1285-1297.

Vergara, D., Merlot, B., Lucot, J. P., Collinet, P., Vinatier, D., Fournier, I. and Salzet, M. (2010) 'Epithelial-mesenchymal transition in ovarian cancer', *Cancer Lett,* 291(1), pp. 59-66.

Versari, D., Daghini, E., Virdis, A., Ghiadoni, L. and Taddei, S. (2009) 'Endothelial dysfunction as a target for prevention of cardiovascular disease', *Diabetes Care,* 32 Suppl 2(Suppl 2), pp. S314-21.

Walker, A. M. N., Warmke, N., Mercer, B., Watt, N. T., Mughal, R., Smith, J., Galloway, S., Haywood, N. J., Soomro, T., Griffin, K. J., Wheatcroft, S. B., Yuldasheva, N. Y., Beech, D. J., Carmeliet, P., Kearney, M. T. and Cubbon, R. M. (2021) 'Endothelial Insulin Receptors Promote VEGF-A Signaling via ERK1/2 and Sprouting Angiogenesis', *Endocrinology,* 162(8).

Wang, A. W., Prieto, J. M., Cauvi, D. M., Bickler, S. W. and De Maio, A. (2020a) 'The Greater Omentum-A Vibrant and Enigmatic Immunologic Organ Involved in Injury and Infection Resolution', *Shock,* 53(4), pp. 384-390.

Wang, L., Jin, X., Lin, D., Liu, Z., Zhang, X., Lu, Y., Liu, Y., Wang, M., Yang, M., Li, J. and Quan, C. (2013) 'Clinicopathologic significance of claudin-6, occludin, and matrix metalloproteinases -2 expression in ovarian carcinoma', *Diagn Pathol,* 8, pp. 190.

Wang, X., Bove, A. M., Simone, G. and Ma, B. (2020b) 'Molecular Bases of VEGFR-2-Mediated Physiological Function and Pathological Role', *Front Cell Dev Biol,* 8, pp. 599281.

Wang, Y., Zang, Q. S., Liu, Z., Wu, Q., Maass, D., Dulan, G., Shaul, P. W., Melito, L., Frantz, D. E., Kilgore, J. A., Williams, N. S., Terada, L. S. and Nwariaku, F. E. (2011) 'Regulation of VEGF-induced endothelial cell migration by mitochondrial reactive oxygen species', *Am J Physiol Cell Physiol,* 301(3), pp. C695-704.

Winiarski, B. K., Acheson, N., Gutowski, N. J., McHarg, S. and Whatmore, J. L. (2011) 'An improved and reliable method for isolation of microvascular endothelial cells from human omentum', *Microcirculation,* 18(8), pp. 635-45.

Winiarski, B. K., Wolanska, K. I., Rai, S., Ahmed, T., Acheson, N., Gutowski, N. J. and Whatmore, J. L. (2013) 'Epithelial ovarian cancer-induced angiogenic phenotype of human omental microvascular endothelial cells may occur independently of VEGF signaling', *Transl Oncol,* 6(6), pp. 703-14.

Xie, Y., Mansouri, M., Rizk, A. and Berger, P. (2019) 'Regulation of VEGFR2 trafficking and signaling by Rab GTPase-activating proteins', *Sci Rep,* 9(1), pp. 13342.

Xu, L., Yoneda, J., Herrera, C., Wood, J., Killion, J. J. and Fidler, I. J. (2000) 'Inhibition of malignant ascites and growth of human ovarian carcinoma by oral administration of a potent inhibitor of the vascular endothelial growth factor receptor tyrosine kinases', *Int J Oncol,* 16(3), pp. 445-54.

Xu, M., Jin, H., Chen, Z., Xie, W., Wang, Y., Wang, Y., Wang, M., Zhang, J. and Acheampong, D. O. (2016) 'A novel bispecific diabody targeting both vascular endothelial growth factor receptor 2 and epidermal growth factor receptor for enhanced antitumor activity', *Biotechnology Progress,* 32(2), pp. 294-302.

Yamada, K. H., Nakajima, Y., Geyer, M., Wary, K. K., Ushio-Fukai, M., Komarova, Y. and Malik, A. B. (2014) 'KIF13B regulates angiogenesis through Golgi to plasma membrane trafficking of VEGFR2', *Journal of Cell Science,* 127(20), pp. 4518-4530.

Yamazaki, T. and Mukouyama, Y. S. (2018) 'Tissue Specific Origin, Development, and Pathological Perspectives of Pericytes', *Front Cardiovasc Med,* 5, pp. 78.

Yang, M. and Huang, C. Z. (2015) 'Mitogen-activated protein kinase signaling pathway and invasion and metastasis of gastric cancer', *World J Gastroenterol,* 21(41), pp. 11673-9.

Yang, N., Zhang, W., He, T. and Xing, Y. (2017) 'Suppression of Retinal Neovascularization by Inhibition of Galectin-1 in a Murine Model of Oxygen-Induced Retinopathy', *J Ophthalmol,* 2017, pp. 5053035.

Yang, Y., Yang, J., Zhao, X. and Wei, X. (2020) 'Tumor Microenvironment in Ovarian Cancer: Function and Therapeutic Strategy', *Front Cell Dev Biol,* 8, pp. 758.

Yau, J. W., Teoh, H. and Verma, S. (2015) 'Endothelial cell control of thrombosis', *BMC Cardiovasc Disord,* 15, pp. 130.

Yeung, T. L., Leung, C. S., Yip, K. P., Au Yeung, C. L., Wong, S. T. and Mok, S. C. (2015) 'Cellular and molecular processes in ovarian cancer metastasis. A Review in the Theme: Cell and Molecular Processes in Cancer Metastasis', *Am J Physiol Cell Physiol,* 309(7), pp. C444-56.

Yoo, E., Kim, J. H., Kim, M. J., Yu, J. S., Chung, J. J., Yoo, H. S. and Kim, K. W. (2007) 'Greater and lesser omenta: normal anatomy and pathologic processes', *Radiographics,* 27(3), pp. 707-20.

Yousefi, M., Dehghani, S., Nosrati, R., Ghanei, M., Salmaninejad, A., Rajaie, S., Hasanzadeh, M. and Pasdar, A. (2020) 'Current insights into the metastasis of epithelial ovarian cancer - hopes and hurdles', *Cell Oncol (Dordr),* 43(4), pp. 515-538.

Yu, L., Liang, X. H. and Ferrara, N. (2011) 'Comparing protein VEGF inhibitors: In vitro biological studies', *Biochem Biophys Res Commun,* 408(2), pp. 276-81.

Zafrakas, M., Grimbizis, G., Timologou, A. and Tarlatzis, B. C. (2014) 'Endometriosis and ovarian cancer risk: a systematic review of epidemiological studies', *Front Surg,* 1, pp. 14.

Zaitoun, I. S., Johnson, R. P., Jamali, N., Almomani, R., Wang, S., Sheibani, N. and Sorenson, C. M. (2015) 'Endothelium Expression of Bcl-2 Is Essential for Normal and Pathological Ocular Vascularization', *PLoS One,* 10(10), pp. e0139994.

Zhang, C., Jang, S., Amadi, O. C., Shimizu, K., Lee, R. T. and Mitchell, R. N. (2013) 'A sensitive chemotaxis assay using a novel microfluidic device', *Biomed Res Int,* 2013, pp. 373569.

Zhang, P., Shi, B., Zhou, M., Jiang, H., Zhang, H., Pan, X., Gao, H., Sun, H. and Li, Z. (2014) 'Galectin-1 overexpression promotes progression and chemoresistance to cisplatin in epithelial ovarian cancer', *Cell Death Dis,* 5(1), pp. e991.

Zhang, X. and Simons, M. (2014) 'Receptor tyrosine kinases endocytosis in endothelium: biology and signaling', *Arterioscler Thromb Vasc Biol,* 34(9), pp. 1831-7.

Zhang, Y., Dong, W., Wang, J., Cai, J. and Wang, Z. (2017) 'Human omental adipose-derived mesenchymal stem cell-conditioned medium alters the proteomic profile of epithelial ovarian cancer cell lines in vitro', *Onco Targets Ther,* 10, pp. 1655-1663.

Zhang, Z., Chen, Y., Zhang, T., Guo, L., Yang, W., Zhang, J. and Wang, C. (2016) 'Role of Myoendothelial Gap Junctions in the Regulation of Human Coronary Artery Smooth Muscle Cell Differentiation by Laminar Shear Stress', *Cell Physiol Biochem,* 39(2), pp. 423-37.

Zhao, T., Wang, X., Xu, T., Xu, X. and Liu, Z. (2017) 'Bevacizumab significantly increases the risks of hypertension and proteinuria in cancer patients: A systematic review and comprehensive meta-analysis', *Oncotarget,* 8(31), pp. 51492-51506.

Zhao, X. Y., Chen, T. T., Xia, L., Guo, M., Xu, Y., Yue, F., Jiang, Y., Chen, G. Q. and Zhao, K. W. (2010) 'Hypoxia inducible factor-1 mediates expression of galectin-1: the potential role in migration/invasion of colorectal cancer cells', *Carcinogenesis,* 31(8), pp. 1367-75.

Zhou, X., Liu, D., You, L. and Wang, L. (2010) 'Quantifying fluid shear stress in a rocking culture dish', *J Biomech,* 43(8), pp. 1598-602.

Zimna, A. and Kurpisz, M. (2015) 'Hypoxia-Inducible Factor-1 in Physiological and Pathophysiological Angiogenesis: Applications and Therapies', *Biomed Res Int,* 2015, pp. 549412.

Zou, Z., Tao, T., Li, H. and Zhu, X. (2020) 'mTOR signaling pathway and mTOR inhibitors in cancer: progress and challenges', *Cell Biosci,* 10, pp. 31.